

*Isolation and cellular characterization of the hemolysin
A type 1 secretion system from Escherichia coli*

Inaugural-Dissertation
zur Erlangung des Doktorgrades
der Mathematisch-Naturwissenschaftlichen Fakultät
der Heinrich-Heine-Universität Düsseldorf

vorgelegt von

Tobias Beer

aus Paderborn

Düsseldorf, April 2020

aus dem Institut für Biochemie
der Heinrich-Heine-Universität Düsseldorf

Gedruckt mit der Genehmigung der
Mathematisch-Naturwissenschaftlichen Fakultät der
Heinrich-Heine-Universität Düsseldorf

Referent: Prof. Dr. Lutz Schmitt

Korreferent: Prof. Dr. Michael Feldbrügge

Tag der mündlichen Prüfung: 16.06.2020

**“Google can bring you back 100,000 answers.
A librarian can bring you back the right one.”**

Neil Gaiman

Contents

1	Introduction	8
1.1.	Lipids, building blocks of biological membranes	8
1.2.	Gram-negative bacteria and the transport across membranes mediated by proteins in general	9
1.3.	The inner membrane secretion system	10
1.4.	The Gram-negative membrane spanning secretion systems	12
1.5.	Resistance-nodulation-division (RND) and T1SS	14
1.6.	Type II Secretion System (T2SS).....	14
1.7.	Type III Secretion System (T3SS)	15
1.8.	Type IV Secretion System (T4SS)	15
1.9.	Type VI Secretion System (T6SS)	16
1.10.	The outer membrane secretion systems	16
1.11.	The Type V Secretion System T5SS	17
1.12.	The Chaperone-usher pathway	18
1.13.	Curli Amyloid biogenesis system or Type VIII Secretion System (T8SS).....	18
1.14.	The hemolysin A (HlyA) T1SS	18
1.15.	ABC-transporter Hemolysin B (HlyB).....	19
1.16.	Hemolysin A (HlyA).	20
1.17.	The membrane fusion protein (MFP) Hemolysin D (HlyD)	22
1.18.	TolC the outer membrane protein (OMP)	23
1.19.	Secretion mechanism of HlyA and stalling of the T1SS	25
2	Aims	27
3	Publications	27
3.1	Chapter I – Secretion rates of substrate translocation of the HlyA Type I secretion system.....	28
3.2	Chapter II – Type I secretion system – it takes three and a substrate	53
3.3	Chapter III – Type I secretion system – One Mechanism for All?	64
3.4	Chapter IV – Quantification of endogenous hemolysin A type one secretion system in UPEC, TolC copy numbers and surface distribution versus the influence of overexpression.....	76
3.5	Chapter V – Isolation of the hemolysin A Type I secretion system in action	110
4	Discussion	142

5	Bibliography	154
6	List of Abbreviations.....	170
7	List of Figures	174
8	Danksagung.....	180
9	Curriculum vitae.....	187
10	Erklärung.....	190

Zusammenfassung

Sekretionssysteme sind essentielle Nanomaschinen in Gram-negativen Bakterien. Sie erlauben die Kommunikation aus der Zelle über den Transport von Proteinen und Signalmolekülen. Das Typ eins Sekretionssystem (T1SS) ist ein Paradebeispiel für Sekretionssysteme in Gram-negativen Bakterien. Das T1SS kann eine Vielfalt an Substraten über beide Membranen, in den extrazellulären Raum, transportieren. Die Substrate können in ihrer Größe von 19 kDa bis 1.5 MDa stark variieren. Dies gilt auch für ihre Funktionen der Substrate: Hämophile, Lipasen, Adhensionsfaktoren, Oberflächenproteine und Toxine. Die Substrate teilen gemeinsame Merkmale. Ein C-terminales Sekretionssignal das nicht während des Transports entfernt wird, während das Substrate in einem ungefalteten Zustand transportiert wird. Ein bekanntes Beispiel für T1SS ist das Hemolysin A (HlyA) T1SS. Es besteht aus dem ABC Transporter Hemolysin B (HlyB), einem Membranfusionsprotein (MFP) Hemolysin D, dem äußeren Membranprotein (OMP) TolC und dem Substrat HlyA, welches zur repeats in toxins (RTX) Familie gehört. In der Anwesenheit von HlyA wird durch den inneren Membrankomplex (IMC), bestehend aus HlyB und HlyD das OMP TolC rekrutiert und ein Translokationspfad wird durch beide Membranen gebildet Während der Forschung für diese Doktorarbeit wurde die Sekretionsrate des HlyA T1SS quantifiziert und der Einfluss von Calcium Ionen untersucht. Dazu wurde ein N-terminales Fusionskonstrukt aus HlyA mit einem schnell faltenden GFP verwendet, dass es ermöglicht das HlyA T1SS während der Translokation zu arretieren. Dieser experimentelle Aufbau ermöglicht die Quantifizierung von ca. 5000 aktiven HlyA T1SS während der Überexpression im Laborstamm *E. coli* BL21(DE3). Die Sekretion von HlyA in Kulturmedium wurde anschließend in Anwesenheit bzw. Abwesenheit verschiedener Calciumionenkonzentrationen beobachtet. Durch die Zahl der aktiven T1SS war es dadurch möglich die Sekretionsrate des HlyA T1SS mit 16 Aminosäuren pro Transporter und Sekunde zu bestimmen. Die Sekretionsrate ist unbeeinflusst vom Verhältnis von Proteinlänge zur Menge der Glycin reichen Wiederholungen und der extrazellulären Calciumionenkonzentration. Mittels Fluoreszenzmikroskopie wurde die Oberflächenlokalisierung der arretierten T1SS charakterisiert. Zur Beurteilung des Oberflächenverteilungsmusters wurde der parentale *E. coli* Stamm UTI89 verwendet. In UTI89 steht das HlyA T1SS unter endogener Expressionskontrolle und wurde untersucht, während es mit dem GFP fusionierten HlyA arretiert wurde. Unabhängig von der Überexpression in BL21(DE3) oder der endogenen Expression in UTI89 war für das HlyA T1SS keine eindeutige Lokalisation auf der Zelloberfläche zu beobachten. Zusätzlich wurde der arretierte Komplex verwendet, um die Menge an aktivem HlyA T1SS in UTI89 zu bestimmen. Während der endogenen Expression wurden etwa 800 aktive HlyA T1SS quantifiziert, verglichen mit etwa 5000 T1SS, die in BL21(DE3) überexprimiert wurden. Weiterhin wurde der Einfluss der TolC Arretierung durch das HlyA T1SS untersucht. Die Zahl der TolC-Trimere wurde quantifiziert während der Expression des HlyA T1SS auf endogenem, überexprimiertem Niveau und dessen abwesenheit. Die Anzahl an TolC waren mit etwa 5000 Trimeren unabhängig vom Besetzungsanteil nicht signifikant beeinflusst. Zuletzt wurde die mögliche Aufreinigung des arretierte T1SS untersucht. Es wurde gezeigt, dass es möglich ist Membranen mit dem T1SS zu isolieren und solubilisieren allerdings ist die Stabilität des Komplexes während der Reinigung nicht gewährleistet. Einführung von Quervernetzung führte zu einer Vielzahl an Quervernetzungsprodukten, weshalb neue Methoden für die Reinigung vorgeschlagen werden.

Abstract

Secretion systems are essential for Gram-negative bacteria as these nanomachineries allow communication with the outside by exporting proteins or signal molecules. The type one secretion system (T1SS) is a prime example for secretion systems in Gram-negative bacteria. It is able to secrete a broad range of substrates across both membranes, into the extracellular space. The substrates can vary drastically in size from 19 kDa up to 1.5 MDa also varying in function like, hemophores, lipases, adhesion factors, surface layer proteins to toxins. All substrates show a common feature the C-terminal secretion signal which is not cleaved during the secretion. One well known example for the T1SS is the hemolysin A (HlyA) T1SS, which consists of an ABC transporter hemolysin B (HlyB), a membrane fusion protein (MFP) hemolysin D (HlyD), the outer membrane protein (OMP) TolC and the substrate HlyA, a member of the repeats in toxins (RTX) family. In the presence of the substrate HlyA the inner membrane complex (IMC), consisting of HlyB and HlyD recruits TolC and forms a translocation pathway through the membranes. During this doctoral research, the secretion rate of the HlyA T1SS was quantified and the influence of calcium ions was investigated. This was established by using an N-terminal fusion construct of HlyA with a fast folding GFP allowing to arrest the T1SS during translocation. This experimental procedure allowed to determine approximately 5000 active HlyA T1SS when overexpressed in the laboratory strain *E. coli* BL21(DE3). The secretion of HlyA in culture medium was subsequently observed in the presence or absence of different calcium ion concentrations. Due to the number of active T1SS it was possible to determine the secretion rate of the HlyA T1SS with 16 amino acids per transporter and second. Revealing that the secretion rate is unaffected by proportion from protein length to amount of glycine rich repeats and the extracellular calcium ion concentration. Via fluorescence microscopy the surface localization of stalled T1SS was characterized. To evaluate the surface distribution pattern the parental *E. coli* strain UTI89 was utilized. In UTI89 the HlyA T1SS is under endogenous expression control and was investigated while arrested with a GFP-HlyA fusion protein. Regardless of overexpression in BL21(DE3) or endogenous expression in UTI89 no distinct localization on the cell surface was observable for the HlyA T1SS. Additionally, the stalled complex was utilized to determine also the amount of active HlyA T1SS in UTI89. During endogenous expression approximately 800 active HlyA T1SS were quantified compared to approximately 5000 T1SS while overexpressed in BL21(DE3). Further, the influence of TolC arrestment through the HlyA T1SS was investigated. The number of TolC trimer was quantified during expression of the HlyA T1SS at endogenous, overexpressed levels and its absence. TolC levels showed no significant influence with approximately 5000 trimers regardless of portion of occupation. Last, the topic of possible purification of the stalled HlyA T1SS was investigated. Showing that obtaining membranes and solubilizing the stalled complex is possible but during purification, the integrity of the complex was compromised. Introduction of crosslinker resulted in a multitude of crosslink products leading to suggestions for novel approaches to purify the T1SS.

1 Introduction

1.1. Lipids, building blocks of biological membranes

Lipids are the fundament of all biological membranes. Insoluble in water while soluble in apolar organic solvents and fat. Membranes capsulate the cytosol and the inner content of organelles of the cell to enable it to control metabolic homeostasis [1]. With the exception of archaea, the double layer lipid membranes are mainly composed of phospholipids, small molecules, which have glycerol as the main building block. A phosphatidyl ester at position C3 provides hydrophilic properties, while two fatty acids chains at positions C1 and C2 provide a hydrophobic character. Fatty acids would form a spherical micelle to minimize the hydrophobic interactions with surrounding water. The phospholipid owns a hydrophilic head group while maintaining a hydrophobic tail. Therefore, the lipid bilayer creates an energetic favorable barrier for molecules inside and outside the bilayer by facing the hydrophilic part on the outside while sandwiching the hydrophobic part [1]. Phospholipid tails are often partially unsaturated which leads to a kink in the carbon chain. The rigid double bound allows a more loose arrangement of the bilayer regulating its fluidity [2]. The overall structure of the major components of the *Escherichia coli* bilayer phosphatidylethanolamine (PE) phosphatidylglycerol (PG) and cardiolipin (CL) [3] [4] are shown in Figure 1.

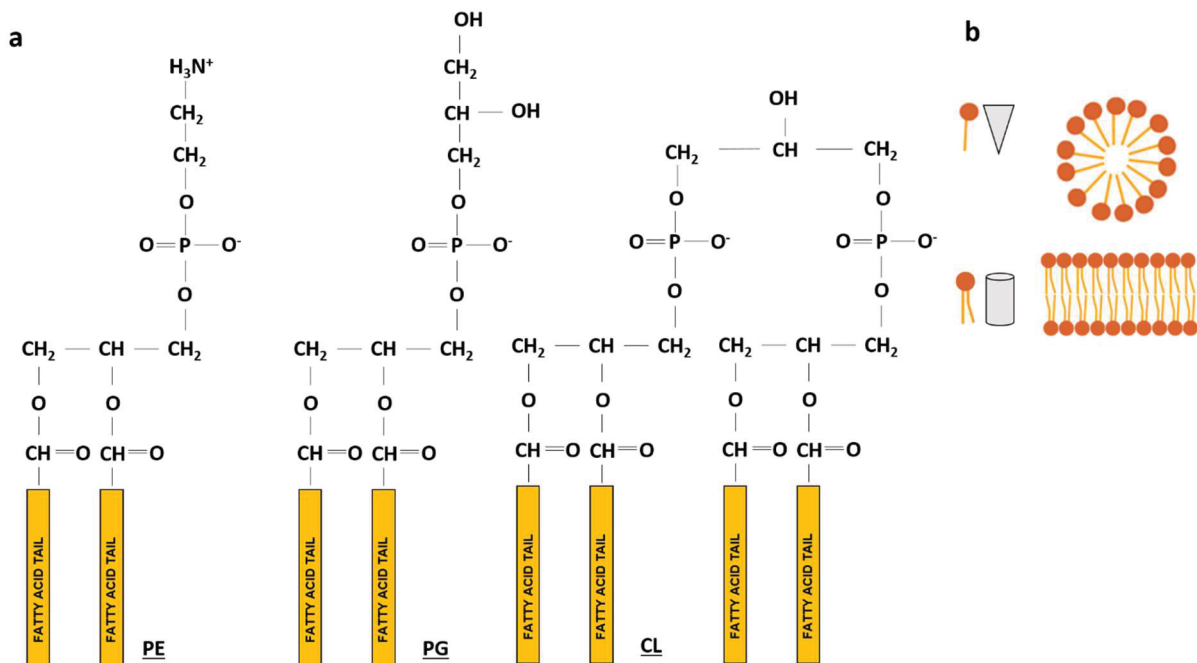


Figure 1 **Phospholipids and the bilayer.** a) Major contributors of the *Escherichia coli* membrane PE, PG and CL. Fatty acid chains are indicated by the dark yellow with the chain length's normally varying between 14 and 19 carbon atoms in *E.coli* [4]. b) Detergents and fatty acids are forming a micelle while phospholipids favorably arrange as a bilayers except pure PE, which will form hexagonal cubic phases [5].

1.2. Gram-negative bacteria and the transport across membranes mediated by proteins in general



Figure 2 Medical illustration of carbapenem-resistant Enterobacteriaceae. A figurative illustration of a Gram-negative carbapenem-resistant bacteria from the CDC-Website for public domain. 2019.09.11[6]

The lipid bilayer forms an energetic barrier, which has to be overcome to provide the cell with nutrition and enable interaction with the environment. Gram-negative (Gram, 1884) bacteria as illustrated for *E. coli* in Figure 1, developed a series of macromolecular nanomachines providing mechanisms to permeabilize the membrane to deliver a broad range of substrates ranging from DNA, small molecules to proteins [7, 8]. While Gram-positive bacteria only have one membrane, Gram-negative possess two membranes. The inner membrane (IM) and the outer membrane (OM) with the periplasm in between. In the periplasm, a peptidoglycan layer is present. The peptidoglycan is built from repeating “*N*-acetylglucosamine (NAG)-*N*-acetylmuramic disaccharide (NAM) [NAG-(β -1,4)-NAM] units having a pentapeptide attached to the d-lactyl moiety of each NAM” [9]., which creates the sacculi providing mechanic stability of the cell [10].

A typical Gram-negative bacterial membrane has a thickness of 40 Å for each, the IM and OM bilayer [11, 12]. In between the peptidoglycan is present in a single layer with a thickness of 25 Å and up to three layers (approximately 70 Å) forming the so-called sacculi [12]. Overall, this periplasm has a diameter 100 to 250 Å [13]. In combination with the IM and OM the distance spanned from the cytosol to the extracellular space is 180 to 330 Å.

Membranes are impermeable for charged molecules respectively ions and less permeable for hydrophilic molecules [14, 15]. To overcome the energetic barrier represented through the bilayer, bacteria developed highly regulated transport mechanisms. Embedding membrane proteins enables the transport of essential molecules for the cell. Metal ions, sugars and peptides

can be transported in and out of the cell by the use of concentration gradients. The usage of gradients as a driving force is called passive transport often observed in membrane spanning channels [16]. The active transport against a concentration gradient requires additional energy to enable the increase of concentration by hydrolysis of energy rich molecules such as ATP [16] or the capture of photons [17]. This mechanism is known as primary transport, while secondary transport is defined as the coupling of transport to an existing gradient to obtain the needed energy. In other words, a substrate is transported against the concentration gradient while a second substrate is transported in line with the gradient to provide the energy needed for transport against the incline in concentration [18]. Known as symporter (import of both substrates into the cell) or antiporter (import against the gradient while exporting with the gradient) [19, 20].

The transport of substrates outside of the cell is referred as secretion. Besides molecules such as ions and sugars, also peptides or even complex proteins can be transported outside of the cell. The secreted substrates can be released in the extracellular space, injected into a target cell or its remains associated with the OM of the bacteria [8, 21]. The machineries can be classified in two subgroups. The single-membrane-spanning secretion systems of the OM / IM, and the double-membrane-spanning secretion systems.

1.3. The inner membrane secretion system

There are two major secretion systems in the inner membrane (IM) of Gram-negative bacteria. The first one is the Sec translocation machinery. The majority of the secretion across the inner membrane is accomplished by this system [22]. During translation of the target protein an N-terminal signal sequence emerges from the ribosome and signal recognition particle (SRP) competes with trigger factor (TF) for binding on the nascent chain [22-24]. A target sequence interact with hydrophobic transmembrane segments (TMSs) [25]. This temporally slows down the translation of the protein on the ribosome and allows the proper interaction of the SRP with the membrane receptor FtsY to transfer the translocation through the SecYEG complex a process that is known as co-translational secretion [22, 26, 27]. Post-translational secretion is initialized through the TF binding, which is not slowing down the translational speed, rather the binding of SecB is mediated and keeps the protein in an unfolded conformation. Subsequently, SecA starts the translocation across the inner membrane (Figure 3) [22, 28, 29].

The twin-arginine translocation (Tat) machinery is in contrast to the Sec machinery able to secret completely folded protein. The Tat system is not used as frequently as the Sec translocon [31], but its property of secreting folded proteins is an important feature for key processes like respiratory energy metabolism, virulence, cell division, iron and phosphate acquisition [32-36]. Some proteins need proper folding to bind cofactors. This results from the fact that some cofactors are only present in the cytosol, or specific ions could compete with undesired ions when not controlled in their environment [32], and additionally oligomerization can be performed in the cytosol before secretion, when needed [37] (Figure 4).

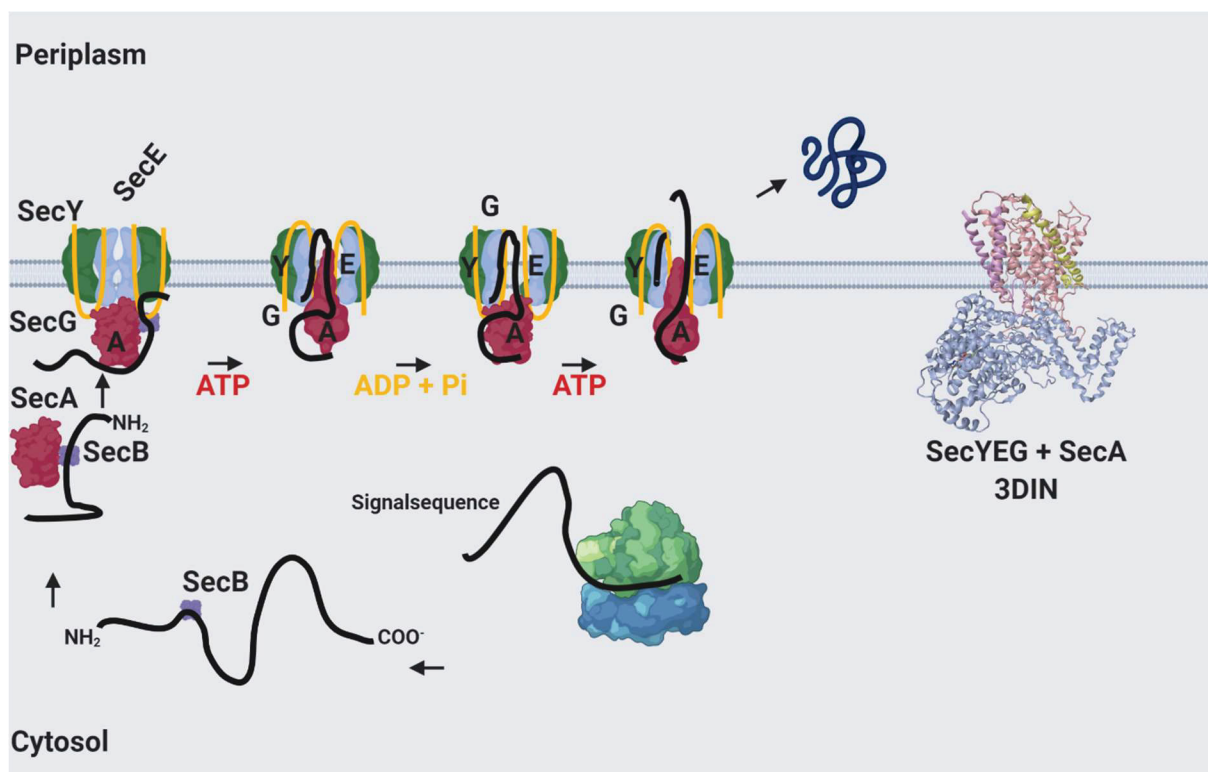


Figure 3 Scheme of the TF path for Sec translocation (post translational secretion). The nascent chain is recognized through the signal peptide and SecB can bind the unfolded protein to prevent aggregation. The precursor protein SecB-complex is recognized by SecA and mediates the binding to the SecYEG translocation complex. The initiation step requires ATP but not its hydrolysis. Continued translocation requires cycles of ATP hydrolysis. The translocation is occurring in a step-wise fashion with a steps of 20–30 amino acid residues and is the released in the periplasm. Figure based on [30]

Another reason for prefolding was observed within archaea. There the folded protein was secreted across the membrane by the Tat system to prevent the aggregation through high extracellular salt concentrations [40]. The Tat translocation machinery is targeted through signal peptides that contain a conserved N-terminal twin-arginine motif ((S/T)RRXFLK)[41]. The signal is cleaved during the translocation. In Gram-negative bacteria the Tat-system is built by the three subunits TatA, TatB and TatC [39]. While TatB and TatC interact with the secretion signal they recruit TatA to form the Tat-complex[42]. The proton motif force powers this translocation across the membrane-spanning channel build by the Tat-complex [43]. For translocation across the outer membrane a translocation machinery has to be utilized. The outer membrane secretion systems are used for this purpose. Together with the Sec and Tat system they are forming a secretion pathway thru the periplasm into the extracellular space. Some of the common outer membrane secretion systems are described in the chapter 1.5.

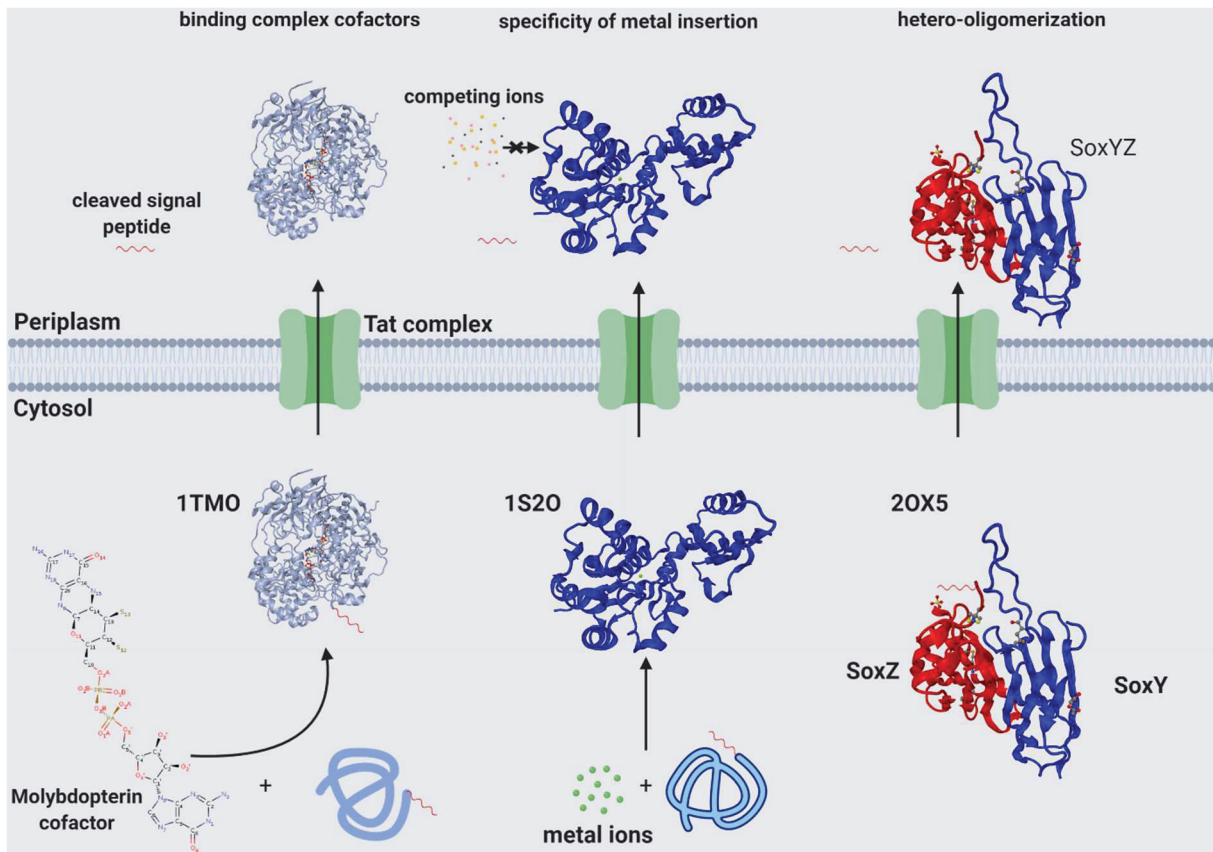


Figure 4 Scheme of the different Tat mediated translocations which have been identified. The first possibility is the acquisition of their cofactor prior to transport across the cytoplasmic membrane. Only certain cofactors are associated with Tat-mediated transport. These can be broadly divided into metal-sulphur clusters and cofactors containing a nucleotide moiety. Metal ions compete for binding sites in proteins. The second case of Tat mediated secretion is the possibility to obtain metal ions under controlled conditions in the cytoplasm. [38]. The third known use of the Tat pathway allows hetero-oligomeric complexes to form in the cytoplasm and then be transported by a signal peptide in just one of the constituent subunits. Figure based on [39]

1.4. The Gram-negative membrane spanning secretion systems

As described above, there are two classes of membrane spanning secretion systems. In contrast to the single spanning secretion systems, Gram-negative bacteria developed systems, which are able to span both membranes. Five double-membrane-spanning secretions systems are identified and classified as type I secretion system (T1SS), T2SS, T3SS, T4SS, T6SS. A selection of some secretion systems is shown in Figure 5. The outer membrane transporters like T5SS, Chaperone-usher pathway and Curli biogenesis system are later subject of discussion in chapter 1.5.

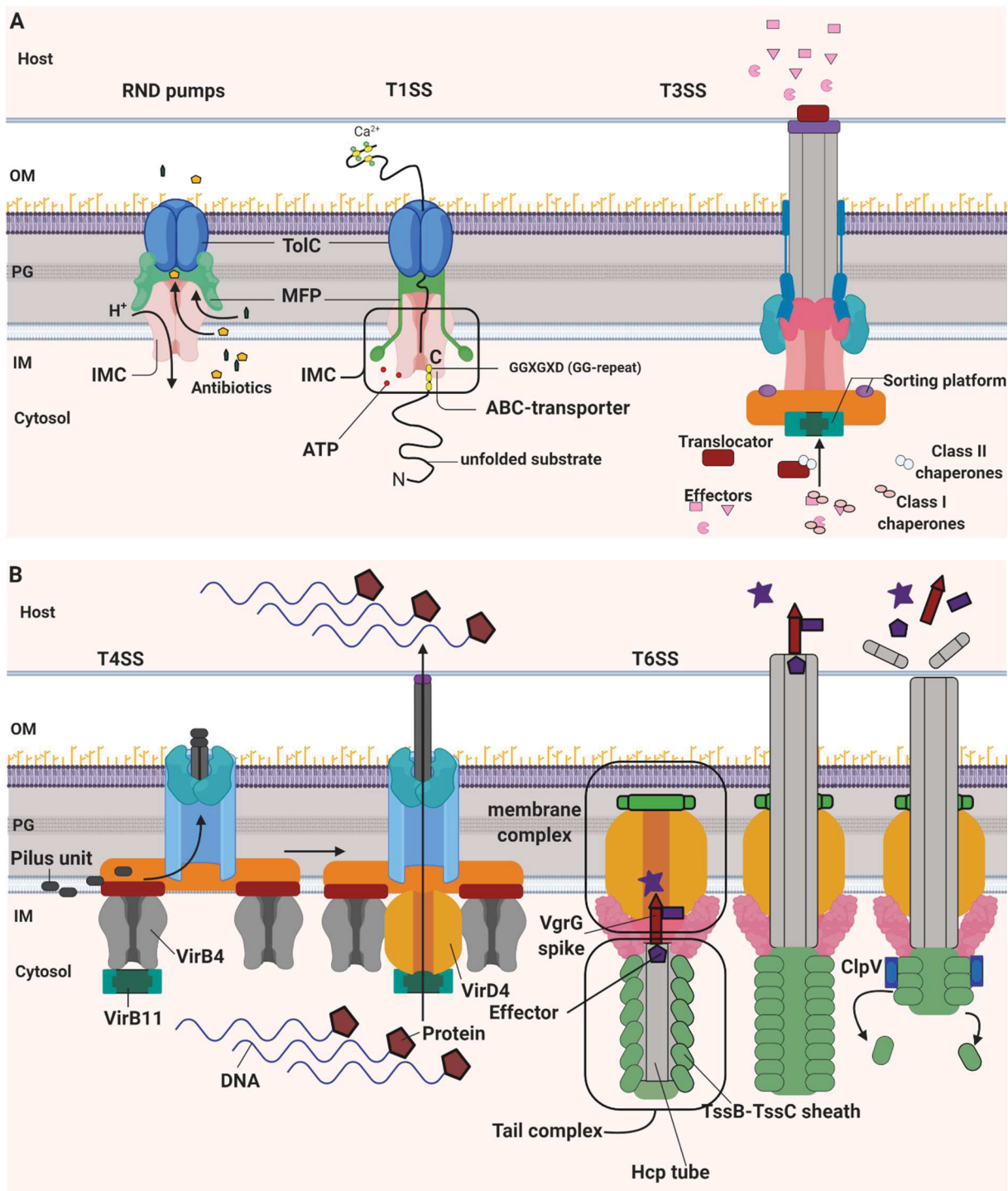


Figure 5 Scheme of the different double-membrane spanning secretion systems. (A) From left to right. Resistance–nodulation–division (RND) pumps are able to secrete a broad range of different substrates in particular small hydrophobic substances. Type I secretion systems (T1SSs) secrete an unfolded substrate across both membranes in a single step (except for some bacteriocins and adhesins which own a cleavable N-terminal secretion signal [44]). The correct folding is induced by Ca²⁺ binding in the extracellular space. The secretion systems T3SS (B) T4SS and T6SS are directly targeting a host cell across a third membrane. These sophisticated machineries are used to directly inject proteins, DNA or effector molecules into the targeted cell to manipulate or infect it. Figure based on [8]

1.5. Resistance-nodulation-division (RND) and T1SS

In regards to the architectural composition the T1SS is closely related to RND systems. The RND acts like a tripartite system, and is divided in different subfamilies. Their classification is derived from their transported substrates. They transport small exogenous molecules, which mostly possess antibacterial properties. This transport contributes to antibiotic resistance [45-47].

The T1SS can secrete a multitude of different substrates into the extracellular space. From small bacteriocins such as ColV [48] to iron scavenging proteins such as HasA [49], pore forming toxins such as HlyA [50], to giant adhesins, which have a molecular weight of up to 1.5 MDa [51].

Both tripartite systems are built in a similar fashion. Both contain an inner membrane protein (IM), an adaptor or the membrane fusion protein (MFP) and as third component an outer membrane protein (OMP), for example TolC [52] which is used as a protein channel to the extracellular space. The three components are forming a membrane spanning secretion machinery with a length of approximately 320 Å [53-55]. While RND pumps are using the proton gradient across the IM to generate the energy for the transport across the membranes [56] the T1SS is using an ATP-binding cassette transporter (ABC transporter) that hydrolyzes ATP to provide the necessary energy for the secretion process. The ABC transporters of T1SS are subdivided in three groups. Two groups possess an N-terminal extension, which is involved in substrate recognition and threading of the substrate into the translocator [50, 57, 58]. This 'appendix' is called C39 peptidase (C39) or C39 peptidase-like domain (CLD), however misses in the third group. While the ABC-transporter containing a C39 domain has a proteolytic activity during translocation and cleaves the secretion signal of the substrate, the CLD has no proteolytic activity. Regardless of activity, this domain is crucial for secretion. When the C39 / CLD is deleted, secretion is abolished [50, 59]. T1SS substrates share the repeat in toxin (RTX) motif (GGXGXDXUX, where X can be any amino acid and U is a large, hydrophobic amino acid). which is also called glycine-rich region (GG-repeat), and is important for substrate recognition in the cytosol and correct folding in the extracellular space [60, 61]. The ABC-transporter is colocalized with the MFP in the inner membrane forming the inner membrane complex (IMC) [62, 63]. The presence of the substrate triggers the assembly of the secretion machinery through substrate recognition and recruitment of the outer membrane protein. The fully assembled secretion machinery can then secrete the substrate into the extracellular space [64, 65].

1.6. Type II Secretion System (T2SS)

T2SS, also known as general secretion pathway (Gsp) in enterotoxigenic *E. coli*, is found in a wide variety of Gram-negative bacteria [66] and secretes folded proteins from the periplasm into the extracellular space [66]. The secreted substrates can vary in function ranging from proteases to phosphatases, lipases [67], virulence factors and toxins such as the cholera toxin from *Vibrio cholera* [68]. The Gsp is composed of 12 – 15 components. In the inner membrane the Gsp forms a IM platform spanning through the membrane together with a cytoplasmic ATPase [67], an OM complex and in the periplasm a pseudopilus to connect the different parts and creating a translocation path [69]. In the OM complex GspD forms a dodecamer also called T2SS

secretin. This GspD is a homologue of T3SS and T4SS pilus-like structures, which displays some relations to the genetic origins [70]. The interaction during the assembly of cytoplasmic ATPase, IM platform and OM complex forms the translocation machinery with a cylindrical shaped structure of 155 Å outer diameter and a length of 200 Å [71]. The substrate for extrusion are transported through the Sec or Tat translocon in a folded or unfolded state across the IM before the secretion is established by the T2SS [66]. The substrate itself is then pushed by the pseudopili out of the translocation pore. The energization of this process is obtained from ATPase hydrolysis in the cytosol and the resulting coupling between GspE and GspG through GspL [72]. While physically moving the substrate through the pore the pili itself is not reaching the extracellular space [71].

1.7. Type III Secretion System (T3SS)

Like the T1SS, the T3SS is a secretion system, which spans both membranes. However and in contrast to the T1SS, the T3SS as the T4 and T6SS (see following chapters) is targeting directly the cell membrane of the host cell inserting effector proteins to modulate the function of the target cell [8, 73, 74]. Found in enteropathogenic *Escherichia coli* (EPEC), *Salmonella*, *Shigella*, *Yersinia* and *Pseudomonas* this secretion machinery is present in a variety of pathogens [75]. An example for the T3SS is the Typhimurium SPI-1 (Salmonella pathogenicity island 1) as a T3SS archetype. It is a 3.5 MDa multi protein complex that forms a ‘syringe like’ structure out of approximately 25 proteins and is organized into two subunits. A double membrane spanning ring and a needle like filament through which injection of effector proteins into the target cell occurs [76-80]. Recently it was shown via cryo electron microscopy (cryo-EM) that the multimeric state of the OM protein InvG of SPI-1 T3SS follows not a 1:1 stoichiometry, rather a 15:16 imbalance (InvG^{secretin} to InvG^{NON1}) [81] was determined. While the inner ring is localized in the IM, the outer ring is inserted in the OM. Together they hold the needle-like filament with a length of 30 - 70 nm and 10 – 13 nm diameter [78]. A tube like structure surrounds the filament and the outer diameter was determined to approximately 80 Å while the internal lumen of the tube is circa 25 Å [82]. Cryo-EM made it possible to obtain snapshots of the secretion process. Secretion through this ‘syringe’ occurs in an unfolded state which indicates that the activation of the effector proteins is induced through secretion [83]. The substrate is recognized by the first 100 amino acids and controlled in a hierarchical and coordinated manner [74, 84]. Chaperones are keeping the substrate stable for secretion, while secretion itself is energized through the T3SS ATPase.

1.8. Type IV Secretion System (T4SS)

T4SS is the most ubiquitous secretion system. It can be found in Gram-negative, Gram-positive bacteria and in some archaea. Furthermore, it has the special feature that it not only can secrete proteins, it also is able to transfer DNA into the targeted cell and to mediate conjugation of plasmid DNA [85-87]. One of the best-studied T4SS is the VirB/D4 system of *Agrobacterium tumefaciens* which serves as a paradigm for T4SS. The VirB/D4 system is built out of 12 different proteins and while the translocation apparatus is built of six proteins, there are three proteins forming the ATPase complex that energizes the translocation process. Two proteins are forming the extracellular pilus, which is the injector for the protein / DNA mixture. The last

protein is located in the periplasm and forms cavities into the peptidoglycan by degradation to allow insertion of the secretion apparatus [88, 89]. The translocator complex is formed out of two sub-structures, the bipartite IM complex and the core-OM complex, respectively, connected by a pore [90-92]. The VirB10 protein is the only building block of the T4SS, which spans the entire cell envelope. Therefore, it interacts with different proteins in the IM and OM of the translocation machinery [93]. Also VirB10 acts as an ATPase sensible relay which can induce conformational changes to gate the OM channel [93]. Studies of VirB11 and its properties of modulation of the secretion of the T4SS suggested that it could switch between two modes. One mode reflects pilus biogenesis, while the other corresponds to a substrate-translocation mode [93, 94]. While it was not possible to obtain a structure of the entire T4SS, recently the structure of the complete IMC of *Helicobacter pylori* was published [95]. The VirB-like proteins showed for VirB4-like a hexamer of dimers at the channel entrance, together with a hexamer of VirB11-like, docked at the base of the VirB4-like protein [95]. For the T4SS in *A. tumefaciens* a study of the pili revealed that while the pili itself is formed of the VirB2 pilin polymer, the VirB5 protein forms the tip and is mediating cell-to-cell adhesion [96].

1.9. Type VI Secretion System (T6SS)

The T6SS was identified in 2006 [97]. Studies showed that the T4SS and T6SS have a common genetic origin in resemblance to bacteriophage tails [98-100]. The T6SS can secrete effector proteins into eukaryotic and prokaryotic cells. It is widely distributed among Protobacteria [101] and essential for pathogenesis and bacterial competition [100, 102]. The T6SS also shows importance in metal ion uptake (iron [103], manganese [104] and zinc [105]) and cell-to-cell communication [106]. The translocation machinery consists of at least 13 proteins called core-components [101, 107] and the IM complex is homologous to T4SS [97, 108]. The T6SS uses a contractile bacteriophage tail in a tail sheath located in an inner tube anchored to a baseplate in the IM [98]. On top of the tubular structure a spike-like protein functions as a nucleation platform for the tube formation [98, 107]. This formation allows a phage-like secretion mechanism to inject the effector proteins upon contact formation into the targeted cell [100, 102, 109]. The secretion cycle can be subdivided in three steps: assembly, contraction and disassembly. The anchored IM complex forms and begins with elongation of a cytoplasmic tubular structure mantled in a sheet like protein. Up on contact to the targeted cell the tube (Hcp tube) is ejected by contracting the sheet like proteins and propelling the tube toward the extracellular space. The contracted sheets are disassembled and can be used for another assembly [100]. As mentioned, the T6SS is also used for cell-to-cell communication. This interaction between sister cells is so essential that parts (shaft or tip) of the T6SS can be exchanged for re-usage or accumulation of T6SS to enhance pathogeny of single sister cells [110].

1.10. The outer membrane secretion systems

Besides the double membrane spanning system, Gram-negative bacteria developed mechanisms to secrete substrates also from the periplasm to the extracellular space. The T5SS, Chaperone-usheer pathway and Curli biogenesis system are localized in the OM and dependent on the SecYEG to transport the substrate from the cytosol into the periplasm. They use the Sec or Tat system for the protein extrusion. An schematic overview is provided in Figure 6.

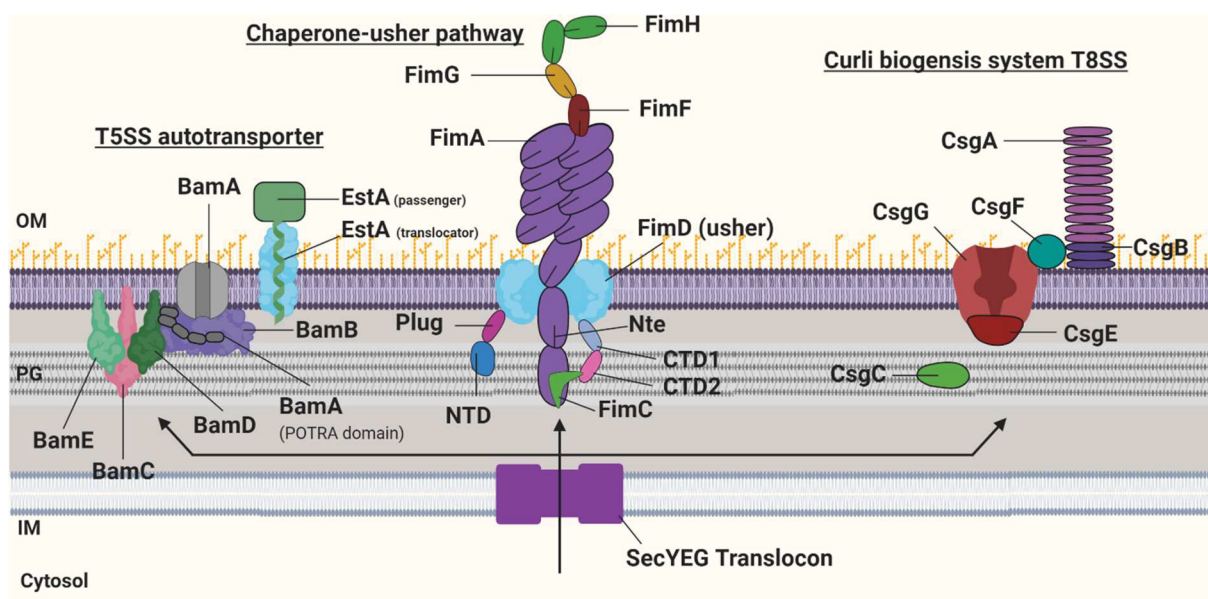


Figure 6. Outer membrane secretion systems. On the left the type V secretion system. T5SS autotransporter (type Va) carboxy-terminal domain (CTD) (the EstA translocator) is inserted into the outer membrane (OM) as a β -barrel, whereas the amino-terminal domain (NTD) of the protein (the EstA passenger) is exposed to the extracellular space after translocation through the β -barrel. The Bam complex (BamA–BamB–BamC–BamD–BamE) is involved in the insertion of the EstA translocator domain into the OM and is also possibly involved in secretion of the EstA passenger domain [111-115]. Shown in the middle is the chaperone–usher pathway. A type I pilus is shown, with the subunits FimH, FimG and FimF forming the tip (known as the fibrillum), and ~1,000 FimA subunits forming a thick rod. The usher (which is composed of FimD) contains a pore, plug, NTD, CTD1 and CTD2. The penultimate FimA subunit traverses the pore, whereas the final FimA subunit is on the periplasmic side of the pore and is still bound to the FimC chaperone [116-118]. The right side displays the curli biogenesis system. The secretion channel in the OM is composed of the protein CsgG and is capped on the periplasmic side by the protein CsgE. The minor curli subunit CsgB anchors the major curli subunit CsgA to the OM and nucleates its polymerization. The secretion process is mediated by the two accessory proteins CsgF and CsgC [119-122]. The Figure is based on [8].

1.11. The Type V Secretion System T5SS

T5SS is an important translocation machinery for virulence factors, cell-to-cell adhesion and biofilm formation [8, 112]. It is localized in the outer membrane and requires the SecYEG translocon to transport the unfolded substrate into the periplasm. The T5SS can be divided in five subclasses, Va to Ve. As described here the autotransporter-secretion system Va, a two-partner secretion Vb, trimeric autotransporter Vc, fused two-partner secretion Vd and inverted autotransporter-secretion Ve [112]. The T5SS is also called autotransporter system, which is derived from the fact that the substrate is able to form a translocation pore in the OM. The pore sequence is fused to the transported substrate in a single polypeptide chain [112, 123]. Thus, the substrate possesses two distinct domains, the secretion domain called ‘passenger’ domain is semi-folded or unfolded in the periplasm and the transmembrane domain, which is also called ‘translocator’ or ‘ β -domain’ [123]. The translocator domain enters the OM to form a β -barrel pore to enable the secretion of the passenger domain. For this process, no ATP hydrolysis or proton gradient is needed. The energy is gained from folding of the passenger domain and the pore [124]. It was shown that the passenger domain is secreted in a C-terminal direction through the β -barrel pore (width approximately 10Å) [124-126]. Some studies showed that for larger

proteins the β -barrel assembly machinery (Bam) supports the T5SS during translocation [111, 113-115]. Structural evidence suggests that during the transport the passenger domains forms a hairpin loop which fold to a β -helix after translocation through the pore. The folding energizes the continuous threading of the passenger domain. When completely transported, the linker between passenger domain and translocator domain forms an α -helix that traverses the β -barrel pore. When complete the protein can be released into the extracellular space by cleavage or remains anchored by the β -barrel in the OM (e.g. for adhesins) [127-129].

1.12. The Chaperone-usher pathway

The chaperone-usher secretion pathway is used to secrete and assemble pili or fimbriae on the bacterial cell surface. These helical rod-like structures can grow up to two μm in length, consisting out of hundreds of pili subunits [116, 118]. The pili and fimbriae showing importance for uropathogenic bacteria while infecting the urinary tract [130] and biofilm formation [131] by mediating host cell recognition [130]. The Type I and P are the best-characterized pili, assembled through chaperone-usher build. To assemble the pili, unfolded subunits are secreted into the periplasm via SecYEG and stabilized there by chaperones [132, 133]. The 'usher' mediates the elongation of the pili. An elongation complex is formed [117] and the single building blocks of the pili are organized through the secretion of the usher pore, where the chaperones establish proper polymerization of the nascent pili. This 'zip-in zip-out' mechanism [134] elongates the pili until the termination subunit binds [135].

1.13. Curli Amyloid biogenesis system or Type VIII Secretion System (T8SS)

Curli are fiber-like structures located on the cell surface of Gram-negative bacteria. Encoded on Curli-specific genes (*csg*) [136-138]. The curli amyloid fibers are important for biofilm formation, host colonization and cell invasion [139-141]. The Csg proteins are transported via SecYEG into the periplasm [119, 122] and kept unfolded by CsgC, a chaperone to prevent fiber formation in the periplasm [119]. The components for self-assembly are stored in the periplasm until a nucleation concentration is reached which also led to the alternative name nucleation-precipitation pathway [138, 142, 143]. It has been assumed that to energize the transport an entropy driven gradient across the membrane is used to transport the *csg* components through the translocation pore CsgG [120, 121]. This would allow the peptide chain to slide via Brownian diffusion into the extracellular space where the nucleation leads to the assembly of 2- to 5-nm -thick, coiled fibers and obtain there the amyloid fold [8, 144-147].

1.14. The hemolysin A (HlyA) T1SS

A prime example for T1SS is the hemolysin A (HlyA) secretion system from *Escherichia coli* (*E. coli*). It is found in most uropathogenic *E. coli* (UPEC) strains and was discovered in the 1980s [64, 148]. The hemolysin secretion system consists of three components and the substrate HlyA. Hemolysin B (HlyB) serves as the ABC transporter, while hemolysin D (HlyD) is the membrane fusion protein (MFP). TolC is recruited as (OMP) outer membrane protein to the complex. Together they form a translocation pore that enables HlyA to be transported across both membranes in a single step without any periplasmic intermediate [149, 150].

1.15. ABC-transporter Hemolysin B (HlyB)

ABC-transporter are ATP dependent primary transporters, they are able to transport a broad range of substrates and can be found in all kingdoms of life: prokaryotes, archaea and eukaryotes [151, 152]. In general, an ABC-transporter consists of four subunits or domains, two transmembrane domains (TMD) and two nucleotide binding domains (NBD). In eukaryotic organisms, the transporter is translated as a single polypeptide, a so-called full-size transporter. In fewer cases, eukaryotes also possess so-called half-size transporters. The name derives from the fact that two units of the ABC-transporter are forming one functional unit. Nevertheless, half-size transporters are more common in prokaryotic organisms [153]. The TMD forms a translocation pathway through the membrane while the NBD is responsible for providing the needed energy for conformational changes and transport of the substrate. To provide this functionality ABC-transporters have highly conserved motifs. The NBD binds ATP coordinated via Mg^{2+} between the Walker A and Walker B motifs [154] and hydrolyzes it to ADP. Every NBD contains six conserved motifs: Walker A, Walker B, Q-loop, A-loop, H-loop and D-loop [155]. The conserved consensus sequence for Walker A is GXXGXXGK (S/T) where X represents any aa. The Walker B motif shows a more restricted sequence $\phi\phi\phi\phi$ DE where ϕ stands for any hydrophobic aa. The sequence motive for ABC-transporters is LSGGQ [156]. The NBD forms a molecular sandwich where the motifs interact thru different interfaces to enable the protein-ATP, Mg^{2+} interaction. While Walker A is coordinating the the α,β,γ -phosphate of ATP (Walker B only γ - phosphate) the second monomer of the NBD faces the γ -phosphate with a α -helical subdomain which is containing the C-loop and coordinates there the γ -phosphate ribose and adenine of ATP [157].

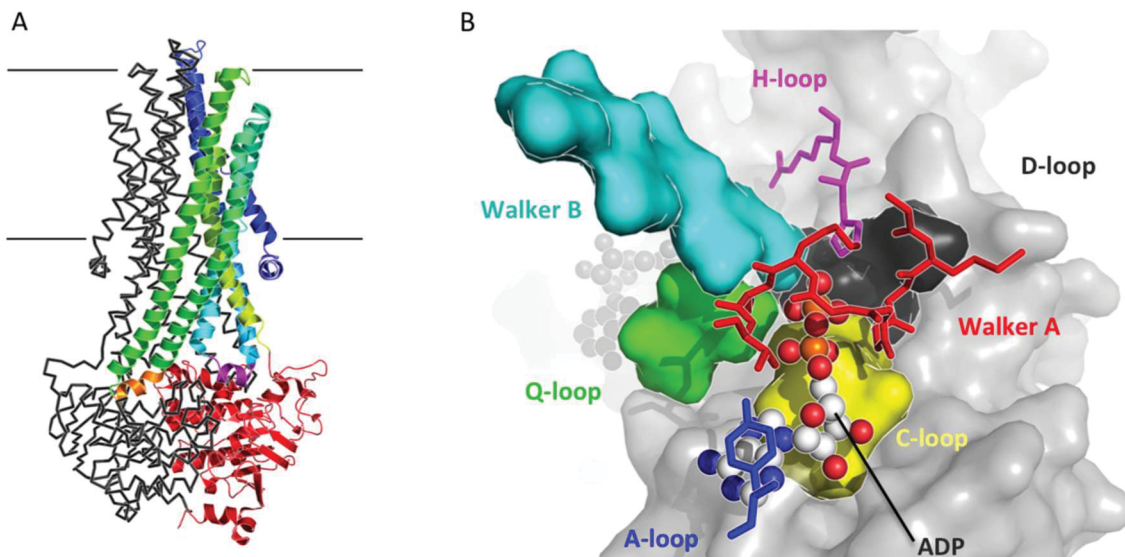


Figure 7. **Structure of Sav1866 from *Staphylococcus aureus* with bound ADP (pdb entry 2HYD).** One of the two monomers is colored dark gray. The other monomer's TMD is colored blue, cyan, yellow and green, while the corresponding NBD is colored red. Coupling helix 1 (magenta helix) is thought to make contact with the *cis* NBDs during formation of the nucleotide sandwich. Coupling helix 2 (orange helix) is always domain swapped to interact with the *trans* NBD. (B) Close-up view of the gray NBD and the sandwiched ADP molecule. Motifs which are directly involved in ATP binding and hydrolysis are colored as follows: Walker A, red; Q-loop, green; H-loop, purple; Walker B, cyan; A-loop, blue; C-loop, yellow; D-loop, black. Figure is taken and modified from [151]

HlyB is a half-size ABC-transporter of 707 aa in size, forms a dimer as functional unit [157, 158] and represents one part of the IM complex of the T1SS. At the N-terminus a C39-peptidase like (CLD) domain is present, followed by the NBD and TMD of HlyB. It was shown via X-ray crystallography that the NBD (240 aa in size) forms a dimer in the presence of ATP in a head-to-tail organization, while building a ‘nucleotide sandwich’ [157, 159]. Surface Plasmon resonance (SRP) revealed that HlyB-NBD interacts with the 50 C-terminal aa of HlyA. This interaction was essential for the correct threading into the translocation pore [160]. The binding and hydrolysis of ATP is suggested to enable conformational changes and energization of the transport across both membranes [151]. However, binding of ATP alone is not enough to enable secretion [52].

The TMD (282 aa) is suggested to contain six transmembrane helices. This agrees with the structure of ABC-transporters and the HlyB analogue (without CLD) AaPrtD from *Aquifex aeolicus* [161, 162]. The TMDs are located antiparallel through the entire IM and connected via loops in the cytosol and periplasm. Interaction studies suggested a fine tuned regulation via interaction of the substrate HlyA directly with TMD and the NBD of HlyB [163]. One hypothesis for these interactions could be that through a coupling helix in the NBD information approximately conformational changes and substrate presence is transmitted into the periplasm to regulate further interactions with the other T1SS components.

The CLD owes its name from the high homology to the C39-peptidase (42%). It is a degenerated cysteine peptidase from the papain superfamily, 123 aa in size and located at the N-terminal part of HlyB. The structure was obtained by NMR spectroscopy and showed that the catalytic triade is not only degenerated but also inactive through a π - π stacking of histidine with a tryptophan [164]. Pulldown assays showed that the CLD interact only with unfolded HlyA and that the interaction can be disrupted by inducing the folding of HlyA by increasing *in vitro* the Ca^{2+} concentration [57]. Because this interaction with unfolded HlyA is essential for secretion it was proposed that the CLD functions to some degree as a chaperone by preventing the aggregation of HlyA during the secretion [165]. The crucial role of the CLD is underlined by the result that with truncation of the CLD the secretion is abolished [50, 57].

1.16. Hemolysin A (HlyA).

Hemolysin A the substrate of the HlyA T1SS is named after its ability to lyse erythrocytes and leukocytes [166, 167]. HlyA is 110 kDa (1024 aa) in size and belongs to the family of repeat in toxins (RTX) proteins [168]. These nonapeptide repeats have the consensus sequence (GGXGXDXUX, where X can be any amino acid and U is a large, hydrophobic amino acid), which possess a high affinity for calcium ions [60]. Through the high number of glycine residues they are also referred as glycine rich (GG-)repeats [167]. Binding of Ca^{2+} to the GG-repeats induces the folding of HlyA. The nonapeptides arrange in parallel β rolls where Ca^{2+} is located in the turn between adjacent β rolls. Calcium ion is buried and periodically coordinated by carboxyl side groups of the aspartic acids and the carbonyl groups of the polypeptide backbone [169]. An X-ray structure of a folded GG-repeat of the CyaA toxin from *Bordetella pertussis* is shown in Figure 7.

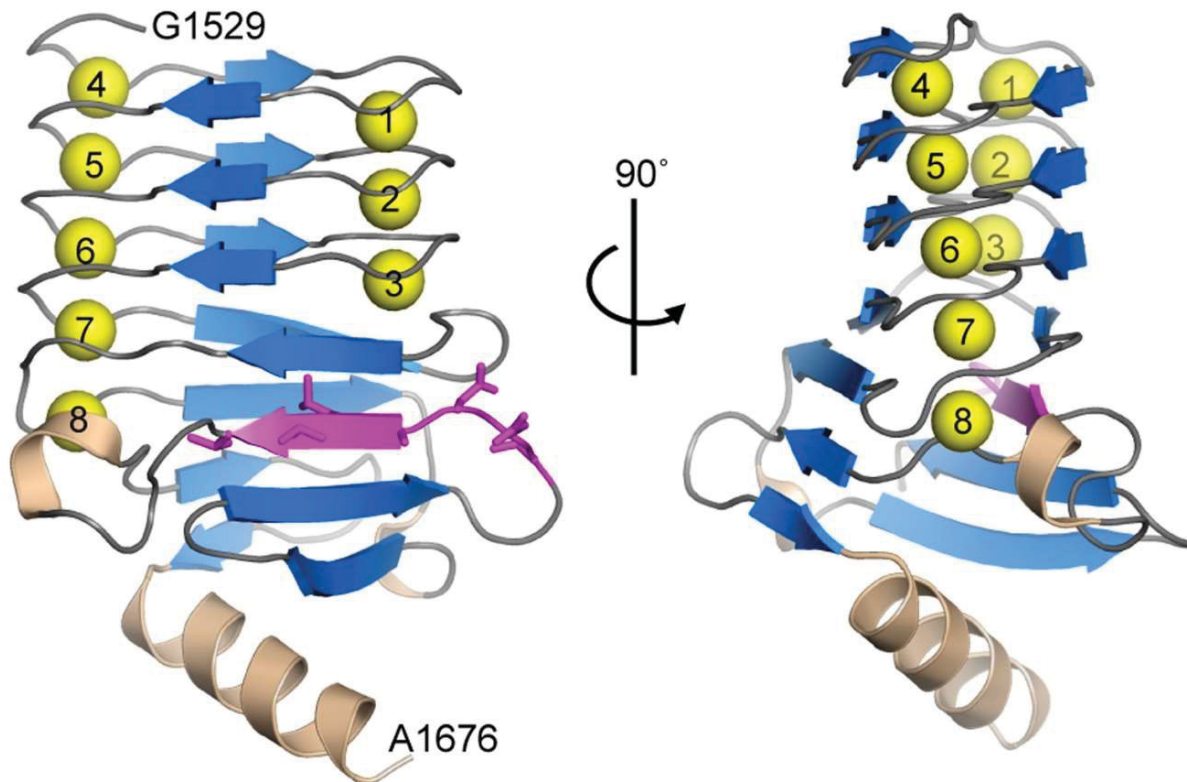


Figure 8. X-ray structure of a folded GG-repeat in *CyaA*. The N-terminal consecutive nonapeptide tandem repeats (GGxGxDxxx) are arranged in a regular right-handed helix of parallel β strands (β -roll). The first six residues of the RTX motif (GGxGxD) constitute a turn with bound calcium ion (yellow ball), while the last three non conserved residues (xxx) form a short β strand. Calcium ions are numbered for clarity, and the residues 1,636–1,642 of the TDDALTV segment involved in initiation of Ca^{2+} -induced folding of the RTX domain are colored in magenta. Taken and modified from [169]

In the peptide sequence of HlyA 13 GG-repeats are present while 6 of them are highly conserved [170]. The Ca^{2+} concentration in *E. coli* is highly regulated and prevents folding of HlyA through the low nM concentration of Ca^{2+} in the cytosol [171, 172]. The maturation of HlyA through correct folding occurs in the extracellular space and is induced by binding Ca^{2+} . On the C-terminus of HlyA the secretion signal is located. It consists of approximately the last 60 aa and is not cleaved during or after secretion. Because of the C-terminal position the whole substrate has to be translated before secretion of the unfolded substrate can occur in a C-terminal direction [173]. The secretion signal consists a cluster of charged residues which are predicted to contain an amphiphilic helix, a largely uncharged tail with predicted structure of turn and β -sheet and an aspartate box, a conserved structure also found in other pathogenic toxins [174]. As mentioned above, the low calcium ion concentration in the cytosol of *E. coli* prevents folding of HlyA; this is combined with the suggested chaperone like function of the IM complex which prevents aggregation in the cytosol [163]. While it was shown that ATP hydrolysis is needed to translocate HlyA across both membranes, the stoichiometry of ATP and HlyA is still unclear. Nevertheless, the secretion rate of the HlyA T1SS was quantified in chapter 3.1 and its dependency on the extracellular Ca^{2+} was investigated. While secreted HlyA in UPEC is hemolytic, the translated HlyA is a non-toxic pre-protein (pro-HlyA) and matures by posttranslational acylation of two lysines, K564 and K690, respectively. The posttranslational acylation is performed by HlyC and the acyl carrier protein acyl-ACP. After acylation in the cytosol and folding in the extracellular

space a pore formation on target cells can be observed [175, 176]. However, the mechanism of pore formation is still unknown, however a two-step mechanism is proposed. While in step one the N-terminal hydrophobic region of HlyA interacts with the target by electrostatic forces, step two follows with an irreversible insertion into the membrane [177, 178]. The pore formation thus leads to target cell turgor increase by Ca^{2+} influx culminating in cell death [179]. The domain organization of HlyA and other variants used in this thesis including fusion proteins is shown in Figure 8.

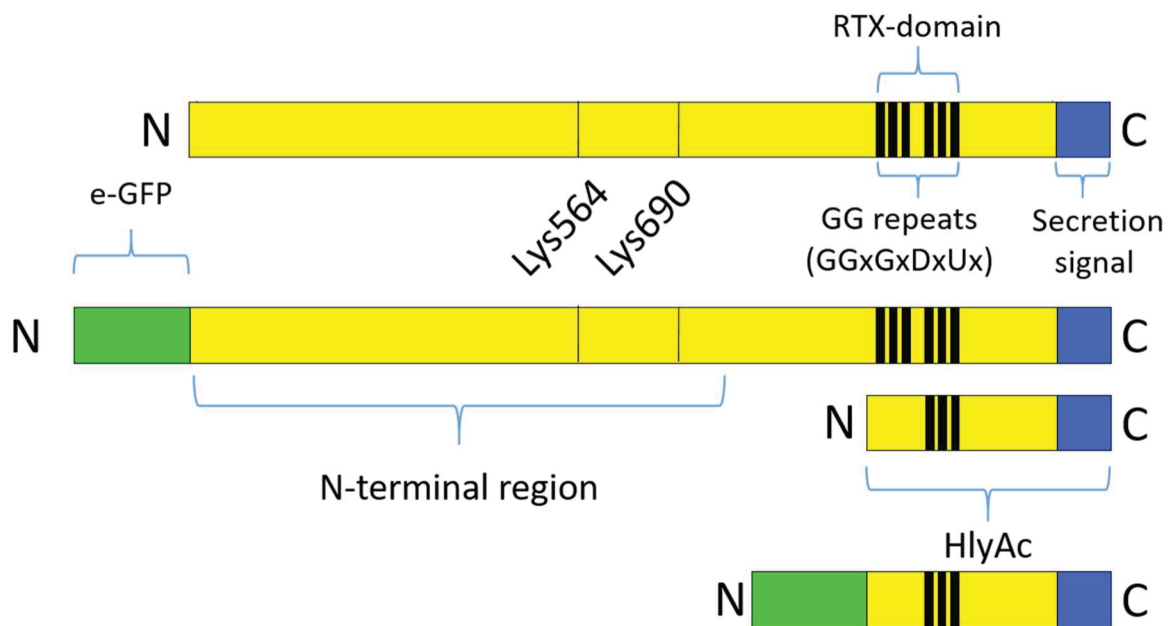


Figure 9. **Domain organization of HlyA, HlyAc and fusion proteins used in the experiments.** Yellow indicates the N-terminal region containing the membrane insertion domain of the toxin. The blue box the C-terminal secretion signal consisting of 50-60 aa. Black boxes represent conserved RTX-domain also called GG-repeats with the conserved consensus sequence GGXGXGUX. The marked aa represent the position for fatty acid acylation via HlyC. Green indicates the N-terminal eGFP in fusion proteins used in for stalling the T1SS.

1.17. The membrane fusion protein (MFP) Hemolysin D (HlyD)

HlyD is the membrane fusion protein of the IM complex from the HlyA T1SS. It is 478 aa in size and can be subdivided in three parts. One segment is the 59 aa cytosolic domain which ranging from residue 1 to 59 is predicted to form an amphipathic helix of charged residues. When deleted the colocalization of HlyD and HlyB is still present, but TolC cannot be recruited [65]. Since TolC is only recruited in the presence of the substrate, it is believed that the cytosolic interaction between HlyB and HlyD with HlyA leads to a conformational change, which recruits TolC [52, 65]. The transmembrane domain follows the cytosolic domain from position 60 to 80. The largest part of HlyD is located in the periplasm, aa 81 to 478. In 2016, Kim *et al.*

reported the structure of a soluble fragment of the periplasmatic domain truncated at the C- and N-terminal sites (Figure 9).

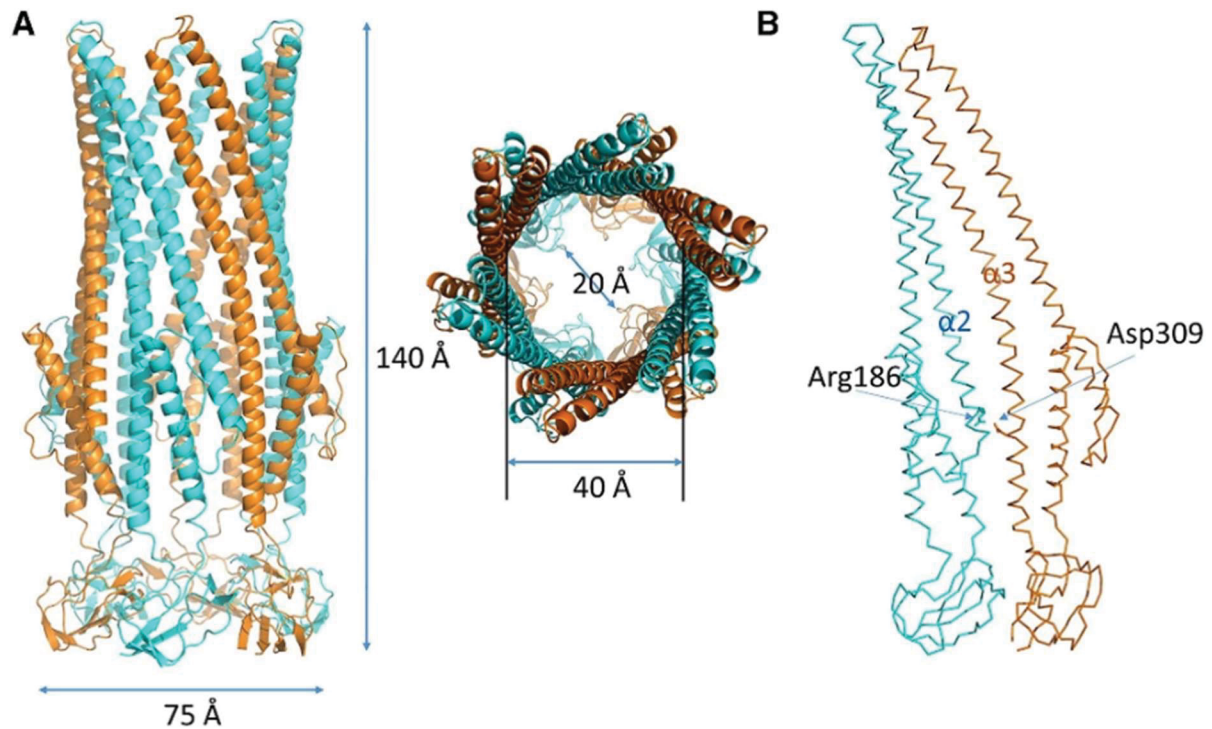


Figure 10. **Hexameric model of HlyD.** (A) Six HlyD protomers (cyan and orange) are assembled in a side-by-side arrangement. This funnel-like hexamer is also observed for MacA and AcrA [53, 180]. (B) Interaction between two adjacent protomers. The intermolecular interaction between $\alpha 2$ and $\alpha 3$ observed while electrostatic interaction of Arg186 and Asp309 also occurs. Figure from [181].

While there is still no structure of the entire HlyD, the periplasmatic part of HlyD shows some important features for the assembly of the T1SS [181]. Like other MFP HlyD has a lipoyl half motif which is highly conserved [182]. The lipoyl motif is followed by an α -hairpin, which has been shown essential for interaction with TolC [183, 184]. Mutation of the half motif leads to a deficient secretion or misfolding of the transported substrate in the extracellular space [182, 183, 185]. While studies for different RND pumps (MacAB-TolC and AcrAB-TolC) showed a tip-to-tip interaction between TolC and the MFP in a cogwheel manner [55, 186, 187] this question is still open for the HlyA T1SS. In addition, the multimeric state of the MFP is not solved yet. The structures of AcrAB and MacAB both showed a hexamer of MFP like proposed for HlyD [53, 55, 181, 184, 186, 188], and shown in Figure 9. However, one study proposed a trimeric state of HlyD based on crosslink studies [52]. Recent publications also suggest that the stability of secretion machineries such as RND pumps and T1SS rely on the interaction with the peptidoglycan. This would indicate that the interaction between TolC and HlyD is also modulated by the peptidoglycan [186].

1.18. TolC the outer membrane protein (OMP)

The outer membrane component of the HlyA T1SS, TolC, is a β -barrel pore located in the outer membrane extending into the periplasm. The overall length is 140 Å while 40 Å are the barrel to span the outer membrane, 100 Å are present in the periplasm [189]. TolC functions as a trimer. The monomer is 493 aa in size with an N-terminal 22 aa signal sequence. This sequence is cleaved in the periplasm and leads to the insertion of the β -barrel into the outer membrane by

the Bam complex [190]. TolC can then be inserted in the nascent peptidoglycan layer [10, 191]. The matured TolC forms a hollow cylindrical translocation pore with an inner diameter of 35 Å on its widest part and 20 Å on the narrowest [189]. The pore shows an iris-like coiled-coil structure, which holds structured water molecules to keep itself closed [192]. Molecular dynamic simulations predict a iris movement to open the duct which controls the entry to the extracellular space [193]. Recently cryo electron tomography (cryo-ET) studies showed how the tip-to-tip (also proposed for other systems that use TolC) interaction between TolC and AcrA leads to an open state of the efflux pump [186]. The same study shows crucial interaction between the PG, the α -hairpin of the MFP and TolC for open or closed conformation. In the lateral helices of TolC motives are present, which would support this finding with the so-called knobs into holes motive [52, 194]. This is proposed for HlyD and was shown for AcrA in the AcrAB-TolC system [192]. Crosslink studies showed that crosslinking events between single helices of TolC on the periplasmatic entrance part of TolC abolished the secretion capability of the HlyA T1SS even when the whole complex was assembled [195]. This leads to the assumption, that TolC not only needs its interaction partner (MFP), also the PG has to be present and the TolC helices need some degree of freedom to properly operate.

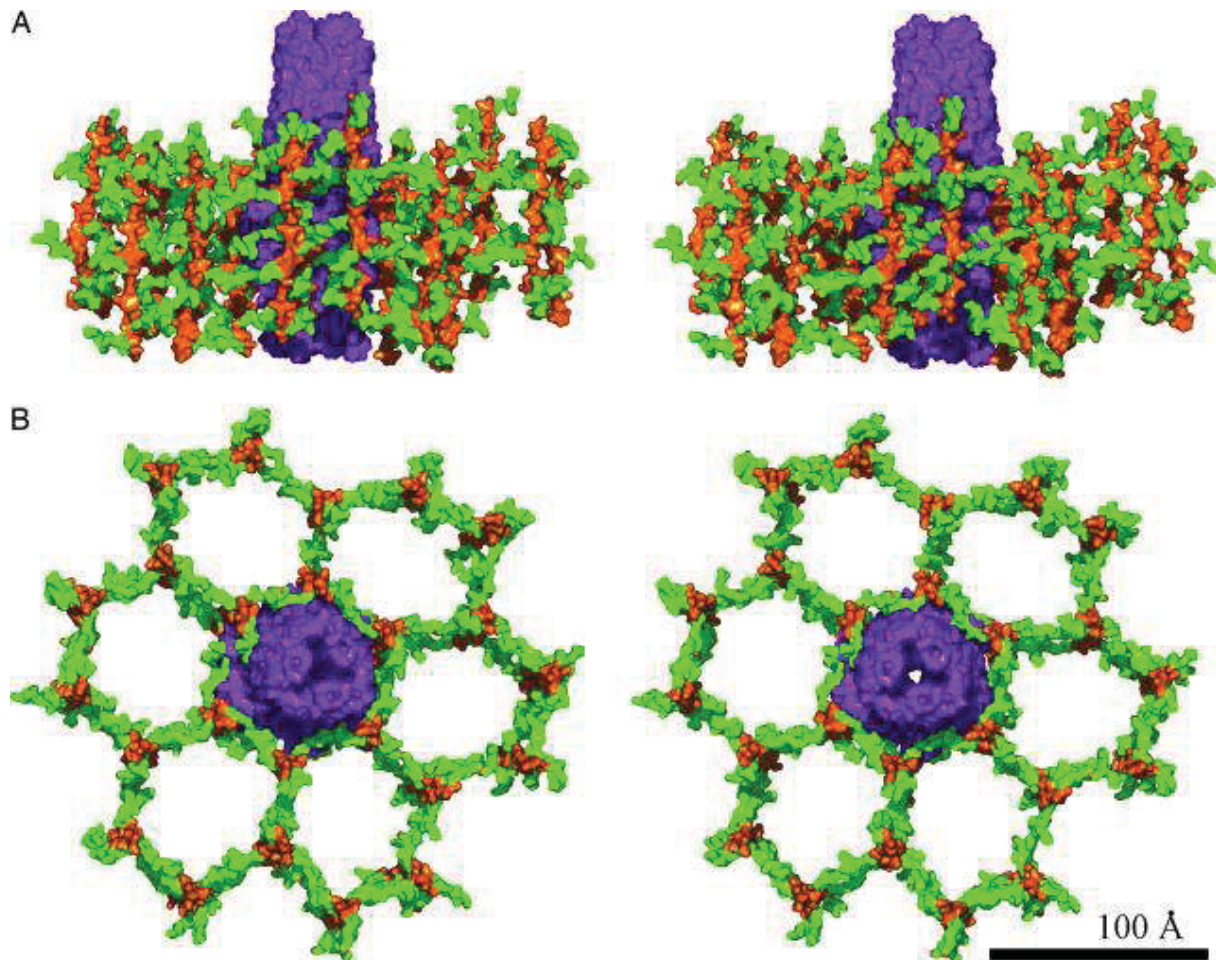


Figure 11. TolC integrated into the peptidoglycan. Stereoviews from the side of (A) and above (B) the crystal structure of TolC outer-membrane channel embedded into a pore of the cell wall. TolC is shown in ribbon and surface representations as a solvent-accessible Connolly surface (purple). The protruding TolC β -barrel domain (shown in ribbon) is fully embedded into the outer-membrane bilayer of the Gram-negative bacterium. As the peptidoglycan is in direct contact with the inner leaflet of the outer membrane bilayer. Figure was taken from [10]

1.19. Secretion mechanism of HlyA and stalling of the T1SS

As described above, HlyB and HlyD interact with unfolded HlyA in the cytosol. This interaction recruits TolC and results in assembly of the secretion machinery. HlyD functions as a relay by translating the presents of the substrate in a conformational change to recruit TolC. TolC is a bottleneck for the secretion by having the narrowest part with an inner diameter of 20 Å. The functional consequence is that only an unfolded substrate can be secreted. Thus, only secondary structures like single helices can pass the translocation pore [151]. By creating MalE-HlyA fusion proteins combined with folding mutants it was demonstrated, that HlyA is not secreted when MalE is folded, but can be secreted when MalE remains unfolded [196]. Secretion experiments with MalE-HlyA and eGFP-HlyA fusions showed not only that the secretion only occurs in an unfolded state but also that the secretion occurs in a vectorial fashion with the C-terminus appearing first at the cell envelope [173, 196, 197]. A competition experiment demonstrated that the T1SS can be arrested during its secretion when a fusion protein with fast folding properties was used [173]. Nevertheless, the C-terminal part of the protein is still able to reach the extracellular space where the GG-repeats can induce the folding by binding calcium ions. The fast folding proteins in the cytosol together with the extracellular folded protein creates something similar to two knots on a string trapping the translocation machinery in between (Figure 11). This new approach allowed the design of new experiments leading to the ability to proof the vectorial transport of the HlyA [173]. A model of the stalling mechanism is shown in Figure 11.

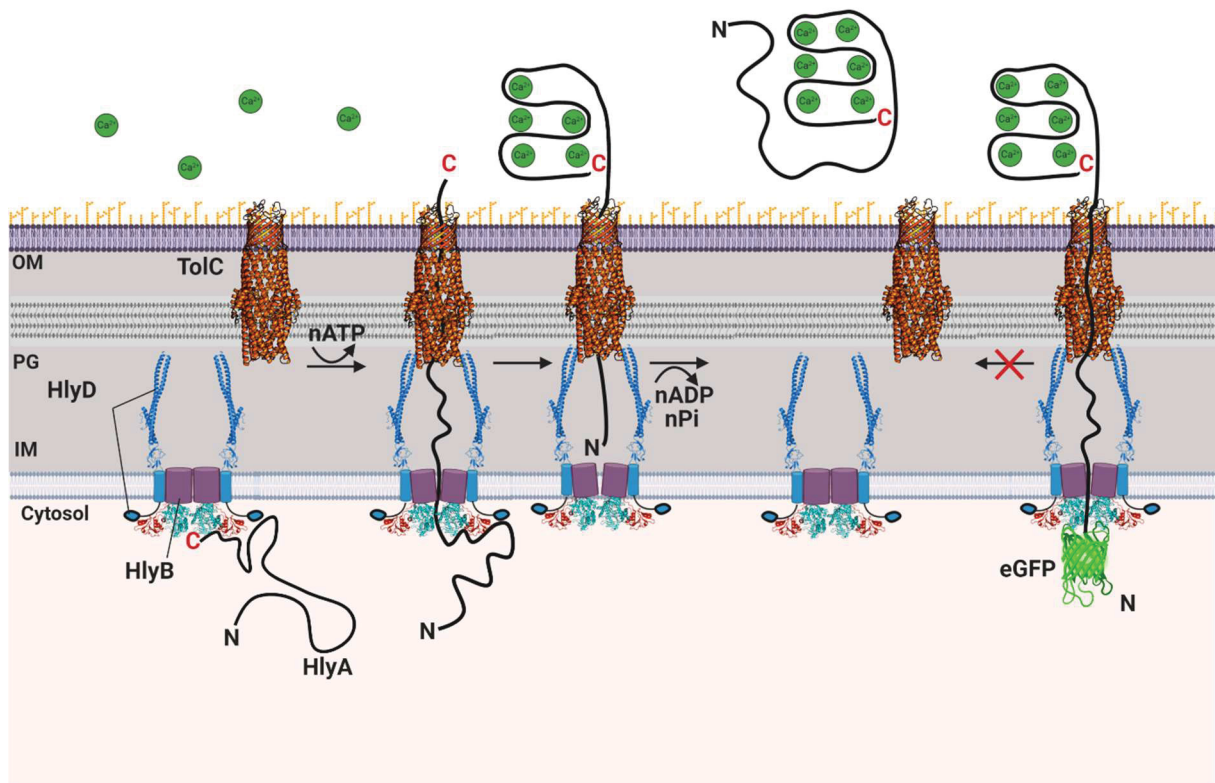


Figure 12. *Assembly, secretion and stalling of the T1SS.* The inner membrane complex of HlyB purple (CLD based on pdb file: 3ZUA in red, NBD based on pdb file: 2PMK cyan) and HlyD in blue (periplasmic part based on pdb file: 5C21) is colocalized. In the presence of the substrate HlyA, HlyB and HlyD recruit TolC, the OMP of the T1SS. The unfolded substrate is threaded into the translocation pore with the C-terminus first, while ATP binding is mediated by the interaction of the

secretion signal with HlyB. The unfolded substrate is displaced into the translocator and moves through TolC until the extracellular space is reached. Here, the GG-repeats bind to extracellular Ca^{2+} (indicated by dark green spheres) which induces folding of the substrate while transport is continued. When HlyA completely passed the translocator, it is presumed that this triggers the release of the OMP and ADP and phosphate is released into the cytosol while the initial state of the IMC is restored. When eGFP (in light green based on the pdb file: 5DY6) or any fast folding protein is fused to the N-terminal site of HlyA the initial secretion occurs until the fast folding N-terminal part reaches the translocation pore. It is too narrow to enter and the secretion system is arrested in this state by preventing the disassembly of the T1SS. In the extracellular space the surface reaching part is folded by binding Ca^{2+} , which prevents backsliding into the translocation pore.

Over many years, the binding of calcium ions was predicted to help energizing the transport of the T1SS substrates [151, 167, 170]. Bumba *et al.* demonstrated a ratchet-like movement induced by the folding of the substrate which apparently prevented backsliding of the substrate [169], while the influence of extracellular Ca^{2+} concentrations on the secretion rate for the HlyA T1SS is shown in the chapter 3.1. How many ATP are hydrolyzed during translocation of HlyA is not clear yet. Furthermore, an additional energetic factor could be the proton motive force (PMF) [176] or usage of the isoelectric properties of T1SS substrates which all have *pI*s of around 5 [170]. These are still open questions. Nevertheless, the secretion is terminated when the substrate is completely translocated into the extracellular space. Accordingly, the T1SS disassembles into IMC and OMP and is primed for the next cycle of secretion cycle (Figure 11).

2 Aims

Gram-negative bacteria have a major impact on human health. A prime example are uropathogenic *Escherichia coli* (UPEC). Alone in the year 2000 urinary tract infections in the United States of America resulted in treatment costs of 3.5 billion \$ and millions of patients [198]. One of the most prominent examples for toxin secretion systems in Gram-negative bacteria is the HlyA type I secretion system of *Escherichia coli*. HlyA is a hemolytic repeats in toxin (RTX) protein and an important virulence factor for UPEC.

To transport the HlyA out of the cell across both membranes of Gram-negative bacteria, *E. coli* has developed a sophisticated secretion machinery consisting of three components. The ABC transporter HlyB that provides the power stroke for the active transport of HlyA [157]. HlyD the membrane fusion protein, forming the inner membrane complex (IMC) in combination with HlyB in the inner membrane [62]. The third component is the outer membrane protein TolC, recruited by the IMC in presence of the substrate HlyA [65]. The unfolded substrate is translocated by the assembled T1SS across both membrane C-directional [173] in the extracellular space without any periplasmic intermediate [52, 196]. HlyA folds after translocation in the extracellular space by binding calcium ions to the RTX motives [61]. The transient assembled state of the T1SS can be arrested by using an N-terminal fusion construct of HlyA with a fast folding GFP. Therefore, further characterization of the T1SS in its transient active state is possible. Based on the arrested HlyA T1SS this thesis aims for development of an experimental method to determine the amount of active T1SS when overexpressed in the lab strain *E. coli* BL21(DE3). This would enable the investigation on the influence of extracellular calcium ions on the secretion of HlyA and investigation of potential energization of the translocation through ratchet motion during the folding of HlyA as proposed [197].

To this day, the localization of the HlyA T1SS on the cell surface is unknown. Utilizing the arrested T1SS, the exposed Substrate HlyA can be used to develop a method to investigate the localization. Further, the overexpression of the T1SS can be compared to the endogenous expression by applying the developing methods also to the parental strain *E. coli* UTI89 (urinary tract infection). An additional aspect is the influence of overexpression respectively endogenous expression of the T1SS on other components like TolC when the T1SS is arrested during secretion [173].

One major obstacle for in depth characterization is the fact that the overall molecular structure of the HlyA T1SS is unknown. Only parts were solved like the HlyB-NBD, CLD [157, 164] TolC [189] and a soluble periplasmic truncated part of HlyD [181]. The concept of stalling used for the investigation of the C-directional transport [173] shall be utilized to stall the complex during secretion, followed by isolation and further purification. The purified complex then should be applied to methods like EM, which were used to solve the related structure of the AcrAB RND efflux pump [53, 186]. Therefore this thesis aims for a novel purification approach for the HlyA T1SS.

3 Publications

3.1 Chapter I – Secretion rates of substrate translocation of the HlyA Type I secretion system

Title In vivo quantification of the secretion rates of the hemolysin A Type I secretion system

Author Michael Lenders, H. H. Tobias Beer. Sander H. J. Smits. Lutz, Schmitt.

Published in Scientific Reports (2016)

Impact Factor 4.525

Own proportion of this work 30 %;

Secretion assay, secretion rate determination, immunofluorescence labeling of formaldehyde treated cells

SCIENTIFIC REPORTS



OPEN

In vivo quantification of the secretion rates of the hemolysin A Type I secretion system

Michael H. H. Lenders, Tobias Beer, Sander H. J. Smits & Lutz Schmitt

Received: 15 April 2016

Accepted: 24 August 2016

Published: 12 September 2016

Type I secretion systems (T1SS) of Gram-negative bacteria secrete a broad range of substrates into the extracellular space. Common to all substrates is a C-terminal secretion sequence and nonapeptide repeats in the C-terminal part that bind Ca^{2+} in the extracellular space, to trigger protein folding. Like all T1SS, the hemolysin A (HlyA) T1SS of *Escherichia coli* consists of an ABC transporter, a membrane fusion protein and an outer membrane protein allowing the one step translocation of the substrate across both membranes. Here, we analyzed the secretion rate of the HlyA T1SS. Our results demonstrate that the rate is independent of substrate-size and operates at a speed of approximately 16 amino acids per transporter per second. We also demonstrate that the rate is independent of the extracellular Ca^{2+} concentration raising the question of the driving force of substrate secretion by T1SS in general.

Many Gram-negative bacteria especially pathogens have evolved dedicated secretion systems to translocate virulence factors into the extracellular medium or directly into the host cell¹. Among these nanomachineries, Type I secretion systems (T1SS) are the most simple systems as they consist of an ATP-binding cassette (ABC) transporter, a membrane fusion protein (MFP), both located in the inner membrane (IM), and an outer membrane protein (OMP). T1SS are able to transport a rather diverse group of proteins with different functions², for example hemophores such as HasA (188 amino acids, 19 kDa) from *S. marcescens*³, lipases such as LipA (613 amino acids, 65 kDa) from *S. marcescens*², adenylate cyclases like CyaA (1706 amino acids, 177 kDa) from *Bordetella pertussis*², proteases like alkaline protease (479 amino acids, 50 kDa) from *Pseudomonas aeruginosa*², pore-forming toxins like hemolysin A (1024 amino acids, 110 kDa) from *E. coli*² or large adhesion factors such as LapA (8682 amino acids, ~900 kDa) from *P. fluorescens*⁴. Common to all these substrates is the presence of a secretion signal that is encoded within the C terminus that in contrast to other secretion systems is not cleaved during or after secretion. In the case of HlyA the last 50 to 60 C-terminal amino acids represent this sequence, which is essential and sufficient for the secretion process^{5–9}.

One prominent family of T1SS substrates is the repeats in toxin (RTX) proteins. Characteristic for these proteins are glycine-rich, nonapeptide repeats (GG repeats) with the consensus sequence GGxGxDxUx (where x can be any amino acid and U is a large or hydrophobic amino acid)¹⁰ that are also located in the C-terminal part of the protein, just upstream of the secretion signal. The number of these repeats depends on the size of the protein with on average one repeat for every 6–12 kDa^{2,10}.

The paradigm of T1SS that translocates RTX toxins is the hemolysin A secretion machinery found in uropathogenic *E. coli* strains. HlyA is a 1024 amino acid (110 kDa) pore-forming toxin, which harbors six conserved GG repeats¹¹. The HlyA T1SS is composed of the ABC transporter hemolysin B (HlyB), the MFP hemolysin D (HlyD) and TolC, the endogenously expressed OMP.

Recently, it was demonstrated that HlyA is secreted in an unfolded form and that the folding rate of the passenger dictates the efficiency of secretion¹². In the extracellular space, Ca^{2+} binds to the GG repeats with an affinity of approximately $100 \mu\text{M}$ ^{13–16} and triggers folding of HlyA or the secreted substrate in general¹⁶. Since the intracellular Ca^{2+} concentration in the cytosol of *E. coli* is roughly 300 nM, HlyA and RTX proteins remain unfolded^{16,17}. The binding of Ca^{2+} (concentration of up to 10 mM in the extracellular space¹⁷) and the subsequent folding of HlyA was consequently proposed to act as driving or 'pulling' force for secretion, acting as a ratchet^{14,18}. However, experimental evidence supporting such a mechanism has only been reported recently for the adenylate cyclase toxin CyaA from *Bordetella pertussis*¹⁹.

Institute of Biochemistry, Heinrich-Heine-Universitaet, 40225 Duesseldorf, Germany. Correspondence and requests for materials should be addressed to L.S. (email: Lutz.Schmitt@hhu.de)

Furthermore, fusions using a fast folding variant of GFP (eGFP) upstream of HlyA or a C-terminal fragment of HlyA (HlyAc) demonstrated that transport is unidirectional with the C-terminal secretion signal appearing first at the cell surface²⁰. HlyAc consists of the last 218 amino acids of HlyA and contains three conserved GG repeats in addition to the secretion sequence. The secretion of HlyAc is as efficient as HlyA, but the protein is more stable and more efficiently purified¹².

It is currently assumed for type 1 secretion that the substrate interacts with the IM components and recruits the OMP to form a continuous tunnel-channel across the periplasmic space. Subsequently, the substrate is transported in an unfolded, secretion-competent state in one step from the cytosol to the extracellular space. Energy is provided through the ABC transporter²¹ and through the proton motif force, which was reported to be essential at an early stage of the secretion process²².

The secretion rate of hemolysin A as well as for any other type 1 protein has not been experimentally determined. However, in the case of the SipA Type 3 secretion system (T3SS), secretion varied between 7–60 molecules SipA per sec per cell, as determined by time-lapse fluorescence spectroscopy²³. As the number of T3SS translocons per cell is not known in this case, a precise secretion rate cannot be deduced. In the case of SecA-dependent transport mediated by SecYEG translocon, the rate limiting step, ATP hydrolysis, was determined experimentally *in vitro*²⁴. Assuming that one ATP molecule energizes the translocation of 20–30 amino acids^{25,26}, a translocation rate of 152–228 amino acids per sec per transporter can be calculated.

To address the question of the secretion rate, we used the concept of a stalled T1SS to quantify the amount of active HlyA T1SS per *E. coli* cell²⁰. This allowed us to calculate the secretion rate of the entire HlyA, or the C-terminal fragment HlyAc. Our data demonstrate that the number of GG repeats has no influence on the secretion rate per amino acid and per transporter, that Ca²⁺ does not influence the secretion rate, and that ATP hydrolysis is necessary for substrate exposure at the extracellular cell surface.

Results

Determination of the amount of active T1SS. The prerequisite for quantification of the substrate secretion rate of any T1SS is an accurate determination of the number of active T1SS translocons per cell. Here, we applied the concept of stalled T1SS complexes that was previously used to determine the directionality of substrate translocation²⁰. Accordingly, an eGFP-HlyAc fusion construct was employed to stall the HlyA T1SS within the membrane²⁰. In the stalled complex, the C-terminal part of the fusion protein, i.e. HlyAc, is exposed at the cell surface, while eGFP remains in the cytosol and plugs the translocation pore²⁰. The extracellular exposed HlyAc was visualized on the cell surface using an HlyA specific, polyclonal antibody, in combination with a secondary antibody labeled with a Cy3 fluorophore (See Fig. 3 of ref. 20). Since the nonspecific binding of both antibodies, anti-HlyA and the Cy3-labeled secondary antibody, is not significant (Fig. 1), these antibodies possess the major advantage that binding to secreted HlyA or parts of HlyA visualizes only active and correctly assembled secretion machineries, that consist of both HlyB and HlyD. We made the assumption that on average one HlyA primary antibody binds to each surface exposed HlyAc and on average one Cy3-labeled secondary antibody binds per primary HlyA antibody. Cells without HlyB and HlyD cannot expose an HlyAc fragment at the cell surface and therefore represent background fluorescence (Fig. 1, right bar, $8.05 \times 10^5 \pm 1.48 \times 10^5$ CPS), which was subtracted from every measurement. The amount of specific fluorescence observed for HlyA-exposed at the surface of *E. coli* is therefore $1.95 \times 10^5 \pm 4.59 \times 10^4$ CPS. To calculate the amount of bound antibody a regression analysis was performed (Supplementary Fig. 1). The intensity of the fluorescence signal was multiplied by the slope of the calibration line resulting in the exact amount of active and stalled translocons present in the *E. coli* membrane, i.e. 0.3 pmol (1.80×10^{11} molecules). Dividing the number of T1SSs by the number of cells (4×10^7 cells in 50 μ L solution of an OD₆₀₀ of 1.0) resulted in an average of 4509 ± 1061 active T1SS cell⁻¹. To validate the determined value, we used a second, commercially available, secondary Cy3-labeled antibody. Following the same experimental procedure, including an antibody specific calibration line (Supplementary Fig. 1), we determined the average number of active HlyA translocons to be 4554 ± 1616 per cell. This value is in excellent agreement with the result of the first Cy3-labeled secondary antibody.

A second method to determine the amount of HlyB in the membrane was applied, namely Western blotting. Cells secreting HlyAc were solubilized, separated by SDS-PAGE and analyzed using a polyclonal HlyB antibody to quantify the HlyB signal by comparison of the signal intensity of a dilution series of purified HlyB of known concentration, which was included on the same Western blot. The signal intensity of the different concentrations of purified HlyB was used to calculate a calibration line (slope: 1.26×10^{-16} mol; Supplementary Fig. 2). This calibration line was subsequently used to determine the number of HlyB molecules present in cells secreting HlyAc or HlyA. Thereby, the determined signal intensity of HlyB within cells secreting HlyA corresponded to 11291 ± 1018 , which is equal to 1.42 ± 0.13 pmol HlyB. Divided by the number of cells (8×10^7 cells), this corresponds to 10710 ± 965 molecules of HlyB per cell. Since HlyB is a functional dimer²⁷, 5355 ± 483 functional units are present per cell. Thus, the Western blot analysis puts an upper limit on the number of T1SS per cell. The results of the fluorescence analysis of the stalled T1SS are in accordance with this upper limit and indicate that nearly all HlyB molecules are recruited to the T1SS.

In summary, the concept of a stalled T1SS allowed us to determine the number of active secretion machineries per cell and resulted in an average value of 4532 ± 966 T1SS cell⁻¹, which was used in the subsequent analysis (Supplementary Table 1).

Quantifying the secretion rate of HlyA and HlyAc. The determined number of T1SS cell⁻¹ provided us with the possibility to quantify the secretion rate for HlyA and HlyAc, respectively both are equally well secreted by the HlyA T1SS²⁸. Furthermore and as described by Lenders *et al.*²⁰, substrate is always present in the cytosol of *E. coli* during secretion. This indicates that the secretion of HlyA is the rate-limiting step and not its synthesis.

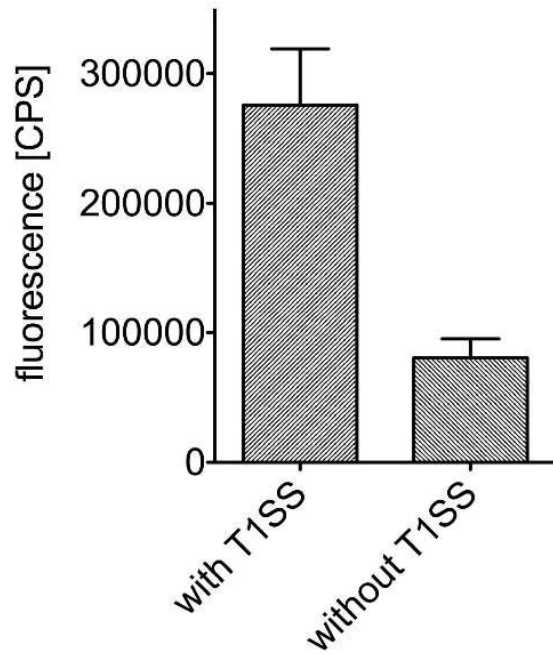


Figure 1. Total cell fluorescence of Cy3. Immunofluorescent labeled *E. coli* cells expressing eGFP-HlyAc in the presence (left bar) and absence (right bar) of HlyB and HlyD, respectively. Error bars represent the standard deviation of the Cy3 fluorescence of at least three biological replicates.

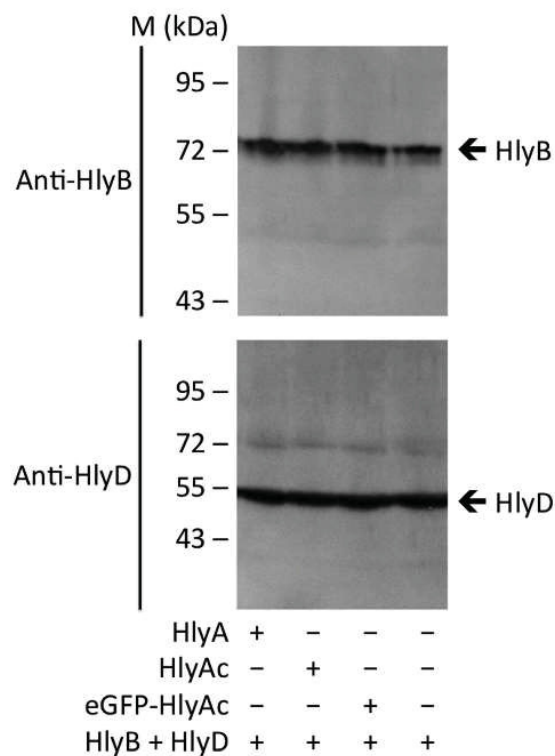


Figure 2. HlyB and HlyD expression levels. Western blot analysis of *E. coli* cells demonstrated that the expression levels of HlyB and HlyD were equal for cells expressing and/or secreting either eGFP-HlyAc, HlyA or HlyAc.

For the purpose of quantification of the secretion rate, HlyA was secreted for four hours and samples of the supernatant were taken every hour. In parallel, cell growth was monitored each hour during secretion by measuring the OD at 600 nm. Based on the optical density, the total number of cells was calculated. Samples of the supernatant and a dilution series of purified HlyA of known concentration were analyzed by SDS-PAGE. The integrated

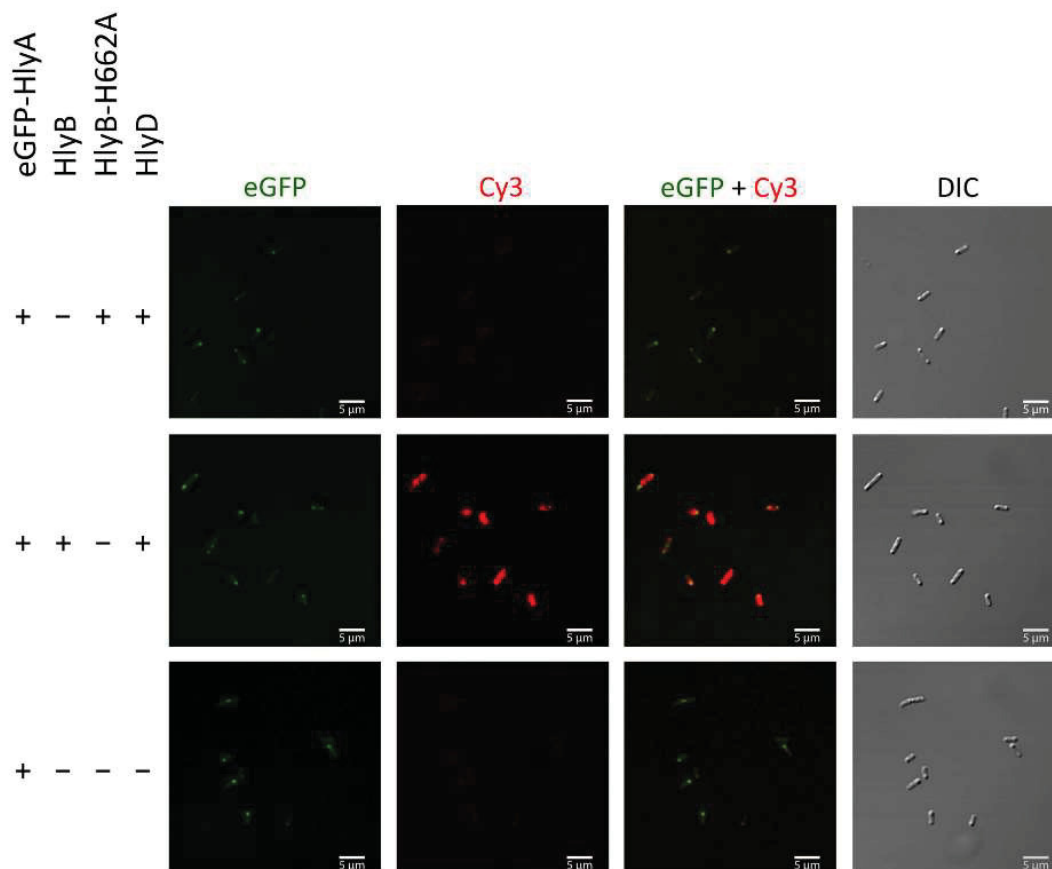


Figure 3. Detection of the surface exposed HlyA fragment of eGFP-HlyA by confocal laser scanning microscopy. *E. coli* cells expressing eGFP-HlyA, HlyD, HlyB or HlyB-H662A in different combinations of the proteins. Shown is the eGFP fluorescence (left panel) of the fusion proteins, the HlyA mediated Cy3 fluorescence at the cell surface (second left panel), merged images of eGFP and Cy3 fluorescence (second right panel) and differential interference contrast (DIC) images of the cells (right panel). The different combinations of proteins employed are indicated to the left.

signal intensity of the samples of purified HlyA at different concentrations was used to generate a regression line. This line allowed the quantification of secreted HlyA over time. Here, the integrated signal intensity of 1.09×10^4 corresponds to 9.6 pmol HlyA (5.781×10^{12} molecules). Knowledge of the amount of secreted HlyA at more than one time point enabled us to determine the secretion level of HlyA per time. Here, a value of $0.13 \text{ pmol min}^{-1}$ ($7.83 \times 10^{10} \text{ HlyA min}^{-1}$). Divided by the number of cells per time ($2.03 \times 10^7 \text{ cells min}^{-1}$), this number corresponds to a value of 3856 secreted HlyA molecules in $\text{cell}^{-1} \text{ min}^{-1}$. If one takes the number of amino acids of HlyA (1024 aa) into account, the calculated secretion rate of HlyA per TISS and per cell (4532), per sec was $14.5 \text{ amino acids (TISS}^{-1} \text{ s}^{-1})$ in this particular example. During the time period of the secretion experiments, HlyA molecules were still present in the cytosol indicating that not the synthesis of HlyA but the translocation step of the substrate is the rate-limiting factor.

The number of cells and the number of secreted HlyA in the exponential cell growth phase of *E. coli* were used for calculation of the secretion rate. This phase is normally present within the first two hours after induction. Supplementary Tables 2 and 3 summarize all values for secreted HlyA and HlyAc, respectively, for the secretion experiments performed for 2 h and 4 h, respectively, the corresponding HlyA secretion level [mol min^{-1}], cell growth [cells min^{-1}] and the final secretion rate of HlyA and HlyAc [$\text{aa TISS}^{-1} \text{ s}^{-1}$].

Using the results of experiments with different durations of secretion, an average value of at least $16.0 \pm 1.3 \text{ aa TISS}^{-1} \text{ s}^{-1}$ was determined for HlyA. Following the same line of experiments (for the corresponding gels see Supplementary Fig. 3 for HlyA and Supplementary Fig. 4 for HlyAc), the secretion rate of HlyAc was calculated to at least $16.6 \pm 1.4 \text{ aa TISS}^{-1} \text{ s}^{-1}$. Western blot analysis using the polyclonal antibodies against HlyB and HlyD confirmed that the expression levels of both proteins were similar in cells expressing the TISS and were not effected by the co-expression of the substrates (Fig. 2).

The results described above demonstrated that the secretion rates of HlyA and HlyAc were identical within experimental error. However, the absolute number of secreted HlyA molecules was 4 to 5 fold lower compared to HlyAc. This simply reflects the difference in number of amino acids, 1024 aa in the case of HlyA and 218 aa in the case of HlyAc. Consequently, the number of secreted molecules of HlyAc is accordingly higher compared to HlyA.

ATP hydrolysis is necessary for early step of secretion. Binding and/or hydrolysis of ATP by the ABC transporter HlyB provides the necessary energy for substrate translocation through the T1SS. Previous studies have demonstrated that substrate secretion is abolished in the absence of ATP hydrolysis but did not affect complex assembly²¹. Nevertheless, since the exact step for which ATPase activity is required remained elusive, the question arises, whether an early step such as entering the translocation pathway or a late step of secretion such as release from the cell envelop or re-setting of the T1SS requires an energetic input.

To analyze the importance of ATP hydrolysis during substrate secretion, the H662A mutant of HlyB, which is deficient in ATP hydrolysis, was used. This mutant is able to bind ATP, dimerization of the NBDs but does not catalyze ATP hydrolysis^{27,29}. In combination with the concept of a stalled T1SS complex described above, the H662A mutant might help to clarify which step of substrate translocation is coupled to ATP hydrolysis.

E. coli cells expressing a T1SS harboring the HlyB H662A mutant (Fig. 3, first row) were analyzed by confocal laser scanning microscopy (CLSM). Homogeneously distributed cytosolic eGFP fluorescence was observed, which sometimes accumulated at the cell poles. However, no Cy3 fluorescence was detected at the cell surface indicating that the C-terminal part of HlyA did not reach the extracellular space. As a control, *E. coli* cells expressing eGFP-HlyA but not HlyB and HlyD were also analyzed (Fig. 3, third row). Here, similar, cytosolic eGFP fluorescence was observed, but again no Cy3 fluorescence was detected (for quantification of the observed eGFP and Cy3 see Supplementary Fig. 5).

In summary, these results demonstrated that the eGFP-HlyA fusion protein was only presented at the cell surface if HlyB was capable of binding and hydrolyzing ATP. This strongly suggests that ATP hydrolysis is essential for an early event in the translocation process.

The role Ca²⁺ on the rate of secretion. The requirement of an unfolded substrate during translocation and the directionality of secretion, i.e. the C-terminal part is presented at the cell surface first, is in line with the hypothesis that binding of Ca²⁺ to the GG repeats and the subsequent folding represents the driving force of substrate secretion by T1SS¹⁰. The affinity of the GG repeats of HlyA and the concentration of Ca²⁺ in the cytosol of *E. coli* and the extracellular medium support this scenario, in which Ca²⁺ induced protein folding creates an inherent driving force that “pulls” the protein out of the translocator^{10,11}.

We addressed the question of a ‘Ca²⁺-triggered pulling mechanism’ by varying the Ca²⁺ concentration in the extracellular medium. If such a ‘pulling’ mechanism indeed provides the inherent driving force for substrate transport, the secretion rate has to depend on the external Ca²⁺ concentration. Below the K_D of the GG repeats for Ca²⁺ (100 μM¹⁶), a clear drop in the rate should be apparent, while the rate should remain constant at Ca²⁺ concentrations exceeding the K_D.

HlyA and HlyAc are unstable in the absence of Ca²⁺, or at concentration below the K_D of the GG repeats and an aggregation of the secreted substrates was observed. However, extracellular aggregation appeared only if HlyA and HlyAc reached a critical concentration, typically after three hours resulting in visible aggregation at the rim of the incubation flasks. Therefore, the time of the secretion experiments was restricted to two hours.

In all of the secretion experiments addressing the role of the concentration of extracellular Ca²⁺, the Ca²⁺ concentration was adjusted either by addition of external Ca²⁺ or EGTA and verified by atomic absorption spectroscopy (for further details see Materials & Methods). The amount of both substrates and HlyB/HlyD remained at the same level during the first two hours of secretion, independently of the external Ca²⁺ concentration (Fig. 4 dark grey bars and Supplementary Fig. 8).

The secretion rates for HlyA and HlyAc at different extracellular Ca²⁺ concentrations are summarized in Supplementary Tables 2 and 3. The results highlight that the secretion rate of HlyA remained constant between 14.3 ± 3.1 and 18.5 ± 4.3 aa T1SS⁻¹ s⁻¹, respectively, while values between 15.8 ± 4.1 aa T1SS⁻¹ s⁻¹ and 17.9 ± 4.1 aa T1SS⁻¹ s⁻¹ were determined for HlyAc. These results demonstrated that therefore a Ca²⁺ concentration between 0 and 5 mM did not alter the secretion rate (Fig. 5).

Ca²⁺ ions are essential for the stability and correct folding of HlyA and HlyAc, respectively. However, our experiments suggest that Ca²⁺ does not provide an inherent driving force for secretion of HlyA and does therefore not impose a “pulling” mechanism during the secretion process. One might speculate that as an alternative to the absolute requirement of ATP hydrolysis, an entropic driving force acts in T1SS as was proposed for protein synthesis at the ribosome³⁰. Here one could envision that confinement of the tunnel-channel of a T1SS translocon, entropically favors formation of secondary structure elements that prevent back-sliding and thereby impose a force that pulls HlyA and some other substrates out of the translocon. However, the question raised is whether the conformation and/or structure of HlyA that is secreted in the absence of Ca²⁺ is similar to the one adopted in the presence of Ca²⁺. Therefore, we measured the intrinsic Trp fluorescence of HlyA in the presence or absence of 2 mM Ca²⁺ at 331 nm and 350 nm, respectively¹⁶. For HlyA secreted in the presence of 2 mM Ca²⁺, we obtained a ratio of the intrinsic Trp fluorescence at 350 nm to 331 nm of 1.44 ± 0.05 indicating a properly folded protein¹⁶. In contrast, the ratio 350 nm over 331 nm of HlyA secreted in the absence of Ca²⁺ was 0.63 ± 0.03 suggesting that HlyA adopted a different conformation under these conditions. To assess this difference further, we secreted acylated HlyA (the lytically active form of HlyA) in the presence and absence (2 mM) Ca²⁺ and placed 10 μl of supernatant on Columbia blood agar plates. After 2 h of incubation at 37 °C, clear halo formation was visible for acylated HlyA secreted in the presence of 2 mM Ca²⁺ (Supplementary Fig. 6). This clearly showed that acylated HlyA was properly folded. In clear contrast, no halo formation was detected in the case of acylated HlyA secreted in the absence of Ca²⁺ suggesting that acylated HlyA adopted a non-lytic conformation under this condition (Supplementary Fig. 6).

Discussion

The concept of a stalled HlyA T1SS by an HlyAc fusion with rapidly folding eGFP was recently used to determine the orientation of HlyA during secretion²⁰. We used this approach to quantify the number of active T1SS

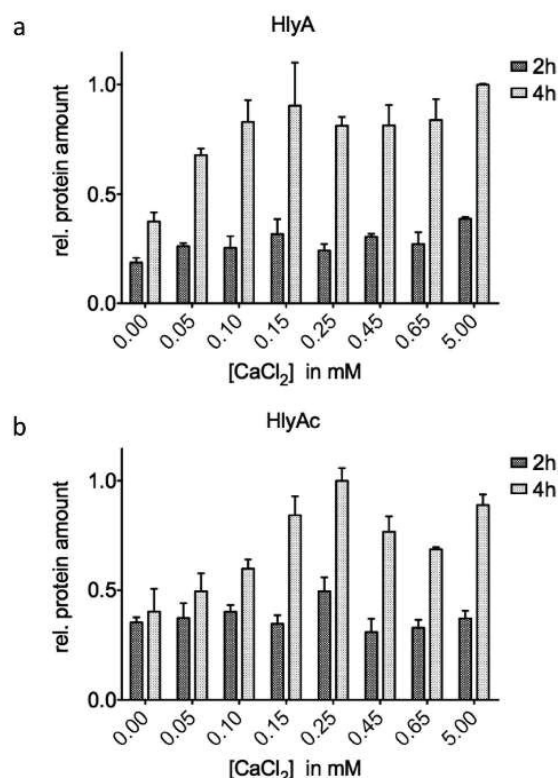


Figure 4. Relative amount of secreted HlyA and HlyAc in the presence of different extracellular Ca²⁺ concentrations. The relative amount of secreted HlyA (a) and HlyAc (b) in the presence of different extracellular Ca²⁺ concentration after 2 h (dark grey bars) and 4 h (light grey bars) is summarized. Values are normalized to the highest mean value of secreted HlyA (a) or HlyAc (b) after 4 h of secretion. Error bars represent the standard deviation of at least three biological replicates.

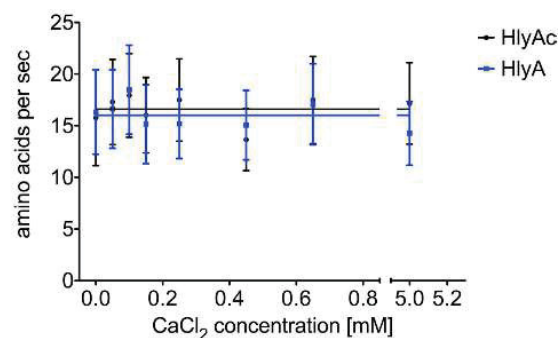


Figure 5. The secretion rate of HlyA and HlyAc is independent of the extracellular Ca²⁺ concentration. Determined secretion rates of HlyA (blue cubes) and HlyAc (black dots) in the presence of different Ca²⁺ concentration. Shown are the mean secretion rates of triplicate secretion experiments as amino acids (aa) T1SS⁻¹ s⁻¹. Error bars represent the standard deviation of at least three biological replicates.

per cell. Here, we assume that on average only one HlyA antibody and one Cy3-labeled secondary antibody binds to a single, surface-exposed HlyAc. Employment of a second, commercially available and Cy3-labeled antibody supported this assumption. Furthermore, we also determined the total number of HlyB molecules that are present in the inner membrane of *E. coli* cells by Western blot analysis. Assuming that HlyB like all ABC transporters analyzed so far forms a dimer as the functional unit³¹, this method revealed the absolute number of HlyB molecules, thus imposing an upper limit to the amount of T1SS present per cell. This value supported our fluorometric-determined value of approximately 4500 active T1SS per cell (Supplementary Table 1). This allowed us to determine the secretion rate of T1SS *in vivo* for the first time. The velocity of secretion of HlyA was determined to be 16.0 ± 1.3 aa T1SS⁻¹ s⁻¹, while HlyAc was secreted at a velocity of 16.6 ± 1.4 aa T1SS⁻¹ s⁻¹. This demonstrates that the secretion rate per transporter and per cell is independent of the size of the substrate.

Previous studies highlighted the importance of ATP hydrolysis for protein translocation in the HlyA T1SS²¹. HlyA secretion is completely abolished by using an HlyB mutant protein deficient in ATP hydrolysis. Nevertheless, cross-linking experiments in the same study confirmed that the translocator still assembled even in the absence of ATP consumption. However, the particular step for which ATP hydrolysis is required was not identified²¹. Our results additionally demonstrate that ATP hydrolysis is essential for the substrate to reach the cell envelope. This leads to two fundamentally different models of how the HlyA T1SS operates. In the first model, continuous ATP consumption is necessary for energizing the transport process. In this case, a defined number of ATP molecules are consumed per transported amino acid(s). Such an iterative mechanism was suggested for SecA-dependent protein translocation^{25,26}. Here, a rate of 152–228 amino acids per sec and transporter can be calculated based on experimental data obtained for SecA *in vivo*²⁴. This process is faster than the secretion rate of at least 16.6 ± 1.4 aa T1SS⁻¹ s⁻¹ determined for the HlyA T1SS. However, the Sec pathway is one of the most essential nanomachineries in Gram-negative bacteria and responsible for the integration of most transmembrane proteins and the transport for many secreted proteins. In the second model, ATP hydrolysis could act as an effector similar to ATP-gated channels. Here, ATP hydrolysis would initiate channel opening and allow translocation of the substrate through the HlyA T1SS pore. In such a scenario, ATP consumption as the driving force for discrete amounts of transported amino acids per ATP consumed is highly unlikely. T1SS substrates can have a size of more than 8000 aa^{2,4} and hydrolysis of only one or two ATP molecules per translocated substrate seems very unlikely.

Other possibilities that can energize the transport process are the proton motive force, which plays an important role in T3SS³² and at an early stage of HlyA secretion²², or diffusion along a concentration or an electrostatic gradient. The proposed Ca²⁺-dependent “pulling” mechanism for HlyA^{14,18} as the inherent driving force is unlikely due to the result of our experiments.

The presence of GG repeats just upstream of the C-terminal secretion sequence is common to a large number of substrates of T1SS². In the case of HlyA, the GG repeats bind Ca²⁺ with an affinity of approximately 100 μM^{13–16} and trigger folding of the protein at the extracellular surface due to the presence of high Ca²⁺ concentration in the extracellular medium^{17,33,34}. Extracellular protein folding could involve an inherent driving force, which ‘pulls’ the protein out of the translocon. Only recently, Bumba *et al.* reported that Ca²⁺ indeed contributed to such a pulling force for the adenylate cyclase toxin CyaA from *Bordetella pertussis*¹⁹. In an elegant set of experiments, it was demonstrated that CyaA, a 1706 amino acid member of the RTX protein family, requires a C-terminal cap and Ca²⁺ ions in the extracellular media to ensure efficient secretion. In this scenario, binding of Ca²⁺ induces a Brownian ratchet mechanism that accelerates secretion. Our results are in contrast to these data¹⁹ and other proposals^{14,18}. After two hours of secretion, the secretion rate did not show any dependence on the extracellular Ca²⁺ concentration. Even in the absence of Ca²⁺ no significant deviation was observed. These results indicate that the proposed “pulling” mechanism is not operational in HlyA and that Ca²⁺ binding to the GG repeats is solely important to ensure proper folding and stability of the substrate. This assumption is supported by our data using intrinsic Trp fluorescence and data on the activity of acylated HlyA (Supplementary Fig. 6). Here, the value of intrinsic Trp fluorescence of 0.63 ± 0.03 (ratio at 331 nm over 350) of HlyA secreted in the absence of Ca²⁺ is identical within experimental error to HlyA unfolded in 8 M urea (0.062 ± 0.05)¹⁶. Thus the secretion rate of HlyA in the absence of Ca²⁺ is not influenced, although the protein adopts a non-active conformation in the absence of Ca²⁺.

Furthermore, one has to stress that HlyA (1024 amino acids) harbors 6 GG repeats, while CyaA (1706 amino acids) harbors 17 GG repeats⁹. Thus, the increased size of CyaA and the higher numbers of GG repeats might give an additional pulling force that is necessary for efficient secretion of this particular type 1 protein.

In summary, our results provided for the first time a quantitative measurement of the *in vivo* secretion rate of a T1SS. Furthermore, the proposed “pulling” mechanism of Ca²⁺ binding to the GG repeats as driving force could be excluded. On the other hand, ATP hydrolysis is essential for the early steps of substrate translocation.

Methods

Bacterial strains and plasmids. *E. coli* DH5α cells were used for all cloning procedures. The pK184 plasmid (Supplementary Fig. 7) was used for HlyB and HlyD expression under the control of a P_{lac} promoter, inducible with IPTG (isopropyl-β-D-1-thiogalactopyranoside)¹². All plasmids and oligonucleotides used in this study are summarized in Supplementary Tables 4 and 5. Plasmids pSOI-eGFP-HlyAc and pSOI-eGFP-HlyA, respectively, were used for eGFP-HlyAc or eGFP-HlyA expression under the control of a P_{BAD} promoter²⁰. Plasmids pSU-*hlyA* and pSU-*hlyA1* were used for HlyA and HlyAc expression, respectively, under the control of a P_{lac} promoter, inducible with IPTG (isopropyl-β-D-1-thiogalactopyranoside)^{16,35}. The HlyB-H662A mutant was expressed using a variant of the pK184 plasmid (pK184-HlyB-H662A-HlyD).

Cell cultivation and protein expression for confocal laser scanning microscopy. Chemically competent *E. coli* BL21 (DE3) cells were transformed with or without pK184-HlyBD or pK184-HlyB-H662A-HlyD and pSOI-eGFP-HlyAc or pSOI-eGFP-HlyA, respectively and grown at 37 °C on LB agar plates supplemented with 100 μg mL⁻¹ ampicillin and/or 30 μg mL⁻¹ kanamycin. *E. coli* BL21 (DE3) cells were prepared and induced as previously described²⁰.

Confocal laser scanning microscopy and image processing. Microscopy and image processing were carried out as previously described²⁰. We present here single confocal planes that do not contain maximum intensity projections composed of z scans.

Fluorescence spectrometry of immunofluorescence labeled formaldehyde treated cells. Immunofluorescence labeled and formaldehyde treated *E. coli* BL21 (DE3) cells expressing eGFP-HlyAc with and without HlyB/HlyD were adjusted to an OD₆₀₀ of 1.0 and were analyzed by a fluorescence spectrometry

(Jobin-Ivon Horiba Fluorolog-3) to quantify the amount of T1SS. All measurements were performed at 25 °C in a 50 μ L cuvette. Excitation was performed at 547 nm and fluorescence emission was monitored at 563 nm with slit widths of 5 nm each. Fluorescence was recorded for 0.5 s. An identical experiment was carried out with PBS buffer and different concentration of free Cy3 fluorophore-linked antibody (0.5 pM–1.5 μ M). To validate the results of the Cy3-labeled antibody, we used another, commercially available (Molecular Probes) Cy3-labeled antibody. This antibody was used as described above for the first Cy3-labeled antibody.

Secretion experiments with HlyA and HlyAc in the presence of different CaCl_2 concentrations.

Chemically competent *E. coli* BL21 (DE3) cells were transformed with pK184-HlyBD and pSU-hlyA or pSU-hlyA1 and grown on LB agar plates supplemented with 100 μ g mL^{-1} ampicillin and 30 μ g mL^{-1} kanamycin. Ca^{2+} concentration of 2YT medium was determined by atomic absorption spectroscopy.

Overnight cultures of single colonies were used to inoculate 25 mL 2YT medium supplemented with 100 μ g mL^{-1} ampicillin and 30 μ g mL^{-1} kanamycin at an OD_{600} of 0.1. Cultures were grown at 37 °C and 180 rpm. The expression of HlyA, HlyAc, HlyB and HlyD was induced by addition of 1 mM IPTG at an OD_{600} of 0.6–0.8. EGTA, respectively CaCl_2 , were added at this point to adjust the final Ca^{2+} concentration in the culture medium. Cells were grown for 4 h at 180 rpm and 37 °C. A 1 mL aliquot was taken each hour during cell growth and centrifuged for 5 min at 14 000 g, 4 °C. The supernatant was diluted one to eight and analyzed by SDS PAGE (Supplementary Figs 3 and 4).

A dilution series of purified HlyA of known concentration ranging from 40 μ g mL^{-1} to 625 ng mL^{-1} or HlyAc of known concentrations ranging from 50 μ g mL^{-1} to 758 ng mL^{-1} were loaded on a SDS-PAGE. Gels were stained using Coomassie Brilliant Blue (CBB). The expression levels of HlyB and HlyD as well as the expression of intracellular amount of HlyA and HlyAc were determined by Western blots (Supplementary Fig. 8) using polyclonal antibodies against HlyA, HlyB and HlyD, respectively, in combination with an horseradish peroxidase (HRP)-conjugated, secondary antibody using the ECL advance kit (GE Healthcare).

Data processing of the secretion experiments. ImageJ³⁶ was used for processing and determination of the band intensities of the proteins of interest on SDS-PAGE gels. The intensity of the band of purified HlyA and HlyAc signals of the dilution series was used to determine the concentration of the secreted HlyA and HlyAc, respectively. The slope of the plotted HlyA or HlyAc amount represents the amount of secreted HlyA or HlyAc per time. This amount can be divided by the growth factor of the cells in their exponential growing phase. The quotient represents the amount of secreted HlyA or HlyAc per time and cell and can be transformed by the amount of T1SS per cell and the number of amino acids of HlyA or HlyAc to finally yield the secretion rate in number of amino acids per sec and T1SS.

Determination of the amount of T1SS by HlyB Western blot analysis. Cells used in the secretion experiments of HlyA and HlyAc, respectively, were used to determine the number of HlyB molecules per cell. For this purpose, we used cells after 2 h of secretion. Here, cells of the 1 mL aliquot were collected by centrifugation (1 min at 14,000 \times g, 4 °C) and the cell pellet was re-suspended in water to obtain 0.5×10^7 cells/ μ L. 16 μ L of this samples and 4 μ L SDS PAGE buffer was loaded on a SDS-PAGE for subsequent analysis by Western blots analysis as described above. A concentration of purified HlyB ranging from 9 μ g mL^{-1} to 144 ng mL^{-1} was analyzed by Western blot and signal intensities of the HlyB signals were determined using the program ImageJ³⁶. The intensity of purified HlyB signals of the dilution series were used to determine the concentration of expressed HlyB per cell. This number was divided by the number of cells. The calculation resulted in the amount of HlyB per cell. Since the functional unit of HlyB is a dimer, division by two resulted in the total number of T1SS per cell.

Purification of HlyA, HlyAc and HlyB for regression analysis. Purification of HlyA and HlyAc was carried out as previously described^{16,35}. HlyB was purified as described²⁹. The concentration of the purified protein was determined spectrophotometrically (Nanodrop-1000, Thermo Scientific) using the calculated (web.expiry.org/protparam) extinction coefficient at 280 nm.

Functional analysis of HlyA and acylated HlyA. HlyA and acylated HlyA were secreted in the absence or presence of Ca^{2+} (2 mM) and purified as described¹⁶. Intrinsic Trp fluorescence of both proteins was measured at 350 nm and 330 nm, respectively. The excitation wavelength was set to 290 nm, slit width to 5 nm and fluorescence was recorded for 0.5 s. The ratio of both values was used as an indicator of the folding state as described¹⁶. The ratio of the intrinsic Trp fluorescence at 350 nm over 331 of HlyA unfolded in 8 M urea is 0.62 ± 0.05 ¹⁶.

Halo assay of the hemolytic activity of acylated HlyA. Acylated HlyA was secreted in the absence or presence of Ca^{2+} (2 mM). Therefore, 25 mL 2YT medium supplemented with 100 μ g mL^{-1} ampicillin and 30 μ g mL^{-1} kanamycin were inoculated with acylated HlyA secreting cells¹⁶ at an OD_{600} of 0.1. Cultures were grown at 37 °C and 180 rpm. The expression of acylated HlyA, HlyB and HlyD was induced by addition of 1 mM IPTG at an OD_{600} of 0.6–0.8. EGTA, respectively CaCl_2 , were added at this point to adjust the final Ca^{2+} concentration in the culture medium. Cells were grown for 2 h at 180 rpm and 37 °C. After 2 h of secretion, cells were separated by centrifugation (5 min at 14 000 g and 4 °C) and 10 μ L of supernatant was put on the Columbia blood agar plates. Plates were incubated for 2 h at 37 °C and halo formation was observed.

References

- Costa, T. R. *et al.* Secretion systems in Gram-negative bacteria: structural and mechanistic insights. *Nature Rev Microbiol* **13**, 343–359 (2015).
- Delepelaire, P. Type I secretion in gram-negative bacteria. *Biochim Biophys Acta* **1694**, 149–161 (2004).
- Letoffe, S., Ghigo, J. M. & Wandersman, C. Secretion of the *Serratia marcescens* HasA protein by an ABC transporter. *J Bacteriol* **176**, 5372–5377 (1994).

4. Hinsä, S. M., Espinosa-Urgel, M., Ramos, J. L. & O'Toole, G. A. Transition from reversible to irreversible attachment during biofilm formation by *Pseudomonas fluorescens* WCS365 requires an ABC transporter and a large secreted protein. *Mol Microbiol* **49**, 905–918 (2003).
5. Ghigo, J. M. & Wandersman, C. A carboxyl-terminal four-amino acid motif is required for secretion of the metalloprotease PrtG through the *Erwinia chrysanthemi* protease secretion pathway. *J Biol Chem* **269**, 8979–8985 (1994).
6. Jarchau, T., Chakraborty, T., Garcia, F. & Goebel, W. Selection for transport competence of C-terminal polypeptides derived from *Escherichia coli* hemolysin: the shortest peptide capable of autonomous HlyB/HlyD-dependent secretion comprises the C-terminal 62 amino acids of HlyA. *Mol Gen Genetics : MGG* **245**, 53–60 (1994).
7. Koronakis, V., Koronakis, E. & Hughes, C. Isolation and analysis of the C-terminal signal directing export of *Escherichia coli* hemolysin protein across both bacterial membranes. *EMBO J* **8**, 595–605 (1989).
8. Omori, K., Idei, A. & Akatsuka, H. *Serratia* ATP-binding cassette protein exporter, Lip, recognizes a protein region upstream of the C terminus for specific secretion. *J Biol Chem* **276**, 27111–27119 (2001).
9. Sebo, P. & Ladant, D. Repeat sequences in the *Bordetella pertussis* adenylate cyclase toxin can be recognized as alternative carboxy-proximal secretion signals by the *Escherichia coli* alpha-hemolysin translocator. *Mol Microbiol* **9**, 999–1009 (1993).
10. Linhartova, I. *et al.* RTX proteins: a highly diverse family secreted by a common mechanism. *FEMS Microbiol Rev* **34**, 1076–1112 (2010).
11. Lenders, M. H., Reimann, S., Smits, S. H. & Schmitt, L. Molecular insights into type I secretion systems. *Biol Chem* **394**, 1371–1384 (2013).
12. Bakkes, P. J., Jenewein, S., Smits, S. H., Holland, I. B. & Schmitt, L. The rate of folding dictates substrate secretion by the *Escherichia coli* hemolysin type I secretion system. *J Biol Chem* **285**, 40573–40580 (2010).
13. Blenner, M. A., Shur, O., Szilvay, G. R., Cropek, D. M. & Banta, S. Calcium-induced folding of a beta roll motif requires C-terminal entropic stabilization. *J Mol Biol* **400**, 244–256 (2010).
14. Chenal, A., Gujjarro, J. L., Raynal, B., Delepierre, M. & Ladant, D. RTX calcium binding motifs are intrinsically disordered in the absence of calcium: implication for protein secretion. *J Biol Chem* **284**, 1781–1789 (2009).
15. Ostolaza, H., Bartolome, B., Serra, J. L., de la Cruz, F. & Goni, F. M. Alpha-hemolysin from *E. coli*. Purification and self-aggregation properties. *FEBS Lett* **280**, 195–198 (1991).
16. Thomas, S., Bakkes, P. J., Smits, S. H. & Schmitt, L. Equilibrium folding of pro-HlyA from *Escherichia coli* reveals a stable calcium ion dependent folding intermediate. *Biochim Biophys Acta* **1844**, 1500–1510 (2014).
17. Jones, H. E., Holland, I. B., Baker, H. L. & Campbell, A. K. Slow changes in cytosolic free Ca^{2+} in *Escherichia coli* highlight two putative influx mechanisms in response to changes in extracellular calcium. *Cell Calcium* **25**, 265–274 (1999).
18. Thomas, S., Holland, I. B. & Schmitt, L. The Type I secretion pathway-The hemolysin system and beyond. *Biochim Biophys Acta* **1621–1649** (2014).
19. Bumba, L. *et al.* Calcium-Driven Folding of RTX Domain beta-Rolls Ratchets Translocation of RTX Proteins through Type I Secretion Ducts. *Mol Cell* **62**, 47–62 (2016).
20. Lenders, M. H., Weidtkamp-Peters, S., Kleinschrodt, D., Jaeger, K. E., Smits, S. H. & Schmitt, L. Directionality of substrate translocation of the hemolysin A Type I secretion system. *Sci Reports* **5**, 12470 (2015).
21. Thanabalu, T., Koronakis, E., Hughes, C. & Koronakis, V. Substrate-induced assembly of a contiguous channel for protein export from *E. coli*: reversible bridging of an inner-membrane translocase to an outer membrane exit pore. *EMBO J* **17**, 6487–6496 (1998).
22. Koronakis, V., Hughes, C. & Koronakis, E. Energetically distinct early and late stages of HlyB/HlyD-dependent secretion across both *Escherichia coli* membranes. *EMBO J* **10**, 3263–3272 (1991).
23. Schlumberger, M. C. *et al.* Real-time imaging of type III secretion: *Salmonella* SipA injection into host cells. *Proc Natl Acad Sci USA* **102**, 12548–12553 (2005).
24. Robson, A., Gold, V. A., Hodson, S., Clarke, A. R. & Collinson, I. Energy transduction in protein transport and the ATP hydrolytic cycle of SecA. *Proc Natl Acad Sci USA* **106**, 5111–5116 (2009).
25. Schiebel, E., Driessen, A. J., Hartl, F. U. & Wickner, W. Delta mu H⁺ and ATP function at different steps of the catalytic cycle of preprotein translocase. *Cell* **64**, 927–939 (1991).
26. Uchida, K., Mori, H. & Mizushima, S. Stepwise movement of preproteins in the process of translocation across the cytoplasmic membrane of *Escherichia coli*. *J Biol Chem* **270**, 30862–30868 (1995).
27. Zaitseva, J., Jenewein, S., Jumpertz, T., Holland, I. B. & Schmitt, L. H662 is the linchpin of ATP hydrolysis in the nucleotide-binding domain of the ABC transporter HlyB. *EMBO J* **24**, 1901–1910 (2005).
28. Nicaud, J. M., Mackman, N., Gray, L. & Holland, I. B. The C-terminal, 23 kDa peptide of *E. coli* hemolysin 2001 contains all the information necessary for its secretion by the haemolysin (Hly) export machinery. *FEBS Lett* **204**, 331–335 (1986).
29. Reimann, S., Poschmann, G., Kanonenberg, K., Stuhler, K., Smits, S. H. & Schmitt, L. Interdomain regulation of the ATPase activity of the ABC transporter hemolysin B from *E. coli*. *Biochem J* (2016).
30. Fulle, S. & Gohlke, H. Statics of the ribosomal exit tunnel: implications for cotranslational peptide folding, elongation regulation, and antibiotics binding. *J Mol Biol* **387**, 502–517 (2009).
31. Locher, K. P. Review. Structure and mechanism of ATP-binding cassette transporters. *Philos Trans R Soc Lond B Biol Sci* **364**, 239–245 (2009).
32. Diepold, A. & Armitage, J. P. Type III secretion systems: the bacterial flagellum and the injectisome. *Philos Trans R Soc Lond B Biol Sci* **370**, (2015).
33. Rhodes, C. R. *et al.* Structural consequences of divalent metal binding by the adenylate cyclase toxin of *Bordetella pertussis*. *Arch Biochem Biophys* **395**, 169–176 (2001).
34. Rose, T., Sebo, P., Bellalou, J. & Ladant, D. Interaction of calcium with *Bordetella pertussis* adenylate cyclase toxin. Characterization of multiple calcium-binding sites and calcium-induced conformational changes. *J Biol Chem* **270**, 26370–26376 (1995).
35. Lecher, J., Schwarz, C. K., Stoldt, M., Smits, S. H., Willbold, D., Schmitt, L. & An, R. T. X. transporter tethers its unfolded substrate during secretion via a unique N-terminal domain. *Structure* **20**, 1778–1787 (2012).
36. Schneider, C. A., Rasband, W. S. & Eliceiri, K. W. NIH Image to ImageJ: 25 years of image analysis. *Nature Meth* **9**, 671–675 (2012).

Acknowledgements

We thank Iris Fey, Protein Production Facility, Heinrich Heine University, for technical support. We are also indebted to Martin Prescher, Sven Reimann, Sandra Peherstorfer and Kerstin Kanonenberg for providing us with the purified proteins HlyB, HlyA and HlyAc, which were used as standard. We thank all members of the Institute of Biochemistry, Heinrich Heine University Düsseldorf, for helpful and very fruitful discussions. We especially acknowledge the fruitful discussion with Prof. Karl-Erich Jaeger and the excellent support of CAi (Center of advanced imaging at HHU). This work was supported by the Bioeconomy Science Center (boost fund BioBreak to L.S.) and in part by the DFG (CRC 1208, project A01 to L.S.).

Author Contributions

M.H.H.L. and T.B. performed the experiments, M.H.H.L., T.B., S.H.J.S. and L.S. designed the experiments, M.H.H.L., T.B., S.H.J.S. and L.S. evaluated the data and M.H.H.L., S.H.J.S. and L.S. wrote the manuscript.

Additional Information

Supplementary information accompanies this paper at <http://www.nature.com/srep>

Competing financial interests: The authors declare no competing financial interests.

How to cite this article: Lenders, M. H. H. *et al.* *In vivo* quantification of the secretion rates of the hemolysin A Type I secretion system. *Sci. Rep.* **6**, 33275; doi: 10.1038/srep33275 (2016).



This work is licensed under a Creative Commons Attribution 4.0 International License. The images or other third party material in this article are included in the article's Creative Commons license, unless indicated otherwise in the credit line; if the material is not included under the Creative Commons license, users will need to obtain permission from the license holder to reproduce the material. To view a copy of this license, visit <http://creativecommons.org/licenses/by/4.0/>

© The Author(s) 2016

Supplementary

***In vivo* quantification of the secretion rates of the
hemolysin A Type I secretion system**

Michael H. H. Lenders¹, Tobias Beer¹, Sander H. J. Smits¹ and Lutz Schmitt^{1*}

¹Institute of Biochemistry, Heinrich-Heine-Universitaet, 40225 Duesseldorf, Germany

*To whom correspondence should be addressed:

Lutz.Schmitt@hhu.de

Tel. +49 211 81-10773

Fax +49 211 81-15310

UniversitaetsstraÙe 1

40225 Duesseldorf

Germany

Figures legends

Supplementary Figure 1

Regression analysis of Cy3 fluorescence of the two (a, b) Cy3-labeled secondary antibodies in solution. The insets show the data at low antibody concentrations.

Supplementary Figure 2

Integrated area of Western blot signals of purified HlyB at different concentrations of HlyB.

Supplementary Figure 3

Secretion level of HlyA in the presence of different extracellular Ca^{2+} concentration. SDS-PAGE analysis of the HlyA secretion level in the culture supernatant over a four-hour time period. (a) SDS-PAGE of purified HlyA at different concentrations. The concentrations are indicated above the gel. (b) Evaluation of the band intensities of HlyA of the SDS PAGE analysis at 5mM Ca^{2+} (black line) and evaluation of the number of cells (blue line) present during the duration of the secretion experiment. (c) SDS-PAGEs show the HlyA secretion levels after every hour. Different extracellular Ca^{2+} concentrations are indicated above the gels. Bar diagrams below the SDS-PAGEs show the relative intensity of the SDS-PAGE bands. Bands are normalized on the highest mean value of secreted HlyA at a particular Ca^{2+} concentration after 4 h secretion time. Error bars represent the standard deviation of at least three biological replicates.

Supplementary Figure 4

Secretion level of HlyAc in the presence of different extracellular Ca^{2+} concentration. SDS-PAGE analysis of the HlyAc secretion level in the culture supernatant over a four-hour time period. (a) SDS-PAGE of purified HlyAc at different concentrations. The concentrations are indicated above the gel. (b) Evaluation of the band intensities of HlyAc of the SDS PAGE analysis at 5mM Ca^{2+} (black line) and evaluation of the number of cells (blue line) present during the duration of the secretion experiment. (c) SDS-PAGEs show the HlyAc secretion level after every hour. Different extracellular Ca^{2+} concentrations are indicated above the gels. Bar diagrams below the SDS-PAGEs show the relative intensity of the SDS-PAGE bands. Bands are normalized on the highest mean value of secreted HlyAc at a particular Ca^{2+} concentration after 4 h secretion time. Error bars represent the standard deviation of at least three biological replicates.

Supplementary Figure 5

(a) Relative cell fluorescence of eGFP. All values were normalized to the eGFP fluorescence of the eGFP-HlyA fusion protein (error bars represent the standard error of the mean of at least three independent experiments). (b) Relative fluorescence of a the secondary Cy3-coupled antibody. All values were normalized to the Cy3 fluorescence of the eGFP-HlyA fusion protein (error bars represent the standard error of the mean of at least three independent experiments). The different combinations of proteins are indicated below the bar plots.

Supplementary Figure 6

Halo assay of the hemolytic activity of acylated HlyA on Columbia blood agar plates. Acylated HlyA was secreted in the absence (left panel) and 2 mM Ca^{2+} (right panel). After 2 h of secretion, cells were separated by centrifugation, 10 μl of supernatant was

put on the agar plates and plates were incubated for 2h at 37 °C (for further details see Materials and Methods).

Supplementary Figure 7

Plasmid map pK184-HlyB-H662A-HlyD

Supplementary Figure 8

Western blot analysis of cell content after 2 h of secretion at different Ca^{2+} concentrations. HlyA, HlyAc, HlyB and HlyD, respectively, are only detected if their expression was induced. Their total amount of the proteins remains constant during the time period of the secretion experiments performed in the presence of different Ca^{2+} concentration.

Tables

Supplementary Table 1

Mean value of transporter

	Transporter
by fluorescence (antibody 1)	4509 ± 1061
by fluorescence (antibody 2)	4554 ± 1616
by fluorescence (average)	4532 ± 966
by western blot	5355 ± 483

Supplementary Table 2

Calculation of HlyA transport rates at different Ca²⁺ concentration

Condition	#	Secreted HlyA after		Secreted HlyA [mol min ⁻¹]	Cell growth [cells min ⁻¹]	Rate by fluorescence [aa T1SS ⁻¹ s ⁻¹]
		2h [pmol]	4h [pmol]			
0.00mM CaCl ₂	1	5.2	9.9	7.46 ± 0.72	1.04 ± 0.09	16.3 ± 4.1
	2	4.4	8.0			
0.05mM CaCl ₂	1	6.8	17	8.93 ± 0.22	1.22 ± 0.09	16.6 ± 3.8
	2	6.4	17			
	3	6.1	16			
0.10mM CaCl ₂	1	5.5	18	10.9 ± 0.80	1.33 ± 0.08	18.5 ± 4.3
	2	5.5	21			
0.15mM CaCl ₂	1	9.6	28	12.6 ± 1.42	1.89 ± 0.14	15.2 ± 3.8
	2	7.5	20			
0.25mM CaCl ₂	1	6.3	20	10.3 ± 0.51	1.53 ± 0.04	15.2 ± 3.4
	2	5.1	21			
	3	6.5	19			
0.45mM CaCl ₂	1	7.9	21	10.4 ± 0.54	1.57 ± 0.06	15.1 ± 3.4
	2	7.2	22			
	3	7.4	17			
0.65mM CaCl ₂	1	5.8	18	10.8 ± 0.69	1.44 ± 0.08	17.1 ± 3.9
	2	6.1	21			
	3	8.2	23			
5.00mM CaCl ₂	1	9.6	25	12.8 ± 0.16	2.03 ± 0.08	14.3 ± 3.1
	2	9.7	24			
	3	9.3	25			

Supplementary Table 3

Calculation of HlyAc transport rates at different Ca²⁺ concentration

Condition	#	Secreted HlyA after		Secreted HlyA [mol min ⁻¹]	Cell growth [cells min ⁻¹]	Rate by fluorescence [aa T1SS ⁻¹ s ⁻¹]
		2h [pmol]	4h [pmol]			
0.00mM CaCl ₂	1	54	70	38.5 ± 6.85	1.18 ± 0.12	15.8 ± 4.6
	2	47	44			
	3	37	45			
0.05mM CaCl ₂	1	50	65	52.2 ± 5.12	1.46 ± 0.06	17.3 ± 4.1
	2	40	56			
	3	36	46			
0.10mM CaCl ₂	1	44	69	53.1 ± 3.38	1.44 ± 0.06	17.9 ± 4.1
	2	43	62			
	3	49	71			
0.15mM CaCl ₂	1	39	55	48.4 ± 3.24	1.46 ± 0.06	16.0 ± 3.6
	2	43	100			
	3	34	88			
0.25mM CaCl ₂	1	47	110	53.9 ± 2.95	1.49 ± 0.09	17.5 ± 4.0
	2	60	120			
	3	60	110			
0.45mM CaCl ₂	1	41	95	42.6 ± 1.96	1.51 ± 0.05	13.7 ± 3.0
	2	36	84			
	3	27	80			
0.65mM CaCl ₂	1	54	130	54.9 ± 5.58	1.52 ± 0.08	17.5 ± 4.2
	2	38	100			
5.00mM CaCl ₂	1	44	110	50.4 ± 1.71	1.42 ± 0.11	17.2 ± 3.9
	2	37	96			
	3	44	98			

Supplementary Table 4

Primers used in this study

Name	Sequence
H662A_5for_B-NBD	5' -CGGTTATAATCATTGCTGCGCGTCTGTCTACAGTAA-3'
H662A_3rev_B-NBD	5' -TTACTGTAGACAGACGCGCAGCAATGATTATAACCG-3'

Supplementary Table 5

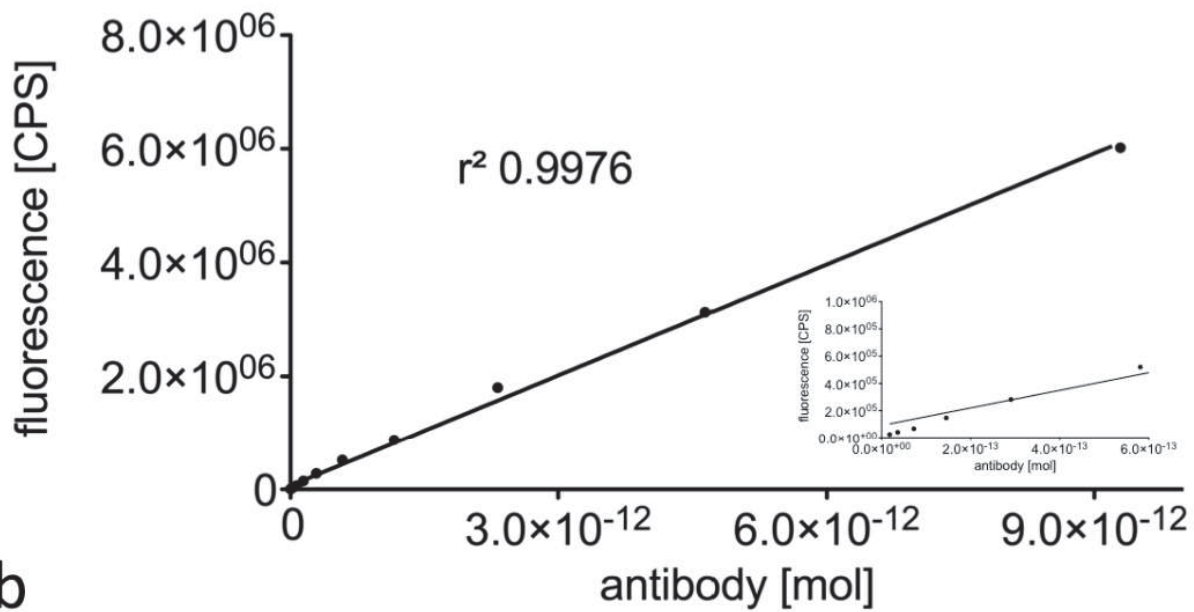
Plasmids used in this study

Name	Description	Reference
pK184-HlyB	Plasmid encoding <i>hlyB</i> and <i>hlyD</i>	1
pK184-HlyB-H662A-HlyD	Plasmid pK184-HlyB with a base pair substitution to generate <i>hlyB-H662A</i> via site-directed mutagenesis; encodes for <i>hlyB-H662A</i> and <i>hlyD</i>	This study
pSU- <i>hlyA</i>	Plasmid encoding <i>hlyA</i>	2
pSU- <i>hlyA1</i>	Plasmid encoding <i>hlyAc</i>	3
pSOI-eGFP-HlyAc	Plasmid encoding <i>eGFP-hlyAc</i>	4
pSOI-eGFP-HlyA	Plasmid encoding <i>eGFP-hlyA</i>	4

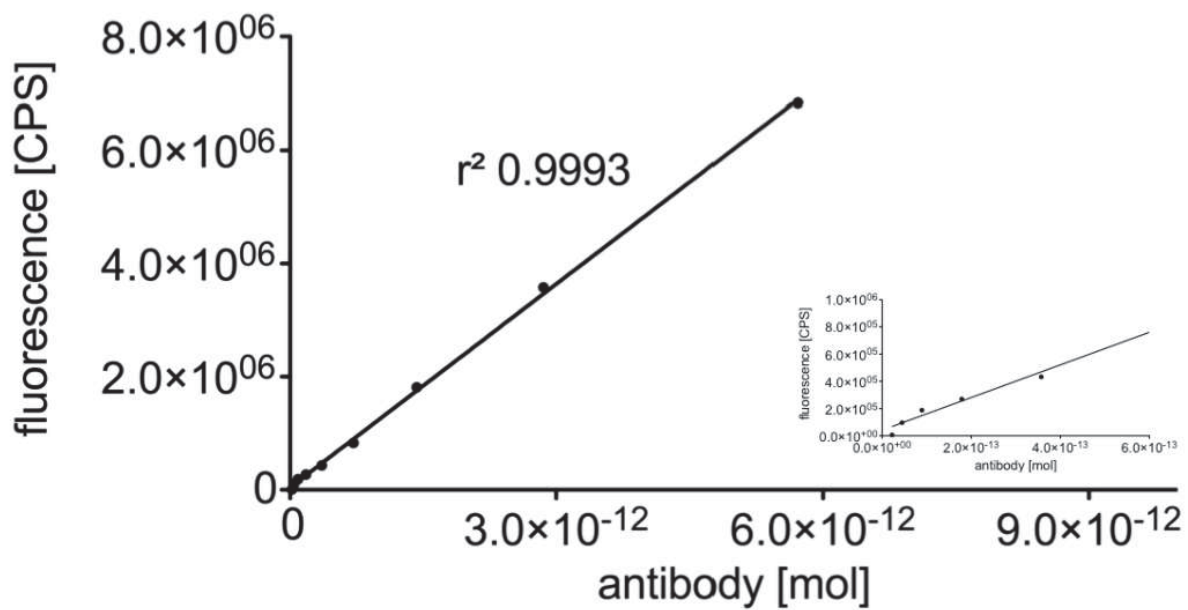
References

1. Bakkes PJ, Jenewein S, Smits SH, Holland IB, Schmitt L. The rate of folding dictates substrate secretion by the Escherichia coli hemolysin type 1 secretion system. *J Biol Chem* **285**, 40573-40580 (2010).
2. Thomas S, Bakkes PJ, Smits SH, Schmitt L. Equilibrium folding of pro-HlyA from Escherichia coli reveals a stable calcium ion dependent folding intermediate. *Biochim Biophys Acta* **1844**, 1500-1510 (2014).
3. Lecher J, Schwarz CK, Stoldt M, Smits SH, Willbold D, Schmitt L. An RTX transporter tethers its unfolded substrate during secretion via a unique N-terminal domain. *Structure* **20**, 1778-1787 (2012).
4. Lenders MH, Weidtkamp-Peters S, Kleinschrodt D, Jaeger KE, Smits SH, Schmitt L. Directionality of substrate translocation of the hemolysin A Type I secretion system. *Sci Rep* **5**, 12470 (2015).

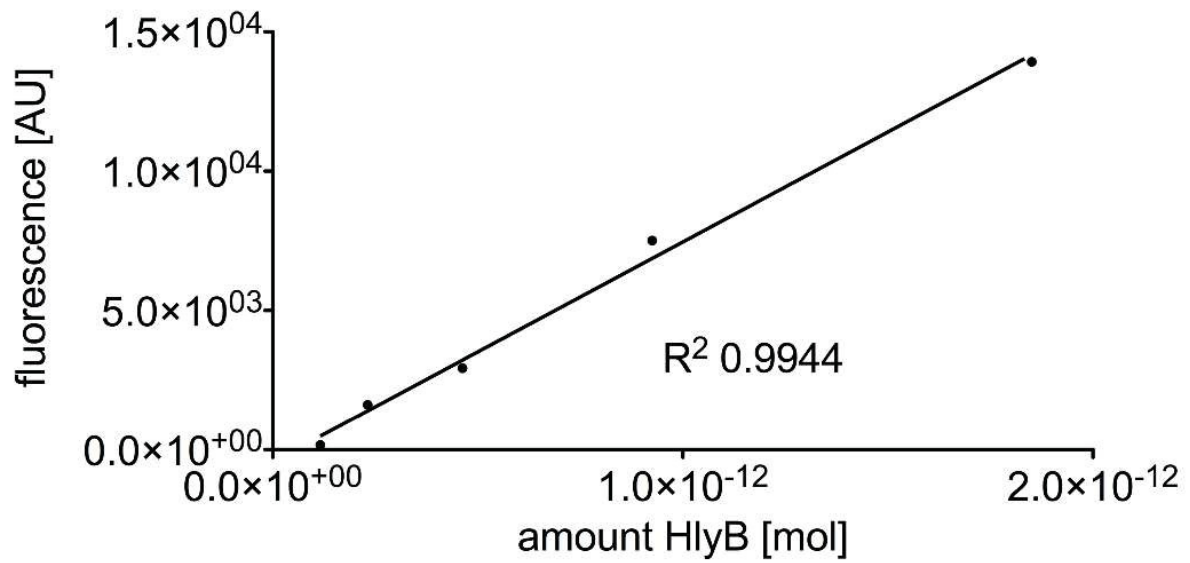
a



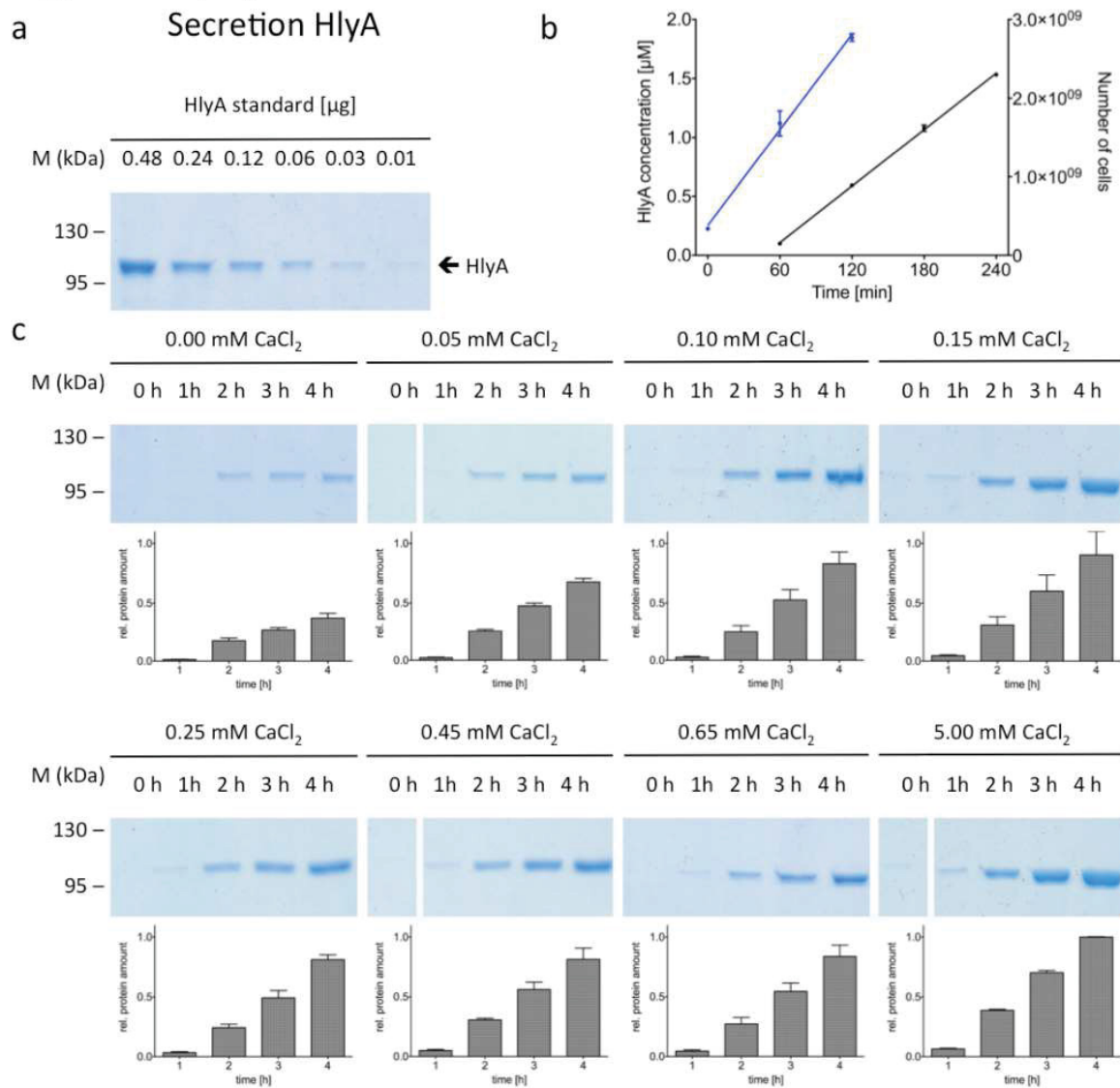
b



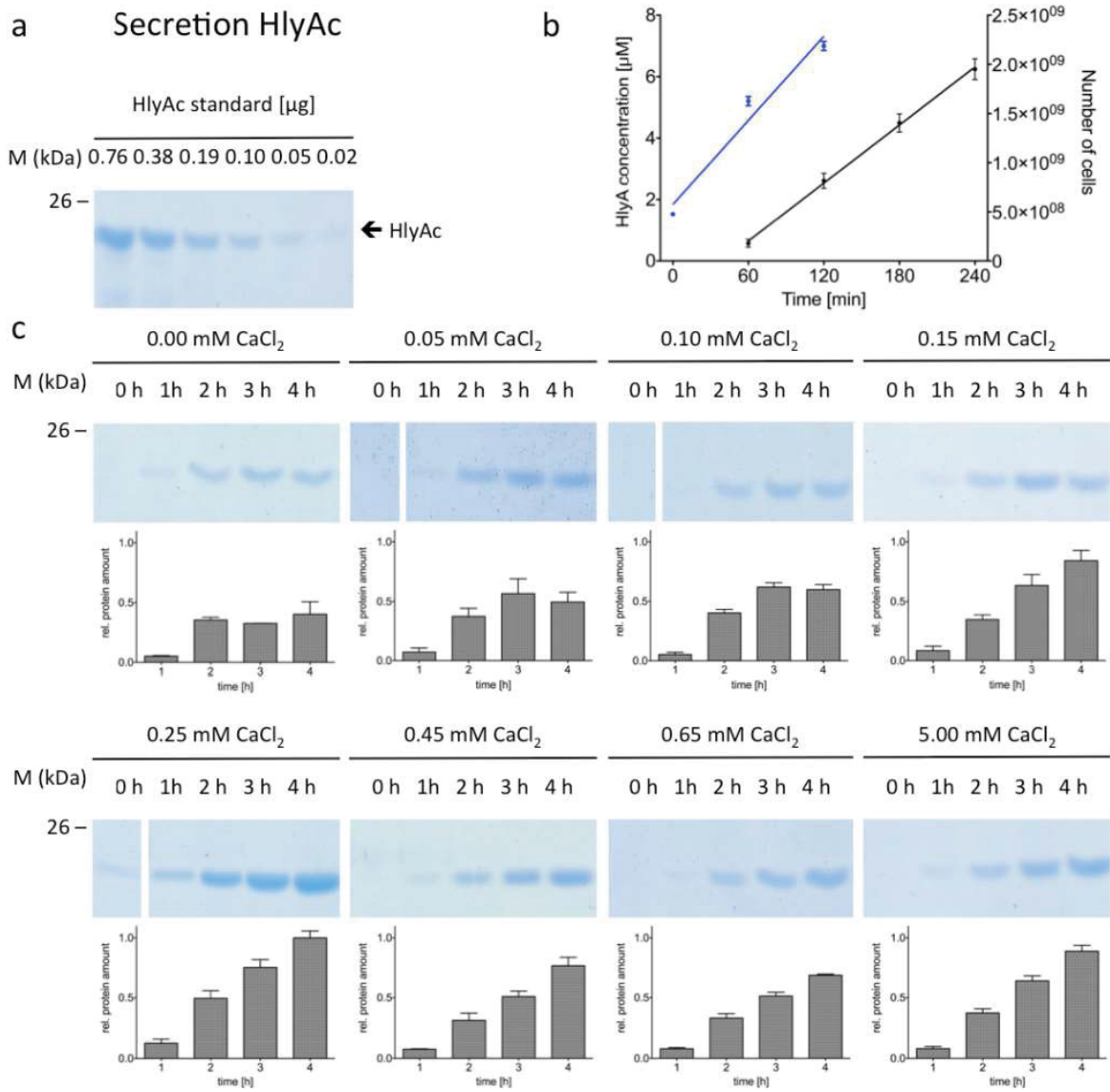
Supplementary Fig. 1



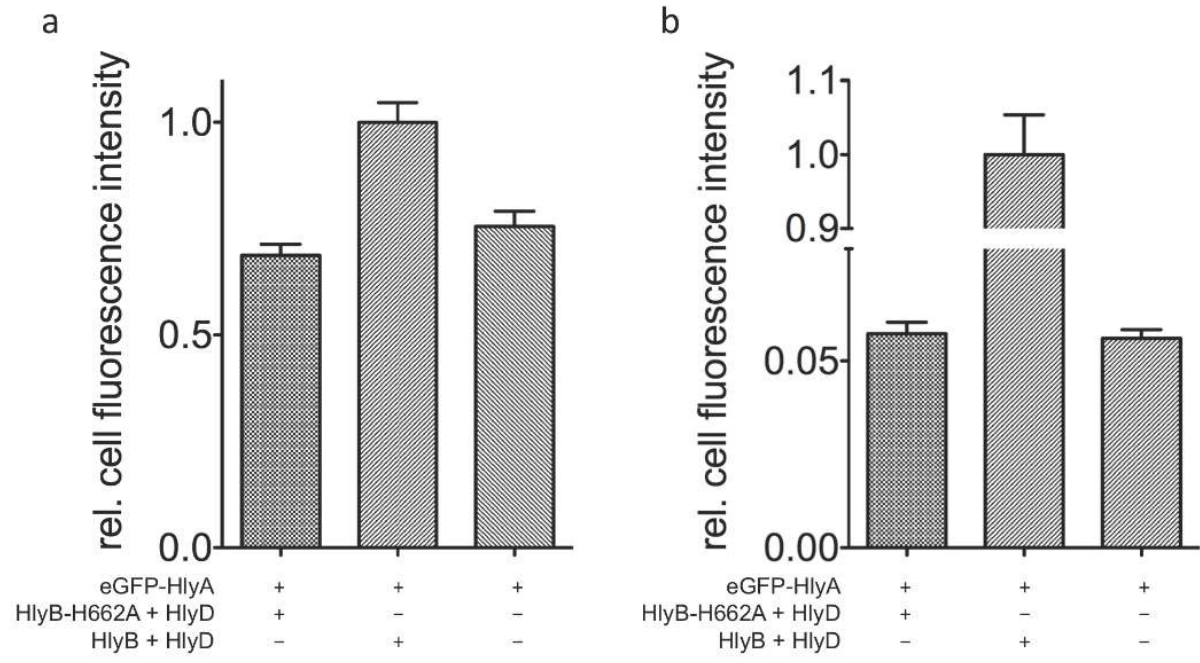
Supplementary Fig. 2



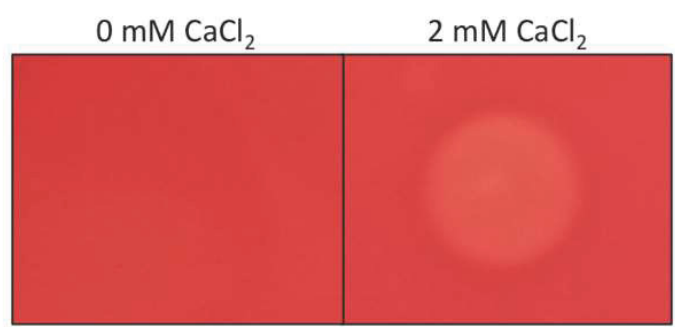
Supplementary Fig. 3



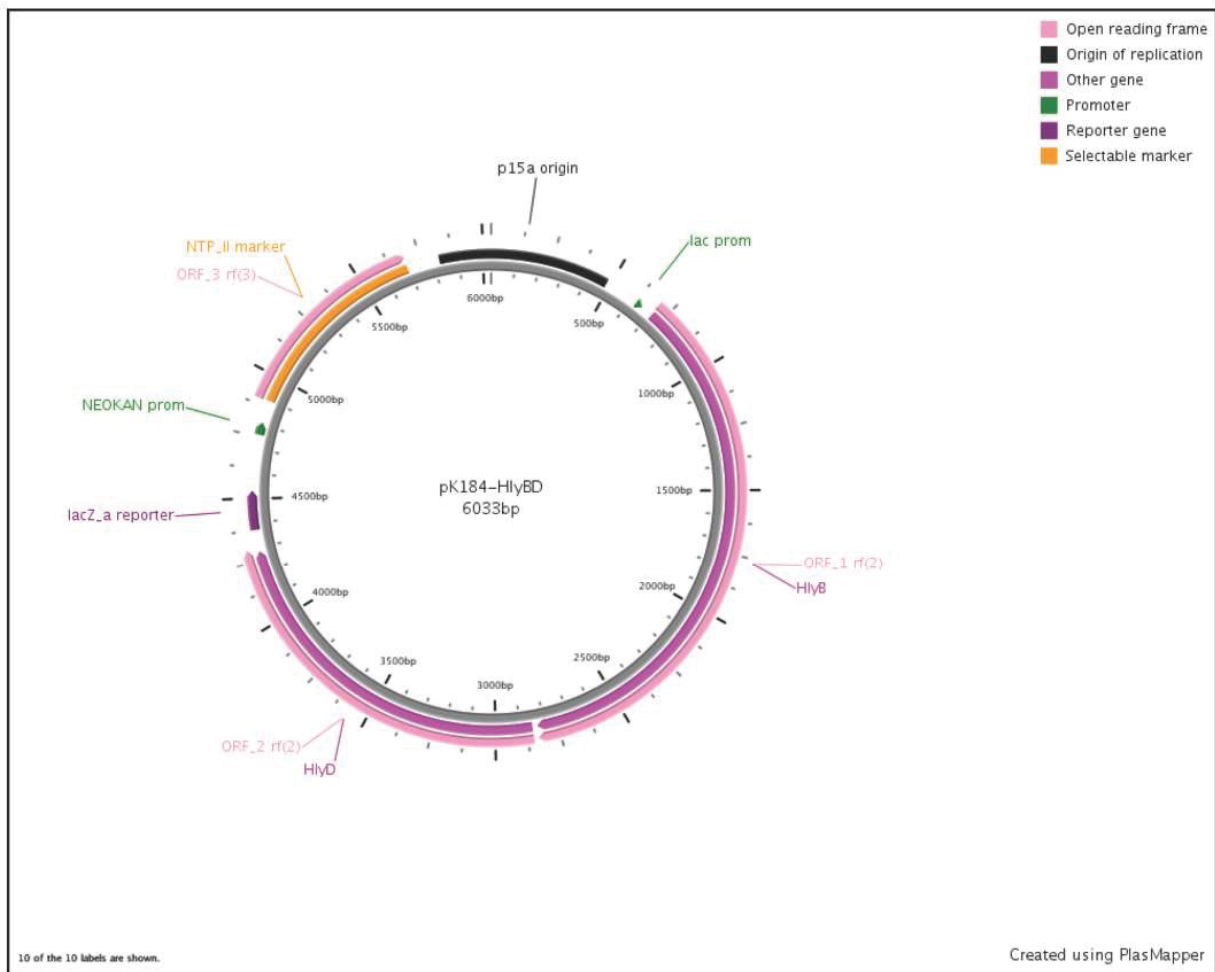
Supplementary Fig. 4



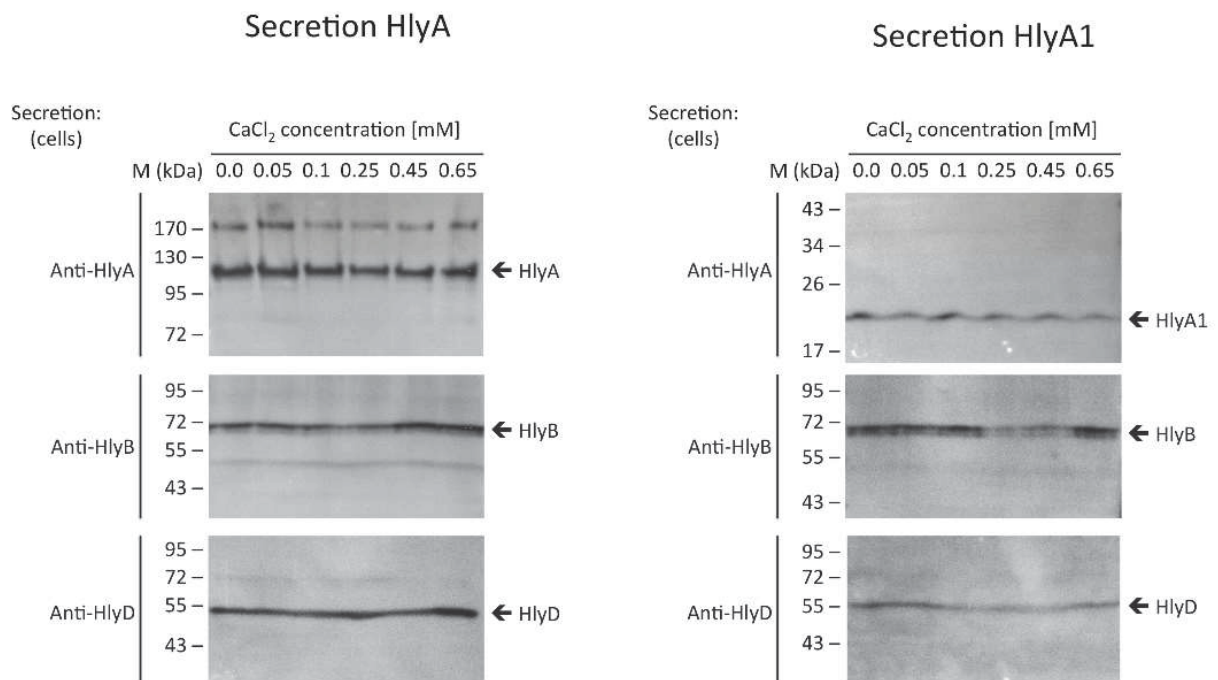
Supplementary Fig. 5



Supplementary Fig. 6



Supplementary Fig. 7



Supplementary Fig. 8

3.2 Chapter II – Type I secretion system – it takes three and a substrate

Title Type I secretion system – it takes three and a substrate
Author Kerstin Kanonenberg. Olivia Spitz. Isabelle N. Erenburg. Tobias Beer. Lutz, Schmitt.

Published in *FEMS Microbiology Letters* (2018)

Impact Factor 1.735

Own proportion of this work 15 %;

Writing of the manuscript

MINIREVIEW – Physiology & Biochemistry

Type I secretion system—it takes three and a substrate

Kerstin Kanonenberg, Olivia Spitz, Isabelle N. Erenburg, Tobias Beer and Lutz Schmitt*

Institute of Biochemistry, Heinrich Heine University, 40225 Düsseldorf, Germany

*Corresponding author: Institute of Biochemistry, Heinrich Heine University, Düsseldorf, Universitätsstr 1, 40225 Düsseldorf, Germany.

Tel: +49-211-81-10773; Fax: +49-211-81-15310; E-mail: lutz.schmitt@hhu.de

One sentence summary: An overview of type I secretion systems of Gram-negative bacteria and a summary of the recent developments is provided.

Editor: Lily Karamanou

ABSTRACT

Type I secretion systems are widespread in Gram-negative bacteria and mediate the one-step translocation of a large variety of proteins serving for diverse purposes, including nutrient acquisition or bacterial virulence. Common to most substrates of type I secretion systems is the presence of a C-terminal secretion sequence that is not cleaved during or after translocation. Furthermore, these protein secretion nanomachineries are always composed of an ABC transporter, a membrane fusion protein, both located in the inner bacterial membrane, and a protein of the outer membrane. These three membrane proteins transiently form a ‘tunnel channel’ across the periplasmic space in the presence of the substrate. Here we summarize the recent findings with respect to structure, function and application of type I secretion systems.

Keywords: protein secretion; ABC transporter; secretion sequence; RTX toxin

INTRODUCTION

Bacteria have a need for secreting a variety of proteins and other molecules to the extracellular space, for nutrient acquisition (e.g. iron-scavenger proteins), biofilm formation (adhesins) or host invasion (virulence factors, e.g. exotoxins).

Secretory pathways have been of major research interest over the past decades and depending on the definition applied, a minimum of 15 different secretion systems has been identified so far in Gram-negative bacteria (reviewed in Costa *et al.* 2015). Here, the outer membrane imposes an additional problem as secreted macromolecules have to cross a second, the outer membrane. These secretion systems are capable of exporting a diverse range of small molecules, DNA and proteins to the extracellular space or even directly into the cytosol of a target cell. They vary greatly in composition and molecular mechanism, but can be easily divided into two major subgroups based on the presence or absence of a periplasmic transport intermediate during the secretion process.

Type I, III and IV secretion systems are double-membrane-spanning export machineries where the substrate is secreted in

one step from the cytosol to the extracellular space (type I). The latter two are even capable of delivering their substrate directly into the cytosol of the target cell, thus traversing three membranes (Fig. 1). Obviously, all these secretion systems require a ‘tunnel channel’-like architecture, composed of a minimum of 3 but up to more than 10 membrane-localized proteins (Fig. 1). For further information, the reader is referred to Economou and Dalbey (2014) and Costa *et al.* (2015) for a review series covering the details of most bacterial secretion systems.

This review highlights the recent advances in research concerning specifically type I secretion systems (TISS), setting the focus mainly on new structural insights that have been obtained over the last years. TISS are often referred to as the most ‘simple’ representative considering that they are composed of only three membrane proteins (also see Delepelaire 2004; Kanonenberg, Schwarz and Schmitt 2013; Thomas, Holland and Schmitt 2014; Holland *et al.* 2016 for various aspects of TISS).

Many Gram-negative pathogens make use of TISS to secrete a great variety of virulence factors. The discovery of the first TISS substrate dates back to as far as 1979 when the Goebel

Received: 6 February 2018; Accepted: 9 April 2018

© FEMS 2018. All rights reserved. For permissions, please e-mail: journals.permissions@oup.com

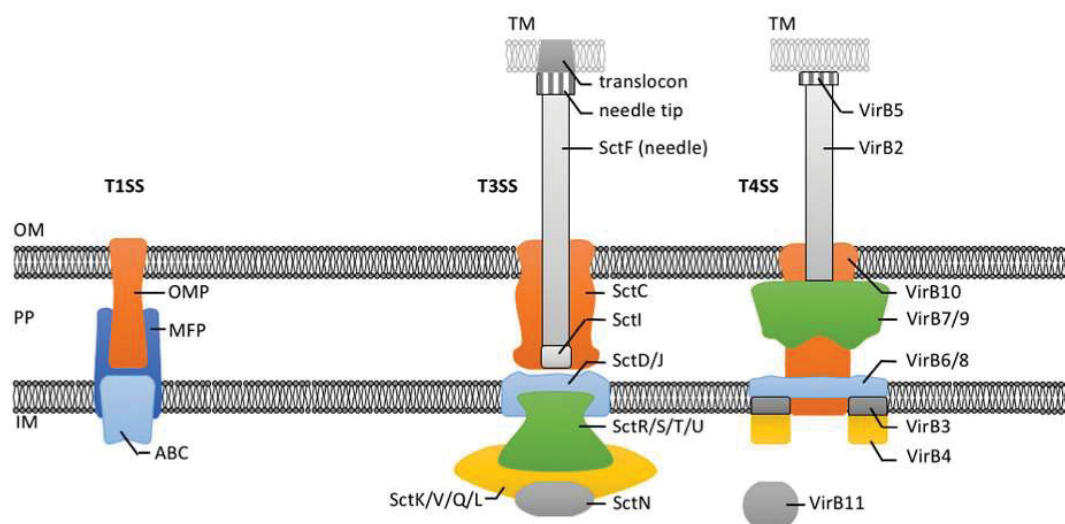


Figure 1. Cartoon of secretion systems from Gram-negative bacteria that translocate their substrates in one step across two (T1SS) or three membranes (T3SS and T4SS). OM: outer membrane, PP: periplasm, IM: inner membrane, OMP: outer membrane protein, MFP: membrane fusion protein, ABC: ABC transporter. Proteins forming the T3SS and T4SS and their putative location are indicated.

laboratory identified hemolysin A (HlyA), named after its ability to lyse erythrocytes from uropathogenic *Escherichia coli* strains (Noegel *et al.* 1979). Subsequently, the nucleotide sequence of HlyA was determined (Felmlee, Pellett and Welch 1985). Additional studies from the laboratories of Koronakis, Holland and Goebel (Mackman and Holland 1984; Mackman *et al.* 1985a,b, 1987; Gray *et al.* 1986, 1989; Felmlee and Welch 1988; Koronakis, Koronakis and Hughes 1989; Gentschev, Hless and Goebel 1990; Chervaux *et al.* 1995) demonstrated that secretion of HlyA occurred without any periplasmic intermediate and was Sec independent. Moreover, HlyA carried a C-terminal secretion signal indicating an unknown secretion mechanism.

The analysis of the sequence of the *hly* operon (Felmlee, Pellett and Welch 1985) revealed the presence of two additional membrane proteins and a third component in addition to the substrate HlyA. The third component, HlyC, turned out to be essential for the activation of HlyA, but not for secretion per se (Nicaud *et al.* 1985). HlyC was shown to act as a cytosolic acyltransferase acylating two internal lysine residues of the unfolded HlyA prior to secretion. This required equimolar amounts of the acyl carrier protein (Issartel, Koronakis and Hughes 1991; Stanley, Koronakis and Hughes 1991; Stanley *et al.* 1994, 1999; Thomas, Smits and Schmitt 2014). Only recently, the crystal structure of an HlyC homolog was reported (Greene *et al.* 2015) that will open up new approaches to understand the function of this unusual acyltransferase at the molecular level.

HlyD, one of the membrane proteins encoded by the *hly* operon, belongs to the family of bacterial membrane fusion proteins (MFPs) (Symmons, Marshall and Bavro 2015) that is unique to Gram-negative bacteria. The second membrane protein, HlyB, is a member of the ABC transporter family (Davidson *et al.* 2008), which is found in all kingdoms of life. Since HlyB and HlyD were localized to the inner membrane (Mackman *et al.* 1985a,b; Wang *et al.* 1991; Pimenta *et al.* 1999), the lack of periplasmic intermediates raised an obvious question—How does HlyA reach the extracellular space? This issue was addressed by the Wandersman group, who identified TolC, a ubiquitous and polyvalent outer membrane protein, as the missing, third component of the HlyA-T1SS (Wandersman and Delepelaire 1990). A complex of the two inner membrane proteins and TolC form the ‘tunnel

channel’ that allows the one-step secretion of HlyA. Apart from T1SS, TolC is involved in the extrusion of toxic components (Koronakis, Eswaran and Hughes 2004), for example by being part of tripartite drug efflux systems such as the AcrA-AcrB/TolC complex (Du *et al.* 2014).

In other T1SS, more than one transport substrate (Letoffe, Delepelaire and Wandersman 1990) or the TolC homolog (Letoffe, Ghigo and Wandersman 1994) can be encoded in the operon. Thus, there are no strict requirements on the genetic level for the operon organization of T1SS, but several lines of evidence suggest that a minimal unit composed of the gene coding for the transport substrate, the ABC transporter and the MFP is present in all operons. In addition, some degree of promiscuity with respect to the transported substrate exists, since the Hly system of *E. coli* was successfully used to secrete, for example, CyaA from *Bordetella pertussis* (Masure *et al.* 1990; Sebo and Ladant 1993), FrpA from *Neisseria meningitidis* (Thompson and Sparling 1993) or PaxA from *Pasteurella aerogenes* (Kuhnert *et al.* 2000).

T1SS SUBSTRATES

For the vast majority of T1SS substrates, all the information necessary and sufficient for secretion is encoded in the extreme C-terminus, which is not cleaved during or after translocation. This was recognized early on (Gray *et al.* 1986) and was one of the first indications that HlyA was secreted independently of the Sec system. However, a small group of substrates (class II microcins) contain an N-terminal propeptide, which is cleaved by a C39 peptidase domain on the ABC transporter prior to secretion (Hwang, Zhong and Tai 1997).

The actual secretion signal of the Hly system was shown to be confined to the last 50 to 60 most extreme C-terminal amino acids (Koronakis, Koronakis and Hughes 1989) but its size and nature varies from system to system. The reader is referred to a review (Holland *et al.* 2016), which summarizes our current knowledge on T1SS secretion signals, still leaving many unanswered questions that need to be addressed in future research.

Upstream to the secretion sequence of HlyA, aspartate and glycine-rich nonapeptide repeats were identified (Welch 1991).

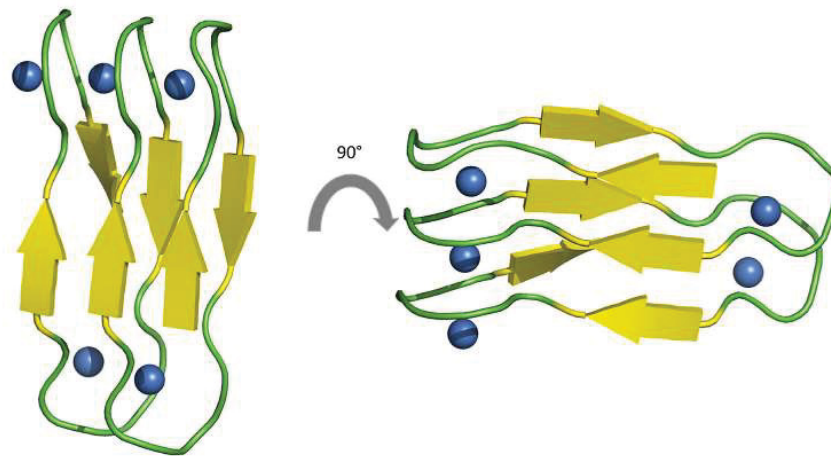


Figure 2. A zoom into the β -roll motif of an alkaline protease (Baumann *et al.* 1993). Ca^{2+} ions and the Ca^{2+} binding region are shown as blue spheres and in cartoon representation, respectively.

These have the consensus sequence GGXGXDXUX (where X can be any amino acid and U is a large hydrophobic amino acid) and the term ‘GG repeats’ or ‘repeats-in-toxins’ (RTX) was coined by Rod Welch. These repeats form the hallmark of an entire family of proteins including lipases, proteases, adhesins, S-layer proteins or toxins (reviewed by Linhartova *et al.* 2010).

Structural studies on the TISS-secreted alkaline protease from *Pseudomonas aeruginosa* (Baumann *et al.* 1993) and other substrates (Baumann *et al.* 1993; Izadi-Pruneyre *et al.* 1999; Meier *et al.* 2007; Griessl *et al.* 2013) revealed that the coordination of one Ca^{2+} by two RTX motifs via the side chains of the aspartate residues and the backbone of the first two glycine residues creates a so-called β -roll or β -helix motif (Fig. 2).

RTX substrates of TISS bind Ca^{2+} ions in the high micromolar range, for example $\sim 500 \mu\text{M}$ for CyaA from *Bordetella pertussis* (Chenal *et al.* 2009; Sotomayor Perez *et al.* 2015) or $\sim 150 \mu\text{M}$ for HlyA from *E. coli* (Ostolaza, Soloaga and Goni 1995; Sanchez-Magraner *et al.* 2007; Thomas *et al.* 2014). This binding induces folding of the entire RTX protein. As the concentration of free Ca^{2+} ions in the bacterial cytosol is in the high nanomolar range (Jones *et al.* 1999), RTX proteins remain unfolded until they reach the extracellular space, where Ca^{2+} concentrations of up to 10 mM result in immediate binding and protein folding.

The N-terminal moiety of TISS substrates encodes for functionality, i.e. lipolytic, hemolytic, proteolytic, adhesive or any other activity. A recent data mining approach of 840 bacterial genome sequences (Linhartova *et al.* 2010) identified ~ 1000 RTX proteins, being extremely variable in size (up to 900 kDa, Hinsa *et al.* 2003) and function, but conforming to the general arrangement of TISS substrates, functional domain/RTX domain/secretion sequence. The number of RTX domains in an individual RTX-protein scales to some extent with the molecular weight (Linhartova *et al.* 2010), but the presence of these characteristic motifs is ubiquitous and highlights their functional importance.

The iron siderophore HasA from *Serratia marcescens* represents an exception (Letroffe, Ghigo and Wandersman 1994). With a size of 19 kDa it is the smallest substrate of a TISS identified so far and interestingly lacks the entire RTX domain, but contains a C-terminal secretion sequence (Izadi-Pruneyre *et al.* 1999). Interestingly, it is the only TISS substrate known which requires a chaperone, SecB, for secretion (Sapriel, Wandersman and Delepelaire 2002; Bakkes *et al.* 2010).

FUNCTIONAL INSIGHTS

Early on, Koronakis and coworkers (Thanabalu *et al.* 1998; Balakrishnan, Hughes and Koronakis 2001) demonstrated for the HlyA TISS that upon interaction of the substrate with the inner membrane proteins (HlyB and HlyD), TolC is recruited and a ‘channel tunnel’ is formed through which HlyA is secreted at the cost of ATP hydrolysis. After substrate translocation is completed, TolC disassembles from the complex, leaving HlyB and HlyD as a stable complex in the inner membrane, ready to start another round of substrate secretion.

Deletion studies proved that the cytosolic domain of HlyD (residues 1–60) forms the hub from which assembly of the secretion complex is initiated (Balakrishnan, Hughes and Koronakis 2001). Complementary data were provided by *in vitro* surface plasmon resonance experiments demonstrating that the isolated nucleotide-binding domain (NBD) of the ABC transporter also interacts with the substrate (Benabdelhak *et al.* 2003). Interestingly, this interaction was strictly limited to the C-terminal secretion signal.

Indirect (Kenny, Haigh and Holland 1991; Debarbieux and Wandersman 2001) and direct evidence (Bakkes *et al.* 2010) demonstrated that substrates of TISS are translocated in an unfolded state. In an elegant set of experiments, Wandersman and colleagues observed that the presence of folded HlyA actually inhibited the secretion of newly synthesized HlyA (Debarbieux and Wandersman 2001). Subsequently, they addressed the underlying principles of this *cis* inhibition (Cescau, Debarbieux and Wandersman 2007) and surprisingly, the results of this study demonstrated that the interaction of unfolded HlyA with the inner membrane complex also occurs outside the region encoding the secretion sequence, identifying a second, non-overlapping binding site. This interaction resulted in stable recruitment of the outer membrane protein TolC, which could be reversed by adding in *cis* the isolated secretion sequence. This pointed toward an intermolecular activity that triggered complex dissociation (Cescau, Debarbieux and Wandersman 2007).

All structural and functional data obtained for ABC transporters so far indicate that the transport mechanism used by these primary active transporters to shuttle their substrates from one side of the membrane to the other follows the ‘alternating two site access model’ for membrane transporters (Jardetzky 1966). However, the unfolded state and the mere

physical length (up to 9000 amino acids) of substrates of T1SS make it impossible to apply this generally accepted mechanism also for ABC transporters involved in T1SS. Although some research has been carried out on this issue, there is still very little understanding of the mechanism of secretion through the transenvelope channel.

In contrast to the canonical organization of ABC transporters, HlyB harbors an additional N-terminal domain, a cytosolic appendix (Kanonenberg, Schwarz and Schmitt 2013). Based on the primary structure of HlyB, the first ~130 amino acids belong to the family of C39 peptidases, a subfamily of the papain superfamily of cysteine proteases (Havarstein, Diep and Nes 1995; Wu and Tai 2004). These peptidases are unique to ABC transporters and are only found in bacteriocin exporters (Havarstein, Diep and Nes 1995). In principle, the protein family of bacteriocins is limited to Gram-positive bacteria, but a few members can also be found in Gram-negative strains, e.g. Colicin V in *E. coli*. Using a type I secretion apparatus but retaining the typical N-terminally cleaved propeptide, these peptides form a small yet unique group amongst type I substrates (Hwang, Zhong and Tai 1997).

However, in many T1SS ABC transporters such as HlyB the catalytically active cysteine residue is replaced by a tyrosine, resulting in a corrupted catalytic triad. Lecher *et al.* (2012) therefore established the term 'C39 peptidase-like domain' (CLD). NMR studies revealed an identical tertiary structure compared to C39 peptidase domains (Ishii *et al.* 2010). A conserved interaction of the histidine residue in the corrupted active center with a tryptophan residue was discovered, which is now commonly used to distinguish C39 peptidase domains from CLDs (Lecher *et al.* 2012; Kanonenberg, Schwarz and Schmitt 2013). In a set of *in vitro* functional and structural studies, Lecher *et al.* (2012) confirmed binding of unfolded substrate to the isolated CLD that was independent of the secretion signal. The substrate-binding site was mapped by chemical perturbation experiments and results were subsequently confirmed by mutational studies. These results suggest that the CLD acts as a receptor that grabs unfolded HlyA and positions it for subsequent translocation. It remains speculative whether the CLD also plays a role in preventing folding and degradation of the substrate in the cytosol and further studies are needed to establish its precise function and mechanism of action.

Within the field of study, the question of directionality of type I secretion has long been under debate. The concept of stalling the HlyA T1SS by using substrate N-terminally fused to fast folding enhanced green fluorescent protein (eGFP) (Evdokimov *et al.* 2006) finally answered this question (Lenders *et al.* 2015). Folded eGFP in the cytosol served as a 'plug' while the C-terminal moiety inserted into the channel tunnel and protruded partially into the extracellular space, where it prevented backsliding by adopting its tertiary structure. A combination of fluorescence and super-resolution microscopy exploiting the autofluorescence of eGFP in the cytosol and immunofluorescence-based methods to detect the secreted C-terminus of the substrate demonstrated that the secretion sequence appears first on the external surface of the cell envelope.

QUANTITATIVE ANALYSIS

The concept of stalling a T1SS (as described in section 'Functional insights') not only offered the possibility to address the directionality of transport but was also exploited to determine the secretion rate of the HlyA T1SS (Lenders *et al.* 2016). Importantly,

the fluorescence of Cy3-labeled antibody was first employed to quantify the total number of active HlyA T1SS translocons per cell. Interestingly, the derived number was in good agreement with the absolute number of HlyB dimers present in the membrane, as determined by quantitative western blot analysis, using a standard of purified HlyB (Reimann *et al.* 2016) of known concentrations. By experimentally quantifying the amount of secreted substrate, the secretion rate of the HlyA T1SS was determined to be 16 amino acids per transporter per second. Thus, it requires 90 s to secrete one complete HlyA molecule. This rate is roughly 10-fold lower than the rate of SecA-dependent protein translocation across the inner membrane, which operates at a calculated rate of ~152–228 amino acids per second per transporter (Schiebel *et al.* 1991; Uchida, Mori and Mizushima 1995). Intriguingly, the rate of HlyA secretion is very similar to the rate of bacterial protein synthesis at the ribosome, which was calculated to be 10–20 amino acids per second (Young and Bremer 1976). Whether this similarity is of any relevance and results from some sort of connection still has to be addressed experimentally.

In earlier studies, the proton motive force (pmf) was identified as being essential for substrate secretion (Koronakis, Hughes and Koronakis 1991). In our hands, however, an influence of the pmf on the secretion rate was not observed (unpublished data), supporting recent results on CyaA, an exotoxin from *B. pertussis* (Bumba *et al.* 2016), whose secretion is also independent from the pmf. This seminal study also demonstrated a clear influence of the extracellular Ca²⁺ concentration on the secretion efficiency. Thus, the presence of Ca²⁺ accelerated CyaA secretion by generating intramolecular Brownian ratchets. In other words, this process is passive but involves ratcheted translocation events. Nevertheless, these data do not support the hypothesis that the binding of Ca²⁺ ions to the RTX domains represents a driving force of prime importance for secretion (Chenal *et al.* 2009; Thomas *et al.* 2014). This is in striking contrast to the secretion of HlyA (Lenders *et al.* 2016), where changes in the Ca²⁺ concentration in the medium or even the complete absence of Ca²⁺ did not influence the secretion rate, which remained at 16 amino acids per transporter per second. However, one has to stress that Ca²⁺ is crucial for the functionality of HlyA and that in the absence of Ca²⁺ the pore-forming activity was abolished (Lenders *et al.* 2016). These findings suggest a certain variety in the molecular mechanism of secretion amongst different T1SS, which may be influenced by the size of the substrate or the arrangement of the RTX domains. Thus, it is suggested that a Brownian ratchet mechanism combined with a pulling force is operational in CyaA (Bumba *et al.* 2016), but absent in HlyA (Lenders *et al.* 2016) and further experiments especially involving other T1SS are required to settle this issue.

STRUCTURAL INSIGHTS

Structural elucidation, together with functional characterization, is a powerful tool to investigate the transport mechanisms of membrane proteins. The very first structural information of a T1SS component was derived from two-dimensional crystals of the outer membrane protein TolC from *E. coli*. Even at a resolution of 12 Å, apart from the trimeric β -barrel nature, the presence of a novel periplasmic domain became evident (Koronakis *et al.* 1997). Only a few years later, solving the crystal structure of TolC at 2.1 Å revealed the novel fold of this funnel-like domain (Koronakis *et al.* 2000). This is composed out of 12 α -helices that protrude 100 Å into the periplasmic space. Including the

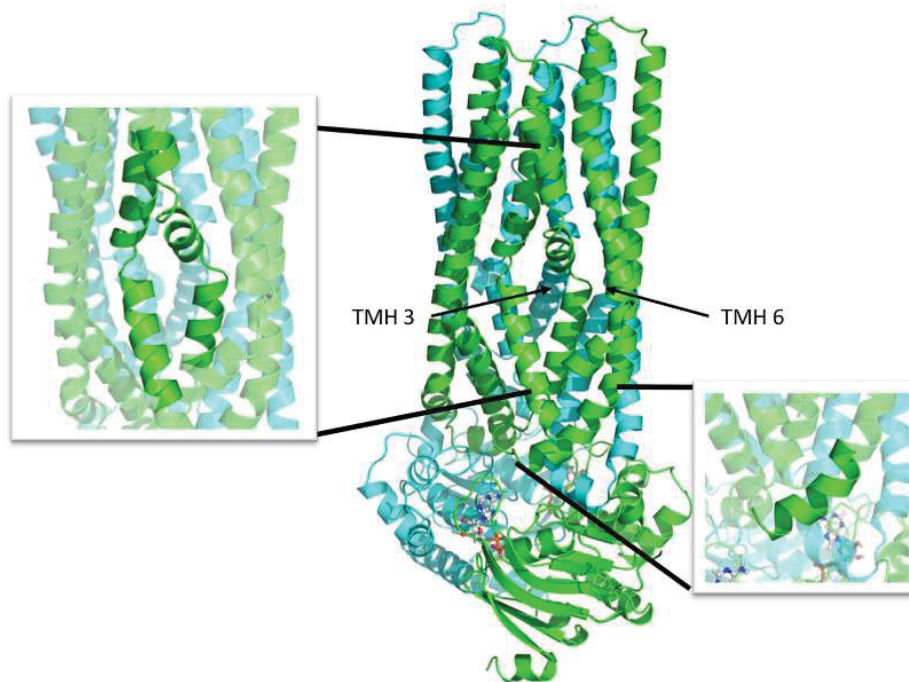


Figure 3. Cartoon representation of AaPrtD (Morgan, Acheson and Zimmer 2017). Monomers are shown in green and cyan. The bound nucleotides are shown in stick representation. The kinked helices 3 and 6 (TMH3 and TMH6) are highlighted for one monomer (left zoom-in). The right zoom-in highlights the coupling helix 1.

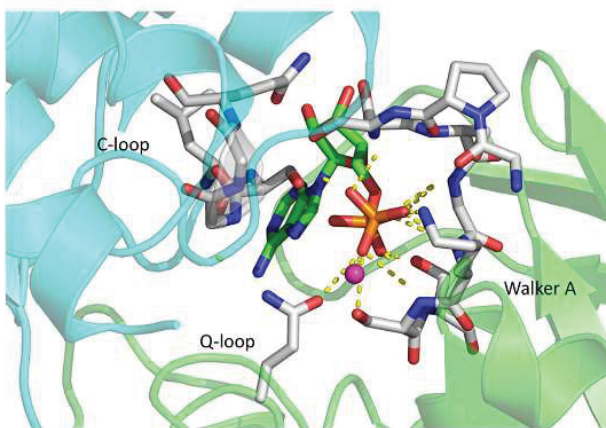


Figure 4. Zoom into the nucleotide-binding site of AaPrtD (Morgan, Acheson and Zimmer 2017) formed by both NBDs colored in green and cyan. ADP is shown in stick representation, the co-factor Mg^{2+} as magenta sphere. The conserved motifs interacting with the bound ADP molecule are labeled and highlighted in stick representation. Interactions are visualized by dashed, yellow lines.

12-stranded β -barrel (3 per monomer) the total length of the protein adds up to 140 Å. The structure was interpreted to represent a closed state as the inner diameter of the water-filled β -barrel of 20 Å narrows to only 3.9 Å at the periplasmic gate of TolC.

Based on this structural information, alanine mutations were placed within the region of the periplasmic gate in order to disrupt the closed state of TolC. Conductivity measurements in black lipid membranes led to a model, in which an ‘iris-like’ opening of the inner helices opens the periplasmic gate and therefore allows substrate translocation (Andersen *et al.* 2002a,b). Later on, this model was confirmed by structural information (Bavro *et al.* 2008; Pei *et al.* 2011).

Starting in 2003, a series of crystal structures paired with functional analysis on the NBD of the ABC transporter HlyB was

published (Benabdelhak *et al.* 2003, 2005; Schmitt *et al.* 2003; Zaitseva *et al.* 2005a, 2006). These studies offered valuable insights into the motor domain of a TISS and its detailed molecular mechanism of ATP hydrolysis (Zaitseva *et al.* 2005b,c; Hanekop *et al.* 2006; Oswald, Holland and Schmitt 2006).

Additional insights into the structure of TISS were obtained only recently, when the crystal structure of the ABC transporter of a putative TISS from the hyperthermophilic Gram-negative bacterium *Aquifex aeolicus* (AaPrtD) was published. It shares a sequence identity of 40% with PrtD from *Dickeya dadantii*, but neither the substrate nor the MFP homolog of AaPrtD was identified (Morgan, Acheson and Zimmer 2017). The structure of the homodimer was determined at a resolution of 3.15 Å and reflected the ADP/ Mg^{2+} -bound state (Fig. 3). The presence of six transmembrane helices (TMH) per monomer and the canonical fold of the NBDs is typical for ABC transporters. Interestingly, the arrangement of the NBDs in the ADP-bound state seems to represent the occluded state (Morgan, Acheson and Zimmer 2017), which contradicts the accepted view that ATP binding induces dimerization of the two NBDs (Locher 2004, 2016; Oswald, Holland and Schmitt 2006).

The ADP molecule is coordinated by residues of the Walker A motif and the glutamine residue of the Q-loop, and also by the serine residue of the C-loop of the opposing NBD resulting in dimerization (Fig. 4). However, a similar architecture has been observed in the crystal structure of Sav1866 from *Staphylococcus aureus* (Dawson and Locher 2006) raising the question of how this architecture fits into the well-established view that only ATP induces formation of the NBD dimer.

The architecture of the TMHs of AaPrtD is distinct from that of other ABC export systems. Generally, ABC transporters contain two coupling helices (CH1 and CH2), which interact with the NBDs. In AaPrtD, the interaction conferred by CH1 is taken over by TMH2, which extends into a loop region that continues without any secondary structure into TMH3.

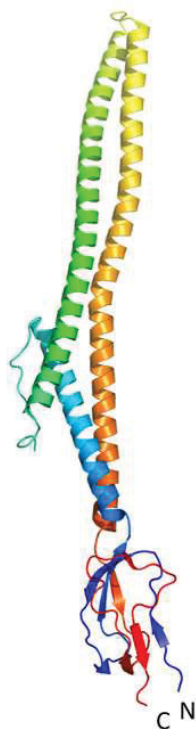


Figure 5. Crystal structure of a soluble fragment of HlyD from *E. coli* (Kim *et al.* 2016) that highlights the coiled-coil interaction of the helices. The lipoyl domain is colored in red and blue. N- and C-termini are indicated.

Furthermore, TMI13 and TMI16 are kinked at the approximate position of the lipid head groups, splitting TMI16 into two and TMH3 into three separate helices—a novel architecture—not been observed before (Morgan, Acheson and Zimmer 2017), neither in the bacteriocin transporter McjD (Choudhury *et al.* 2014) nor in the peptide transporter TAP 1/2 (Oldham, Grigorieff and Chen 2016). The kinks create a restriction within the putative substrate channel. The fact that residues lining this restriction are stabilized by interactions with conserved amino acids emphasizes their functional importance. Although the functionality of AalPrfD has not been demonstrated yet and the identity of the MFP and the transport substrate remain elusive, the structure provided the first glimpse of a T1SS ABC transporter and presents a platform to design new and exciting experiments.

Proteins from the family of MFPs are not only an indispensable part of T1SS but have also been intensively studied in the context of bacterial tripartite drug efflux pumps, such as the AcrB-AcrA-TolC system (Du *et al.* 2014) or the MacA-MacB-TolC system (Fitzpatrick *et al.* 2017). Until 2016, structural information was limited to MFPs involved in drug efflux (for a recent review, see Symmons, Marshall and Bavro 2015), while for T1SS MFPs only recently has some limited structural information become available (Kim *et al.* 2016). In 2016, the crystal structure of a soluble fragment of HlyD, comprising the α -helical domain and lipoyl domain, was published (Kim *et al.* 2016). However, the construct used for structure determination lacked not only the first 95 N-terminal amino acids, including the cytoplasmic domain (residues 1–59) and the single TMH of HlyD (residues 60–80), but also the last 106 C-terminal residues (residues 373–478), corresponding to the entire membrane proximal domain (Fig. 5).

In contrast to the majority of structurally described MFPs that contain two α -helices, the unusually long (115 Å) α -helical domain of HlyD is built out of three helices, of which helix 3 in-

teracts in an anti-parallel coiled-coil fashion with helix 1 and 2. Based on structural comparison with AcrA (Kim *et al.* 2010) and sequence conservation analysis, a model was proposed, where the α -helical tip located between helix 2 and 3 forms the interaction site with TolC (Kim *et al.* 2016). Only recently, in 2017, the crystal structure of the α -helical domain and the lipoyl domain of LipC, the MFP of the lipase secretion system from *Serratia marcescens*, was reported (Murata *et al.* 2017). Interestingly, the α -helical domain also contained three helices, which might be a common feature of T1SS MFPs.

The AcrA-AcrB-TolC (Du *et al.* 2014) and the MacA-MacB-TolC (Fitzpatrick *et al.* 2017) structures revealed a hexameric arrangement of the corresponding MFPs. Contradictory findings provided by cross-linking studies in *E. coli* suggest a trimeric state of HlyD as the functional unit (Thanabalu *et al.* 1998). Even though in principle a hexameric state seems more likely and is also supported by a model (Kim *et al.* 2016) based on the available crystal structure of MacA (Yum *et al.* 2009), the oligomeric state of T1SS MFPs is still under debate and the subject is still in need of further investigation.

BIOTECHNOLOGICAL APPLICATIONS

By achieving the secretion of fusion proteins in high amounts into the extracellular medium, large-scale purification can be significantly simplified, which reflects an attractive approach for biotechnological applications.

The relatively simple nature of T1SS and the C-terminal secretion signal raised interest in their use in biotechnological applications. Two main areas became the focus of intensive research: heterologous protein secretion, in general (Blight and Holland 1994) and antigen production for vaccination (Sebo *et al.* 1999; Spreng *et al.* 1999).

Here, we will only focus on the applicability of T1SS for the secretion of heterologous proteins. Based on the T1SS of TliA, a thermostable lipase from *P. fluorescens* (Park *et al.* 2012), a versatile secretion system was engineered (Ryu *et al.* 2015). The C-terminal secretion signal of TliA was fused either to GFP or alkaline phosphatase, and both proteins were secreted into the medium. The hydrophobic nature of the secretion signal even allowed subsequent purification via hydrophobic interaction chromatography. Secretion of fusion proteins was further enhanced by engineering a negative net charge by introducing aspartate clusters in the fusion proteins of interest (Byun *et al.* 2017). These constructs go hand in hand with the direction of the membrane potential, which is positive on the surface of bacteria. This favors the translocation of negatively charged proteins since the directionality of the potential acts electrophoretically (Cao, Kuhn and Dalbey 1995).

The other T1SS that has been extensively studied for the purpose of heterologous protein secretion is the HlyA T1SS from *E. coli*. With the identification of HlyA1 (Nicaud *et al.* 1986), a 23 kDa, C-terminal fragment of HlyA encouraging the secretion sequence and three of six RTX domains, research efforts were intensified to exploit the system for the secretion of heterologous proteins. The studies of Debarbieux and Wandersman (2001) and Bakkes *et al.* (2010) stressed the importance of folding rates in the successful secretion of fusion proteins. Remarkably, the natural folding rate of a protein fused to HlyA1 decreased dramatically, which increased the range of possible fusion partners and increased the yields of the proteins of interest (Bakkes *et al.* 2010).

Only recently, a new expression vector was established that impressively improved secretion efficiencies of various

fusion proteins (Khosha *et al.* 2018). Here, a 5'-untranslated region (UTR) was identified that increased the amount of secreted HlyA1 several-fold and that, most surprisingly, does contain nucleotides belonging to the coding sequence of HlyC. The region was mapped to an area enriched in adenosine- and uracil nucleotides, located ~36 base pairs upstream from the start codon of HlyA1. Nevertheless, the most striking result to emerge from this data in terms of biotechnological application is that besides boosting the secretion efficiency of HlyA1, the vector enabled the secretion of fast-folding fusion proteins that could not be secreted until then (Khosha *et al.* 2018). This is likely due to the fact that this 5'-UTR is recognized by ribosomal protein S1 and targeted to the ribosome for faster and more efficient translation. Certainly, these findings could open up new avenues for the exploitation of T1SS and highlights their potential biotechnological and pharmaceutical value. Furthermore, they emphasize the necessity not to limit biotechnological engineering to the mere coding sequence of a protein.

OUTLOOK

Since its discovery nearly 40 years ago, T1SS have been the subject of numerous fruitful studies and the basic outline of the secretion process is by now well established. However, much uncertainty still exists about the detailed mechanism of transport. Ongoing, exciting research should address, for example, additional structural information, the stoichiometry of the T1SS complexes, the nature of the secretion signal and biochemical insights into recognition and processing of the substrate.

ACKNOWLEDGEMENTS

We apologize to all our colleagues whose research could not be appropriately referenced due to space limitation. We thank all current and former members of the Institute of Biochemistry for support and valuable discussion. LS wishes to gratefully acknowledge his long term and highly fruitful collaboration with Prof. I. Barry Holland and his laboratory at the University of Orsay, France.

FUNDING

Research on the hemolysin T1SS is funded by the DFG through CRC 1208 (project A01 to LS) and the Manchot Graduate School Molecules of Infections III (to LS).

Conflict of interest. None declared.

REFERENCES

Andersen C, Koronakis E, Bokma E *et al.* Transition to the open state of the TolC periplasmic tunnel entrance. *P Natl Acad Sci USA* 2002a;**99**:11103–8.

Andersen C, Koronakis E, Hughes C *et al.* An aspartate ring at the TolC tunnel entrance determines ion selectivity and presents a target for blocking by large cations. *Mol Microbiol* 2002b;**44**:1131–9.

Bakkes PJ, Jenewein S, Smits SH *et al.* The rate of folding dictates substrate secretion by the *Escherichia coli* hemolysin Type 1 secretion system. *J Biol Chem* 2010;**285**:40573–80.

Balakrishnan L, Hughes C, Koronakis V. Substrate-triggered recruitment of the TolC channel-tunnel during type I export of hemolysin by *Escherichia coli*. *J Mol Biol* 2001;**313**:501–10.

Baumann U, Wu S, Flaherty KM *et al.* Three-dimensional structure of the alkaline protease of *Pseudomonas aeruginosa*: a two-domain protein with a calcium binding parallel beta roll motif. *EMBO J* 1993;**12**:3357–64.

Bavro VN, Pietras Z, Fumham N *et al.* Assembly and channel opening in a bacterial drug efflux machine. *Mol Cell* 2008;**30**:114–21.

Benabdelhak H, Kiontke S, Hom C *et al.* A specific interaction between the NBD of the ABC-transporter HlyB and a C-terminal fragment of its transport substrate haemolysin A. *J Mol Biol* 2003;**327**:1169–79.

Benabdelhak H, Schmitt L, Horn C *et al.* Positive cooperative activity and dimerization of the isolated ABC-ATPase domain of HlyB from *E. coli*. *Biochem J* 2005;**368**:1–7.

Blight MA, Holland IB. Heterologous protein secretion and the versatile *Escherichia coli* haemolysin translocator. *Trends Biotechnol* 1994;**12**:450–5.

Bumba L, Masin J, Macek P *et al.* Calcium-driven folding of RTX domain beta-Rolls ratchets translocation of RTX proteins through type I secretion ducts. *Mol Cell* 2016;**62**:47–62.

Byun H, Park J, Kim SC *et al.* A lower isoelectric point increases signal sequence-mediated secretion of recombinant proteins through a bacterial ABC transporter. *J Biol Chem* 2017;**292**:19782–91.

Cao G, Kuhn A, Dalbey RE. The translocation of negatively charged residues across the membrane is driven by the electrochemical potential: evidence for an electrophoresis-like membrane transfer mechanism. *EMBO J* 1995;**14**:866–75.

Cescou S, Debarbieux L, Wandersman C. Probing the in vivo dynamics of type I protein secretion complex association through sensitivity to detergents. *J Bacteriol* 2007;**189**:1496–504.

Chenal A, Guijarro JI, Raynal B *et al.* RTX calcium binding motifs are intrinsically disordered in the absence of calcium. *J Biol Chem* 2009;**284**:1781–9.

Chervaux C, Sauvonnet N, Le Clainche A *et al.* Secretion of active beta-lactamase to the medium mediated by the *Escherichia coli* haemolysin transport pathway. *Mol Gen Genet* 1995;**249**:237–45.

Choudhury HG, Tong Z, Mathavan I *et al.* Structure of an antibacterial peptide ATP-binding cassette transporter in a novel outward occluded state. *P Natl Acad Sci USA* 2014;**111**:9145–50.

Costa TR, Felisberto-Rodrigues C, Meir A *et al.* Secretion systems in Gram-negative bacteria: structural and mechanistic insights. *Nat Rev Microbiol* 2015;**13**:343–59.

Davidson AL, Dassa E, Orelle C *et al.* Structure, function, and evolution of bacterial ATP-binding cassette systems. *Microbiol Mol Biol R* 2008;**72**:317–64, table of contents.

Dawson RJ, Locher KP. Structure of a bacterial multidrug ABC transporter. *Nature* 2006;**443**:180–5.

Debarbieux L, Wandersman C. Folded HasA inhibits its own secretion through its ABC exporter. *EMBO J* 2001;**20**:4657–63.

Delepelaire P. Type I secretion in gram-negative bacteria. *BBA-Mol Cell Res* 2004;**1694**:149–61.

Du D, Wang Z, James NR *et al.* Structure of the AcrAB-TolC multidrug efflux pump. *Nature* 2014;**509**:512–5.

Economou A, Dalbey RE. Preface to special issue on protein trafficking and secretion in bacteria. *Biochim Biophys Acta* 2014;**1843**:1427.

Evdokimov AG, Pokross ME, Egorov NS *et al.* Structural basis for the fast maturation of Arthropoda green fluorescent protein. *EMBO Rep* 2006;**7**:1006–12.

- Felmlee T, Pellett S, Welch RA. Nucleotide sequence of an *Escherichia coli* chromosomal hemolysin. *J Bacteriol* 1985;163:94–105.
- Felmlee T, Welch RA. Alterations of amino acid repeats in the *Escherichia coli* hemolysin affect cytolytic activity and secretion. *PNatl Acad Sci USA* 1988;85:5269–73.
- Fitzpatrick AWP, Llabres S, Neuberger A *et al.* Structure of the MacAB-TolC ABC-type tripartite multidrug efflux pump. *Nat Microbiol* 2017;2:17070.
- Gentschev I, Hess J, Goebel W. Change in the cellular localization of alkaline phosphatase by alteration of its carboxy-terminal sequence. *Mol Gen Genet* 1990;222:211–6.
- Gray L, Baker K, Kenny B *et al.* A novel C-terminal signal sequence targets *Escherichia coli* haemolysin directly to the medium. *J Cell Sci* 1989;11:45–57.
- Gray L, Mackman N, Nicaud JM *et al.* The carboxy-terminal region of haemolysin 2001 is required for secretion of the toxin from *Escherichia coli*. *Mol Gen Genet* 1986;205:127–33.
- Greene NP, Crow A, Hughes C *et al.* Structure of a bacterial toxin-activating acyltransferase. *P Natl Acad Sci USA* 2015;112:E3058–66.
- Griessl MH, Schmid B, Kassler K *et al.* Structural insight into the giant Ca²⁺-binding adhesin SiiE: implications for the adhesion of salmonella enterica to polarized epithelial cells. *Structure* 2013;21:741–52.
- Hanekop N, Zaitseva J, Jenewein S *et al.* Molecular insights into the mechanism of ATP-hydrolysis by the NBD of the ABC-transporter HlyB. *FEBS Lett* 2006;580:1036–41.
- Havarstein LS, Diep DB, Nes IF. A family of bacteriocin ABC transporters carry out proteolytic processing of their substrates concomitant with export. *Mol Microbiol* 1995;16:229–40.
- Hinsa SM, Espinosa-Urgel M, Ramos JL *et al.* Transition from reversible to irreversible attachment during biofilm formation by *Pseudomonas fluorescens* WCS365 requires an ABC transporter and a large secreted protein. *Mol Microbiol* 2003;49:905–18.
- Holland IB, Peherstorfer S, Kanonenberg K *et al.* Type I protein secretion—deceptively simple yet with a wide range of mechanistic variability across the family. *EcoSal Plus* 2016;7:1–46.
- Hwang J, Zhong X, Tai PC. Interactions of dedicated export membrane proteins of the colicin V secretion system: CvaA, a member of the membrane fusion protein family, interacts with CvaB and TolC. *J Bacteriol* 1997;179:6264–70.
- Ishii S, Yano T, Ebihara A *et al.* Crystal structure of the peptidase domain of *Streptococcus* ComA, a Bifunctional ATP-binding cassette transporter involved in the quorum-sensing pathway. *J Biol Chem* 2010;285:10777–85.
- Issartel JP, Koronakis V, Hughes C. Activation of *Escherichia coli* prohaemolysin to the mature toxin by acyl carrier protein-dependent fatty acylation. *Nature* 1991;351:759–61.
- Izadi-Pruneyre N, Wolff N, Redeker V *et al.* NMR studies of the C-Terminal secretion signal of the haem-binding protein, HasA. *Eur J Biochem* 1999;261:562–8.
- Jardetzky O. Simple allosteric model for membrane pumps. *Nature* 1966;211:969–70.
- Jones HE, Holland IB, Baker HL *et al.* Slow changes in cytosolic free Ca²⁺ in *Escherichia coli* highlight two putative influx mechanisms in response to changes in extracellular calcium. *Cell Calcium* 1999;25:265–74.
- Kanonenberg K, Schwarz CK, Schmitt L. Type I secretion systems – a story of appendices. *Res Microbiol* 2013;164:596–604.
- Kenny B, Haigh R, Holland IB. Analysis of the haemolysin transport process through the secretion from *Escherichia coli* of PCM, CAT or beta-galactosidase fused to the Hly C-terminal signal domain. *Mol Microbiol* 1991;5:2557–68.
- Khosa S, Scholz R, Schwarz C *et al.* An A/U-Rich enhancer region is required for high-level protein secretion through the HlyA Type I secretion system. *Appl Environ Microb* 2018;84:e01163–17.
- Kim HM, Xu Y, Lee M *et al.* Functional relationships between the AcrA hairpin tip region and the TolC aperture tip region for the formation of the bacterial tripartite efflux pump AcrAB-TolC. *J Bacteriol* 2010;192:4498–503.
- Kim JS, Song S, Lee M *et al.* Crystal structure of a soluble fragment of the membrane fusion protein HlyD in a Type I secretion system of gram-negative bacteria. *Structure* 2016;24:477–85.
- Koronakis V, Eswaran J, Hughes C. Structure and function of TolC: the bacterial exit duct for proteins and drugs. *Annu Rev Biochem* 2004;73:467–89.
- Koronakis V, Hughes C, Koronakis E. Energetically distinct early and late stages of HlyB/HlyD-dependent secretion across both *Escherichia coli* membranes. *EMBO J* 1991;10:3263–72.
- Koronakis V, Koronakis E, Hughes C. Isolation and analysis of the C-terminal signal directing export of *Escherichia coli* hemolysin protein across both bacterial membranes. *EMBO J* 1989;8:595–605.
- Koronakis V, Li J, Koronakis E *et al.* Structure of TolC, the outer membrane component of the bacterial type I efflux system, derived from two-dimensional crystals. *Mol Microbiol* 1997;23:617–26.
- Koronakis V, Sharff A, Koronakis E *et al.* Crystal structure of the bacterial membrane protein TolC central to multidrug efflux and protein export. *Nature* 2000;405:914–9.
- Kuhnert P, Heyberger-Meyer B, Nicolet J *et al.* Characterization of PaxA and its operon: a cohemolytic RTX toxin determinant from pathogenic *Pasteurella aerogenes*. *Infect Immun* 2000;68:6–12.
- Lecher J, Schwarz CK, Stoldt M *et al.* An RTX transporter tethers its unfolded substrate during secretion via a unique N-terminal domain. *Structure* 2012;20:1778–87.
- Lenders MH, Beer T, Smits SH *et al.* In vivo quantification of the secretion rates of the hemolysin A Type I secretion system. *Sci Rep* 2016;6:33275.
- Lenders MH, Weidtkamp-Peters S, Kleinschrodt D *et al.* Directionality of substrate translocation of the hemolysin A Type I secretion system. *Sci Rep* 2015;5:12470.
- Letoffe S, Delepelair P, Wandersman C. Protease secretion by *Erwinia chrysanthemi*: the specific secretion functions are analogous to those of *Escherichia coli* alpha-haemolysin. *EMBO J* 1990;9:1375–82.
- Letoffe S, Ghigo JM, Wandersman C. Secretion of the *Serratia marcescens* HasA protein by an ABC transporter. *J Bacteriol* 1994;176:5372–7.
- Linhartova I, Bumba L, Masin J *et al.* RTX proteins: a highly diverse family secreted by a common mechanism. *FEMS Microbiol Rev* 2010;34:1076–112.
- Locher KP. Structure and mechanism of ABC transporters. *Curr Opin Struct Biol* 2004;14:426–31.
- Locher KP. Mechanistic diversity in ATP-binding cassette (ABC) transporters. *Nat Struct Mol Biol* 2016;23:487–93.
- Mackman N, Baker K, Gray L *et al.* Release of a chimeric protein into the medium from *Escherichia coli* using the C-terminal secretion signal of haemolysin. *EMBO J* 1987;6:2835–41.
- Mackman N, Holland IB. Functional characterization of a cloned haemolysin determinant from *E. coli* of human origin, encoding information for the secretion of a 107K polypeptide. *Mol Gen Genet* 1984;196:129–34.

- Mackman N, Nicaud JM, Gray L *et al.* Genetical and functional organisation of the *Escherichia coli* haemolysin determinant 2001. *Mol Gen Genet* 1985a;201:282–8.
- Mackman N, Nicaud JM, Gray L *et al.* Identification of polypeptides required for the export of haemolysin 2001 from *E. coli*. *Mol Gen Genet* 1985b;201:529–36.
- Masure HR, Au DC, Gross MK *et al.* Secretion of the *Bordetella pertussis* adenylate cyclase from *Escherichia coli* containing the hemolysin operon. *Biochemistry* 1990;29:140–5.
- Meier R, Drepper T, Svensson V *et al.* A Calcium-gated lid and a large beta-roll sandwich are revealed by the crystal structure of extracellular lipase from *Serratia marcescens*. *J Biol Chem* 2007;282:31477–83.
- Morgan JL, Acheson JF, Zimmer J. Structure of a Type-I secretion system ABC transporter. *Structure* 2017;25:522–9.
- Murata D, Okano H, Angkawidjaja C *et al.* Structural basis for the *Serratia marcescens* lipase secretion system: Crystal structures of the membrane fusion protein and Nucleotide-Binding domain. *Biochemistry* 2017;56:6281–91.
- Nicaud JM, Mackman N, Gray L *et al.* Regulation of haemolysin synthesis in *E. coli* determined by HLY genes of human origin. *Mol Gen Genet* 1985;199:111–6.
- Nicaud JM, Mackman N, Gray L *et al.* The C-terminal, 23 kDa peptide of *E. coli* haemolysin 2001 contains all the information necessary for its secretion by the haemolysin (Hly) export machinery. *FEBS Lett* 1986;204:331–5.
- Noegel A, Rdest U, Springer W *et al.* Plasmid cistrons controlling synthesis and excretion of the exotoxin alpha-haemolysin of *Escherichia coli*. *Mol Gen Genet* 1979;175:343–50.
- Oldham ML, Grigorieff N, Chen J. Structure of the transporter associated with antigen processing trapped by herpes simplex virus. *Elife* 2016;5:e21289.
- Ostolaza H, Soloaga A, Goni FM. The binding of divalent cations to *Escherichia coli* alpha-haemolysin. *Eur J Biochem* 1995;228:39–44.
- Oswald C, Holland IB, Schmitt L. The motor domains of ABC-transporters. *N-S Arch Pharmacol* 2006;372:385–99.
- Park Y, Moon Y, Ryoo J *et al.* Identification of the minimal region in lipase ABC transporter recognition domain of *Pseudomonas fluorescens* for secretion and fluorescence of green fluorescent protein. *Microb Cell Fact* 2012;11:60.
- Pei XY, Hinchliffe P, Symmons MF *et al.* Structures of sequential open states in a symmetrical opening transition of the TolC exit duct. *P Natl Acad Sci USA* 2011;108:2112–7.
- Pimenta AL, Young J, Holland IB *et al.* Antibody analysis of the localisation, expression and stability of HlyD, the MFP component of the *E. coli* haemolysin translocator. *Mol Gen Genet* 1999;261:122–32.
- Reimann S, Poschmann G, Kanonenberg K *et al.* Interdomain regulation of the ATPase activity of the ABC transporter haemolysin B from *Escherichia coli*. *Biochem J* 2016;473:2471–83.
- Ryu J, Lee U, Park J *et al.* A vector system for ABC transporter-mediated secretion and purification of recombinant proteins in pseudomonas species. *Appl Environ Microb* 2015;81:1744–53.
- Sanchez-Magraner L, Viguera AR, Garcia-Pacios M *et al.* The Calcium-binding C-terminal domain of *Escherichia coli* alpha-hemolysin is a major determinant in the surface-active properties of the protein. *J Biol Chem* 2007;282:11827–35.
- Sapriel G, Wandersman C, Delepeleire P. The N terminus of the HasA protein and the SecB chaperone cooperate in the efficient targeting and secretion of HasA via the ATP-binding cassette transporter. *J Biol Chem* 2002;277:6726–32.
- Schiebel E, Driessen AJ, Hartl FU *et al.* Delta mu H⁺ and ATP function at different steps of the catalytic cycle of preprotein translocase. *Cell* 1991;64:927–39.
- Schmitt L, Benabdellhak H, Blight MA *et al.* Crystal structure of the nucleotide-binding domain of the ABC-transporter haemolysin B: identification of a variable region within ABC helical domains. *J Mol Biol* 2003;330:333–42.
- Sebo P, Ladant D. Repeat sequences in the *Bordetella pertussis* adenylate cyclase toxin can be recognized as alternative carboxy-proximal secretion signals by the *Escherichia coli* alpha-haemolysin translocator. *Mol Microbiol* 1993;9:999–1009.
- Sebo P, Moukrim Z, Kalhous M *et al.* In vivo induction of CTL responses by recombinant adenylate cyclase of *Bordetella Pertussis* carrying multiple copies of a viral CD8(+) T-cell epitope. *FEMS Immunol Med Mic* 1999;26:167–73.
- Sotomayor Perez AC, Karst JC, Davi M *et al.* Characterization of the regions involved in the calcium-induced folding of the intrinsically disordered RTX motifs from the *Bordetella pertussis* adenylate cyclase toxin. *J Mol Biol* 2015;397:534–49.
- Spreng S, Dietrich G, Goebel W *et al.* The *Escherichia coli* haemolysin secretion apparatus: a potential universal antigen delivery system in gram-negative bacterial vaccine carriers. *Mol Microbiol* 1999;31:1596–8.
- Stanley P, Hyland C, Koronakis V *et al.* An ordered reaction mechanism for bacterial toxin acylation by the specialized acyl-transferase HlyC: formation of a ternary complex with acyl-LACP and protoxin substrates. *Mol Microbiol* 1999;34:887–901.
- Stanley P, Koronakis V, Hughes C. Mutational analysis supports a role for multiple structural features in the C-terminal secretion signal of *Escherichia coli* haemolysin. *Mol Microbiol* 1991;5:2391–403.
- Stanley P, Packman LC, Koronakis V *et al.* Fatty acylation of two internal lysine residues required for the toxic activity of *Escherichia coli* hemolysin. *Science* 1994;266:1992–6.
- Symmons MF, Marshall RL, Bavro VN. Architecture and roles of periplasmic adaptor proteins in tripartite e fflux assemblies. *Front Microbiol* 2015;6:513.
- Thanabalu T, Koronakis E, Hughes C *et al.* Substrate-induced assembly of a contiguous channel for protein export from *E. coli*: reversible bridging of an inner-membrane translocase to an outer membrane exit pore. *EMBO J* 1998;17:6487–96.
- Thomas S, Bakkes PJ, Smits SH *et al.* Equilibrium folding of pro-HlyA from *Escherichia coli* reveals a stable calcium ion dependent folding intermediate. *BBA-Proteins Proteom* 2014;1844:1500–10.
- Thomas S, Holland IB, Schmitt L. The Type 1 secretion pathway - The hemolysin system and beyond. *Biochim Biophys Acta* 2014;1843:1621–41.
- Thomas S, Smits SH, Schmitt L. A simple in vitro acylation assay based on optimized HlyA and HlyC purification. *Anal Biochem* 2014;464:17–23.
- Thompson SA, Sparling PF. The RTX cytotoxin-related FrpA protein of *Neisseria meningitidis* is secreted extracellularly by meningococci and by HlyBD+ *Escherichia coli*. *Infect Immun* 1993;61:2906–11.
- Uchida K, Mori H, Mizushima S. Stepwise movement of preproteins in the process of translocation across the cytoplasmic membrane of *Escherichia coli*. *J Biol Chem* 1995;270:30862–8.
- Wandersman C, Delepeleire P. TolC, an *Escherichia coli* outer membrane protein required for hemolysin secretion. *P Natl Acad Sci USA* 1990;87:4776–80.
- Wang RC, Seror SJ, Blight M *et al.* Analysis of the membrane organization of an *Escherichia coli* protein translocator, HlyB, a

- member of a large family of prokaryote and eukaryote surface transport proteins. *J Mol Biol* 1991;**217**:441–54.
- Welch RA. Pore-forming cytolysins of gram-negative bacteria. *Mol Microbiol* 1991;**5**:521–8.
- Wu KH, Tai PC. Cys 32 and His 105 are the critical residues for the calcium-dependent cysteine proteolytic activity of CvaB, an ATP-binding cassette transporter. *J Biol Chem* 2004;**279**:901–9.
- Young R, Bremer H. Polypeptide-chain-elongation rate in *Escherichia coli* B/r as a function of growth rate. *Biochem J* 1976;**160**:185–94.
- Yum S, Xu Y, Piao S *et al.* Crystal structure of the periplasmic component of a tripartite macrolide-specific efflux pump. *J Mol Biol* 2009;**387**:1286–97.
- Zaitseva J, Jenewein S, Jumpertz T *et al.* H662 is the linchpin of ATP hydrolysis in the nucleotide-binding domain of the ABC transporter HlyB. *EMBO J* 2005a;**24**:1901–10.
- Zaitseva J, Jenewein S, Oswald C *et al.* A molecular understanding of the catalytic cycle of the nucleotide-binding domain of the ABC transporter HlyB. *Biochem Soc Trans* 2005b:990–5.
- Zaitseva J, Jenewein S, Wiedenmann A *et al.* Functional characterization and ATP-induced dimerization of the isolated ABC-domain of the haemolysin B transporter. *Biochemistry* 2005c;**44**:9680–90.
- Zaitseva J, Oswald C, Jumpertz T *et al.* A structural analysis of asymmetry required for catalytic activity of an ABC-ATPase domain dimer. *EMBO J* 2006;**25**:3432–43.

3.3 Chapter III – Type I secretion system – One Mechanism for All?

Title Type I secretion system – One Mechanism for All?
Author Olivia Spitz. Isabelle N. Erenburg. Tobias Beer. Kerstin Kanonenberg. Barry I. Holland. Lutz, Schmitt.

Published in *Microbiology Spectrum* (2019), American Society for Microbiology

Impact Factor - (eliminated by ASM [199])

Own proportion of this work 15 %;

Writing of the manuscript

18

Type I Secretion Systems— One Mechanism for All?

OLIVIA SPITZ,¹ ISABELLE N. ERENBURG,¹ TOBIAS BEER,¹
KERSTIN KANONENBERG,¹ I. BARRY HOLLAND,² and LUTZ SCHMITT¹

INTRODUCTION

Gram-negative bacteria are equipped with at least seven dedicated secretion systems that mediate the export of proteins beyond the outer membrane (1, 2). These are called type 1 to 6 and type 9 secretion systems (T1SS to T6SS and T9SS). Among those, T3SS, T4SS, and T6SS are even capable of delivering their cargo directly into the cytosol of the host cell. In this minireview, we place the major emphasis on the hemolysin A (HlyA) secretion system in *Escherichia coli*. This is by far the most studied and illustrates very well the largely conserved, essential features of T1SS. Interestingly, however, an important mechanistic variation in the translocation of some of the unusually extended giant RTX proteins—adhesins—was discovered recently (3) and is also discussed.

T1SS substrates are usually defined by the presence of several blocks of nonapeptide-binding sequences with the consensus GGxGxDxUx (4, 5), where x can be any amino acid and U is a large hydrophobic amino acid. The exceptions are the SiiE-like adhesins (Fig. 1) (6). These nonapeptides gave rise to the abbreviation RTX (repeats in toxins), the name for the family.

¹Institute of Biochemistry, Heinrich Heine University Düsseldorf, Düsseldorf, Germany

²Institute of Genetics and Microbiology, University of Paris-Sud, Orsay, France

Protein Secretion in Bacteria

Edited by Maria Sandkvist, Eric Cascales, and Peter J. Christie

© 2019 American Society for Microbiology, Washington, DC

doi:10.1128/microbiolspec.PSIB-0003-2018

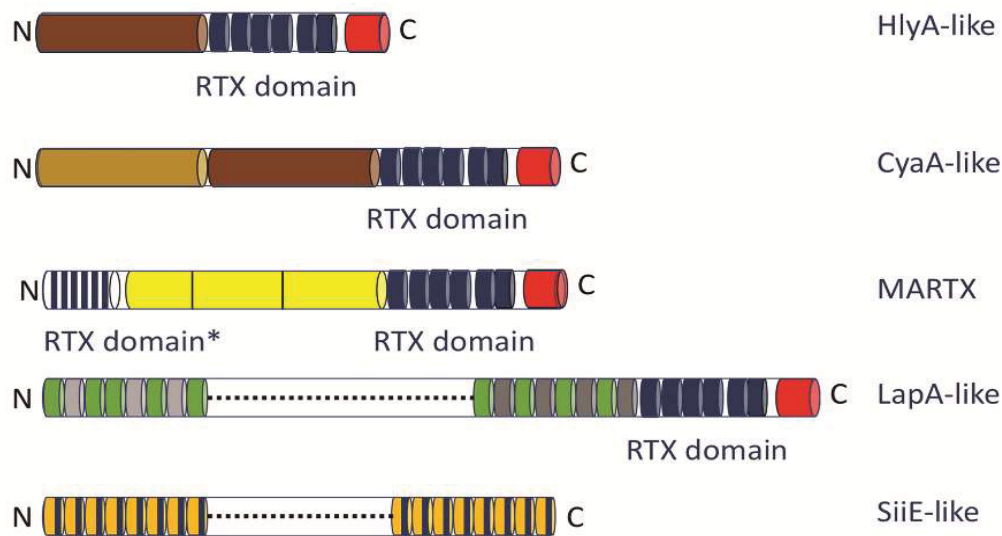


FIGURE 1 Architecture of substrates of T1SS. The primary structure of a canonical substrate of a T1SS is shown as white cylinder with the N and C termini labeled by “N” and “C,” respectively. The secretion sequence (approximately 50 to 100 amino acids depending on the substrate) at the C terminus is in red, the GG repeats forming the classic RTX domain are in blue (six GG repeats as in the case of HlyA have been chosen as an example), and the functional, N-terminal domain is in brown. However, the number and types of architectures of this functional domain have increased in recent years. HlyA-like proteins contain only one domain with dedicated activity (pore-forming activity in the case of HlyA), while, for example, CyaA-like proteins contain two domains, which possess an adenylate cyclase (light brown) and a pore-forming (brown) activity in the case of CyaA. A third class are MARTX proteins (exemplified here by a MARTX protein from *V. cholerae*). The effector domains (yellow and separated by black vertical lines) that are autocatalytically excised after secretion are flanked by an N-terminal RTX-like domain (marked as RTX domain*) and a C-terminal RTX domain. The C-terminal domain corresponds to the canonical sequence, while the conserved aspartate is missing in the N-terminal one. Another architecture is present in LapA-like adhesins (or bacterial transglutaminase-like cysteine proteinases) that contain multiple, different domains. In the case of LapA, two different colors indicate two different domains. However, the number of different domains is not restricted to two. Additionally, the double-alanine motif in the N termini of LapA-like RTX adhesins is not shown. Finally, SiiE-like adhesins contain multiple identical domains, such as the 53 copies of the Blg domain in the case of SiiE (6, 71). The vertical blue line indicates that the GG repeats are integrated within the Ig-like domains and do not form a separate RTX domain. Please note that the drawing of the functional domains is not to scale.

These motifs, also called GG repeats, specifically bind Ca^{2+} (see below) and are implicated in posttranslocation folding. The RTX domain (Fig. 1) is located N terminal to the secretion signal at the extreme C terminus.

Like T1SS substrates, the very large and widespread group of peptide bacteriocins in Gram-negative bacteria (7–9) also require an ABC transporter, a membrane fusion protein (MFP), and an outer membrane (OM) protein for secretion. However, these antimicrobials lack RTX repeats, have a cleavable N-terminal secretion sequence instead of the “classical” C-terminal signal, and have

a quite distinctive translocation mechanism (10, 11): alternating access rather than extrusion through an OM “tunnel.” In view of these properties, we decided not to include them in this minireview. The interested reader is directed to references 7 to 11.

The first molecular identification of a T1SS, the secretion machinery of the pore-forming toxin HlyA from *E. coli* (12), was made in the 1980s and 1990s (13–15) with the demonstration that two inner membrane proteins, an ABC transporter and an MFP, encoded together with the toxin in the same operon were required for secretion. A fourth

gene in the *hly* operon encoded an acyltransferase, HlyC (16), catalyzing the posttranslational modification of two internal lysine residues (17–19). This modification, with fatty acids ranging from C₁₄ to C₁₇ in length, requires acyl carrier protein (20) and is essential for HlyA to form a pore in the host membrane. Thus, only the acylated, toxic form of hemolysin should be called HlyA, while the nonacylated form should correctly be called pro-HlyA. Such acylation conferring toxicity is observed not only in HlyA but also in other hemolysins, leukotoxins, and cytotoxins that are members of the RTX family (4). The recently published crystal structure of a homologue of the *E. coli* HlyC (21) allows a more detailed understanding of how acylation is installed. Notably, however, acylation is not required for secretion into the extracellular space. On the other hand, the proteins encoded in the *hly* operon are not sufficient for secretion of (pro-)HlyA. The OM component of the translocon is TolC. The TolC protein is encoded elsewhere in the chromosome and was first described for a related T1SS by Wandersman and Delepelaire (22).

Equally important, the work by the laboratories of Koronakis, Holland, and Goebel demonstrated that substrate secretion by the T1SS is a one-step process, i.e., directly from the cytosol into the extracellular space without any periplasmic intermediate. Furthermore, these data established that the entire process was Sec independent, relying on a novel C-terminal secretion signal (5, 23–31).

However, the view that T1SS is mediated by the one-step translocation of proteins has been challenged. Recently, so-called periplasmic intermediates for a proposed two-step secretion process were described for the adhesins LapA and IBA (3). The exciting results identified a “retention module” (RM) at the N terminus that anchors the adhesion to the cell surface by stalling further translocation. This leaves a stalled short stub in the periplasm, apparently stuck in TolC, and a fully translocated, functional adhesin in the extracellular space. When conditions change,

for example, in the case of LapA, to conditions unfavorable for biofilm formation, proteolysis removes the RM and releases the adhesin. Therefore, the secretion of the adhesin, as the authors described it, occurs in two steps. Our interpretation is that this is an exciting and important variation of the T1SS but that translocation is still effectively one step, and therefore, we prefer to call the adhesin-TolC-RM complex a pseudoperiplasmic intermediate.

Here we summarize our current knowledge of the molecular processes that underlie the T1SS and focus on the molecular events that result in secretion of substrates that harbor a C-terminal secretion sequence.

THE SUBSTRATES OF THE T1SS

The N-terminal domain of an RTX protein like HlyA contains one functional domain, the HlyA pore-forming toxin. CyaA from *Bordetella pertussis* (32) harbors an HlyA-like toxin but also an adenylate cyclase that, following translocation into the cytosol of a host cell, manipulates cAMP levels. More complex architectures are present in MARTX (multifunctional autoprocessing repeats in toxins), LapA, and SiiE-like proteins. MARTX proteins are of enormous size (approximately 500 to 900 kDa). This protein family is encoded in a chromosomal island in human pathogens such as *Vibrio cholerae* (33, 34). The extreme N-terminal part of these proteins is composed of an RTX-like domain that, however, lacks the conserved aspartate residue that normally coordinates the Ca²⁺ ion. Spaced between this domain and the RTX domain near the C terminus are effector proteins that are autoprocessed, posttranslocationally, to release a cocktail of different effectors into a host cell (35). However, little is still known about the mechanism of secretion of MARTX proteins. The RTX adhesins, LapA from *Pseudomonas fluorescens*, and SiiE, the RTX-like protein from *Salmonella*, are even larger, reaching up to 1.5 MDa (3, 36, 37). In LapA

(3, 38), the functional domain contains a varying number of domains that mediate adhesin functions. Strikingly, the SiiE-like adhesins deviate from the canonical architecture of RTX proteins, particularly with respect to calcium binding (39). Ca^{2+} binding sites are distributed virtually throughout the entire molecule, which is composed of 53 bacterial immunoglobulin-like (BIg) domains constituting the functional domain—the adhesin (Fig. 1). Ca^{2+} type I sites (three aspartate residues) fulfill the role of RTX repeats in secretion and are positioned at all the interfaces between two BIg domains (6). On the other hand, the translocon is composed of the familiar tripartite complex; translocation depends on a C-terminal secretion sequence (40) inferred to be extruded first (39).

A C-terminal secretion signal remains as a signature characteristic of RTX substrates. Signals appear to be conserved only within groups of related proteins, with no evidence of widespread conservation as far as we are aware. For the hemolysin group, competitive hypotheses have postulated a specific linear code, a structural code, or a combination of the two, but the question remains unresolved (see the extensive discussion in reference 41).

RTX Motifs and Ca^{2+} Promote Extracellular Folding of Substrates

A bioinformational approach based on the presence of the GG repeats revealed more than 1,000 putative RTX proteins in approximately 250 bacterial species (4). Since that study was published in 2010, the number of putative RTX proteins is necessarily much larger today, given the enormous number of genomes now sequenced. However, only the compilation of Linhartová et al. (4) is currently available. The number of identified RTX repeats ranged from below 10 to more than 40, with a slight tendency of the number of repeats to correlate with molecular weight. Additionally, more than 90% of the putative RTX proteins displayed an isoelectric point below 5.0, suggesting that electrophoretic

mobility (42) might be important for the secretion process.

Structural studies of the alkaline protease from *Pseudomonas aeruginosa* (43) and other substrates of the TISS (6, 44, 45) confirmed that the nonapeptide repeats bind Ca^{2+} ions. Two GG repeats coordinate one Ca^{2+} ion by interaction of the side chain of the aspartate residue and the carbonyl oxygens of the amino acids forming the repeat. This architecture creates a right-handed, so-called β -roll motif (Fig. 2). Functional *in vitro* studies demonstrated that Ca^{2+} ions are a strict requirement for folding. In other words, in the absence of Ca^{2+} ions, substrates, such as HlyA from *E. coli* (46–49) or CyaA from *Bordetella pertussis* (50–52), remain unfolded or in a molten globular state (53). Subsequent studies revealed that the dissociation constant of Ca^{2+} ions from the RTX domain is in the high micromolar range. The concentration of free Ca^{2+} ions in the bacterial cytosol is strictly regulated and remains in the high nanomolar range (100 to 300 nM in *E. coli*) (54). Secretion of RTX proteins therefore presumably occurs in the unfolded state. This hypothesis was indeed experimentally verified by the fusion of maltose binding protein to a C-terminal fragment of HlyA that only harbored the secretion signal and three of the six GG repeats (55). Given that the extracellular concentration of Ca^{2+} ions is normally in the millimolar range (54), this suggests that RTX repeats immediately bind Ca^{2+} upon exit from the bacterium. Elegant *in vitro* studies with CyaA have also demonstrated that binding of Ca^{2+} ions to the RTX domain induces immediate folding of the entire protein (46–48), suggesting that Ca^{2+} ions act as a chemical foldase.

CURRENT WORKING MODEL FOR CLASSIC TISS

The process of secreting a substrate by a TISS starts at the ribosome. However, only after the extreme C terminus of the substrate

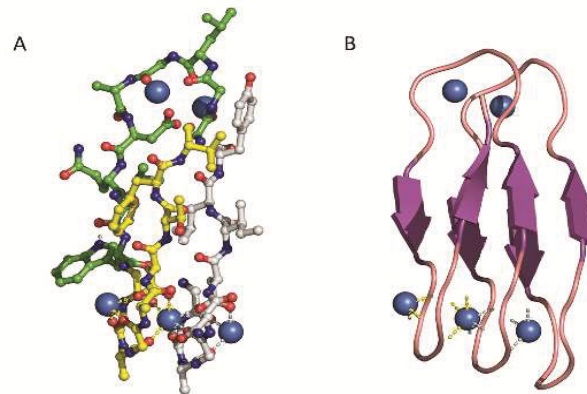


FIGURE 2 Structure of GG repeats of alkaline protease (PDB entry 1KAP) from *P. aeruginosa* in its Ca^{2+} -bound state, resulting in the classic β -roll motif. (A) The five Ca^{2+} ions are shown as blue spheres. For simplicity, only the first three GG repeats are shown in ball-and-stick representation. The carbon atoms of GG repeat one are in gray, the carbon atoms of the second GG repeat in green, and the ones of the third repeat in yellow. The interactions of repeat one with the bound Ca^{2+} ion are indicated by gray dashed lines, and the interaction of the third repeat with the bound Ca^{2+} ions is in yellow. As it is evident, one Ca^{2+} ion is coordinated by repeat n and repeat $n + 2$. (B) RTX domain of alkaline protease from *P. aeruginosa* in cartoon representation. The orientation is identical to that in panel A, and the gray and yellow dashed lines indicate the interactions.

containing the secretion signal (Fig. 1), around 50 to 100 amino acids, has been synthesized will secretion be initiated, since all information necessary and sufficient for secretion is encoded in the secretion signal. Bearing in mind that the sizes of T1SS proteins range from 20 kDa up to 1,500 kDa, two obvious questions arise: why do substrates of T1SS not aggregate and precipitate prior to secretion, and why are these proteins not immediately degraded by cytosolic proteases? Unfortunately, we do not yet have answers to these important questions.

In the second step, the unfolded substrate interacts with both of the two membrane proteins of the inner membrane, the ABC transporter and the MFP (56, 57). Based on cross-linking studies with the HlyA system, these two proteins were shown to form a stable complex in the inner membrane, a dimer of the ABC transporter and a trimer of the MFP (57). However, the remarkable similarity of the T1SS translocon to tripartite drug efflux pumps, such as the AcrB-AcrA-TolC system from *E. coli*, in which there is a 2:6 stoichiometry (ABC:MFP) (58), makes it

most likely that the T1SS MFP is also a hexamer. Nevertheless, further research should be undertaken to resolve this obvious discrepancy. Deletion studies by the Koronakis laboratory showed that the cytoplasmic domain of the MFP is required to recruit the OM component, TolC in the case of the HlyA machinery (56). However, the engagement occurred only in the presence of the substrate, indicating that docking of HlyA with the inner membrane complex transmits a signal to the periplasmic domain of HlyD that results in the formation of a transient HlyB-HlyD-TolC complex, a so-called “channel-tunnel” bridging the entire distance from the cytosol to the extracellular space across the periplasm and two membranes. The timing of these events also explains why deletion or inactivation of one of the three translocon components completely abolishes secretion without the appearance of a periplasmic intermediate. Finally, biophysical studies with the isolated nucleotide binding domain of HlyB, the ABC transporter of the HlyA secretion machinery, demonstrated an interaction with the substrate in

the low micromolar range that required the secretion signal (59).

As soon as the outer membrane protein is engaged and a continuous channel tunnel has formed, the substrate enters the translocation pathway (Fig. 3A). For HlyA, it was experimentally demonstrated that secretion is directional, with the C terminus extended first onto the cell surface (60). Furthermore, the entire process proceeds with a secretion rate of 16 amino acids per transporter per second (61). At this stage, Ca^{2+} ions must bind to the RTX motifs and induce folding as soon as the substrate appears at the cell surface

(Fig. 3A). This should prevent backsliding of the entire protein. Interestingly, reducing the external Ca^{2+} concentration below the dissociation constant of the ion from the RTX motif did not reduce the secretion rate in the HlyA system (61). This clearly demonstrates that the secretion rate is independent of Ca^{2+} and that Ca^{2+} -induced folding does not represent a driving force for secretion. A seemingly different scenario was observed for the much larger adenylate cyclase toxin (CyaA) from *B. pertussis* (62). A Ca^{2+} concentration of 2 mM in the media accelerated the efficiency of secretion. However, even when the Ca^{2+}

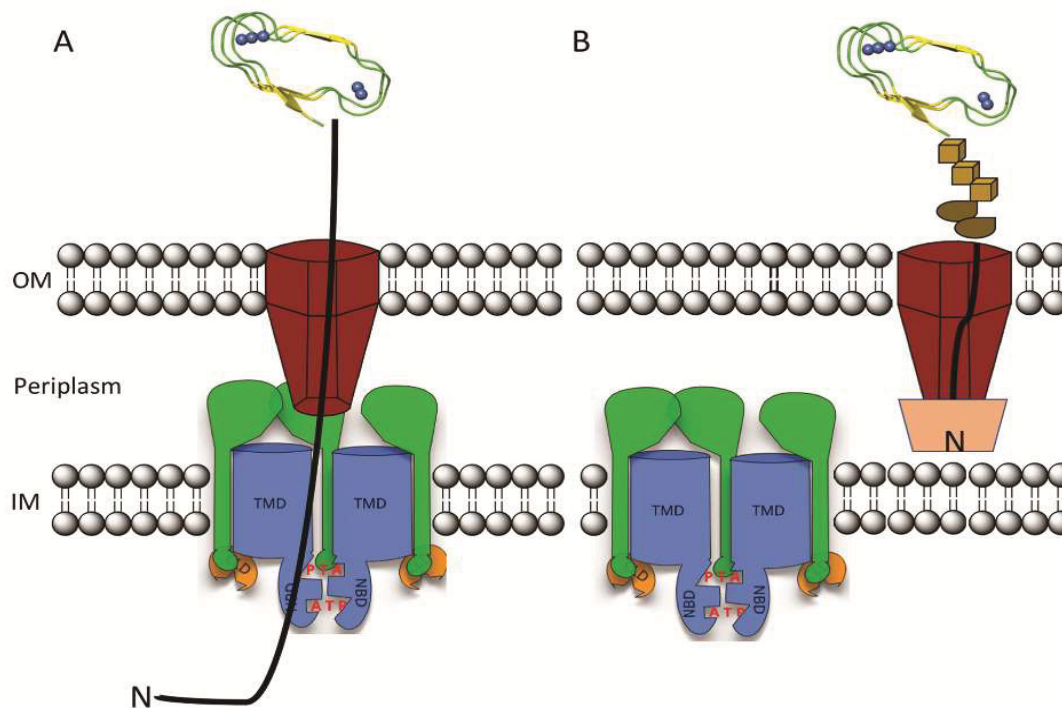


FIGURE 3 Schematic summary of the classic T1SS-mediated substrate secretion (A) and the recently discovered secretion mechanism for some RTX adhesins in which secretion stalls just before completion, creating a so-called two-step process with a pseudoperiplasmic intermediate (B). The ABC transporter and the MFP are shown in blue and green, respectively, and the OM protein is in maroon. (A) The unfolded substrate is secreted with its C terminus first. At the cell surface, Ca^{2+} ions (blue spheres) bind to the GG repeats and induce folding, which results in formation of the β -roll (indicated in cartoon representation). (B) In the case of adhesins such as IBA or LapA, the N-terminal domain starts folding prior to or during secretion, which plugs the translocon (indicated by the light brown polygon) and tethers the entire substrate at the cell surface within the OM component of the translocon of the T1SS. The brown cubes and distorted ellipse represent folded domains of the substrate. This scheme clearly demonstrates that the classic T1SS disassembles only after the entire substrate is translocated, while in two-step T1SS disassembly earlier, e.g., when the N-terminal plug domain has not passed the OM. For further details, see the text. IM, inner membrane; NBD, nucleotide binding domain; TMD, transmembrane domain.

concentration was reduced to 0.1 mM (which does not allow folding of CyaA), 50% of produced CyaA still reached the cell surface. These differences might be due to the diverging sizes of the two RTX proteins or details of the architecture of the RTX domain. Thus, further experimental approaches and analysis of additional TISS substrates are required to completely understand the molecular mechanisms of secretion, the influence of Ca^{2+} ion folding and secretion (if any), and the molecular signals that regulate substrate translocation across two membranes in one step for this group of classic TISS substrates.

RTX ADHESINS—NEW KIDS ON THE BLOCK

RTX proteins include not only toxins but also lipases, S-layer proteins, MARTX, and adhesins, which are extremely large in size. Recently, the structure of an ice-binding adhesin (IBA) of the marine Gram-negative bacterium *Marinomonas primoryensis* (molecular mass, 1.5 MDa) was determined and the putative mechanism of translocation modeled (37). IBA contains the hallmarks of substrates of a TISS, an RTX domain and a C-terminal secretion sequence. N terminal to the RTX domain, three additional domains are located, namely, peptide-, sugar-, and ice-binding domains. While interactions of the peptide- and sugar-binding domains with surface receptors of other microorganisms allow formation of mixed aggregates of microorganisms, the ice-binding domain anchors *M. primoryensis* to ice in seas, lakes, or rivers. Surprisingly, and in contrast to the classical RTX proteins described earlier that are directly secreted into the extracellular space, IBA is translocated but then retained on the cell surface (Fig. 3B). Guo et al. (37) identified a conserved region (homologous to RM in LapA described above) at the extreme N terminus of IBA that they proposed could plug the channel-tunnel of the TISS. Based on their structural analysis, Guo et al. proposed

that this N-terminal region forms two domains: a proximal sequence that folds and a distal region that is sufficiently unfolded to traverse the TolC homologue into the outer membrane. This prevents further translocation and retains the adhesin at the cell surface. In 2018, exciting new data concerning the LapA adhesin from *Pseudomonas fluorescens* (3; for a summary, see reference 38) provided direct experimental evidence for this model in a comprehensive multidisciplinary study. The 160-residue RM was shown to be essential to tether the adhesin to the translocator and thus to the cell surface (Fig. 3B). Moreover, the RM consists of two domains, folded and unfolded, with the former specifically cleaved by a dedicated protease, LapG, to release the adhesin. In another exciting twist, LapG is normally inactivated by binding to its membrane receptor, LapD. Binding is controlled by c-di-GMP to favor binding under conditions suitable for biofilm formation (63). Finally, we note that both of these studies (for IBA and LapA) confirm the directionality of translocation, C terminal first, for TISS secretion.

Finally, it must be stressed that while IBA and LapA are anchored to the surface by stalling translocation, other strategies are used to retain adhesins at the cell surface. SiiE from *Salmonella enterica* contains a putative coiled-coil motif that facilitates immobilization of the entire protein on the surface of the cell envelope, which is controlled by SiiA and SiiB (36). Thus, continued efforts are needed to see whether additional mechanisms and modifications of the classic TISS exist that are used by Gram-negative bacteria to cope with the demands of their ecological niches.

SUMMARY AND OUTLOOK

An enormous amount of data on TISS has been gathered since the discovery of the first system. The amount of available structural information on the components of the translocon machinery is increasing constantly.

These components include the OM protein TolC (64), a closely related homologue of HlyC (21), isolated domains of the ABC transporter HlyB (65–67) and other ABC transporters (68), a soluble fragment of the MFP HlyD (69), and an entire structure of an ABC transporter (70) of a putative TISS with unknown substrate from *Aquifex aeolicus*. This article is unable to cover all aspects of type I secretion; however, it provides a broad summary of the accumulating data on functional aspects of the secretion process. The review does not engage with the possibilities of the TISS in biotechnological applications (for a recent summary, see reference 41) that go well beyond basic research and would allow large-scale protein production and isolation via protein secretion.

However, we are still some distance from a systematic understanding of the TISS since the nature of molecular signals and intramolecular communication within this nanomachinery remains unclear. In summary, there are still many open questions that have to be addressed and many more fascinating variations and novel insights to be discovered for the TISS in Gram-negative bacteria.

ACKNOWLEDGMENTS

We apologize to all our colleagues whose work is not cited due to space limitations. We thank all current and former members of the group for fruitful discussions.

Research on hemolysin A and the hemolysin A secretion machinery is funded by the MOI III graduate school under project name Molecules of Infection and the DFG through CRC 1208 under project name Identity and Dynamics of Membrane Systems—From Molecules to Cellular Functions (project A01 to L.S.).

CITATION

Spitz O, Erenburg IN, Beer T, Kanonenberg K, Holland IB, Schmitt L. 2019. Type I secretion systems—one mechanism for all? *Microbiol Spectrum* 7(2):PSIB-0003-2018.

REFERENCES

1. Costa TR, Felisberto-Rodrigues C, Meir A, Prevost MS, Redzej A, Trokter M, Waksman G. 2015. Secretion systems in Gram-negative bacteria: structural and mechanistic insights. *Nat Rev Microbiol* 13:343–359.
2. Veith PD, Glew MD, Gorasia DG, Reynolds EC. 2017. Type IX secretion: the generation of bacterial cell surface coatings involved in virulence, gliding motility and the degradation of complex biopolymers. *Mol Microbiol* 106:35–53.
3. Smith TJ, Font ME, Kelly CM, Sondermann H, O'Toole GA. 2018. An N-terminal retention module anchors the giant adhesin LapA of *Pseudomonas fluorescens* at the cell surface: a novel sub-family of type I secretion systems. *J Bacteriol* 200:e00734-17.
4. Linhartová I, Bumba L, Mašín J, Basler M, Osička R, Kamanová J, Procházková K, Adkins I, Hejnová-Holubová J, Sadílková L, Morová J, Sebo P. 2010. RTX proteins: a highly diverse family secreted by a common mechanism. *FEMS Microbiol Rev* 34:1076–1112.
5. Felmlee T, Welch RA. 1988. Alterations of amino acid repeats in the *Escherichia coli* hemolysin affect cytolytic activity and secretion. *Proc Natl Acad Sci U S A* 85:5269–5273.
6. Griessl MH, Schmid B, Kessler K, Braunsmann C, Ritter R, Barlag B, Stierhof YD, Sturm KU, Danzer C, Wagner C, Schäffer TE, Sticht H, Hensel M, Müller YA. 2013. Structural insight into the giant Ca²⁺-binding adhesin SiiE: implications for the adhesion of *Salmonella enterica* to polarized epithelial cells. *Structure* 21:741–752.
7. Håvarstein LS, Diep DB, Nes IF. 1995. A family of bacteriocin ABC transporters carry out proteolytic processing of their substrates concomitant with export. *Mol Microbiol* 16:229–240.
8. Håvarstein LS, Holo H, Nes IF. 1994. The leader peptide of colicin V shares consensus sequences with leader peptides that are common among peptide bacteriocins produced by gram-positive bacteria. *Microbiology* 140:2383–2389.
9. Michiels J, Dirix G, Vanderleyden J, Xi C. 2001. Processing and export of peptide pheromones and bacteriocins in Gram-negative bacteria. *Trends Microbiol* 9:164–168.
10. Choudhury HG, Tong Z, Mathavan I, Li Y, Iwata S, Zirah S, Rebuffat S, van Veen HW, Beis K. 2014. Structure of an antibacterial peptide ATP-binding cassette transporter in a novel outward occluded state. *Proc Natl Acad Sci U S A* 111:9145–9150.

11. Husada F, Bountra K, Tassis K, de Boer M, Romano M, Rebuffat S, Beis K, Cordes T. 2018. Conformational dynamics of the ABC transporter McjD seen by single-molecule FRET. *EMBO J* 37:e100056.
12. Felmler T, Pellett S, Welch RA. 1985. Nucleotide sequence of an *Escherichia coli* chromosomal hemolysin. *J Bacteriol* 163:94–105.
13. Härtelein M, Schiessl S, Wagner W, Rdest U, Kreft J, Goebel W. 1983. Transport of hemolysin by *Escherichia coli*. *J Cell Biochem* 22:87–97.
14. Noegel A, Rdest U, Springer W, Goebel W. 1979. Plasmid cistrons controlling synthesis and excretion of the exotoxin alpha-hemolysin of *Escherichia coli*. *Mol Gen Genet* 175:343–350.
15. Springer W, Goebel W. 1980. Synthesis and secretion of hemolysin by *Escherichia coli*. *J Bacteriol* 144:53–59.
16. Nicaud JM, Mackman N, Gray L, Holland IB. 1985. Characterisation of HlyC and mechanism of activation and secretion of haemolysin from *E. coli* 2001. *FEBS Lett* 187:339–344.
17. Stanley P, Hyland C, Koronakis V, Hughes C. 1999. An ordered reaction mechanism for bacterial toxin acylation by the specialized acyltransferase HlyC: formation of a ternary complex with acylACP and protoxin substrates. *Mol Microbiol* 34:887–901.
18. Stanley P, Packman LC, Koronakis V, Hughes C. 1994. Fatty acylation of two internal lysine residues required for the toxic activity of *Escherichia coli* hemolysin. *Science* 266:1992–1996.
19. Trent MS, Worsham LM, Ernst-Fonberg ML. 1998. The biochemistry of hemolysin toxin activation: characterization of HlyC, an internal protein acyltransferase. *Biochemistry* 37:4644–4652.
20. Issartel JP, Koronakis V, Hughes C. 1991. Activation of *Escherichia coli* prohaemolysin to the mature toxin by acyl carrier protein-dependent fatty acylation. *Nature* 351:759–761.
21. Greene NP, Crow A, Hughes C, Koronakis V. 2015. Structure of a bacterial toxin-activating acyltransferase. *Proc Natl Acad Sci U S A* 112:E3058–E3066.
22. Wandersman C, Delepelaire P. 1990. TolC, an *Escherichia coli* outer membrane protein required for hemolysin secretion. *Proc Natl Acad Sci U S A* 87:4776–4780.
23. Chervaux C, Sauvonnnet N, Le Clainche A, Kenny B, Hung AL, Broome-Smith JK, Holland IB. 1995. Secretion of active beta-lactamase to the medium mediated by the *Escherichia coli* haemolysin transport pathway. *Mol Gen Genet* 249:237–245.
24. Gentschev I, Hess J, Goebel W. 1990. Change in the cellular localization of alkaline phosphatase by alteration of its carboxy-terminal sequence. *Mol Gen Genet* 222:211–216.
25. Gray L, Baker K, Kenny B, Mackman N, Haigh R, Holland IB. 1989. A novel C-terminal signal sequence targets *Escherichia coli* haemolysin directly to the medium. *J Cell Sci Suppl* 11:45–57.
26. Gray L, Mackman N, Nicaud JM, Holland IB. 1986. The carboxy-terminal region of haemolysin 2001 is required for secretion of the toxin from *Escherichia coli*. *Mol Gen Genet* 205:127–133.
27. Koronakis V, Koronakis E, Hughes C. 1989. Isolation and analysis of the C-terminal signal directing export of *Escherichia coli* hemolysin protein across both bacterial membranes. *EMBO J* 8:595–605.
28. Mackman N, Baker K, Gray L, Haigh R, Nicaud JM, Holland IB. 1987. Release of a chimeric protein into the medium from *Escherichia coli* using the C-terminal secretion signal of haemolysin. *EMBO J* 6:2835–2841.
29. Mackman N, Holland IB. 1984. Functional characterization of a cloned haemolysin determinant from *E. coli* of human origin, encoding information for the secretion of a 107K polypeptide. *Mol Gen Genet* 196:129–134.
30. Mackman N, Nicaud JM, Gray L, Holland IB. 1985. Genetical and functional organisation of the *Escherichia coli* haemolysin determinant 2001. *Mol Gen Genet* 201:282–288.
31. Mackman N, Nicaud JM, Gray L, Holland IB. 1985. Identification of polypeptides required for the export of haemolysin 2001 from *E. coli*. *Mol Gen Genet* 201:529–536.
32. Goyard S, Sebo P, D'Andria O, Ladant D, Ullmann A. 1993. *Bordetella pertussis* adenylate cyclase: a toxin with multiple talents. *Zentralbl Bakteriol* 278:326–333.
33. Satchell KJ. 2011. Structure and function of MARTX toxins and other large repetitive RTX proteins. *Annu Rev Microbiol* 65:71–90.
34. Satchell KJF. 2015. Multifunctional-autoprocessing repeats-in-toxin (MARTX) toxins of vibrios. *Microbiol Spectr* 3(3):VE-0002-2014.
35. Kim BS, Gavin HE, Satchell KJ. 2015. Distinct roles of the repeat-containing regions and effector domains of the *Vibrio vulnificus* multifunctional-autoprocessing repeats-in-toxin (MARTX) toxin. *mBio* 6:e00324-15.
36. Barlag B, Hensel M. 2015. The giant adhesin SiiE of *Salmonella enterica*. *Molecules* 20:1134–1150.
37. Guo S, Stevens CA, Vance TDR, Olijve LLC, Graham LA, Campbell RL, Yazdi SR, Escobedo C, Bar-Dolev M, Yashunsky V, Braslavsky I,

- Langelaan DN, Smith SP, Allingham JS, Voets IK, Davies PL. 2017. Structure of a 1.5-MDa adhesin that binds its Antarctic bacterium to diatoms and ice. *Sci Adv* 3:e1701440.
38. Smith TJ, Sondermann H, O'Toole GA. 2018. Type 1 does the two-step: type 1 secretion substrates with a functional periplasmic intermediate. *J Bacteriol* 200:e00168-18.
39. Peters B, Stein J, Klingl S, Sander N, Sandmann A, Taccardi N, Sticht H, Gerlach RG, Muller YA, Hensel M. 2017. Structural and functional dissection reveals distinct roles of Ca²⁺-binding sites in the giant adhesin SiiE of *Salmonella enterica*. *PLoS Pathog* 13:e1006418.
40. Wagner C, Polke M, Gerlach RG, Linke D, Stierhof YD, Schwarz H, Hensel M. 2011. Functional dissection of SiiE, a giant non-fimbrial adhesin of *Salmonella enterica*. *Cell Microbiol* 13:1286–1301.
41. Holland IB, Peherstorfer S, Kanonenberg K, Lenders M, Reimann S, Schmitt L. 2016. Type I protein secretion—deceptively simple yet with a wide range of mechanistic variability across the family. *EcoSal Plus* 7:ESP-0019-2015.
42. Cao G, Kuhn A, Dalbey RE. 1995. The translocation of negatively charged residues across the membrane is driven by the electrochemical potential: evidence for an electrophoresis-like membrane transfer mechanism. *EMBO J* 14:866–875.
43. Baumann U, Wu S, Flaherty KM, McKay DB. 1993. Three-dimensional structure of the alkaline protease of *Pseudomonas aeruginosa*: a two-domain protein with a calcium binding parallel beta roll motif. *EMBO J* 12:3357–3364.
44. Baumann U, Bauer M, Létoffé S, Delepelaire P, Wandersman C. 1995. Crystal structure of a complex between *Serratia marcescens* metalloprotease and an inhibitor from *Erwinia chrysanthemi*. *J Mol Biol* 248:653–661.
45. Meier R, Drepper T, Svensson V, Jaeger KE, Baumann U. 2007. A calcium-gated lid and a large beta-roll sandwich are revealed by the crystal structure of extracellular lipase from *Serratia marcescens*. *J Biol Chem* 282:31477–31483.
46. Ostolaza H, Soloaga A, Goñi FM. 1995. The binding of divalent cations to *Escherichia coli* alpha-haemolysin. *Eur J Biochem* 228:39–44.
47. Sánchez-Magraner L, Viguera AR, García-Pacios M, Garcillán MP, Arrondo JL, de la Cruz F, Goñi FM, Ostolaza H. 2007. The calcium-binding C-terminal domain of *Escherichia coli* alpha-hemolysin is a major determinant in the surface-active properties of the protein. *J Biol Chem* 282:11827–11835.
48. Soloaga A, Ramírez JM, Goñi FM. 1998. Reversible denaturation, self-aggregation, and membrane activity of *Escherichia coli* alpha-hemolysin, a protein stable in 6 M urea. *Biochemistry* 37:6387–6393.
49. Thomas S, Bakkes PJ, Smits SH, Schmitt L. 2014. Equilibrium folding of pro-HlyA from *Escherichia coli* reveals a stable calcium ion dependent folding intermediate. *Biochim Biophys Acta* 1844:1500–1510.
50. Blenner MA, Shur O, Szilvay GR, Cropek DM, Banta S. 2010. Calcium-induced folding of a beta roll motif requires C-terminal entropic stabilization. *J Mol Biol* 400:244–256.
51. Chenal A, Guijarro JI, Raynal B, Delepierre M, Ladant D. 2009. RTX calcium binding motifs are intrinsically disordered in the absence of calcium: implication for protein secretion. *J Biol Chem* 284:1781–1789.
52. Sotomayor Pérez AC, Karst JC, Davi M, Guijarro JI, Ladant D, Chenal A. 2010. Characterization of the regions involved in the calcium-induced folding of the intrinsically disordered RTX motifs from the *Bordetella pertussis* adenylate cyclase toxin. *J Mol Biol* 397:534–549.
53. Zhang L, Conway JF, Thibodeau PH. 2012. Calcium-induced folding and stabilization of the *Pseudomonas aeruginosa* alkaline protease. *J Biol Chem* 287:4311–4322.
54. Jones HE, Holland IB, Baker HL, Campbell AK. 1999. Slow changes in cytosolic free Ca²⁺ in *Escherichia coli* highlight two putative influx mechanisms in response to changes in extracellular calcium. *Cell Calcium* 25:265–274.
55. Bakkes PJ, Jenewein S, Smits SH, Holland IB, Schmitt L. 2010. The rate of folding dictates substrate secretion by the *Escherichia coli* hemolysin type 1 secretion system. *J Biol Chem* 285:40573–40580.
56. Balakrishnan L, Hughes C, Koronakis V. 2001. Substrate-triggered recruitment of the TolC channel-tunnel during type I export of hemolysin by *Escherichia coli*. *J Mol Biol* 313:501–510.
57. Thanabalu T, Koronakis E, Hughes C, Koronakis V. 1998. Substrate-induced assembly of a contiguous channel for protein export from *E. coli*: reversible bridging of an inner-membrane translocase to an outer membrane exit pore. *EMBO J* 17:6487–6496.
58. Du D, Wang Z, James NR, Voss JE, Klimont E, Ohene-Agyei T, Venter H, Chiu W, Luisi BF. 2014. Structure of the AcrAB-TolC multi-drug efflux pump. *Nature* 509:512–515.
59. Benabdelhak H, Kiontke S, Horn C, Ernst R, Blight MA, Holland IB, Schmitt L. 2003. A

- specific interaction between the NBD of the ABC-transporter HlyB and a C-terminal fragment of its transport substrate haemolysin A. *J Mol Biol* 327:1169–1179.
60. Lenders MHH, Weidtkamp-Peters S, Kleinschrodt D, Jaeger K-E, Smits SHJ, Schmitt L. 2015. Directionality of substrate translocation of the hemolysin A type I secretion system. *Sci Rep* 5:12470.
 61. Lenders MH, Beer T, Smits SH, Schmitt L. 2016. In vivo quantification of the secretion rates of the hemolysin A type I secretion system. *Sci Rep* 6:33275.
 62. Bumba L, Masin J, Macek P, Wald T, Motlova L, Bibova I, Klimova N, Bednarova L, Veverka V, Kachala M, Svergun DI, Barinka C, Sebo P. 2016. Calcium-driven folding of RTX domain β -rolls ratchets translocation of RTX proteins through type I secretion ducts. *Mol Cell* 62:47–62.
 63. Monds RD, Newell PD, Gross RH, O'Toole GA. 2007. Phosphate-dependent modulation of c-di-GMP levels regulates *Pseudomonas fluorescens* Pf0-1 biofilm formation by controlling secretion of the adhesin LapA. *Mol Microbiol* 63:656–679.
 64. Koronakis V, Sharff A, Koronakis E, Luisi B, Hughes C. 2000. Crystal structure of the bacterial membrane protein TolC central to multidrug efflux and protein export. *Nature* 405:914–919.
 65. Lecher J, Schwarz CK, Stoldt M, Smits SH, Willbold D, Schmitt L. 2012. An RTX transporter tethers its unfolded substrate during secretion via a unique N-terminal domain. *Structure* 20:1778–1787.
 66. Zaitseva J, Jenewein S, Jumpertz T, Holland IB, Schmitt L. 2005. H662 is the linchpin of ATP hydrolysis in the nucleotide-binding domain of the ABC transporter HlyB. *EMBO J* 24:1901–1910.
 67. Zaitseva J, Oswald C, Jumpertz T, Jenewein S, Wiedenmann A, Holland IB, Schmitt L. 2006. A structural analysis of asymmetry required for catalytic activity of an ABC-ATPase domain dimer. *EMBO J* 25:3432–3443.
 68. Murata D, Okano H, Angkawidjaja C, Akutsu M, Tanaka SI, Kitahara K, Yoshizawa T, Matsumura H, Kado Y, Mizohata E, Inoue T, Sano S, Koga Y, Kanaya S, Takano K. 2017. Structural basis for the *Serratia marcescens* lipase secretion system: crystal structures of the membrane fusion protein and nucleotide-binding domain. *Biochemistry* 56:6281–6291.
 69. Kim JS, Song S, Lee M, Lee S, Lee K, Ha NC. 2016. Crystal structure of a soluble fragment of the membrane fusion protein HlyD in a type I secretion system of Gram-negative bacteria. *Structure* 24:477–485.
 70. Morgan JLW, Acheson JF, Zimmer J. 2017. Structure of a type-I secretion system ABC transporter. *Structure* 25:522–529.
 71. Gerlach RG, Jäckel D, Stecher B, Wagner C, Lupas A, Hardt WD, Hensel M. 2007. *Salmonella* pathogenicity island 4 encodes a giant non-fimbrial adhesin and the cognate type I secretion system. *Cell Microbiol* 9:1834–1850.

3.4 Chapter IV – Quantification of endogenous hemolysin A type one secretion system in UPEC, TolC copy numbers and surface distribution versus the influence of overexpression

Title Quantification and surface localization of the hemolysin A type one secretion system at the endogenous level and under conditions of overexpression

Author Tobias Beer*, Sebastian Hänsch*, Klaus Pfeffer, Sander H.J. Smits, Stefanie Weidtkamp-Peters & Lutz Schmitt.

Published to be submitted

Own proportion of this work 30 %;

Secretion system quantification, immunofluorescence labeling of formaldehyde treated cells, quantification of TolC, writing of the manuscript.

* Both authors contributed equally

Quantification and surface localization of the hemolysin A type one secretion system at the endogenous level and under conditions of overexpression

Tobias Beer^{1§}, Sebastian Hänsch^{2§}, Klaus Pfeffer³, Sander H.J. Smits¹, Stefanie Weidtkamp-Peters² & Lutz Schmitt^{1†}

1 Institute of Biochemistry, Heinrich-Heine-Universität, D-40225 Düsseldorf, Germany.

2 Center for Advanced Imaging (CAi), Heinrich-Heine-Universität, D-40225 Düsseldorf, Germany.

3 Institute of Medical Microbiology and Hospital Hygiene, Heinrich-Heine-Universität, D-40225 Düsseldorf, Germany.

§ Both authors contributed equally

Abstract

Secretion systems are essential for Gram-negative bacteria as these nanomachineries allow a communication with the outside by exporting proteins into the extracellular space or directly into the cytosol of a host cell. For example, type one secretion systems (T1SS) secrete a broad range of substrates across both membranes into the extracellular space. One well-known example is the hemolysin A (HlyA) T1SS, which consists of an ABC transporter (HlyB), a membrane fusion protein (HlyD), the outer membrane protein TolC and the substrate HlyA, a member of the family of RTX (repeats in toxins) toxins. In a previous study, we determined the amount of the HlyA T1SS under conditions of overexpression in *E. coli* BL21(DE3) to approximately 4500 copies. Interestingly, the overall amount of TolC as quantified in this study under identical conditions was also approximately 4500 TolC trimers. Since this observation might be a result of overexpression, we turned to the parental uropathogenic strain UTI89. Here, no significant changes in the number of TolC trimers regardless of endogenous or overexpression background of the HlyA T1SS system was determined. Additionally, the amount of the HlyA T1SS was quantified on the endogenous level in UTI89 by fluorescence spectroscopy. These studies were complemented by localization studies at the cell surface applying super-resolution microscopy.

†Corresponding author: Institute of Biochemistry, Heinrich-Heine-University, Düsseldorf, Universitätsstr 1, 40225 Düsseldorf, Germany. Tel: +49-211-81-10773; Fax: +49-211-81-15310; E-mail: lutz.schmitt@hhu.de

Introduction

Gram-negative bacteria such as *Bordetella pertussis*[1-3], *Vibrio cholerae*[4] or uropathogenic *Escherichia coli* (UPEC)[5, 6] are responsible for a variety of human diseases. They developed a series of mechanisms to ensure their own survival in different, often hostile environments. This requires strategies to exchange information between the inside and the outside of the cell, across the inner membrane (IM) and the outer membrane (OM) to adjust to environmental conditions. A minimum of 15 different secretion systems were identified in Gram-negative bacteria so far [7]. These secretion machineries have a variety of functions. The type III secretion system (T3SS) for example uses a rod like structure with a tip as warhead to distribute its payload in the host cell [8]. Also, the type IV secretion system (T4SS) can use a pili like structure to deliver a mix of target proteins and DNA into a cell to infect it [9]. The Type VI secretion system (T6SS) translocates toxic effector proteins through a long tubular structure directly into the target cell, thus spanning three membrane systems [10, 11]. The IM part possesses a significant degree of homology to T4SS and resemble bacteriophage tails, which indicates a common origin [12]. The T3SS, T4SS and T6SS have in common that they simultaneously span the IM and OM [8, 9]. This feature is shared by one other secretion system, the type I secretion system (T1SS). However, T1SS deliver their cargo only into the extracellular space. The secretion of the substrate occurs in an unfolded state with the C-terminus appearing first at the cell surface [13]. The substrates vary in size from large adhesins such as LapA [14] with a molecular weight of approximately 900 kDa, SiiE with 595 kDa [15] or the ice-binding protein MpIBP from *M. primoryensis* with a molecular weight of 1.5 MDa [16], to iron scavenger proteins such as HasA with a molecular weight of approximately 19kDa, which is one of the smallest known secreted T1SS substrate containing a C-terminal secretion signal [17, 18]. In contrast, bacteriocins such like ColV [19] are secreted by a T1SS in a folded state and with a cleavable N-terminal secretion signal [20]. Additionally, the classical view, which developed over decades, that the substrates of the T1SS are secreted in a single step was recently extended[14]. In case of LapA from *Pseudomonas fluorescens* the substrate is clogged at the OM through a so-called retention module, which allows adhesion and biofilm formation [14].

One well-known substrate of T1SS is hemolysin A (HlyA), named after its ability to lyse for example erythrocytes [21]. Hemolysin is a member of the family of RTX-toxins (repeat in toxins) [22]. These nonapeptide repeats have the consensus sequence (GGXGXDXUX, where X can be any amino acid and U is a large, hydrophobic amino acid), which possess a high affinity for calcium ions [23]. The binding of calcium ions induces the folding of the substrates in the extracellular space [24]. To energize substrate translocation an ABC-transporter generates the power stroke. The half-size transporter hemolysin B (HlyB) is located in the IM and colocalizes with the membrane fusion protein (MFP) hemolysin D (HlyD). HlyB and HlyD are supposed to form an inner membrane complex (IMC) of the T1SS [25-28]. To secrete substrates simultaneously across the inner and outer membrane, a third protein in the OM, TolC, is required. TolC [29] is a channel-like protein which reaches into the periplasm and interacts with different secretion systems and drug efflux pumps such as AcrAB, which is also located in the IM, and acts as a connector to the extracellular space across the OM [30-34]. TolC is recruited by the IMC in the presence of the substrate HlyA [28, 35].

Recently, we determined 4500 copies of a stalled HlyA T1SS in BL21(DE3) under conditions of overexpression of HlyA, HlyB and HlyD [36]. To evaluate whether this amount is limited by the endogenous amounts of TolC present in BL21(DE3), we quantified the copy number of TolC in the presence of an actively secreting HlyA T1SS and a stalled complex. In both cases, approximately 4500 copies of trimeric TolC were determined. In the next step, the endogenous number of active HlyA T1SS was quantified using the concept of a stalled secretion complex [13] in UTI89 with 800 secretion machineries compared to 4,500 in BL21(DE3). Finally and as mentioned above, T1SS, T3SS and T4SS secrete their substrates in one step from the cytosol to the extracellular space (T1SS) or into the cytosol of the host cell (T3SS, T4SS). The T3SS of *Shigella* [37] or the T4SS of *Legionella* [38] possess a distinct and polar localization within the bacterial cell envelop. Furthermore, this distinct localization appears to be important for the pathogenicity of these bacteria[37]. We analyzed the surface localization of the HlyA T1SS again employing the concept of a stalled secretion system [13] by biochemical approaches and super resolution microscopy. For the latter, an automated evaluation routine was developed. Interestingly we determined no distinct or polarized surface localization. However, a study investigated the diffusion of the SiiE T1SS components and showed clustering for SiiE from *Salmonella enterica* by single particle tracking[39] and was also evident for the HlyA T1SS.

Methods

Bacterial strains and plasmids.

E. coli DH5 α cells were used for cloning. The generation of the pK184 plasmid coding for HlyB and HlyD, the pBAD plasmid coding for eGFP-HlyAc and eGFP-HlyA, respectively, was previously described [13]. Plasmid pK184 is under the control of a P_{lac} promoter [40], while the two pBAD-derived plasmids are under the control of a P_{BAD} promoter. A synthetic, codon-optimized TolC gene (GenScript) was created based on the genomic sequence of TolC from *E. coli* BL21(DE3) and inserted into a pET-25b(+) plasmid. Additionally, a C-terminal His-tag and a thrombin cleavage site were introduced. All plasmids and oligonucleotides used in this study are summarized in supplementary Table S1.

Two strains were used in this study. *E. coli* BL21(DE3) for overexpression of HlyB and HlyD as well as eGFP-HlyAc or eGFP-HlyA and the uropathogenic *E. coli* strain UTI89 (urinary tract infection) [41], which is the parental strain of HlyB, HlyD and HlyA.

Cell cultivation and protein expression for structured illumination microscopy (SIM).

In the case of *E. coli* BL21(DE), chemically competent cells were transformed with or without pK184-HlyBD and pBAD-eGFP-HlyAc or pBAD-eGFP-HlyA and grown at 37 °C on 2YT agar plates supplemented with 100 $\mu\text{g mL}^{-1}$ carbenicillin and 30 $\mu\text{g mL}^{-1}$ kanamycin, respectively. Overnight cultures of a single colony were used to inoculate 25 mL 2YT supplemented with 100 $\mu\text{g mL}^{-1}$ carbenicillin and 30 $\mu\text{g mL}^{-1}$ kanamycin, respectively, at an OD₆₀₀ of 0.1. Cultures were grown at 180 rpm, 37 °C. The expression of HlyB and HlyD was induced by the addition of 1 mM IPTG. The expression of eGFP-HlyAc or eGFP-HlyA was induced by the addition of 10 mM arabinose and additionally 5 mM CaCl₂ was added to the media. Induction was started at an OD₆₀₀ of 0.6- 0.8 for 2 hours. 1 ml aliquots were harvested

by centrifugation for 3 min at 13,000xg at room temperature (RT). Cells were adjusted with water to an OD_{equivalent} of 0.1 and analyzed by Western blot. Growth behavior of UTI89 cells was analyzed by taking aliquots every hour for up to seven hours with a final sample taken after overnight growth (approximately 14 h). Additionally, a growth curve was recorded in a TECAN (SunriseTM) reader at 25 °C with fast Plate shaking.

The expression levels of HlyB and HlyD as well as the expression levels of eGFP-HlyAc or eGFP-HlyA were determined by Western blot analysis using polyclonal antibodies against HlyA, HlyB or HlyD in combination with a horseradish peroxidase (HRP)-conjugated, secondary antibody.

In the case of *E. coli* UTI89, electrical competent cells were transformed with pBAD-eGFP-HlyAc or pBAD-eGFP-HlyA and grown at 37 °C on 2YT agar plates supplemented with 100 µg mL⁻¹ carbenicillin. Overnight cultures of a single colony were used to inoculate 25 mL 2YT supplemented with 100 µg mL⁻¹ carbenicillin and 30 µg mL⁻¹ kanamycin, respectively, at an OD₆₀₀ of 0.1. Cultures were grown at 180 rpm at 37 °C. The expression of eGFP-HlyAc or eGFP-HlyA were induced by 10 mM arabinose and additionally 5 mM CaCl₂ were added to the media. Induction was started at an OD₆₀₀ of 0.6-0.8 for 2 hours. 1 ml aliquots were harvested by centrifugation for 3 min at 130,00xg at RT. Cells were adjusted with water to an OD_{equivalent} of 0.1 and analyzed by Western blot as described above.

TolC quantification experiments were performed with biological quintuplicates. The growth controls for UTI89, were performed in triplicates with technical quadruplicates for each clone. The quantification of T1SS polarization, was done as quadruplicates.

Expression controls are summarized in the supplementary Figures S1 (BL21(DE)) and S2 (UTI89)

The complete sample preparation protocol including fixation with paraformaldehyde (PFA) different antibodies, DAPI, post-fixation on cover glasses, structured illumination microscopy (SIM) and image processing can be found in detail in the supplementary materials and methods section.

Fluorescence spectroscopy of immunofluorescence labeled and PFA treated *E. coli* UTI89 cells.

Immunofluorescence labeled and paraformaldehyde treated *E. coli* UTI89 cells expressing eGFP-HlyAc were adjusted to an OD₆₀₀ of 1.0 and analyzed by a fluorescence spectroscopy in a Horiba Fluorolog-3 to quantify the amount of T1SS in *E. coli* UTI89. All measurements were performed at 25 °C in a 100 µL cuvette. Excitation was performed at 547 nm and fluorescence emission was monitored at 563 nm with slit widths of 5 nm each. Fluorescence was recorded for 0.5 s. An identical experiment was carried out with PBS buffer and different concentration of free Cy3 fluorophore-linked antibody (0.5 pM–1.5 µM). To validate the results of the Cy3-labeled antibody, we used another, commercially available Cy3-labeled antibody (Molecular Probes). This antibody was used as described above to quantify the amount of T1SS in *E. coli* BL21(DE)[36]. To obtain a background fluorescence for endogenous expression of HlyB, HlyD and HlyA, UTI89 cells were treated as described above. To obtain the background fluorescence for eGFP-HlyAc, a sample of cells was induced and fixed without staining. The average signal

count of unstained *E. coli* UTI89 with overexpressed eGFP-HlyAc at 563 nm was used as background.

Expression and purification of TolC in *E. coli* BL21(DE3) and *E. coli* UTI89.

Chemically competent *E. coli* BL21(DE3) cells were transformed with pET-25b(+) TolC-6His and grown at 37 °C on 2YT agar plates supplemented with 100 µg mL⁻¹ carbenicillin. Overnight cultures of a single colony were used to inoculate 6L 2YT supplemented with 100 µg mL⁻¹ carbenicillin at an OD₆₀₀ of 0.1. Cultures were grown at 180 rpm at 37 °C. The expression of TolC was induced by 1 mM IPTG at an OD₆₀₀ of 0.6-0.8 for 2 hours. Cells were harvested by centrifugation for 15 min at 8,000xg at 4 °C. 12 g of cells were resuspended in lysis buffer (20 mM TRIS pH 7.8, 100 mM NaCl) and disrupted by three rounds at 1.5 kbar in a microfluidic cell disruptor (Microfluidics M-110P).

Cell debris was collected by centrifugation for 30 min at 30,000xg 4 °C. The supernatant was applied to a high spin centrifugation step for 90 min (200,000 g at 4 °C). The membrane pellet was resuspended in solubilization buffer (20 mM TRIS pH 7.8, 250 mM NaCl). For storage at -80 °C, 50 % glycerol was added. For solubilization, the membranes were thaw on ice and adjusted to 20 mg / ml overall protein concentration. Membranes were solubilized with 2 % (w/v) Triton X-100 for 2 hours at 4 °C with gentle agitation in 20 mM TRIS pH 7.8, 250 mM NaCl. Aggregates were separated by centrifugation at 100,000xg for 10 min at 4 °C. Solubilized membranes were diluted 1:1 with solubilization buffer and 10 mM imidazole was added. IMAC purification was performed with a Ni²⁺ loaded 5ml GE High Trap Chelating column (GE Healthcare). After loading, detergent was exchanged. 30 column volumes (CV) washing buffer (20 mM TRIS pH 8, 300 mM NaCl, 0.01 % DDM and 10 mM imidazole) was used. Followed by a 15 CV washing step with washing buffer supplemented with 100 mM imidazole. Elution was performed with washing buffer supplemented with 250 mM imidazole. The eluted protein was dialyzed overnight against 20 mM TRIS pH 8, 300 mM NaCl, 0.01 % DDM and 10 U thrombin per mg protein. The dialyzed protein was concentrated using a Millipore ultrafiltration device (MWCO of 100 kDa) and loaded on a Superdex 200 increased 300/10 column (GE Healthcare). Fractions containing TolC were pooled, concentrated and used for raising polyclonal TolC antibodies and quantification. Protein concentration was measured by a BCA assay (Thermo Fischer).

Quantification of TolC in *E. coli* BL21(DE3) and *E. coli* UTI89.

For the quantification of TolC, purified TolC was used in serial dilutions for quantitative Western blot analysis. Together with the serial dilutions, a reference sample of *E. coli* BL21(DE3) was applied three times as a technical replicate to create an external standard for other Western blots. A polyclonal rabbit antibody against TolC was used for a quantitative Western blot analysis of *E. coli* BL21(DE3) and *E. coli* UTI89. All blots used for quantification are summarized in the supplementary data supplementary Figures S5 and S6.

Results

Quantification of TolC in *E. coli* BL21(DE3) and *E. coli* UTI89.

In our previous study [36], we stalled the T1SS during secretion and quantified the amount of active T1SS in BL21(DE), while overexpressing HlyB, HlyD and eGFP-HlyAc. HlyAc is a N-terminal truncated version of HlyA, and consists of the C-terminal 223 amino acids (aa) of HlyA. This approach resulted in an amount of approximately 4500 active T1SSs indicating that also at least 4500 copies of TolC are present in *E. coli* BL21(DE3). In a previous study investigating the *Resistance-Nodulation-Division* (RND) pump AcrAB, the single components AcrA, AcrB and TolC were also quantified [42]. Here, approximately 5000 – 7000 copies of AcrA per cell during exponential growth phase, compared with only approximately 500 copies of AcrB and approximately 1500 copies of TolC were determined. These results indicate, that the amount of TolC is not sufficient to form 4500 copies of an active T1SS, even if the entire pool of TolC is engaged in the active T1SS. Thus, we decided to determine the amount of TolC under endogenous conditions in the uropathogenic *E. coli* strain UTI89 [5] and to investigate the influence of overexpression of the HlyA T1SS on the amount of TolC. Also, the question arose how many active T1SS are present under these conditions in UTI89. Therefore, we applied our previously established method to quantify the T1SS in BL21(DE3) to UTI89.

Purified TolC was used to determine the amount of TolC in *E. coli* BL21(DE3) by quantitative Western blot analysis. Stepwise dilution of TolC and a technical triplicate of BL21(DE3) cells allowed the calculation of the amount of TolC, which was based on a calibration line of TolC samples of known concentration. These BL21(DE3) cells were subsequently used as a standard to quantify the amount of TolC in BL21(DE3) and UTI89 cells, respectively. In the case of BL21(DE3) cells, different plasmids containing different components of the T1SS, i.e. HlyB, HlyD and eGFP-HlyAc respectively eGFP-HlyA were transformed and overexpressed. In UTI89, only eGFP-HlyAc respectively HlyA was used to investigate its influence on the amount of TolC in the presence of endogenous level of HlyB and HlyD. The different combinations were quantified by quantitative Western blot analysis under conditions of protein expression and no expression. A statistical investigation via ANOVA and Turkey's multiple comparison indicated no significant differences between the analyzed cells. Western blots of the different permutations to quantify TolC are summarized in Figure S7 and Figure S8. In all cases, the amount of TolC was not significantly influenced and remained at a copy number of approximately 4500 TolC trimers per cell (Figure 1 and Tables S3 and S4). This resulted in an average value of 4472 ± 1231 TolC trimers.

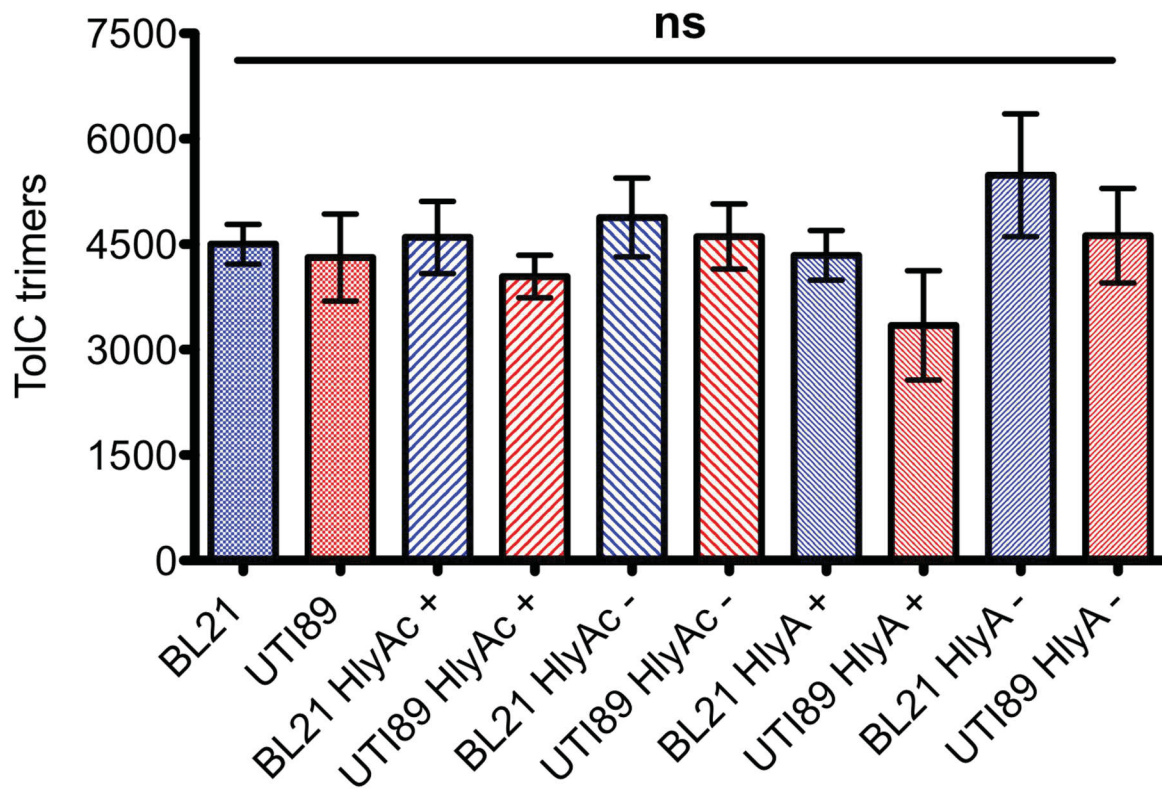


Figure 1. Quantification of TolC trimers. Bar diagram of the quantification of TolC by quantitative Western blot analysis. Blue: BL21(DE3) cells and red UTI89 cells. '+' indicates induction of eGFP-HlyA and eGFP-HlyAc, respectively, while '-' indicates no induction during the experiment. In the case of UTI89 HlyB and HlyD were not overexpressed and only the endogenous protein levels were present. In BL21(DE3), HlyB and HlyD were also overexpressed. ANOVA One-way analysis ($P < 0.05$) and Turkey's Multiple Comparison Test indicated no significance. Bars represent the average of at least five independent quantifications and the error bars represent the standard error of the mean.

Quantification of active T1SS in *E. coli* UTI89.

While no distinguishable difference in the amount of TolC was measured the number of active HlyA T1SS remained unknown in the UTI89 strain. Therefore, the amount of active T1SS was determined by immunofluorescence. This method was also used to determine the amount of active T1SS in BL21(DE3) in a previous study [36]. For the measurements in UTI89, an N-terminal truncated version of eGFP-HlyA, eGFP-HlyAc, was expressed. The reduced size of eGFP-HlyAc obviously reduces the proportion of HlyAc reaching the cell envelope and consequently only one antibody can bind per translocator on the cell surface because of steric reasons [36]. For quantification, a polyclonal HlyA specific primary antibody was used in combination with a Cy3-labeled secondary antibody for fluorescent readout. To determine the amount of unspecific antibody binding on the cell surface and the fluorescence background two approaches were used. First, UTI89 cells expressing eGFP-HlyAc were measured without any antibody staining to determine the background fluorescence in the Cy3 channel caused by eGFP. Wildtype UTI89 cells were stained with primary and secondary antibodies to determine residual/unspecific antibody signal, which is considerably low, because eGFP-HlyAc is not expressed and stalling of the T1SS and thus does not occur. The eGFP-HlyAc fluorescence at

the emission wavelength of Cy3 was then used for fluorescence background (Figure S4). The intensity of the fluorescence signal was multiplied by the slope of a Cy3-antibody calibration line to calculate the amount of active T1SS [36]. The number of T1SS was then divided by the number of cells in the cuvette (8×10^7 cells in 100 μ l at an OD₆₀₀ of 1 [43]). This calculation resulted in number of 796 ± 62 active T1SS per UTI89 cell. In comparison, 4532 ± 966 active T1SS are present in BL21(DE3) when HlyB and HlyD were overexpressed [36] (Figure 2).

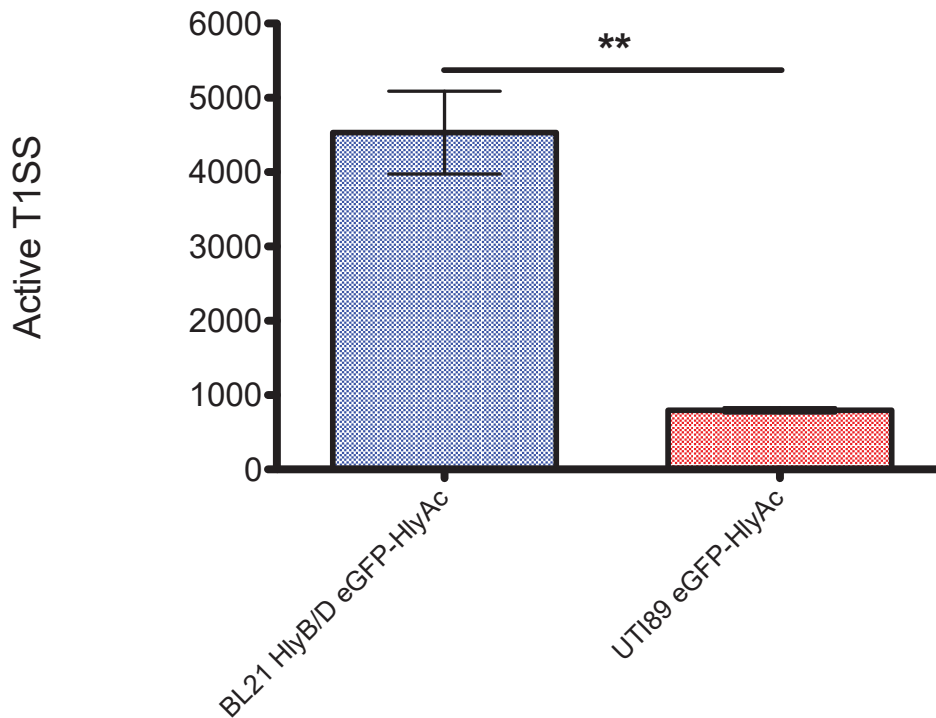
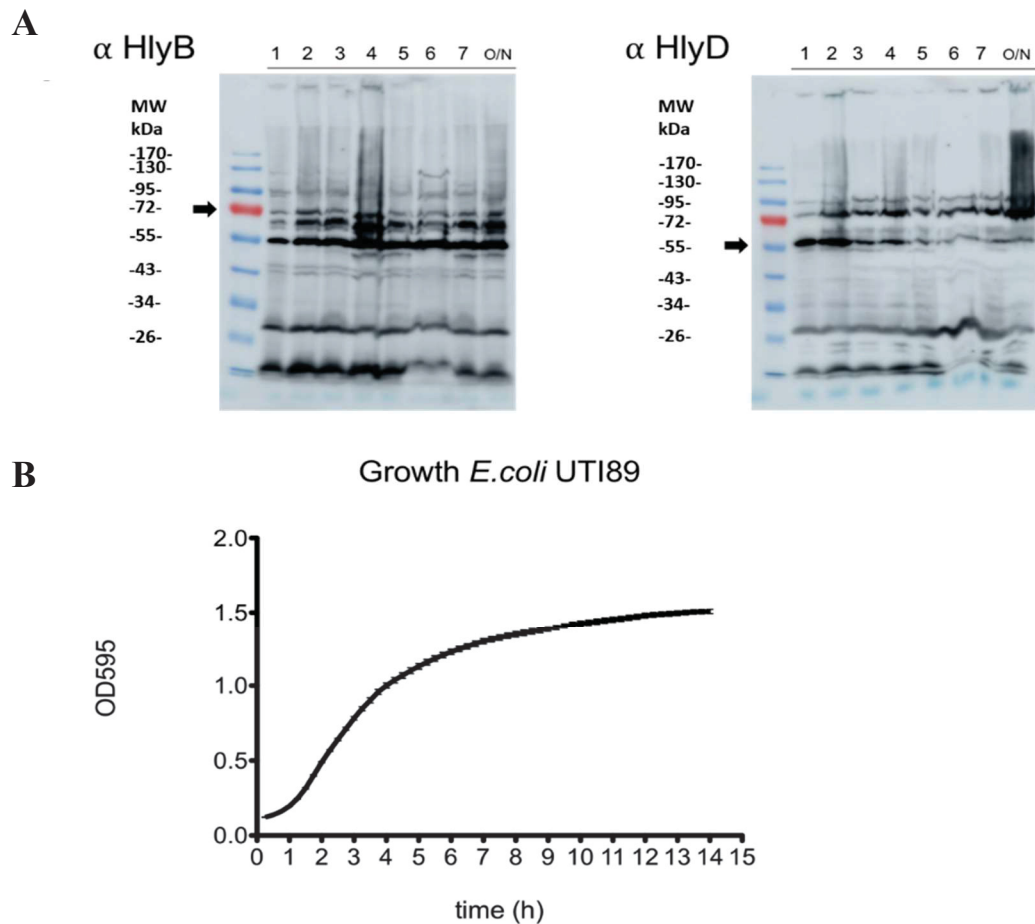


Figure 2. Quantification of active T1SS in *E. coli* BL21(DE3) and UTI89. Error bars represent the standard error of the mean of three independent experiments. $P < 0.01$

The expression of the *hlyCABD* operon is highly regulated [44-47] (for a review see [48]) and the endogenous expression levels of the individual components vary during cell growth. For example, the *rfaH* and *cnfI* genes are major regulation factors. Moreover, the *rfaH* gene is involved in the lipopolysaccharide (LPS) synthesis regulation and therefore linked to the growth of *E. coli* [49]. Furthermore, secretion only occurs in a time window ranging from early to mid-exponential phase and is switched off during the transition to stationary phase [50]. To ensure that the maximal amount of the T1SS was present during our analysis, a growth curve was recorded and the endogenous expression levels of HlyB and HlyD were investigated (Figure 3(A) and 3(B)). An unexpected high proteolytic activity in UTI89 resulted in a substantial amount of degradation products (Figure 3) and complicated an accurate determination of the absolute concentration of HlyB and HlyD. Nevertheless, it was still visible that the expression of HlyB and HlyD increased during the initial growth phase and plateaus off when growth changed from exponential to stationary phase. This is in line with published data [50] and suggested a very defined time window for the secretion of HlyA. More important, it indicated

that the amount of HlyB and HlyD and thus the amount of active T1SS was maximal within the time frame of our analysis.

Figure 3. Growth analysis of *E. coli* UTI89. (A) Western blots against HlyB (left panel) and HlyD



(right panel) of wildtype UTI89. Time points after inoculation in hours, at which the samples were taken, are indicated. Overnight culture (O/N) corresponded to approximately 14 h. Polyclonal antibodies were used as stated. Arrows indicate the size of the corresponding full length protein. (B) Growth curve of *E. coli* UTI89 in a 96 well plate (for further details see Materials & Methods). The curve represents the average of three biological replicates, each of which was performed as quadruplicate.

Surface localization of the T1SS in *E. coli*.

With our result of approximately 800 active T1SS in UTI89 on endogenous level compared to approximately 4500 copies in BL21(DE3) under conditions of overexpression, the question arose if this fivefold change had implications on the localization on the cell surface. Therefore, we analyzed the sub-cellular localization and distribution of the T1SS utilizing structured illumination microscopy (SIM) as a super-resolution imaging technique to integrate detailed spatial information into our understanding of the T1SS machinery in UTI89 and BL21(DE3).

Bacterial secretion systems can be polarized such as the T3SS of *Shigella* [37], the T4SS of *Legionella* [38], both of which localize almost exclusively to the tip of the cell (e.g. ~70% *Shigella* T3SS; > 92% *Legionella* T4SS), or SecYEG of *Bacillus subtilis*, which is arranged in clusters in a spiral-like manner [51]. Barlag *et al.* showed for SiiE T1SS via single particle tracking clustering of signals on the cell surface [39]. However, it is unknown

whether such an arrangement also exists for the HlyA T1SS. To address the question of polarization and clustering for HlyA T1SS, we applied the concept of a stalled T1SS [13, 36]. Here, the substrate, HlyA, was fused to eGFP at its N-terminus. Since, the C-terminus of HlyA appears first at the cell surface [13, 36], N-terminal eGFP [13] can fold prior to secretion and arrests the entire T1SS. This stalled system exposes the C-terminal part to the extracellular space and is accessible to antibodies, a fact that was used to visualize the transporter by immunolabeling. Obviously, this process only recognizes secretion-competent T1SS. Figure 4A shows DAPI (blue channel) stained BL21(DE3) and UTI89 *E. coli* cells expressing HlyA-eGFP (green channel) and α -HlyA staining (red channel). They display significant intensities in the eGFP-channel compared to cells without expression as shown in the unprocessed SIM maximum intensity projections (MIPs) of the acquired z-stacks (Figure 4A and Figure S1)

Subsequently, the red channel was processed to improve resolution and the whole dataset projected as maximum intensity. For the large amount of data in form of microscopy images a self-written semi-automatically script for “*Fiji*” [52] was developed to investigate polarization and signal distribution. The script was also successfully tested *in silico* and on *Schizosaccharomyces pombe* (the script together with the raw data can be found in the supplement). We analyzed the data for possible accumulation of the HlyA T1SS in the bacterial tip zone in comparison to the remaining cell body (Figure 4A and 4B).

The bacterial outlines were generated based on the widefield DAPI signal (Figure 4B, middle panel). The HlyA signal on the surface of the bacteria was semi-automatically located and intensity-weighted to include possible effects of clustered signals. We defined a signal in the tip as accumulated if it achieved a weighted intensity value that was at least 50% larger than the one of the cell body.

According to this criterion, bacteria were classified as single-sided tip-accumulated, double-sided tip-accumulated or no accumulation at all (Figure 4C and Figure S2). For a detailed description of the workflow, see supplementary material. In both strains, BL21(DE3) and UTI89, we observed a small fraction of bacteria with accumulation of the HlyA T1SS in both tips of the cell ($\sim 10\% \pm 7\%$). Roughly a quarter of the cells showed accumulation of signals in one of the tips ($\sim 29\% \pm 8\%$), while the majority of all analyzed cells did not show any specific accumulation of the stalled HlyA T1SS ($\sim 61\% \pm 9\%$) (Figure 4C). In summary, the result lead to the conclusion that stalled HlyA-eGFP, and therefore the T1SS does not significantly accumulate at the tip of the cell.

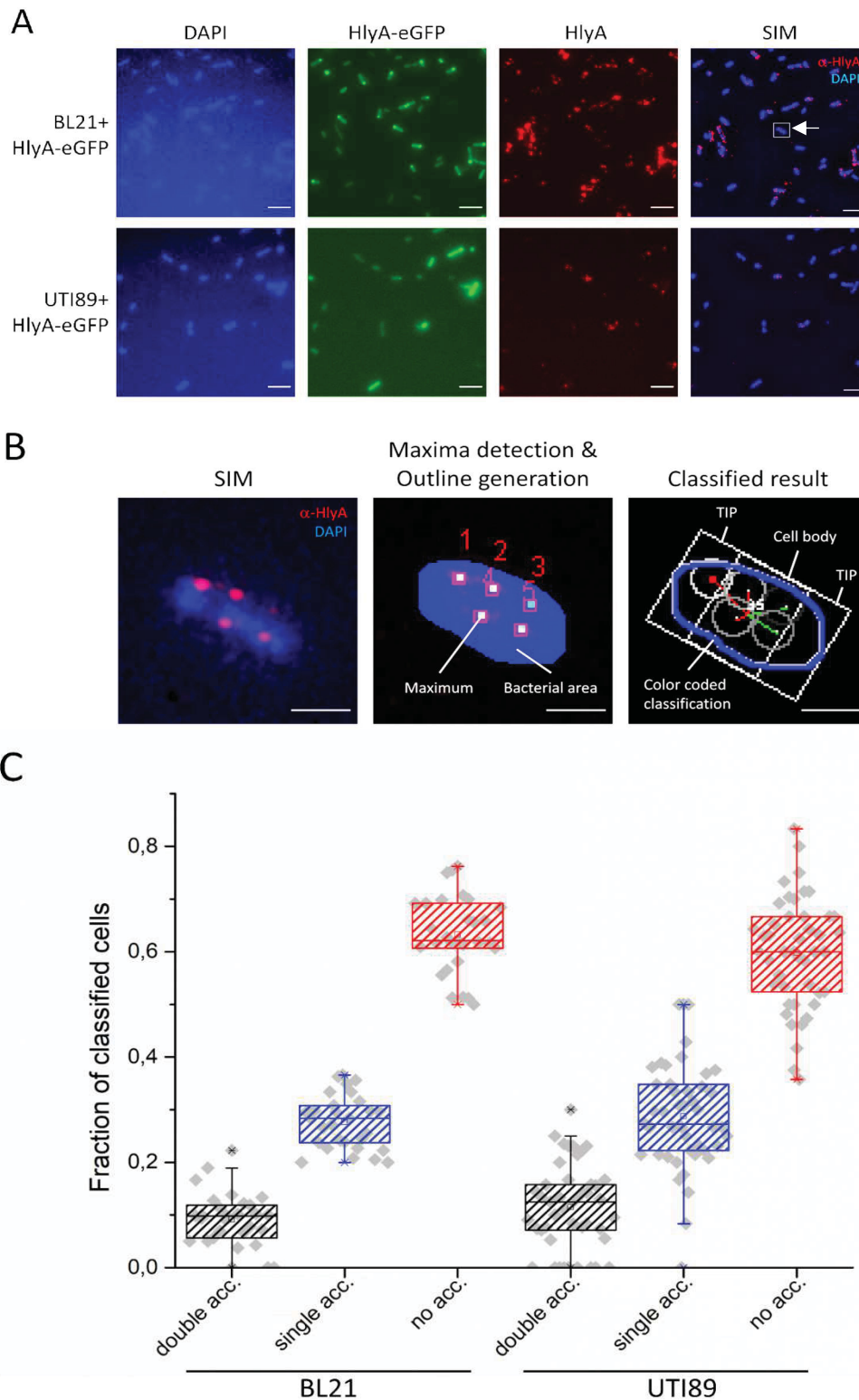


Figure 4. Surface-staining of stalled eGFP-HlyA TISS does not indicate a specific accumulation at the tip. (A) eGFP-HlyA expression was induced in BL21(DE3) or UTI89 and cells were fixed after 2 h of expression. DNA was stained by DAPI and cell surface exposed HlyA was stained by immunofluorescence labelling. Cells were imaged by SIM. Maximum intensity projections (MIPs) of raw data before processing show the DAPI channel in blue (DAPI), the eGFP channel in green (eGFP-HlyA) and the HlyA channel in red (α -HlyA). Contrast was identical to the conditions applied to non-expressing BL21(DE3) and wild type UTI89 cells (Figure S1). Processed SIM MIPs are shown on the right (SIM). The white square marked by arrow indicates the area displayed in (B). Scale bar was 5 μ m. (contrast and brightness was modified for better

visibility) **(B)** (*Left panel*) Inset of SIM processed MIP (contrast and brightness was modified for better visibility). (*Middle panel*) The first analysis step discriminated the area of the bacterial cell (blue), and the detected maxima (white). (*Right panel*) The final output of the analysis included a color-coded classification for each bacterium highlighting the two tip and the cell body areas. The exemplary bacterium displayed no specific accumulation at any tip, indicated by blue outline. Details on colour coding can be found in the supplementary Classification & Quality management. Scale bar 1 μm . **(C)** Quantification of non-accumulating, one-sided and two-sided accumulated HlyA signals. Staining and analysis were performed in duplicates using 3-5 different clones and at least 15 images for each replicate. In total, 1411 UTI89 bacteria were analysed with respect to a potential accumulation of the stalled HlyA T1SS at the tips and 771 bacteria were analysed in the case of BL21(DE3).

Discussion

Environmental conditions have a regulating effect on TolC expression [53] including for example antibiotics [53], pH [54], metal ions, indole, flavonoids [55], ethanol or EDTA [56]. The absence of TolC leads to upregulation of TolC homologues or phenotypes, which were similar to strains carrying a deletion of *acrAB* [57, 58]. Taken together, these data suggest that the expression of TolC is sensitive towards environmental clues. However, the overexpression of the T1SS had no influence on the amount of TolC. In both cases, BL21(DE3) or UTI89, no significant difference (overall 4472 ± 1231 trimers) were detected. This implies that the recruiting through the HlyA T1SS does not directly influence the expression of TolC, but the entire TolC pool becomes engaged in substrate secretion under conditions of T1SS overexpression. However, no influence on cell growth was detected. This raises the interesting question if a feedback loop or a network exists that co-regulates the expression of the HlyA T1SS and TolC, which is encoded outside of the *hlyCABD* operon.

The T1SS surface pattern itself was not influenced by the overexpression of the single components of the secretion system. Under conditions of overexpression, an only fivefold increase of the HlyA T1SS from approximately 800 copies in the endogenous system to approximately 4500 copies was determined. Obviously, these numbers have to be fine-tuned as TolC is part of other the tripartite systems such as AcrAB or MacAB [30, 33, 42, 59, 60]. In 2004, Zgurskaya and coworkers quantified the amount of AcrA, AcrB and TolC to approximately 5000 – 7000 copies of AcrA per cell during the exponential phase compared with only approximately 500 copies of AcrB and approximately 1500 copies of TolC [42]. Currently, we cannot explain this differences, but the amount of TolC in comparison to the amount of completely assembled AcrAB-TolC complexes confirms that only a part of the TolC pool is constantly engaged in this tripartite efflux pump [61]. Even in light of the approximately 800 copies of the HlyA T1SS in UTI89, the number of TolC trimers is still sufficient to ensure the formation of other essential complexes. However, the number of TolC and the amount of T1SS under conditions of overexpression [36] are nearly identical.

In *Salmonella typhimurium* transmission electron microscopy (TEM) was used to determine the number of T3SS [62]. Here, between 10 and 100 T3SS were observed on the cell surface. This is a 8 fold difference compared to the HlyA T1SS of UTI89. This difference is maybe due to the different function of the two secretion systems. While a T1SS targets the host cell by secretion of the substrate in the extracellular space and subsequent diffusion until a host cell is engaged and pore formation can result in cell lysis, the T3SS directly targets the infected cell and injects its pathogenic cargo into the host's cytosol. For SipA, transport started 10-90 sec

after the injection needle penetrated the host cell's plasma membrane and lasted between 100-600 sec [63]. In contrast, secretion of HlyA occurred in a time window ranging from early to mid-exponential phase and was turned off during the transition to the stationary phase [50]. Thus, a T1SS operates similar to a broadly acting weapon, while the T3SS is more similar to a 'precision strike' attack directly on the identified target. This difference in toxin versus effector action could be a reason for the 8 fold difference in the amount of the two secretion systems. The T3SS can deliver its pool of " $6 \pm 3 \times 10^3$ cargo molecules" within 110 seconds [63], while the secretion of a single HlyA requires approximately 67 seconds [36]. This further suggests that a larger amount of T1SS is required to reach a sufficient concentration of extracellular HlyA. Interestingly, the copy number of the Sec translocon, SecYEG, ranges between 200 - 600 [64-67]. Thus the HlyA T1SS and SecYEG are present in a similar copy numbers.

Studies demonstrated that certain secretion systems such as the *Legionella* type IV secretion system[38], the type III secretion system from *Shigella*[37] possess specific polarization or revealed a helical distribution in the case of the SecYEG translocon of *Bacillus subtilis*[51], a possible polarization of a T1SS was so far not investigated. We demonstrate here that the HlyA T1SS adopts no discrete pattern on the cell surface or polarization. Also, we show that this is not an artefact caused by overexpression as the endogenous system (*E. coli* UTI89) displayed the same pattern. For HlyB the insertion mechanism in the membrane is not known yet, however it very likely occurs via the Sec-translocation in a co-translational manner. In contrast, TolC is inserted in the OM while also threaded through the peptidoglycan layer [68]. The peptidoglycan is in steady reconstruction for inserting new proteins in the sacculus [69]. Thus, the more restricted part of the T1SS with respect to diffusion is TolC. This is in line with experiments performed in *Salmonella enterica* [39]. The TolC homolog SiiC of the SiiE T1SS was Halo-tagged, while the ABC-transporter SiiF was SNAP-tagged and its localization was examined by super-resolution microscopy. The SiiA T1SS clustered in a few unspecific spots and SiiF possessed a low diffusion coefficient [39]. Additionally it was shown for the *E. coli* Tol-Pal complex that the components in the inner membrane can lateral diffuse until the substrate colicin is bound and the inner membrane complex mirrors the OMP [70]. The OMPs were observed forming OMP islands restricted due to their sequestration [71]. Shown for proteins inserted by the Bam complex, like TolC by fluorescence microscopy. Based on these and our results, it is tempting to speculate that the pattern of the surface distribution is determined by the interaction of TolC and the peptidoglycan. The measured surface distribution was derived from fully assembled and functional T1SS and the clustering could be a consequence of this. The peptidoglycan grows from patches, which are inserted in the sacculus. When TolC is inserted via the Bam machinery [72] in the peptidoglycan, a 'patch like growing' [69] leads to clustering on the cell surface as recently proposed [39, 68]. In the continuous growth of the sacculus, an individual T1SS would grow in different directions and the signals would become more separated. Bergmiller et al. showed this signal separation by investigating the AcrAB complex with GFP tagged AcrB in the presence of TolC and observed the distribution of fluorescence in the cell during several cell divisions while focusing on the long-lived phenotypic type of the maternal cell [73]. The fluorescence measurement showed an uneven distribution of AcrB during cell division. 42 % of eGFP-AcrB would be remain in the newly formed cell compared to 58 % in the maternal cell. It was concluded that this distribution has a long-term effect (observation started after 100 minutes peaked and ended at 900 minutes) on

the accumulation of AcrAB-TolC to one pole of the cell. While the cells in this experiment were fixated after 2 h of expression. The asymmetry of in the Bergmiller experiment had shown an asymmetry of roughly 10 % in the 2h time window from parental to the daughter cells. While our cells showed signals in one of the tips with roughly $\sim 29\% \pm 8\%$. Therefore some of the one sided polarized cell could show the observed polarization through a parental ancestry. Nevertheless, the accumulation had no influence on the overall cell distribution compared to the cohort of processed cells.

We could show that the T1SS distribution on the cell surface in wild type *E. coli* UTI89 and BL21(DE3) shows no specific pattern except clustering and no distinct polarization. The clustered but even distribution allows secretion in all directions to ensure fast and efficient biological response. Furthermore, the T1SS in *E. coli* strain UTI89 was quantified approximately 800 copies of the HlyA T1SS on an endogenous level, compared to approximately 4500 copies under conditions of overexpression of HlyB, HlyD and eGFP-HlyA in BL21(DE). The stalling of the T1SS during secretion had also no effect on the expression level of TolC, (4500 trimers). This indicates that the different T1SS and RND pumps, which employ TolC (AcrAB, MacAB and ColV T1SS [20, 42, 60]), can still recruit TolC when the HlyA T1SS is expressed in UTI89. The stalling of the HlyA T1SS on endogenous level will not deplete the TolC pool. Regulation of the T1SS expression ensures that a sufficient amount of TolC is present for assembly of the tripartite efflux pumps regarding their vital role in resistance mechanisms [42, 58, 60, 74].

Acknowledgement

We thank, Prof. Rodney Welch (University of Wisconsin, Madison) for the kind gift of UTI89. We also thank all members of the Institute of Biochemistry for stimulating discussions. This project was funded by the DFG (CRC 1208 project A01 to L.S. and project Z02 to S.W.-P.).

References

1. Moullem, M., Z. Farfel, and E. Hanski, *Bordetella pertussis adenylate cyclase toxin: intoxication of host cells by bacterial invasion*. Infect Immun, 1990. **58**(11): p. 3759-64.
2. Carbonetti, N.H., *Pertussis toxin and adenylate cyclase toxin: key virulence factors of Bordetella pertussis and cell biology tools*. Future Microbiol, 2010. **5**: p. 455-69.
3. Hasan, S., et al., *Bordetella pertussis Adenylate Cyclase Toxin Disrupts Functional Integrity of Bronchial Epithelial Layers*. Infect Immun, 2018. **86**(3).
4. Tam, V.C., et al., *A type III secretion system in Vibrio cholerae translocates a formin/spire hybrid-like actin nucleator to promote intestinal colonization*. Cell Host Microbe, 2007. **1**(2): p. 95-107.
5. Ristow, L.C. and R.A. Welch, *Hemolysin of uropathogenic Escherichia coli: A cloak or a dagger?* BBA-MOL CELL RES., 2016. **1858**(3): p. 538-45.

6. Hooton, T.M. and W.E. Stamm, *Diagnosis and treatment of uncomplicated urinary tract infection*. Infect Dis Clin North Am, 1997. **11**(3): p. 551-81.
7. Costa, T.R., et al., *Secretion systems in Gram-negative bacteria: structural and mechanistic insights*. Nat Rev Microbiol, 2015. **13**(6): p. 343-59.
8. Buttner, D., *Protein export according to schedule: architecture, assembly, and regulation of type III secretion systems from plant- and animal-pathogenic bacteria*. Microbiol Mol Biol Rev, 2012. **76**(2): p. 262-310.
9. Alvarez-Martinez, C.E. and P.J. Christie, *Biological Diversity of Prokaryotic Type IV Secretion Systems*. Microbiol. Mol. Biol. Rev., 2009. **73**(4): p. 775-808.
10. Zoued, A., et al., *Architecture and assembly of the Type VI secretion system*. BBA-MOL CELL RES., 2014. **1843**(8): p. 1664-73.
11. Pukatzki, S., et al., *Identification of a conserved bacterial protein secretion system in Vibrio cholerae using the Dictyostelium host model system*. Proc Natl Acad Sci U S A, 2006. **103**(5): p. 1528-33.
12. Leiman, P.G., et al., *Type VI secretion apparatus and phage tail-associated protein complexes share a common evolutionary origin*. Proc Natl Acad Sci U S A, 2009. **106**(11): p. 4154-9.
13. Lenders, M.H.H., et al., *Directionality of substrate translocation of the hemolysin A Type I secretion system*. Sci. Rep., 2015. **5**: p. 12470.
14. Smith, T.J., et al., *An N-Terminal Retention Module Anchors the Giant Adhesin LapA of Pseudomonas fluorescens at the Cell Surface: a Novel Subfamily of Type I Secretion Systems*. J. Bacteriol., 2018. **200**(8): p. e00734-17.
15. Barlag, B. and M. Hensel, *The Giant Adhesin SiiE of Salmonella enterica*. Molecules, 2015. **20**(1): p. 1134-1150.
16. Guo, S., et al., *Structure of a 1.5-MDa adhesin that binds its Antarctic bacterium to diatoms and ice*. Sci. Adv., 2017. **3**(8): p. e1701440.
17. Delepelaire, P., *The SecB chaperone is involved in the secretion of the Serratia marcescens HasA protein through an ABC transporter*. Embo J 1998. **17**(4): p. 936-944.
18. Izadi-Pruneyre, N., et al., *NMR studies of the C-terminal secretion signal of the haem-binding protein, HasA*. Eur. J. Biochem 1999. **261**(2): p. 562-568.
19. Šmajš, D., et al., *Bacteriocin synthesis in uropathogenic and commensal Escherichia coli: colicin E1 is a potential virulence factor*. BMC Microbiol., 2010. **10**(1): p. 288.
20. Zhang, L.H., et al., *Genetic analysis of the colicin V secretion pathway*. Genetics, 1995. **141**(1): p. 25-32.
21. Noegel, A., et al., *Plasmid cistrons controlling synthesis and excretion of the exotoxin alpha-haemolysin of Escherichia coli*. Mol Gen Genet, 1979. **175**(3): p. 343-50.

22. Welch, R.A., *Pore-forming cytolysins of gram-negative bacteria*. Mol Microbiol, 1991. **5**(3): p. 521-8.
23. Ostolaza, H., A. Soloaga, and F.M. Goni, *The binding of divalent cations to Escherichia coli alpha-haemolysin*. Eur J Biochem, 1995. **228**(1): p. 39-44.
24. Chenal, A., et al., *RTX calcium binding motifs are intrinsically disordered in the absence of calcium: implication for protein secretion*. J Biol Chem, 2009. **284**(3): p. 1781-9.
25. Mackman, N., et al., *Genetical and functional organisation of the Escherichia coli haemolysin determinant 2001*. Mol Gen Genet, 1985. **201**(2): p. 282-8.
26. Wang, R.C., et al., *Analysis of the membrane organization of an Escherichia coli protein translocator, HlyB, a member of a large family of prokaryote and eukaryote surface transport proteins*. J Mol Biol, 1991. **217**(3): p. 441-54.
27. Pimenta, A.L., et al., *Antibody analysis of the localisation, expression and stability of HlyD, the MFP component of the E. coli haemolysin translocator*. Mol Gen Genet, 1999. **261**(1): p. 122-32.
28. Balakrishnan, L., C. Hughes, and V. Koronakis, *Substrate-triggered recruitment of the TolC channel-tunnel during type I export of hemolysin by Escherichia coli*. J Mol Biol, 2001. **313**(3): p. 501-10.
29. Wandersman, C. and P. Delepelaire, *TolC, an Escherichia coli outer membrane protein required for hemolysin secretion*. Proc Natl Acad Sci U S A, 1990. **87**(12): p. 4776-80.
30. Koronakis, V., et al., *Crystal structure of the bacterial membrane protein TolC central to multidrug efflux and protein export*. Nature, 2000. **405**(6789): p. 914-919.
31. Du, D., et al., *Structure of the AcrAB-TolC multidrug efflux pump*. Nature, 2014. **509**(7501): p. 512-5.
32. Bavro, V.N., et al., *Assembly and channel opening in a bacterial drug efflux machine*. Mol. Cell, 2008. **30**(1): p. 114.
33. Shi, X., et al., *In situ structure and assembly of the multidrug efflux pump AcrAB-TolC*. Nat. Commun., 2019. **10**(1): p. 2635.
34. Koronakis, V., J. Eswaran, and C. Hughes, *Structure and function of TolC: the bacterial exit duct for proteins and drugs*. Annu Rev Biochem, 2004. **73**: p. 467-89.
35. Thanabalu, T., et al., *Substrate-induced assembly of a contiguous channel for protein export from E.coli: reversible bridging of an inner-membrane translocase to an outer membrane exit pore*. Embo J, 1998. **17**(22): p. 6487-96.
36. Lenders, M.H., et al., *In vivo quantification of the secretion rates of the hemolysin A Type I secretion system*. Sci Rep, 2016. **6**: p. 33275.
37. Jaumouillé, V., et al., *Cytoplasmic targeting of IpaC to the bacterial pole directs polar type III secretion in Shigella*, in Embo J. 2008. p. 447-57.

38. Jeong, K.C., et al., *Polar delivery of Legionella type IV secretion system substrates is essential for virulence*. Proc Natl Acad Sci U S A, 2017. **114**(30): p. 8077-8082.
39. Barlag, B., et al., *Single molecule super-resolution imaging of proteins in living Salmonella enterica using self-labelling enzymes*. Sci. Rep., 2016. **6**: p. 31601.
40. Bakkes, P.J., et al., *The rate of folding dictates substrate secretion by the Escherichia coli hemolysin type I secretion system*. J Biol Chem, 2010. **285**(52): p. 40573-80.
41. Mulvey, M.A., J.D. Schilling, and S.J. Hultgren, *Establishment of a Persistent Escherichia coli Reservoir during the Acute Phase of a Bladder Infection*. Infect. Immun., 2001. **69**(7): p. 4572-4579.
42. Tikhonova, E.B. and H.I. Zgurskaya, *AcrA, AcrB, and TolC of Escherichia coli Form a Stable Intermembrane Multidrug Efflux Complex*. J Biol Chem, 2004. **279**(31): p. 32116-24.
43. F.M. Ausubel et al., ed., John Wiley & Sons, *Short protocols in molecular biology*. 5th ed. 2. 2002, New York: Wiley.
44. Lemonnier, M., L. Landraud, and E. Lemichez, *Rho GTPase-activating bacterial toxins: from bacterial virulence regulation to eukaryotic cell biology*. FEMS Microbiol Rev, 2007. **31**(5): p. 515-34.
45. Bailey, M.J.A., C. Hughes, and V. Koronakis, *RfaH and the ops element, components of a novel system controlling bacterial transcription elongation*. Mol. Microbiol., 1997. **26**(5): p. 845-851.
46. Leeds, J.A. and R.A. Welch, *RfaH enhances elongation of Escherichia coli hlyCABD mRNA*. J Bacteriol, 1996. **178**(7): p. 1850-7.
47. Leeds, J.A. and R.A. Welch, *Enhancing transcription through the Escherichia coli hemolysin operon, hlyCABD: RfaH and upstream JUMPStart DNA sequences function together via a postinitiation mechanism*. J Bacteriol, 1997. **179**(11): p. 3519-27.
48. Thomas, S., I.B. Holland, and L. Schmitt, *The Type I secretion pathway — The hemolysin system and beyond*. (BBA) - Mol. Cell Res., 2014. **1843**(8): p. 1629-1641.
49. Schnaitman, C.A. and J.D. Klena, *Genetics of lipopolysaccharide biosynthesis in enteric bacteria*. Microbiol. Rev., 1993. **57**(3): p. 655-682.
50. Nicaud, J.-M., et al., *Regulation of haemolysin synthesis in E. coli determined by HLY genes of human origin*. Mol. Gen. Genet., 1985. **199**(1): p. 111-116.
51. Campo, N., et al., *Subcellular sites for bacterial protein export*. Mol Microbiol, 2004. **53**(6): p. 1583-99.
52. Schindelin, J., et al., *Fiji: an open-source platform for biological-image analysis*. Nat. Methods, 2012. **9**: p. 676.

53. Zhang, A., J.L. Rosner, and R.G. Martin, *Transcriptional activation by MarA, SoxS and Rob of two tolC promoters using one binding site: a complex promoter configuration for tolC in Escherichia coli*. Mol. Microbiol., 2008. **69**(6): p. 1450-1455.
54. Masuda, N. and G.M. Church, *Regulatory network of acid resistance genes in Escherichia coli*. Mol. Microbiol., 2003. **48**(3): p. 699-712.
55. Leblanc, S.K.D., C.W. Oates, and T.L. Raivio, *Characterization of the Induction and Cellular Role of the BaeSR Two-Component Envelope Stress Response of Escherichia coli*. J. Bacteriol., 2011. **193**(13): p. 3367-3375.
56. Bury-Moné, S., et al., *Global Analysis of Extracytoplasmic Stress Signaling in Escherichia coli*. PLOS Genet., 2009. **5**(9): p. e1000651.
57. Nichols, R.J., et al., *Phenotypic Landscape of a Bacterial Cell*. Cell, 2011. **144**(1): p. 143-156.
58. Sulavik, M.C., et al., *Antibiotic Susceptibility Profiles of Escherichia coli Strains Lacking Multidrug Efflux Pump Genes*. Antimicrob. Agents Chemother., 2001. **45**(4): p. 1126-1136.
59. Fralick, J.A., *Evidence that TolC is required for functioning of the Mar/AcrAB efflux pump of Escherichia coli*. J. Bacteriol., 1996. **178**(19): p. 5803-5805.
60. Fitzpatrick, A.W.P., et al., *Structure of the MacAB-TolC ABC-type tripartite multidrug efflux pump*. Nat Microbiol, 2017. **2**: p. 17070.
61. Krishnamoorthy, G., et al., *On the role of TolC in multidrug efflux: the function and assembly of AcrAB–TolC tolerate significant depletion of intracellular TolC protein*. Mol. Microbiol., 2013. **87**(5): p. 982-997.
62. Kubori, T., et al., *Supramolecular structure of the Salmonella typhimurium type III protein secretion system*. Science, 1998. **280**(5363): p. 602-5.
63. Schlumberger, M.C., et al., *Real-time imaging of type III secretion: Salmonella SipA injection into host cells*. 2005. **102**(35): p. 12548-12553.
64. Matsuyama, S.-I., et al., *Overproduction, purification and characterization of SecD and SecE, integral membrane components of the protein translocation machinery of Escherichia coli*. BBA Prot. Struc. and Mol. Enzymology, 1992. **1122**(1): p. 77-84.
65. Drew, D., et al., *Assembly and overexpression of membrane proteins in Escherichia coli*. BBA Prot. Struc. and Mol. Enzymology, 2003. **1610**(1): p. 3-10.
66. Moran, U., R. Phillips, and R. Milo, *SnapShot: Key Numbers in Biology*. Cell, 2010. **141**(7): p. 1262-1262.e1.
67. Kudva, R., et al., *Protein translocation across the inner membrane of Gram-negative bacteria: the Sec and Tat dependent protein transport pathways*. Res Microbiol., 2013. **164**(6): p. 505-534.

68. Meroueh, S.O., et al., *Three-dimensional structure of the bacterial cell wall peptidoglycan*, in *Proc Natl Acad Sci U S A*. 2006. p. 4404-9.
69. Typas, A., et al., *From the regulation of peptidoglycan synthesis to bacterial growth and morphology*. *Nat. Rev. Microbiol.*, 2011. **10**: p. 123.
70. Rassam, P., et al., *Intermembrane crosstalk drives inner-membrane protein organization in Escherichia coli*. *Nat. Commun.*, 2018. **9**(1).
71. Rassam, P., et al., *Supramolecular assemblies underpin turnover of outer membrane proteins in bacteria*. *Nature*, 2015. **523**(7560): p. 333-336.
72. Hagan, C.L., T.J. Silhavy, and D. Kahne, *beta-Barrel membrane protein assembly by the Bam complex*. *Annu Rev Biochem*, 2011. **80**: p. 189-210.
73. Bergmiller, T., et al., *Biased partitioning of the multidrug efflux pump AcrAB-TolC underlies long-lived phenotypic heterogeneity*. *Science*, 2017. **356**(6335): p. 311-315.
74. Sennhauser, G., et al., *Drug export pathway of multidrug exporter AcrB revealed by DARPin inhibitors*. *PLoS Biol*, 2007. **5**(1): p. e7.

Supplementary:

The *Saccharomyces pombe* strain expressing lifeact-GFP (UFY2999: *Pact1*-LAGFP::*leu1*⁺ *ura4*-D18 *leu1*-32 h⁻ + pmCherry/URA4) harbors an additional *ura4*⁺ plasmid encoding mCherry under the control of the *nmt1*⁺ promoter. This strain was generated based on the lifeact-eGFP expressing *S. pombe* strain MBY6656 (*Pact1*-LAGFP::*leu1*⁺ *ura4*-D18 *leu1*-32 h⁻), which was a kind gift of Dr. M. Balasubramanian (Division of Biomedical Sciences, Warwick) [1].

Materials:

DAPI (Sigma Aldrich)

FM4-64FX (Thermo Fischer Scientific)

ProLong Diamond (Thermo Fischer Scientific)

Microscopy:

Structured illumination microscopy was performed using the Zeiss ELYRA PS.1 microscope system (Zeiss Microscopy GmbH, Oberkochen, Germany) equipped with a Plan-Apochromat 63x/1.4 oil immersion objective lens. For excitation of DAPI we used a 405 nm diode laser, a eGFP the 488 nm diode laser and for Abberior Star 635P a 642 nm diode laser, respectively. Detection filter were set for the different channels as follows: for DAPI BP 420-480 + LP 750, for eGFP-HlyA BP 495-570 + LP 750, and for α -HlyA + Abberior Star 635P LP 655. Three rotations with no averaging were set as parameters for SIM imaging. We acquired z-stacks, that were processed internally with the ZEN black at a fixed signal-to noise filter of -6. Resulting data files contained super-resolution and widefield data for all acquired channels. For downstream image analysis, the widefield of the DAPI channel and the super-resolution data of HlyA signal in the red channel were used as *maximum intensity projections* of the acquired Z-stacks.

As a positive control we acquired lifeact-eGFP signal in *S. pombe* yeast cells that display clear accumulation of fluorescent signal depending on the life cycle with a Zeiss LSM880 Airyscan microscope system (Zeiss Microscopy GmbH, Oberkochen, Germany), equipped with a Plan-Apochromat 63x/1.4 oil immersion objective lens. Imaging parameters were set in

Fast-airyscan mode as follows. The pixel dwell time was set to 0.66 μ s, with a line averaging of 4 at an excitation wavelength of 488 nm to excite lifeact-eGFP and 633 nm as excitation wavelength of FM4-64FX dye (Thermo Fischer Scientific) for membrane staining. Detection filters were set as BP 420-480 + BP 495-550 for lifeact-eGFP and BP 570-620 + LP 645 for FM4-64FX. Resulting Z-stacks were processed with the Zeiss Airyscan processing using the

automatic standard filter settings and converted into *maximum intensity projections* before analysis with Fiji.

Staining:

After two hours of induction, an OD_{equivalent} of 0.1 from the induced cells was taken and centrifuged for 2 min at 13,000x g at RT. The supernatant was discarded and cells were resuspended in 100 µl fresh 2YT media. BSA in PBS, pH 7.4 was added to a final concentration of 1 % and incubated for 10 min at RT. Primary antibody (polyclonal Rabbit) [2] against HlyA was added (1:50) and incubated under gentle agitation for 1 h at RT. Cells were collected by centrifugation for 2 min at 13,000x g at RT and washed 3 times with 1 ml 2YT. After washing, the pellet was resuspended in 2 ml 4 % paraformaldehyde (PFA) in PBS, pH 7.4. Cells were incubated under gentle agitation for 1 h at RT, collected again by centrifugation for 2 min at 13,000x g at RT and washed 2 times with 1 ml PBS, pH 7.4, followed by a third washing step with 100 mM NH₄Cl in PBS, pH 7.4 for 20 min under gentle agitation to quench residual active PFA. Subsequently, cells were collected by centrifugation for 2 min at 13,000x g at RT and washed 2 times with 1 ml PBS. Each aliquot was resuspended in 100 µl PBS containing 1 % BSA. The secondary antibody (1:100) against rabbit was added, either with Cy3 label for the quantification experiment, or AbberiorStar635P for the surface localization. Samples were incubated under gentle agitation for 1h at RT, collected by centrifugation for 2 min at 13,000x g at RT and washed 3 times with 1 ml PBS pH 7.4. Each aliquot was resuspended in 100 µl PBS. The DNA was stained by the addition of DAPI and incubated under gentle agitation for 5 min at RT before collecting by centrifugation for 2 min at 13,000x g at RT and washing 3 times with 1 ml PBS. The cells were then resuspended in 100 µl PBS.

Slide preparation and post-fixation:

For the sample preparation poly-L-lysine slides were prepared freshly as follows. Cover glasses grade #1.5H were cleaned with 70 % Ethanol and dried by pressured air. Per cover glass 500 µl of poly-L-lysine (0.1 % w/v in H₂O) was spread on top and incubated for 5 min. Residual poly-L-lysine was removed and dried with pressured air. The coated glass was placed cover up in a 12-well plate and overlaid with 1 ml PBS. 10 µl of the stained sample were added to the well and mixed. The plate was centrifuged for 15 min at 4°C and 1,500 x g. The supernatant was discarded and each sample was fixed to the coating by adding 1 ml PFA 4 % in PBS to each sample for 10 min, washed with 1 ml PBS and in addition with 1 ml PBS containing 100 mM NH₄Cl for 10 min. The sample was finally washed 3 times with 1 ml PBS each. The cover glass with attached cells was then rinsed of residual PBS and embedded on a glass slide with one drop (~10µl) ProLong Diamond.

Cell treatment (*S. pombe*):

Saccharomyces pombe cells expressing lifeact-eGFP were inoculated in minimal medium (MM) with supplements as described before [3] and incubated for approximately 20 h at 25°C and 170 RPM. 50 µl of the resulting cell culture were then mixed with 1 ml of fresh MM and centrifuged for 15 min at RT and 1500 x g on Poly-L-Lysin coated coverslips as described before (slide preparation). The coated slides were then mounted into a live cell chamber, overlaid carefully with 500 µl MM containing FM4-64FX (Thermo Fischer Scientific) at a final concentration of 5µg/ml and imaged directly.

Workflow (Supplements / Material and Methods):

Resulting images of stained bacteria were analyzed applying a self-written Fiji [4] macro according to the following steps.

Bacteria outline generation:

The widefield DAPI channel was processed using a *pseudo-flatfield correction* (radius 50 px) of the BioVoxel-Toolbox [5], in order to create an equal DAPI intensity for subsequent thresholding. Next, the DAPI channel was smoothed using a *Gaussian blur* of 1px radius and a *median filter* of 10px radius. To create a binary image for the bacterial area, thresholding using *Li's Minimum Cross Entropy* [6] was performed. To include all associated HlyA signals in the red channel, the resulting outlines were *dilated* by the factor of 5 and artificially fused bacteria outlines were manually removed from the analysis.

Signal-identification:

HlyA signals were first identified by the *detect maxima* function of Fiji. As a threshold approximation for this function an auto-threshold procedure was implemented. During this HlyA signals are limited to those overlapping with the generated bacteria outlines. To increase robustness, potential signals outside of the bacteria are ignored by the workflow. Next, a threshold according to the *triangle* method [7] was applied to identify HlyA signals and the *mean intensity* of those identified regions was set as a threshold for the *maxima detection* procedure.

Intensity weighting:

Furthermore, all HlyA signals assigned to bacteria are weighted on a scale of 0-10 based on their intensity to include the effect and influence of clustered signals. A *Gaussian fit* was carried out, based on the measured intensity of a 6 px rectangle around the signal to set a more accurate intensity. In case of a less well-defined *Gaussian fit*, the measured maximum value of the 6 px rectangle was used, which occurred on average in less than 3 % of the cases of exemplary analyzed datasets. For each signal an intensity score from 0 to 10 was generated as quotient of the signal intensity divided by the *maximum signal* intensity found in the image

multiplied by 10. This results in a score of 0 for no intensity signals and 10 for the most intense signal found in the image.

Definition of cell body and tip zone:

For each bacterium an approximation of its area is set as a rectangle which is scaled according to the *ferets length* of bacteria outline and its *minimum ferets diameter* with additional 20 %. Because half of the *minimum ferets diameter* matches the radius of the curved tip in rod-shaped *E. coli*, another rectangle with the length of the *ferets diameter* without the size of two tips (once the *minimum ferets diameter*) and the width of the *minimum ferets diameter* additional 20 % is generated. This smaller area resembles the area of the cell body without tip zones.

Accumulation check:

Each detected HlyA signal, which overlaps with the bacteria cell, was checked if it was part of the smaller cell body area. If this is the case, the weighted intensity score was added to the cell body. If this was not the case, the corresponding intensity score was added to the tip. By using the angle of a line between the HlyA signal and the geometrical center of the bacterium compared to the *ferets angle*, the tip signal was then assigned to the left or the right handed tip. The summed signal scores of the cell body and the two tip zones were then divided by the area of the cell body or the tip zone to rule out the effect, that slightly elongated cells have a higher chance to accumulate signal in the cell body compared to the tip zones.

Classification & Quality management:

Finally, the area normalized intensity scores were compared between the tip zone and the cell body. Here, we set an accumulation threshold of 1.5, meaning that the area normalized intensity score in the tip must be at least 1.5-fold higher (50% higher) compared to the cell body. This threshold had been chosen according to toy simulations as described later. The classification was performed according to the following criteria and quality management aspects to exclude bacteria from the analysis, which were not within the limitations of this tool (Fig. S2). The counted classes were: No accumulation at any tip (blue outline in results file) was counted as non-accumulated; accumulation on the right tip (green outline) or on the left tip (red outline) was counted as single sided accumulation; accumulation at both sides (white outline) was counted as double sided accumulation. Bacterial cells were excluded from the analysis, if a bacterium had no signal at all (yellow outline), less than 3 signals (magenta outline), or the cell body of a bacterium was smaller than the size of the tip zone (cyan outline). As another quality management step the output (results file and display of bacteria area overlaid with the HlyA signals and *maxima detection*) was visually inspected at the end of the analysis.

Controls:

As a control for the resulting macro a toy simulation was performed to assure that the analysis is assigning the weighted intensities correctly and detects simulated accumulated signal. Random signal distribution does not give false positive results (Fig. S3, left & middle). The accumulation-threshold was set to 1.5, because this did not result in false positive classification in the random distribution, and could detect the clear accumulated situations correctly. Furthermore, as a proof of principle *Saccharomyces pombe* cells expressing lifeact-eGFP were analyzed for accumulated localization of actin patches. Since the localization of these patches changed throughout the cell cycle ([1]), the pattern of these cells served as another control. The *S. pombe* cells stained with FM4-64FX and imaged under live-cell conditions using the Airyscan technique. *Maximum-intensity projection* was performed for the resulting Airyscan micrograph and processed similar to the *E. coli* measurements with the following exceptions: Due to the lack of a fluorescent internal marker and the heterogeneity of the FM4-64FX staining, the threshold for the outlines was set manually to achieve a closed cellular outline. The outlines were not dilated by the factor of 5 px, because of the tendency of *S. pombe* to aggregate and a *watershed-filter* was used to separate *S. pombe* outlines. As seen from the result (Fig. S3, right panel) obviously polarized cells were detected and highlighted in the corresponding color (green, red and white). Accordingly, cells with no clear polarization were highlighted in blue, while smaller artifacts were detected and excluded.

Table S1.: List of plasmids used:

Name	Description	Reference
pK184-HlyB/D	Plasmid encoding <i>hlyB</i> and <i>hlyD</i>	[8]
pET25b(+)-TolC-6His	Plasmid encoding for TolC with a thrombine cleavable 6-His tag on the C-terminal site	This study
pBAD-eGFP-HlyAc	Plasmid encoding <i>eGFP-hlyAc</i>	[9]
pBAD-eGFP-HlyA	Plasmid encoding <i>eGFP-hlyA</i>	[9]

Table S2.: List of antibodies used:

Name	Description	Host
α HlyA	<i>Polyclonal against proHlyA, serum</i>	Rabbit
α HlyB	<i>Polyclonal against the NBD of HlyB, purified</i>	Rabbit
α HlyD	<i>Polyclonal against the periplasmic part of HlyD, serum</i>	Rabbit
α TolC	<i>Polyclonal against TolC, serum</i>	Rabbit
α Rabbit-HRP	<i>Polyclonal against rabbit IgG, conjugated with HRP, purified, (Thermo)</i>	Goat
α Rabbit-Cy3	<i>Polyclonal against rabbit IgG, conjugated with Cy3, purified (Abcam)</i>	Goat
α Rabbit-Ab635	<i>Polyclonal against rabbit IgG, conjugated with Abberior STAR 635P, purified (Abberior)</i>	Goat

Sequence of TolC inserted in pET25b(+) restriction sides BamHI and EcoRI:

GGATCCGCTGGTGCCGCGCGGCAGCATGAAGAAATTGCTCCCCATTCTTATCGGC
CTGAGCCTTTCTGGGTTTCAGTTCGTTGAGCCAGGCCGAGAACCTGATGCAAGTTT
ATCAGCAAGCACGCCTTAGTAACCCGGAATTGCGTAAGTCTGCCGCCGATCGTGA
TGCTGCCTTTGAAAAAATTAATGAAGCGCGCAGTCCATTACTGCCACAGCTAGGT
TTAGGTGCAGATTACACCTATAGCAACGGCTACCGCGACGCGAACGGCATCAACT
CTAACGCGACCAGTGCGTCCTTGCAGTAACTCAATCCATTTTTGATATGTCGAAA
TGGCGTGCGTTAACGCTGCAGGAAAAGCAGCAGGGATTCAGGACGTCACGTAT
CAGACCGATCAGCAAACCTTGATCCTCAACACCGCGACCGCTTATTTCAACGTGT
TGAATGCTATTGACGTTCTTTCCTATACACAGGCACAAAAAGAAGCGATCTACCG
TCAATTAGATCAAACCACCCAACGTTTTAACGTGGGCCTGGTAGCGATCACCGAC
GTGCAGAACGCCGCGCACAGTACGATACCGTGCTGGCGAACGAAGTGACCGCA
CGTAATAACCTTGATAACGCGGTAGAGCAGCTGCGCCAGATCACCGGTA ACTACT
ATCCGGA ACTGGCTGCGCTGAATGTCGAAA ACTTTAAAACCGACAAACCACAGC

CGGTTAACGCGCTGCTGAAAGAAGCCGAAAAACGCAACCTGTCGCTGTTACAGG
CACGCTTGAGCCAGGACCTGGCGCGCGAGCAAATTCGCCAGGGCGCAGGATGGTC
ACTTACCGACTCTGGATTTAACGGCTTCTACCGGGATTTCTGACACCTCTTATAGC
GGTTCGAAAACCCGTGGTGCCGCTGGTACCCAGTATGACGATAGCAATATGGGCC
AGAACAAGTTGGCCTGAGCTTCTCGCTGCCGATTTATCAGGGCGGAATGGTTAA
CTCGCAGGTGAAACAGGCACAGTACAACCTTTGTCGGTGCCAGCGAGCAACTGGA
AAGTGCCCATCGTAGCGTCGTGCAGACCGTGCGTTCCTCCTTCAACAACATTAAT
GCATCTATCAGTAGCATTAAACGCCTACAAACAAGCCGTAGTTTCCGCTCAAAGCT
CATTAGACGCGATGGAAGCGGGCTACTCGGTTCGGTACGCGTACCATTGTTGATGT
GTTGGATGCGACCACCACGTTGTACAACGCCAAGCAAGAGCTGGCGAATGCGCG
TTATAACTACCTGATTAATCAGCTGAATATTAAGTCAGCTCTGGGTACGTTGAAC
GAGCAGGATCTGCTGGCACTGAACAATGCGCTGAGCAAACCGGTTTCCACTAATC
CGGAAAACGTTGCACCGCAAACGCCGGAACAGAATGCTATTGCTGATGGTTATGC
GCCTGATAGCCCGGCACCAGTCGTTTCAGCAAACATCCGCACGCACTACCACCAGT
AACGGTCATAACAGCAGCGGCCTGGTGCCGCGCGGCAGCCATCATCATCATCATC
ATTGAGAATTC

Table S3.: Statistical analysis of the quantification of TolC trimers in *E. coli*

Construct	Number of TolC trimers mean	Std. Deviation	Std. Error
BL21	4500	695	284
BL21 proHlyA +	4341	789	352
BL21 proHlyA -	5482	1953	873
BL21 HlyAc +	4597	1151	514
BL21 HlyAc -	4880	1253	560
UTI89	4309	1515	618
UTI89 proHlyA +	3344	1739	777
UTI89 proHlyA -	4622	1506	673
UTI89 HlyAc +	4040	677	302
UTI89 HlyAc -	4609	1037	463

Table S4.: Number of TolC trimers quantified in *E. coli*

BL21	BL21 proHlyA +	BL21 proHlyA -	BL21 HlyAc +	BL21 HlyAc -	UTI89	UTI89 proHlyA +	UTI89 proHlyA -	UTI89 HlyAc +	UTI89 HlyAc -
4708	5069	4267	5848	2703	4530	1922	4878	4486	5741
3535	5050	7261	4876	4939	3592	3286	6920	4983	5446
4859	3177	7929	5454	5425	4841	4949	4772	3789	3819
4128	4383	4187	3229	5608	5708	1345	3397	3602	4722
4219	4024	3765	3574	5722	1636	5215	3138	3340	3314
5546					5547				

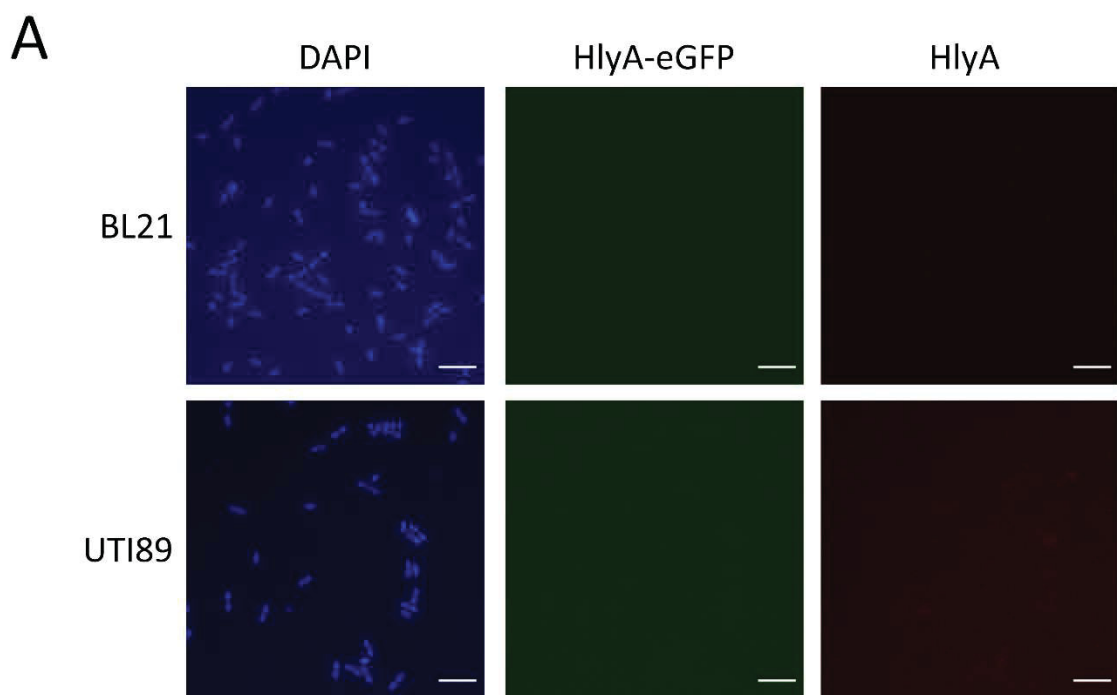


Figure S1. *Surface-staining of stalled eGFP-HlyA T1SS does not show signals in non-expressing BL21 and wild type UTI89.* BL21 without expression plasmid and UTI89 wild type *E. coli* were treated in an identical way as the corresponding expressing cells (Fig 1A). Cells were imaged by SIM and processed as described in Fig. 1.

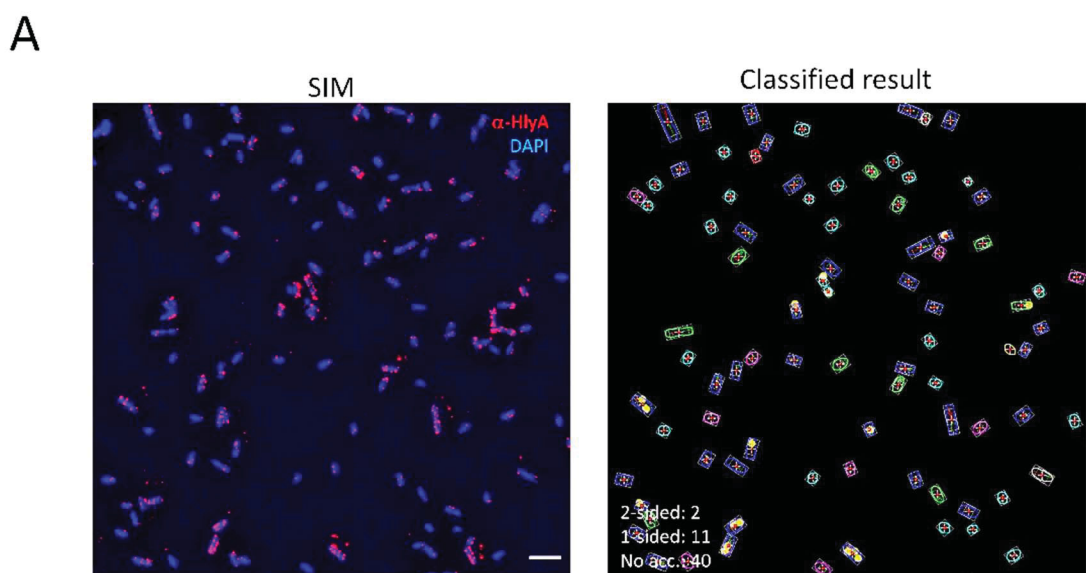


Figure S2. *Exemplary classification of BL21 expressing HlyA-eGFP.* (Left panel) comparison between one exemplary input file of a processed SIM MIP and (right) the resulting output file, displaying the classification of each bacterium in the full field of view (contrast and brightness was modified for better visibility in print). Highlighted are the rectangular area approximations for the tip zones and the cell body as well as the color coded classification: No accumulation at any tip (blue outline); accumulation at the right tip (green outline) or at the left

tip (red outline); accumulation at both sides (white outline); an a bacterial cell without a signal (yellow outline), less than 3 signals (magenta outline) or the cell body of a bacterium that is smaller than the size of the tip zone (cyan outline); the last three cases were excluded from the analysis. Scale Bar 5 μm .

A

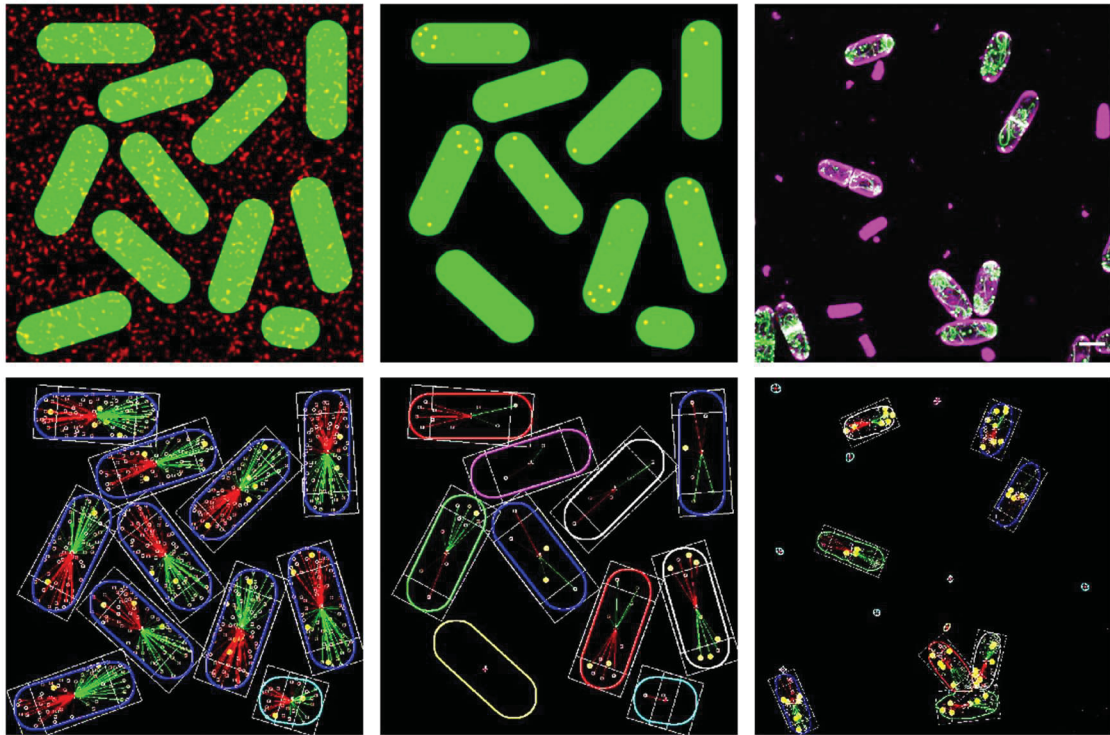


Figure S3. Analysis of toy simulation and *S. pombe* expressing *Lifeact-eGFP* as control for accumulation analysis. (Upper left panel) Toy simulation of manually generated outlines of bacteria and random scattered signal across the field of view shows no false positive detected accumulation (blue outlines, lower left), using an accumulation threshold of 1.5. (upper middle panel) Toy simulation of different types of accumulation by manually placed signal on rod-shaped outlines result in correct assignment of classification (lower middle panel). (Upper right panel) MIP of *S. pombe* cells expressing lifeact-eGFP and stained by membrane marking dye FM4-64FX. (lower right panel) Analysis for accumulated signal results in correct classification, indicated by 2-sided (white), 1-sided (green, red) and cells with no accumulation (blue). Scale bar was 5 μm . (contrast and brightness of all panels was modified for better visibility in print)

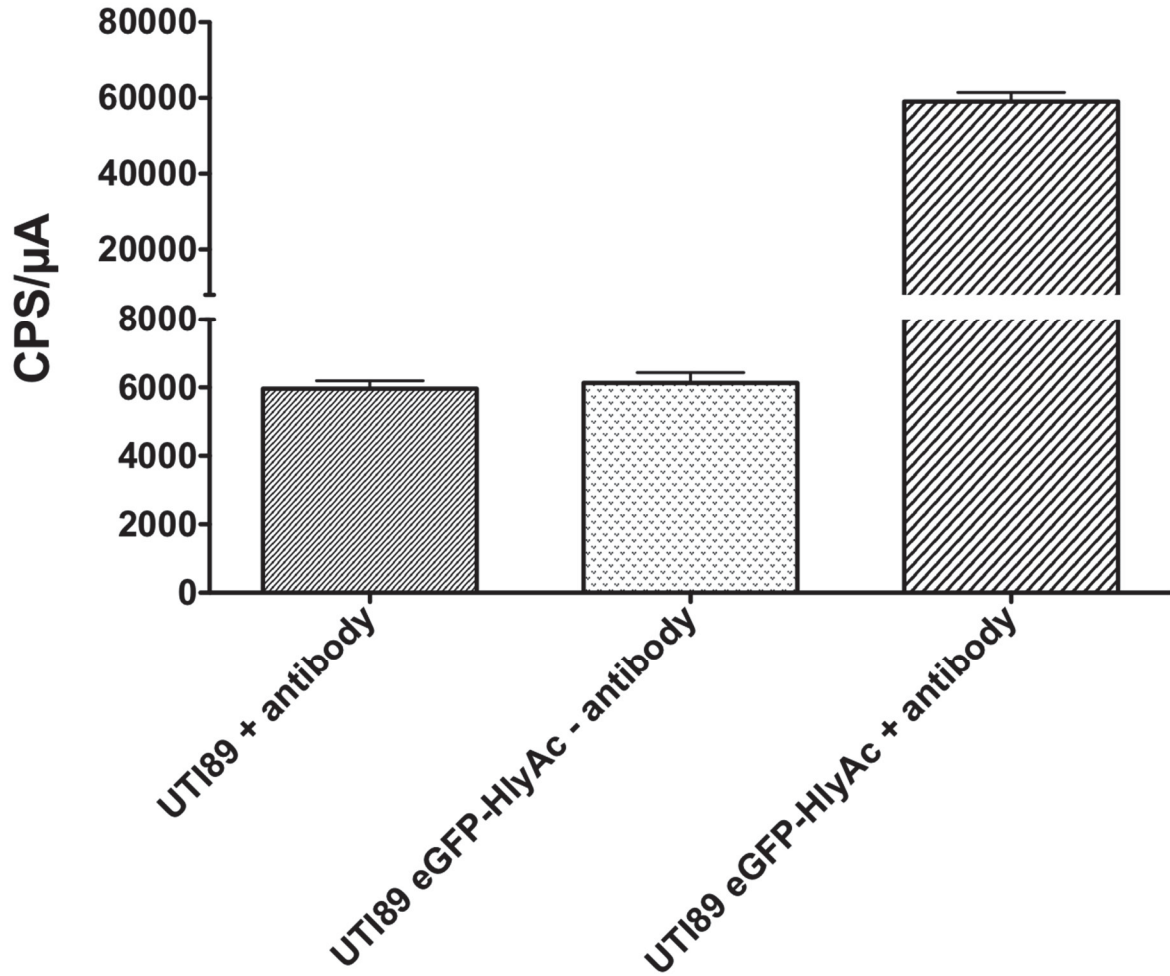


Figure S4. Total cell fluorescence of Cy3 at 563 nm from stained and un-stained *E.coli* UTI89 cells. Excitation was performed at 547 nm and fluorescence emission was monitored at 563 nm. UTI89 + antibody (left bar) represents the labeling antibody against HlyA and a secondary antibody labeled with Cy3 in the absence of eGFP-HlyAc. UTI89 eGFP-HlyAc - antibody (middle bar) represents the background of emission at 563 nm, while eGFP-HlyAc is expressed, but cells are not labeled with antibodies. UTI89 eGFP-HlyAc + antibody (right bar) is the immunofluorescent labeled UTI89, while eGFP-HlyAc is present. HlyB/D is present in all cases present at endogenous levels. Error bars represent the standard deviation of the fluorescence of at least three biological replicates.

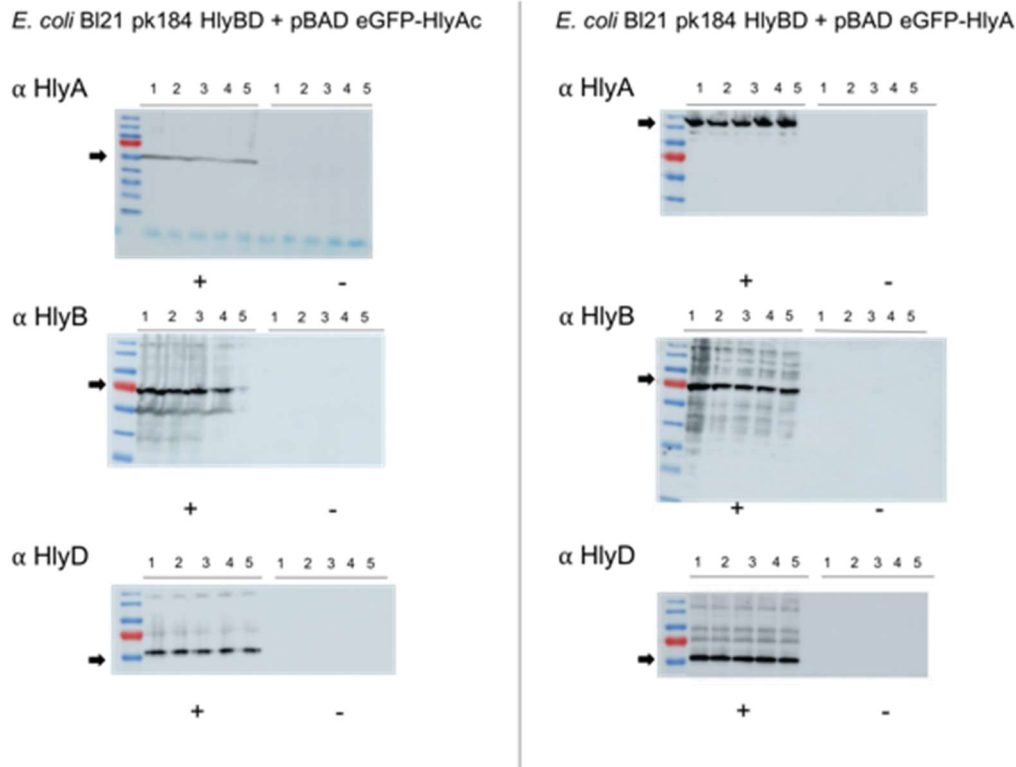


Figure S5. Western blots for expression control in BL21. ‘+’ indicates the induction of eGFP-HlyA respectively eGFP-HlyAc. HlyB and HlyD were also overexpressed. ‘-’ indicates no induction during the experiment. Numbers indicate the clone used with an OD₆₀₀ equivalent of 0.1

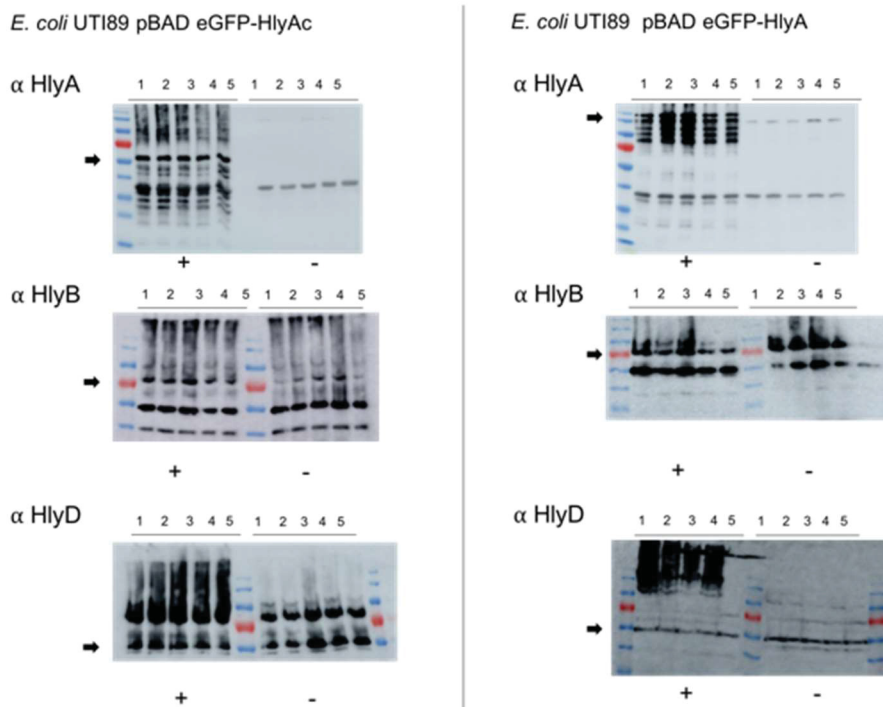


Figure S6. Western blots for expression control of T1SS in UTI89 background. The ‘+’ mark indicates the induction of eGFP-HlyA respectively eGFP-HlyAc. HlyB and HlyD are on an endogenous level expressed. The ‘-’ mark indicates no induction during the experiment. Numbers indicate the clone used with an OD₆₀₀ equivalent of 0.1

E. coli BL21 (DE3) Reference with TolC calibration

TolC dilutive calibration

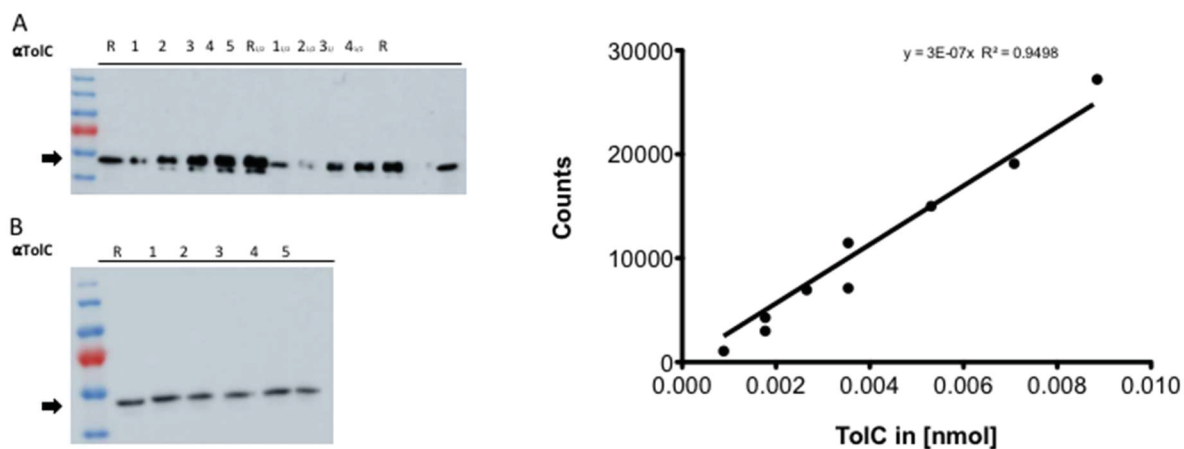


Figure S7. Dilutive calibration of the quantification the number of TolC in the reference sample. (A) R is the indicator for reference, TolC was applied as a 1.7 μM solution 1 to 5 μl and then again in a 1:1(0.85 μM) dilution 1-4 μl . The reference sample was applied 3 times. 2 times with an OD_{600} equivalent of 0.1 (R) and one time as 0.05 ($R_{1/2}$). Calculation resulted in 4708 ± 462 trimers of TolC for the reference. (B) R is the indicator for reference. Numbers indicate the *E. coli* BL21 clone used with an OD_{600} equivalent of 0.1

E. coli UTI89

E. coli BL21 (DE3)

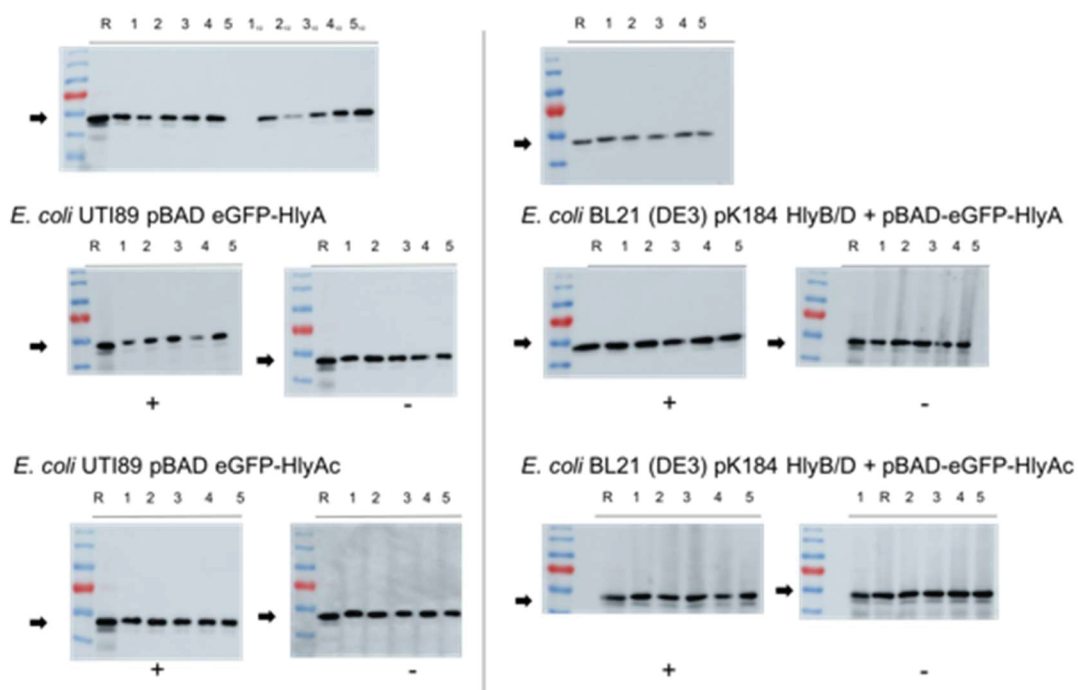


Figure S8. Western blots for quantification of TolC trimers in BL21 and UTI89 background. The '+' mark indicates the induction of eGFP-HlyA respectively eGFP-HlyAc. For UTI89 HlyB and HlyD are on an endogenous level expressed. In BL21 HlyB and HlyD are also overexpressed. The '-' mark indicates no induction during the experiment. Numbers indicate the clone used with an OD_{600} equivalent of 0.1 e.g. R1 and when applied with an OD_{600} 0.05 an index is used like 1/2.

Accessible files:

Code of the self-written Fiji-macro:

<https://github.com/SHAensch/Etact---E.coli-tip-accumulation-tool>

Exemplary raw dataset of SIM measurement:

https://omero-cai.hhu.de/webgateway/img_detail/71085/

Exemplary raw MIP of SIM measurement:

https://omero-cai.hhu.de/webgateway/img_detail/71102/

Exemplary processed dataset of SIM measurement:

https://omero-cai.hhu.de/webgateway/img_detail/71084/

Exemplary processed MIP (α -HlyA SIM processed and DAPI widefieldA):

https://omero-cai.hhu.de/webgateway/img_detail/71086/

Exemplary result file 1 (area and maxima detection):

https://omero-cai.hhu.de/webgateway/img_detail/71087/

Exemplary result file 2 (classification result):

https://omero-cai.hhu.de/webgateway/img_detail/71089/

Additional acknowledgements:

We thank Dr. Mohan Balasubramanian (Division of Biomedical Sciences, Warwick) for providing the *S. pombe* strain expressing lifeact-eGFP and Dr. **Abel Alcázar-Román (Eukaryotic Microbiology, Duesseldorf)** for support in cultivating and handling the *S. pombe* cells.

1. Huang, J., et al., *Nonmedially assembled F-actin cables incorporate into the actomyosin ring in fission yeast*. J Cell Biol, 2012. **199**(5): p. 831-47.
2. Lenders, M.H., et al., *In vivo quantification of the secretion rates of the hemolysin A Type I secretion system*. Sci Rep, 2016. **6**: p. 33275.
3. Moreno, S., A. Klar, and P. Nurse, *Molecular genetic analysis of fission yeast Schizosaccharomyces pombe*. Methods Enzymol, 1991. **194**: p. 795-823.
4. Schindelin, J., et al., *Fiji: an open-source platform for biological-image analysis*. Nat Methods, 2012. **9**(7): p. 676-82.
5. Brocher, J., *The BioVoxel Image Processing and Analysis Toolbox*. EuBIAS-Conference, 2015.

6. C.H. Li, P.K.S.T., *An iterative algorithm for minimum cross entropy thresholding*. Pattern Recognition Letters, 1998. **19**(8): p. 771-776.
7. Zack, G.W., W.E. Rogers, and S.A. Latt, *Automatic measurement of sister chromatid exchange frequency*. J Histochem Cytochem, 1977. **25**(7): p. 741-53.
8. Bakkes, P.J., et al., *The rate of folding dictates substrate secretion by the Escherichia coli hemolysin type I secretion system*. J Biol Chem, 2010. **285**(52): p. 40573-80.
9. Lenders, M.H., et al., *Directionality of substrate translocation of the hemolysin A Type I secretion system*. Sci Rep, 2015. **5**: p. 12470.

3.5 Chapter V – Isolation of the hemolysin A Type I secretion system in action

Title Isolation of the hemolysin A Type I secretion system in action

Author Tobias Beer, Michael H.H. Lenders, Sander H.J. Smits & Lutz Schmitt.

In Preparation

Own proportion of this work 60 %;

Construction of plasmids, purification of the used constructs, development for PAGE and immunofluorescence verification of T1SS components, writing of the manuscript.

Isolation of the hemolysin A Type I secretion system in action

Tobias Beer, Michael H.H. Lenders, Sander H.J. Smits and Lutz Schmitt^{†2}

Institute of Biochemistry, Heinrich-Heine-Universität,
40225 Düsseldorf, Germany

Abstract

Gram-negative bacteria are able to secrete a multitude of proteins in the extracellular space by a broad range of membrane-localized nanomachineries. The Type I secretion system (T1SS) is a prime example for this machines. They transport a broad range of unfolded substrates across both cell membranes. The hemolysin A (HlyA) T1SS from *Escherichia Coli* secretes the 110kDa toxin HlyA which. The hemolytic toxin is secreted in a single step without any periplasmatic intermediate directly from the cytosol to the extracellular space. Three different proteins form the HlyA T1SS machinery. In the inner membrane the ABC transporter hemolysin B (HlyB) is colocalized with the membrane fusion protein (MFP) hemolysin D (HlyD) forming the inner membrane complex (IMC). In presence of the substrate, HlyA the outer membrane protein (OMP) TolC is recruited and the T1SS assembles forming a translocation pathway across the membranes. However, the stoichiometry of the assembling proteins is unknown as well as structural information about the assembled T1SS. To address this question, we use an GFP-HlyA fusion protein to arrest the HlyA T1SS during translocation. *E. coli* membranes with the stalled complex were obtained and purification was established. The purification via affinity chromatography was introduced in presence and absence of crosslinker. Additionally the influence of different expression strains was investigated. The experiments revealed the instability of the T1SS when no crosslinker is present and a complex variety of crosslink products in presence of crosslinker. Illustrating the challenge of obtaining the correct assembled complex from *in vivo*.

Introduction

Gram-negative bacteria harbor a broad range of proteogenic machineries that enables transport across both cell membranes directly into the extracellular space or into a host cell [8]. This nanomachineries are called secretion systems and can be divided in subgroups ranging from type I secretion systems (T1SS) up to type VIII. They transport various substrates, ranging from small molecules, proteins and deoxyribonucleic acid [8]. In case of the T1SS, the substrate is secreted out of the cytoplasm directly into the extracellular space. This kind of one-step secretion occurs for type III, IV and VI secretions systems, too. Only type II and V secretion

² † To whom correspondence should be addressed: Lutz.Schmitt@hhu.de Tel. +49 211 81-10773
Universitätsstraße 1, 40225 Düsseldorf, Germany

systems have a preliminary substrate translocation into the periplasm whereas the secretion occurs over the outer membrane [8]. T1SS are prominent examples for transport systems that are able to transport a broad range of substrates like toxins, hemophores, adenylate cyclases, lipases, proteases, nodulation or adhesion factors [170]. The size of the substrates varies between 19 kDa in the case of the hemophore HasA from *Serratia marcescens* and 900 kDa for the surface layer proteins LapA from *Pseudomonas fluorescens* up to 1.5 MDa like the cell-surface protein from the Antarctic bacterium *Marinomonas primoryensis* [51, 200, 201]. All substrates in common is the unfolded respectively partially folded secretion [196, 202]. One of the best characterized T1SS, is the hemolysin A (HlyA) secretion system. It consists out of the ABC transporter hemolysin B (HlyB) and the membrane fusion protein (MFP) hemolysin D (HlyD) [52]. Both proteins are located in the inner membrane. Together with the outer membrane factor (OMP) TolC they build up the fully assembled HlyA T1SS that creates a continuous channel across both membranes, and allows substrate secretion in one step from the cytoplasm directly into the extracellular space [52]. Secretion of the 110 kDa repeats in toxin (RTX) protein HlyA occurs without any periplasmic intermediate [170]. Furthermore, the C-terminal localized HlyA secretion signal that contains all necessary information for secretion is not cleaved during or after secretion [203, 204]. Many biochemical information about the HlyA T1SS are available. For example, the role of the secretion signal, the substrate orientation during secretion and interaction studies between the translocator building proteins as well as their interaction with the substrate [52, 65, 173, 183, 205]. Nevertheless, structurally the main transport pathway is barely understood. Only structural information about TolC, a soluble part of the periplasmic part of HlyD and the HlyB NBD and CLD, are available [157, 164, 181, 189]. The translocator stoichiometry is unknown so far. Nevertheless while HlyB is suggested to be a dimer [157, 158] some studies suggest a trimer of HlyD [52] or a hexamer of HlyD [181, 183]. Further, nearly nothing is known about structural changes of the different T1SS components during secretion [52]. For that purpose, we use an eGFP-HlyA fusion protein to stall the HlyA T1SS [173]. *E. coli* membranes with the intact stalled complex could be isolated and initially solubilized. Affinity trials suggest that an isolation of the stalled system out of membranes is possible, but the integrity of the complex is not lasting the purification.

Methods

Bacterial strains and plasmids

E. coli BL21 (DE3), *E. coli* C41 (DE3) $\Delta ompF \Delta acrAB$, *E. coli* C43 (DE3) $\Delta acrAB$ and *E. coli* C43 (DE3) $\Delta ompF \Delta acrAB$ cells were used for protein expression. The eGFP-HlyA expressing plasmid pSOI-eGFP-HlyA was generated as previous described [Lenders et al., 2015]. Protein expression is under the control of a PBAD promoter, inducible with arabinose. Further, the pSOI-eGFP-HlyA plasmid was modified by substitution of the N-terminal six His-tag with a CBP-tag and a deca-histidine instead of the six-histidine tag. HlyB and HlyD expressions were done by using the pK184 plasmid that is under the control of a Plac promoter, inducible with IPTG (isopropyl β -D-1-thiogalactopyranoside) [Bakkes et al., 2010].

Cell cultivation and protein expression

Chemically competent cells were transformed with pK184-HlyBD and pSOI-eGFP-HlyA (His- respectively CBP-tagged) and grown on LB agar plates supplemented with 100 $\mu\text{g mL}^{-1}$ ampicillin and 30 $\mu\text{g mL}^{-1}$ kanamycin. Overnight cultures of single colonies were used to inoculate 10 L 2 YT medium supplemented with 100 $\mu\text{g mL}^{-1}$ ampicillin and 30 $\mu\text{g mL}^{-1}$ kanamycin at an OD_{600} of 0.1. Cells were grown at 37 °C and 160 rpm in 5 L flasks with baffles to an OD_{600} of 0.6-0.8. Protein expression was induced with 10 mM arabinose and 1 mM IPTG. Additionally, 5 mM CaCl_2 was added to the cell culture. After induction cells were grown for additional 3 h at 25 °C and 160 rpm. The cells were harvested by centrifugation and stored at -80 °C.

Membrane preparation of the stalled HlyA T1SS

Complex expressing *E. coli* cells were resuspended in buffer A1 (150 mM NaCl, 100 mM HEPES, 5 mM CaCl_2 , pH 8.0). Cell were disrupted by sonication (Bandelin Sonopuls HD 2200). The cells were cracked by five 1 min cycles at 4 °C, 20 kHz and an amplitude at 50 %, interrupted by 1 min breaks. Lysate was centrifuged for 30 min at 18 000 x g. Resulting supernatant was again centrifuged for 90 min at 200 000 x g. Pelleted membranes were resolved and homogenized in buffer A2 (250 mM NaCl, 100 mM HEPES, 5 mM CaCl_2 , 10 % (w/v) glycerol, pH 8.0). Membranes were adjusted with buffer A2 to 10 mg mL^{-1} , shock frosted in liquid nitrogen and stored at -80 °C.

Crosslinking of the stalled HlyA T1SS

Crosslinking *in vivo* at 37°C. After expression of the T1SS, the collected cells were washed with Buffer A1, adjusted to an OD_{600} of 7.0 for DSP and 2 for formaldehyde and crosslinking was initialized with 0.2 mM DSP or 3.5 % formaldehyde and agitated vigorously for 1h at 37 °C 700 RPM. After 1 h 2 mM Tris-HCL pH 7.4 was added and agitated vigorously for 15 min at 37 °C 700 RPM to quench free crosslinker.

Crosslinking *in vitro* at 37 °C. To the homogenized membranes (5 mg ml^{-1}) 0.2 mM DSP or 3.5 % formaldehyde were added and agitated vigorously for 1h at 37 °C 700 RPM. After 1 h 2 mM Tris-HCL pH 7.4 was added and agitated vigorously for 15 min at 37 °C 700 RPM to quench free crosslinker.

Crosslinking *in vitro* at 4 °C. To the homogenized membranes (5 mg ml^{-1}) 0.2 mM DSP were added and agitated mildly for 6 h at 4 °C. After 6 h 2 mM Tris-HCL pH 7.4 was added and agitated mildly for 30 min at 4 °C to quench free crosslinker.

Membrane preparation of the stalled HlyA T1SS with peptidoglycan digest

Complex expressing *E. coli* cells were resuspended in buffer A1 (150 mM NaCl, 100 mM HEPES, 5 mM CaCl_2 , pH 8.0) supplemented with 0.4 mg ml^{-1} lysozyme, protease inhibitor tablet and desoxyribonuclease. Followed by 30 min incubation on ice. Cell were disrupted by sonication (Bandelin Sonopuls HD 2200). They were broken by five 1 min cycles at 4 °C, 20 kHz and an amplitude at 50 %, interrupted by 1 min breaks (MS72 tip). Lysate was centrifuged for 30 min at 18 000 x g. Resulting supernatant was again centrifuged for 90 min at 200 000 x g. Pelleted membranes were resolved and homogenized in buffer B1 (300 mM NaCl, 100 mM

HEPES, 2 mM CaCl₂, 5 % (w/v) glycerol, 2 mM MgCl₂, pH 8.0). Membranes were adjusted with 50 % glycerol and buffer B1 to 10 mg mL⁻¹ + 10 % glycerol, shock frosted in liquid nitrogen and stored at -80 °C.

Whole cell preparation of the stalled HlyA T1SS with peptidoglycan digest and CBP-affinity purification

To obtain the complex from T1SS expressing *E. coli* cells a whole cell predigest and solubilization was tested analog to Jinhong Hu et al[81]. Cells were resuspended in buffer A1 (150 mM NaCl, 100 mM HEPES, 5 mM CaCl₂, pH 8.0) supplemented with 0.4 mg ml⁻¹ lysozyme, protease inhibitor tablet, desoxyribonuclease and 1 % Lauryldimethylamine-N-oxid (LDAO). The resuspended mix was mildly agitated at 8 °C for 2.5 h. Lysate was centrifuged for 30 min at 18 000 x g. Resulting supernatant was again centrifuged for 90 min at 200 000 x g. Pelleted membranes were resolved and homogenized in buffer B1 (300 mM NaCl, 100 mM HEPES, 2 mM CaCl₂, 5 % (w/v) glycerol, 2 mM MgCl₂, 0.2 % LDAO pH 8.0).

The volume of solubilized membranes was supplemented with the same amount of binding buffer. 1 ml CBP-resin was added per 400 mg solubilized Protein and incubated while mildly agitated over night at 4 °C.

The followed purification procedure was applied at 4 °C. The resin was collected as a column bed in a gravity flow column. The resin was washed with 5 CV buffer B1 (300 mM NaCl, 100 mM HEPES, 2 mM CaCl₂, 5 % (w/v) glycerol, 2 mM MgCl₂, pH 8.0, 0.2 % LDAO) and supplemented with 5 mM ATP pH 8. After the ATP containing buffer was dripped into the stationary phase B1 was added in 4 washing steps each 5 CV. The bound protein was eluted by adding 5 CV buffer E (300 mM NaCl, 100 mM HEPES, 2 mM EGTA, 5 % (w/v) glycerol, pH 8.0, 0.2 % LDAO). The washing and elution fractions were collected and the complex containing fractions concentrated, using a Millipore ultrafiltration device (MWCO of 100 kDa).

The concentrated elution fraction was loaded on a Superose6 increased column with SEC-buffer C (300 mM NaCl, 100 mM HEPES, 5 % (w/v) glycerol, pH 8.0, 0.2 % LDAO). The Fractions with UV-absorbance were analyzed and collected for further studies.

Solubilization screen via dot blot technique

Membranes were solubilized in buffer A2 and adjusted to 10 mg mL⁻¹. Detergents were used at a concentration of 1 or 2 % according to their critical micellar concentration (see table 1 for used concentration). Samples were solubilized for 1 h at 4 °C and agitated at 750 rpm. Afterwards, solubilized samples were centrifuged for 30 min at 120 000 x g. Supernatant was supplemented with SDS sample buffer and 3 µL samples were spotted onto a dry nitrocellulose membrane. Membranes were dried over night and than blocked for an additional night in TBS-T with 5 % (w/v) milk powder. Blocked dot blots were incubated for 3 h in the corresponding primary rabbit antibody solutions. Afterwards, blots were washed three times in TBS-T buffer and incubated 1 h in a HRP-conjugated, secondary antibody solution. Incubated blots were again washed two times in TBS-T and one time in TBS buffer. The ECL advance kit (GE Healthcare) was used for the visualization of the protein signals. Signal intensity of dot blots were quantified by using the program ImageJ.

Table 1. List of detergents for the solubilization screening of the HlyA TISS

Number	Detergent	Used [%]	Nature
A1	Anameg®-7	1 %	N
A2	Anapoe®-20	1 %	N
A3	Anapoe®-35	1 %	N
A4	Anapoe®-58	1 %	N
A5	Anapoe®-80	1 %	N
A6	Anapoe®-C10E6	1 %	N
A7	Anapoe®-C10E9	1 %	N
A8	Anapoe®-C12E8	1 %	N
A9	Anapoe®-C12E9	1 %	N
A10	Anapoe®-C12E10	1 %	N
A11	Anapoe®-C13E8	1 %	N
A12	Anapoe®-X-100	1 %	N
B1	Anapoe®-X-114	1 %	N
B2	Anapoe®-X-305	1 %	N
B3	Anapoe®-X-405	1 %	N
B4	Big CHAP	1 %	N
B5	Big CHAP deoxy	1 %	N
B6	CYGLU®-3	2 %	N
B7	CYMAL®-1	2 %	N
B8	CYMAL®-2	2 %	N
B9	CYMAL®-3	1 %	N
B10	2,6-Dimethyl-4-heptyl- α -D-maltopyranoside	2 %	N

B11	n-Decyl- α -D-maltopyranoside	2 %	N
B12	n-Decyl- β -D-maltopyranoside	2 %	N
C1	n-Decyl- β -D-thiomaltopyranosid	2 %	N
C2	n-Decyl-N,N-Dimethylglycin	2 %	N
C3	n-Dodecyl- α -D-maltopyranoside	1 %	N
C4	n-Dodecyl- β -D-maltopyranoside (DDM)	1 %	N
C5	n-Heptyl- β -D-thioglucopyranoside	2 %	N
C6	n-Heptyl- β -D-Glucopyranoside	2 %	N
C7	n-Nonyl- β -D-thiomaltopyranoside	1 %	N
C8	n-Dodecyl- β -D-thiomaltopyranoside (LTM)	1 %	N
C9	CYMAL®-4	2 %	N
C10	CYMAL®-5	2 %	N
C11	CYMAL®-6	1 %	N
C12	CYMAL®-7	1 %	N
D1	Anzergent®3-8	2 %	Z
D2	Anzergent®3-10	2 %	Z
D3	Anzergent®3-12	1 %	Z
D4	Anzergent®3-14	1 %	Z
D5	CHAPS	2 %	Z
D6	CHAPSO	2 %	Z
D7	Cyclofos™-4	2 %	Z
D8	Cyclofos™-5	1 %	Z
D9	Cyclofos™-6	1 %	Z
D10	Cyclofos™-7	1 %	Z
D11	Fos-Choline®-9	2 %	Z

D12	Fos-Choline®-10	2 %	Z
E1	Cyclofos™-3	2 %	Z
E2	Fos-Choline®-11	1 %	Z
E3	Fos-Choline®-12	1 %	Z
E4	Fos-Choline®-13	1 %	Z
E5	Fos-Choline®-14	1 %	Z
E6	Fos-Choline®-15	1 %	Z
E7	Fos-Choline®-16	1 %	Z
E8	Fos-Choline®-Iso-9	2 %	Z
E9	Fos-Choline®-Iso-11	2 %	Z
E10	Fos-Choline®-Unisat-11-10	1 %	Z
E11	Fos-Choline®-8	2 %	Z
E12	n-Dodecyl-N,N-dimethylglycine	1 %	Z
F1	n-Dodecyl-N,N-dimethylamine-N-oxide (DDAO)	1 %	Z
F2	Cholic acid, sodium salt	1 %	A
F3	Deoxycholic acid, sodium salt	1 %	A
F4	Fosmea®-8	1 %	A
F5	Fosmea®-10	1 %	A
F6	Hexaethylene Glycol Monooctyl Ether (C8E6)	1 %	N
F7	n-Hexyl- β -D-Glucopyranoside	2 %	N
F8	n-Hexyl- β -D-Maltopyranoside	2 %	N
F9	n-Nonyl- β -D- Glucopyranoside	1 %	N
F10	n-Nonyl- β -D-Maltopyranoside	1 %	N
F11	n-Nonyl- β -D-Thiomaltopyranoside	1 %	N
F12	Octaethylene Glycol Monodecyl Ether (C12E8)	1 %	N

G1	n-Octyl- β -D-Glucopyranoside	1 %	N
G2	n-Octyl- β -D-Thiomaltopyranoside	1 %	N
G3	n-Octyl- β -D-Maltopyranoside	2 %	N
G4	Pentaethylene Glycol Monodecyl Ether (C10E5)	1 %	N
G5	PMAL-C8	1 %	N
G6	Hexaethylene Glycol Monoethyl Ether (C8E6)	1 %	Z
G7	2-Propyl-1-Pentyl Maltopyranoside	2 %	N
G8	Sodium Dodecanoyl Sarcosine	1 %	A
G9	Sucrose Monododecanoate	1 %	N
G10	n-Tetradecyl- β -D-Maltopyranoside	1 %	N
G11	n-Tetradecyl-N,N-Dimethylamine-N-Oxide (TDAO)	1 %	Z
G12	Tetraethylene Glycol Monoethyl Ether (C8E4)	1 %	N
H1	n-Tridecyl- β -D-Maltopyranoside	1 %	N
H2	n-Undecyl- β -D-Maltopyranoside	1 %	N
H3	n-Undecyl- β -D-Maltopyranoside	1 %	N
H4	n-Undecyl- β -D-Thiomaltopyranoside	1 %	N
H5	Digitonin	1 %	N
H6	propyl(bi)cyclohexyl- β -maltoside (PCC- β -M)	1 %	N
H7	sodium dodecyl sulfate (SDS)	1 %	A
H8	Buffer		
H9	MEGA-8	2 %	N
H10	Cyclofos TM -2	1 %	Z

Density gradient centrifugation

100g H₂O-MQ were added to 100g sucrose. The sucrose solution was diluted with buffer (250 mM NaCl, 100 mM HEPES, 5 mM CaCl₂, pH 8.0) to 50 % w/w sucrose. The gradient was stacked in 5 % steps from 50 % w/w to 5 % w/w sucrose. After applying each gradient step the emerging gradient was frozen by using liquid nitrogen until the whole gradient was stacked to 10 % w/w. The gradient then thawed at 4 °C over night. Each gradient step had a volume of 3 mL, except the 5 % w/w fraction which was the membrane sample (BL21 DE3) adjusted with sucrose to a total volume 5 mL and 10 mg / mL solubilized protein (Fos16). The gradient centrifugation was done in a Surespin 630 rotor with a total volume of 38 mL for 24 h at 4 °C at 24.000 RPM. After centrifugation the single gradient steps were collected and the fractions analyzed via Western blot.

Solubilization of stalled HlyA T1SS followed by CBP-affinity purification

Membranes containing the T1SS complex adjusted to 10 mg ml⁻¹ were thawed at room temperature or in a water bath with cold water. The solubilization was conducted with 0.5 % Fos-Choline®-16 at 8 °C for 1 h with mild agitation. The volume of solubilized membranes was supplemented with the same amount of binding buffer B1 to reduce the amount of free detergent in solution. 1 ml CBP-resin was added per 400 mg solubilized protein and incubated while mildly agitated over night at 4 °C.

The followed purification procedures were applied at 4 °C. The resin was collected as a column bed in a gravity flow column. The resin was washed with 5 CV buffer B2 ((300 mM NaCl, 100 mM HEPES, 2 mM CaCl₂, 5 % (w/v) glycerol, 2 mM MgCl₂, pH 8.0, 0.0011 % Fos16)) and supplemented with 5 mM ATP pH 8. After the ATP containing buffer was dripped into the stationary phase B2 was added in 4 washing steps each 5 CV. The bound protein was eluted by adding 5 CV buffer E (300 mM NaCl, 100 mM HEPES, 2 mM EGTA, 5 % (w/v) glycerol, pH 8.0, 0.0011 % Fos16). The washing and elution fractions were collected and the complex containing fractions were concentrated using a Millipore ultrafiltration device (MWCO of 100 kDa).

Size exclusion chromatography for T1SS

The concentrated elution fraction was loaded on a Superose6 increased column using SEC-buffer C (300 mM NaCl, 100 mM HEPES, 5 % (w/v) glycerol, pH 8.0, 0.0011 % Fos16). The Fractions with UV-absorbance were analyzed and collected for further studies.

Native PAGE and analysis via Western blot

For analyzing, the sample on the integrity of the complex native PAGE was introduced. Precast gels from Novex 4 % - 16 % Bis-Tris were used in the Novex Gel system. For running of the gels the NativePAGE™ running buffer was used (50 mM BisTris, 50 mM Tricine, pH 6.8). Coomassie G-250 was selected as a cathode additive. The sample size applied for the gel was 10 µL composed of: 2.5 µL, 4 x native PAGE sample buffer (50 mM BisTris, 2.3 mM HCl, 50 mM NaCl, 10 % (w/v) glycerol, 0.001 % Ponceau S, pH 7.2). 0.25 µL cathode additive (Coomassie G250 0.4 % or Ponceau S 0.1 % 50 % glycerol). 5 µL Protein sample and 10 µL

ad H₂O. To disassemble complexes and disulfide bonds from the crosslinker DSP: DTT, SDS respectively LDS and urea can be added.

For maximum resolution of the native PAGE initial dark blue buffer (200 mL running buffer plus 10 ml Coomassie G250 0.4 %) was used at 100 V (fixed voltage, variable current) for 15 min. After the 15 min the dark blue buffer was exchanged with running buffer and the voltage was set to 150 – 180 V until the dye front reaches the bottom of the gel. The completed Native PAGE then was used for colloidal Coomassie stain, silver stain or Western blot.

For blotting the Criterion™ Blotter or Trans-Blot® Turbo™ system was used. For both applications PVDF membrane, activated with methanol, was utilized. For tankblotting a single buffer system was applied. The buffer contains 20 mM Tris-HCl, 150 mM Glycin, 10 methnaol and 40 mM 6-aminocaproic acid. For transfer 85 V for 2 h at 4 – 8 °C. The Trans-Blot® system was operated with a two buffer system. At the anode the buffer contained 60 mM Tris, 40mM CAPS and 15 % methanol pH 9.6. For the cathode 60 mM Tris, 40 mM CAPS 0.1 % SDS. For transfer 15 min 25 V with up to 2.5 A. Membranes were blocked over night in TBS-T with 5 % (w/v) milk powder. Blocked Western blots were incubated for 3 to 4 h in the corresponding primary rabbit antibody solutions. Afterwards, blots were washed three times in TBS-T buffer and incubated 1 h in a HRP-conjugated, secondary antibody solution. Incubated blots were again washed two times in TBS-T and one time in TBS buffer. The WESTAR EtacC Ultra 2.0 kit (Cyanagen) was used for the visualization of the protein signals.

Results

Stalling of the HlyA T1SS

In previous studies, it was shown that the HlyA T1SS is not able to secret HlyA when fast folding proteins are fused to the N-terminal part [196]. When eGFP is used the system can be stalled during the secretion process [173]. The fast folded eGFP cannot pass the translocator while the unfolded HlyA can still be threaded into the T1SS and can reach the extracellular space. The folding of the HlyA near the extracellular surface prevents the backsliding of the substrate. While eGFP fusion constructs of HlyA are present the secretion of HlyA is abolished by stalling all active T1SS. This finding made the determination of active T1SS in *E.coli* possible. About 4500 in *E.coli* BL21 DE3 when overexpressed [206] and approximately 800 on endogenous level in UTI89 (See chapter 3.4). A similar setup was also used for purification of the injectisome of *Salmonella enterica* serovar Typhimurium by Radics et al. [83]. The injectisome was purified while stalled and structurally investigated via cryo-EM. While being able to use this approach for different in vivo studies this method was also tried to initiate the purification of the stalled HlyA T1SS complex for further studies.

Membrane preparation of stalled HlyA T1SS

Cells expressing the HlyA T1SS stalled with eGFP-HlyA were disrupted by sonification and membranes were prepared. By immunofluorescence the interaction of the eGFP-HlyA, stalled T1SS was investigated. If the interaction between the components is strong enough the whole complex of membrane protein consisting of HlyB, HlyD and TolC, including the soluble eGFP-

HlyA is present in the membrane fraction. When the cells are disrupted, next to the endogenous membrane proteins the T1SS components HlyB, HlyD and TolC should be found in the membrane. Free expressed eGFP-HlyA does not interact with the membrane which allows to draw conclusion on the integrity of the T1SS containing membranes. The immunofluorescence analysis of the collected membranes is highlighted in Figure 1 where the presence of TolC, HlyB, HlyD and eGFP-HlyA is shown. These results indicated that the stalled translocator is still assembled and could be used for further purification and analyzation steps.

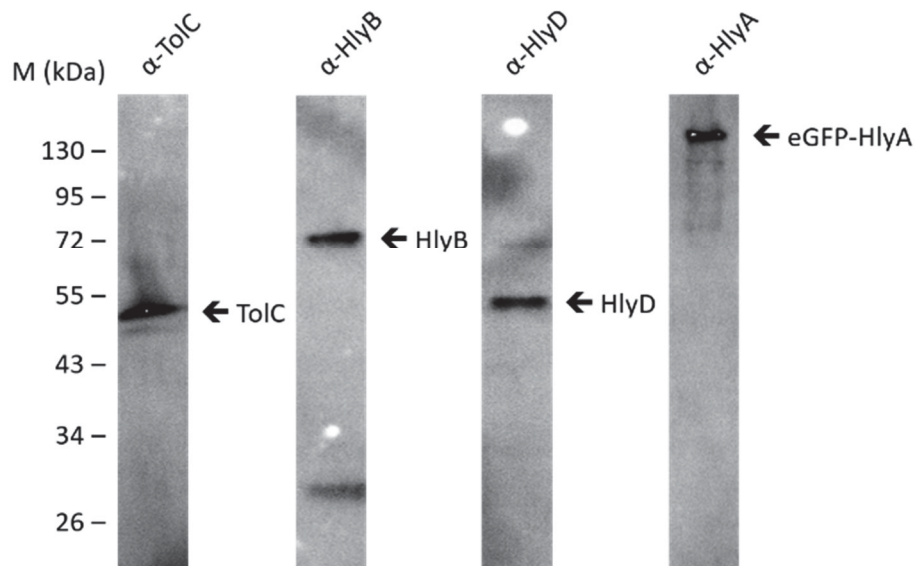


Figure 13. Western blot of prepared *E.coli* membranes containing stalled HlyA T1SS. All parts of the HlyA T1SS were detected by immunofluorescence in the collected membranes from *E. coli* BL21 DE3. The used antibody is labeled above while specific bands (eGFP-HlyA, HlyB, HlyD and TolC) are indicated by arrows.

Solubilization screen of the stalled HlyA T1SS

While it was shown that, all components are present in the collected membrane, the suitable detergent had to be identified. The desired detergent should solubilize all membrane proteins involved in the T1SS (TolC, HlyB, HlyD) and be compatible with eGFP-HlyA. Therefore, the dot blot technique was used for a detergent screening. The signals of the immunofluorescence for the different T1SS components were compared by intensity level. For further investigations only detergents that showed overall intense signals for all HlyA T1SS components were consider as potential candidate for further purification. If the signals were only obtained for a part of the T1SS a disruption of the translocation system during the solubilization is possible.

Signal intensity of dot blots were quantified by using the program ImageJ. The solubilization screen indicated that especially the zwitterionic Fos-CholinesR_-14, 15 and 16 and CyclofosTM-5 showed a very efficient solubilization behavior (see Figure 2). Further, the non-ionic pyranoside n-Dodecyl- β -D-maltopyranoside and n-Dodecyl- β -D-thiomaltopyranoside as well as digitonin seemed to be prominent candidates for solubilization (see Figure 2).

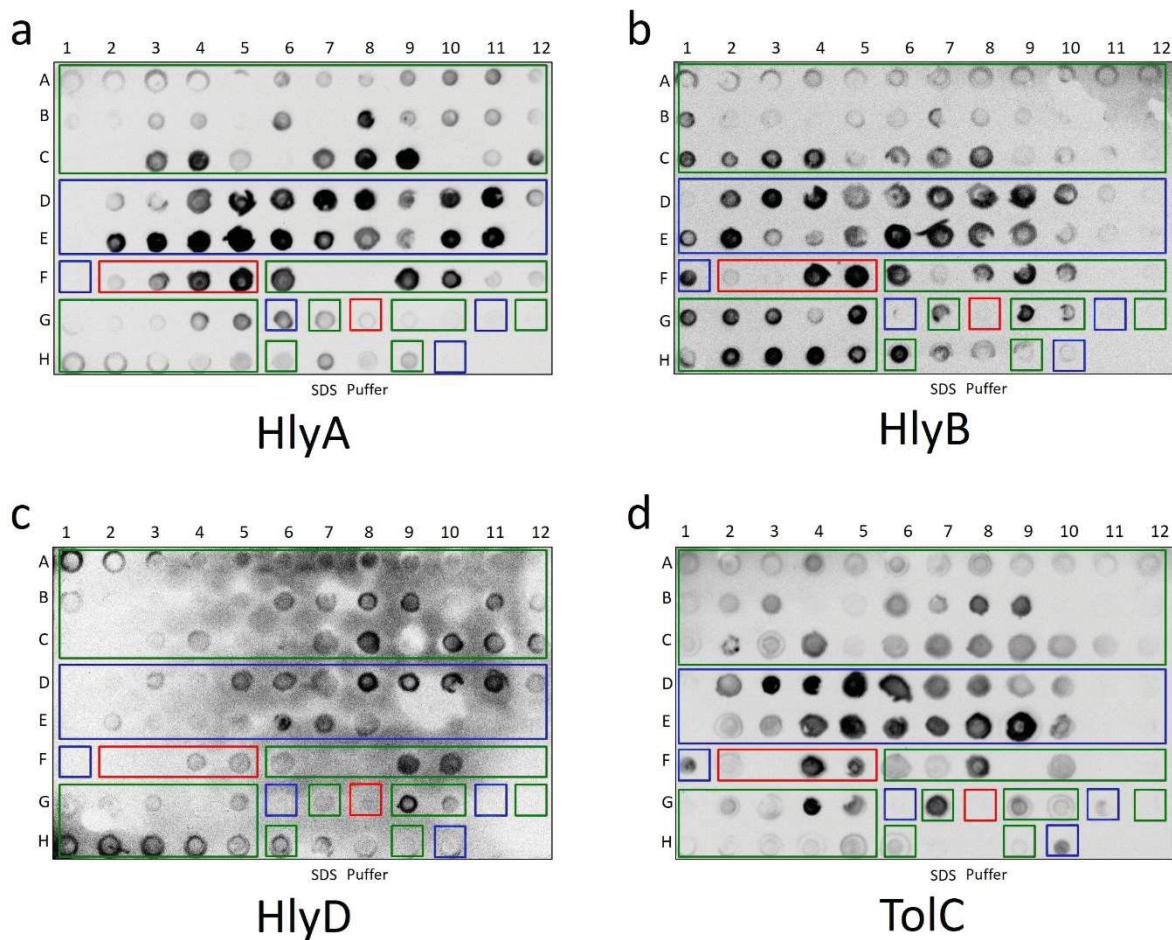


Figure 14. Solubilization screen from membranes containing the stalled HlyA TISS. Solubilization screen of *E. coli* membranes containing the via eGFP-HlyA stalled HlyA TISS. For the screen 92 different detergents were tested. Non-ionic detergents are marked by green boxes, zwitterionic by blue boxes and anionic are marked by red boxes. SDS and the solubilization buffer without detergent are used as control in line H7 and H8. The list of all used detergents is shown in Table 1. The solubilized membranes were spotted on a nitrocellulose membrane via dot blot method. The blotted membranes then were examined by using specific antibodies against (a) HlyA, (b) HlyB, (c) HlyD and (d) TolC.

Density gradient centrifugation

To ensure the complex integrity a stepwise sucrose gradient was used. The fractions after the centrifugation were analyzed via Western blot, shown in Figure 3.

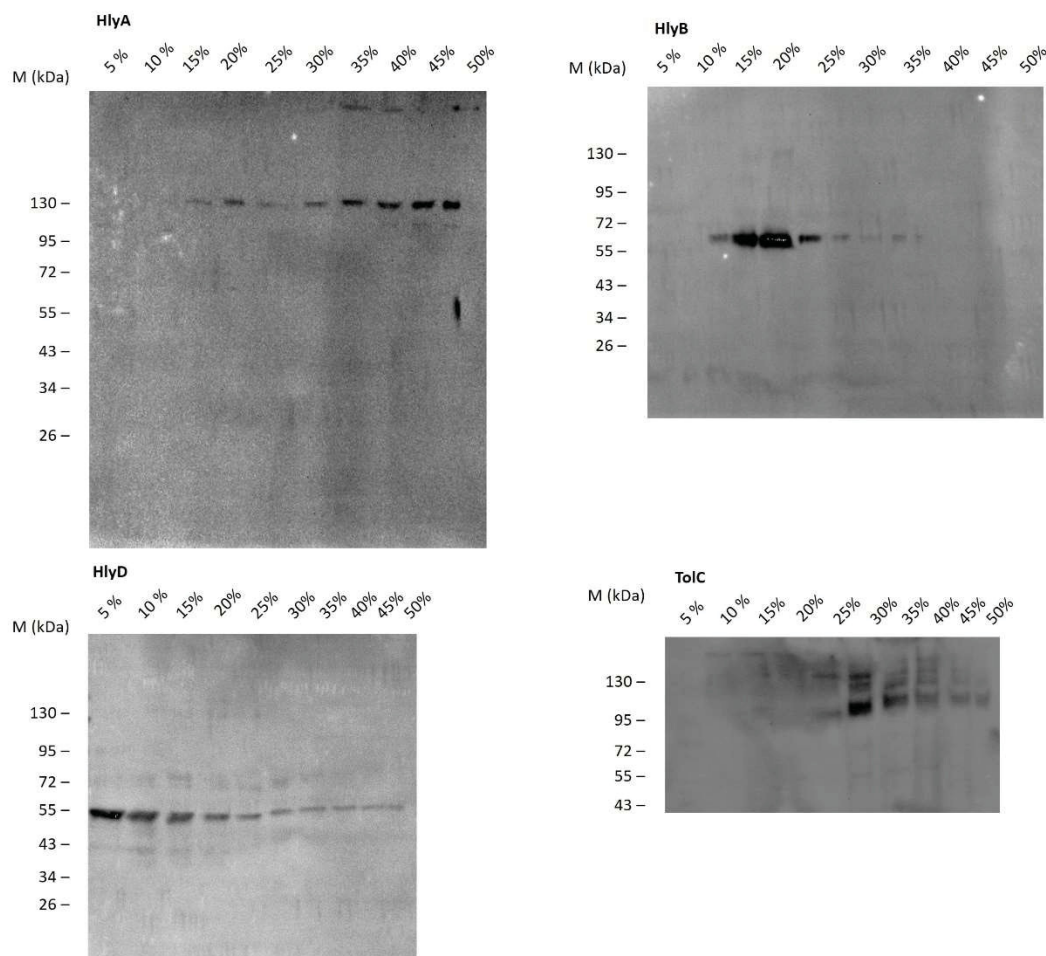


Figure 3. Western blot from sucrose gradient with the solubilized TISS membrane. All parts of the HlyA TISS were detected by immunofluorescence in the collected gradient fractions. The used sample derived from, Fos16 solubilized membranes from E.coli BL21(DE3) The sample was applied to SDS-PAGE with a continuous 10 % polyacrylamide gel. The Protein was transferred by tank-blot to the PVDF membrane. The blotted membranes then were examined by using specific antibodies against eGFP, HlyB, HlyD and TolC

The analysis via Western blot revealed signals for every component of the TISS. HlyA is present in all fractions with a sucrose content greater than 15 % w/w. with the highest intensity around 45 % to 50 % w/w sucrose. The major signals for HlyB were identified in the gradient fraction around 20 % sucrose. While HlyD also was present at 20 % w/w sucrose but showed the most intense signal at 5 %. TolC had the major signal at 25 % and some signals 20 % w/w sucrose. From the signal distribution the assumption was that the TISS is located in the gradient fractions around 20 to 25 % w/w sucrose. Also, the signal spread of some components showed hints that the overall stability could not be enough when solubilized to allow proper purification. Therefore, the first purification experiments were planned using the crosslinker (DSP).

Initial affinity purification and size exclusion chromatography of solubilized T1SS

The initial purification was performed in BL21 (DE3) with 0.2 mM DSP crosslinked cells. The solubilized membrane containing the stalled T1SS were then used for affinity purification. On the N-terminal site of eGFP-HlyA a six His-tag was present. Therefore, a pull-down with Ni-NTA agarose was used to investigate the binding properties of the T1SS. No binding to the resin was detectable. Also no binding on a stationary IMAC-column was observable. To establish a feasible purification the pBAD-plasmid containing the eGFP-HlyA was modified. The six histidine tag was elongated to eight respectively twelve histidine. Additionally a His-tag independent construct was created with the calmodulin binding protein (CBP).

The elongated His-tags showed no binding to Ni-NTA resin or pre packed columns. In contrast to the His-tag constructs the CBP tagged eGFP-HlyA showed sufficient binding to the CBP-resin. Further solubilized membranes containing the T1SS were applied to the CBP-resin to initialize the further purification. The by affinity purified Protein was used for size exclusion chromatography (SEC), showed in Figure 4. The SEC fractions were analyzed by Native PAGE -Western blot and SDS-PAGE Western blot (Figure 5). Some fractions (peak 1 and 2 indicated in Figure 4) showed all components of the T1SS, displayed in Figure 5 (HlyA, HlyB, HlyD, TolC).

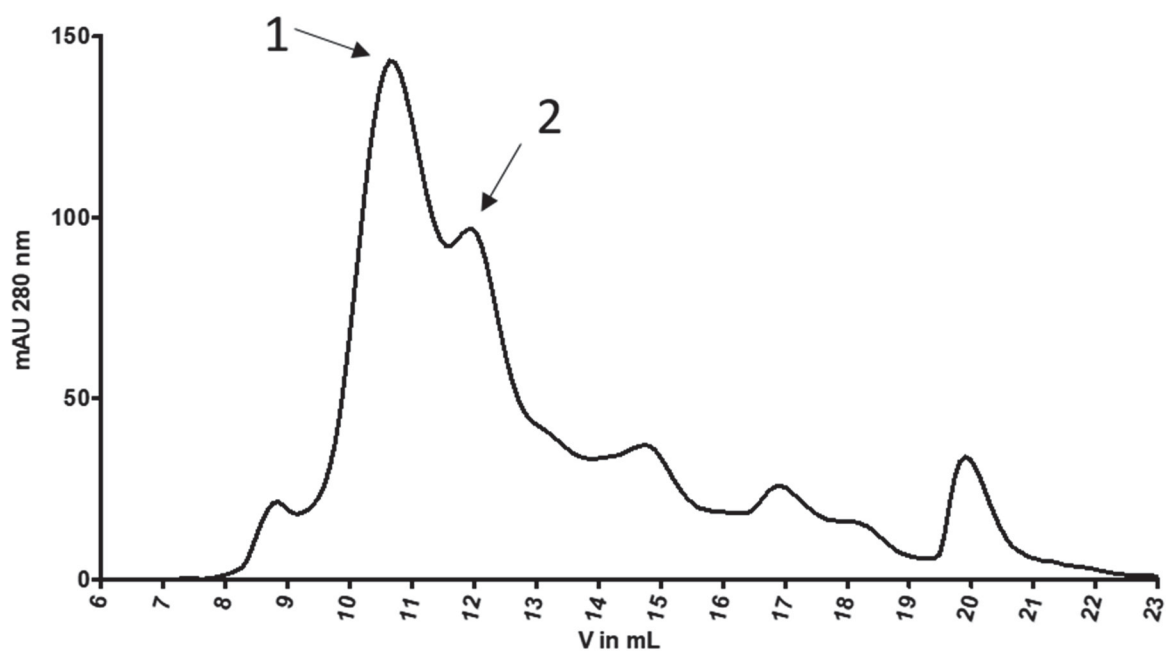


Figure 4. SEC profile of DSP cross-linked CBP-eGFP-HlyA stalled T1SS. The eluted fractions from the CBP-resin containing the T1SS were concentrated using an Amicon Ultra centrifugal filter unit and 500 μ L was loaded on a Superose6 increase 10/300 column. 1 indicates the first major peak (near 10 to 11 mL) for further investigation. 2 indicates the second major peak (around 12-13 mL) for further investigation. Peak 1 and 2 was applied to NativePAGE and SDS-PAGE for immunoblot analysis (Figure 4).

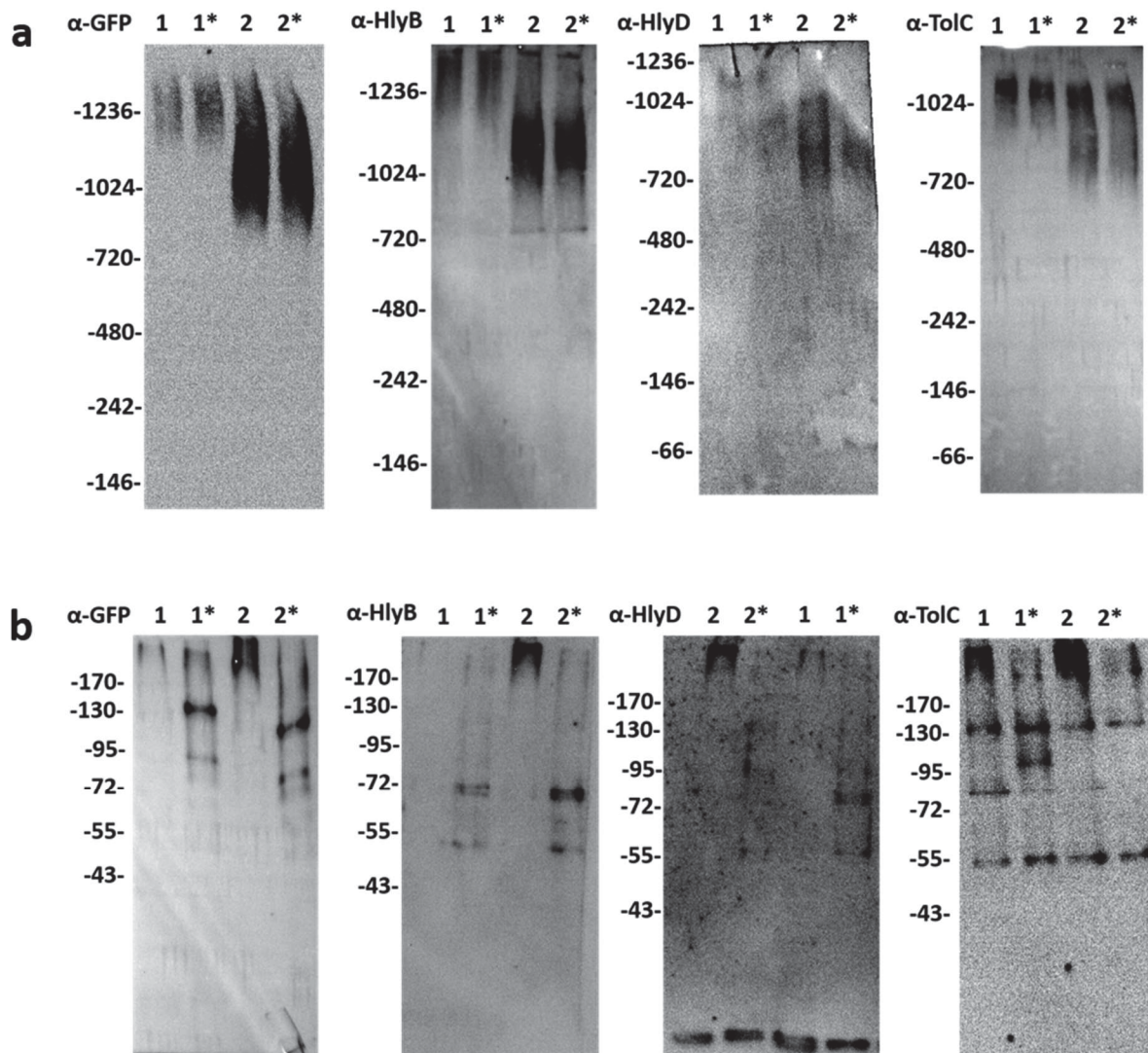


Figure 15. Immunoblot analysis of the SEC fractions from TISS purification. All parts of the HlyA TISS were detected by immunofluorescence in the collected SEC fractions. The sample derived from DSP crosslinked, solubilized membranes from *E. coli* BL21(DE3). (a) the sample was applied to a Native PAGE with a Bis-Tris 4-16 % gradient gel. The protein was transferred by tank-blot to the PVDF membrane. (b) the sample was applied to SDS-PAGE with a continuous 10 % polyacrylamide gel. The Protein was transferred by tank-blot to the PVDF membrane. The blotted membranes then were examined by using specific antibodies against eGFP, HlyB, HlyD and TolC. The * indicates an addition of 50mM DTT during sample preparation to reduce the DSP disulfide bonds.

All components were shown via immunofluorescence even though the signal for HlyD was very faint. The application on NativePAGE showed blots resulting in specific signals against the different components of the TISS in a molecular weight range between 720 kDa to 1236 kDa. The signals did not vanished when the DSP crosslink was resolved by adding DTT. The signals for HlyB and especially eGFP showed a severe smearing of the signal. The signals obtained from Peak 2 lead to reason that the TISS is in the second peak fraction. Additionally to the NativePAGE the SDS PAGE was used to further investigate the samples from SEC to individualize the TISS components and check for identity via immunofluorescence. Here the results from NativePAGE as well indicated that the TISS could be eluted in peak 2. The crosslinked sample was not able to enter the separation gel and migrated only to the stacking

gel. While the sample in addition with DTT showed signals for the monomers of eGFP-HlyA (140.0 kDa), HlyB (79.5 kDa), HlyD (54.4 kDa) and the trimer (154.2 kDa) and monomer (51.4 kDa) of TolC.

The possible MW for the T1SS consisting of one eGFP-HlyA for stalling (and purification via CBP-tag), a dimer of HlyB, a trimer of TolC and a trimer of HlyD would be 616 kDa while the same complex with a hexamer of HlyD would have a MW around 779 kDa. From this approximation the results of Native PAGE can be a hint but no clear result, because of smearing no clear signals are present. An aspect in the favor for presence of the T1SS is the immunofluorescence of the specific antibodies. Therefore, the purification was further developed to reduce signal smearing and investigate the influence of crosslinking.

Affinity purification and reinject of sample for second size exclusion chromatography

The affinity purification and SEC was stated as before. To improve the purification the fractions which were suggested for containing the T1SS was pooled (shown in Figure 6 (a)) and concentrated using an Amicon Ultra centrifugal filter (MWCO of 100 kDa). The eluted fractions of the second SEC (displayed in Figure 6 (b)) were further investigated via immunofluorescence (Western blot against HlyA, HlyB, HlyD, TolC shown in Figure 7) and silver stain (Figure 8).

The first SEC (Figure 6(a) first SEC) showed a peak around 12 mL which was poorly separated from other signals while overall signal was at the same range as the purification before. The reinjection resulted in a broad peak from 10 to 16 mL (Figure 6(b) second SEC). To further investigate the identity and integrity of the T1SS in the sample the peak was pooled from 11 to 15 mL and applied to NativePAGE (Figure 7 [Western blot] & 8 [silver stain]).

The Western blot (Figure 7) showed specific immunofluorescence for every component of the T1SS. The signal was detected a little above the height of the 720 kDa marker band. This would correspond with the signals from the former purification and the hexameric state of HlyD. To dissolve the complex and check for the single components of the T1SS DTT and SDS was used. The use of both additives resulted in the disbandment of the “720 kDa” signal and resulted in smaller signals. For eGFP-HlyA a signal around 242 kDa was observable. HlyB at 146 kDa and TolC also for 242 kDa. For HlyD no clear band was detectable when SDS and DTT was added, but a clear signal for native protein.

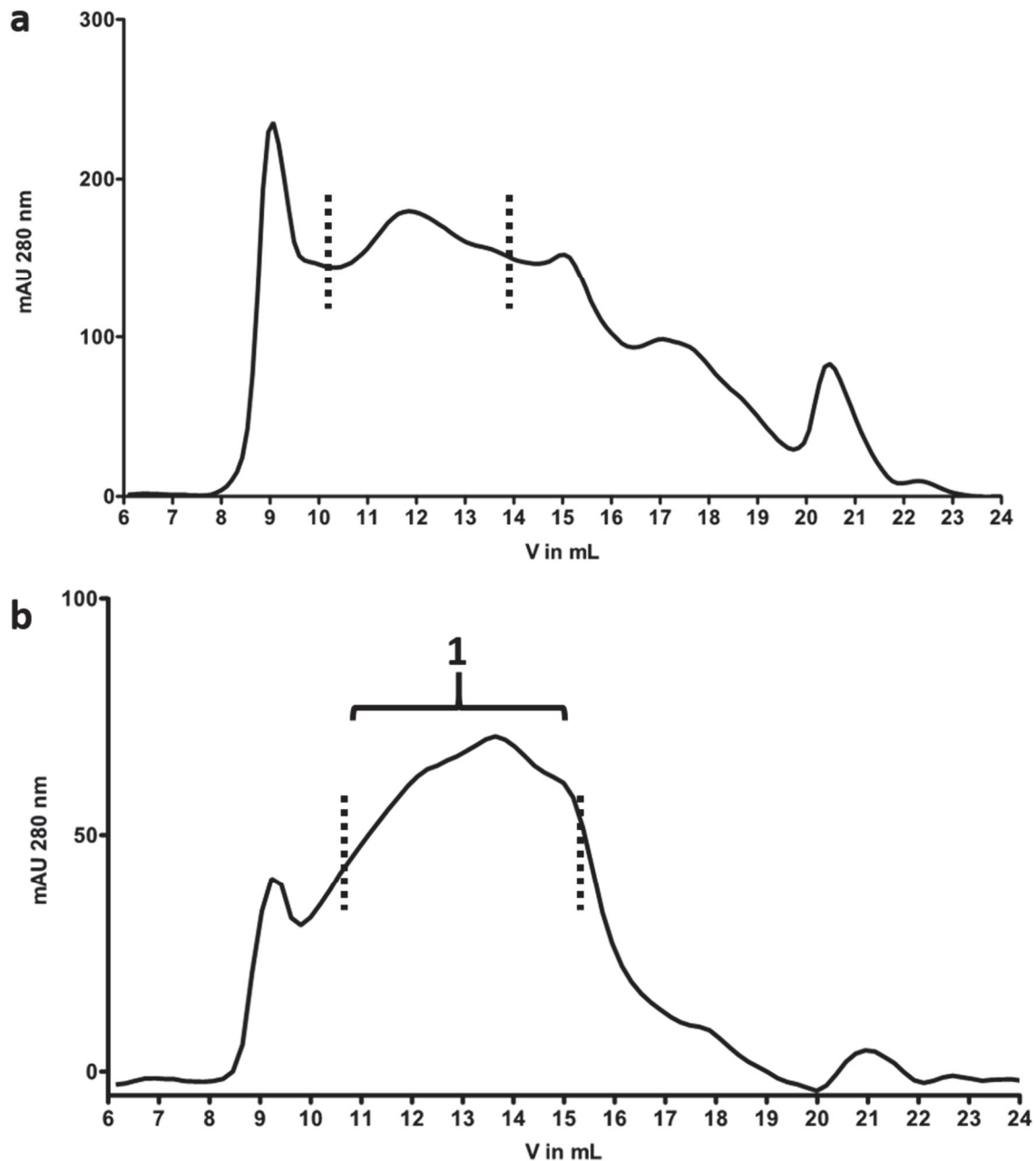


Figure 6. SEC profile of DSP cross-linked CBP-eGFP-HlyA stalled TISS and reinject of selected fractions on same column. (a) The eluted fractions from the CBP-resin containing the TISS were concentrated using an Amicon Ultra centrifugal filter unit and 500 μ L was loaded on a Superose6 increase 10/300 column. The dotted line indicates the selected peak (about 10 to 14 mL) for reinject. (b) The selected 4 mL fraction were concentrated using an Amicon Ultra centrifugal filter unit to 500 μ L and was reinjected on the Superose6 increase. The dotted lines indicates the selected peak (about 11-15 mL) for further investigation. The pooled peak (indicated as 1) was applied to NativePAGE and for immunoblot analysis and silver stain (Figure 7 & 8).

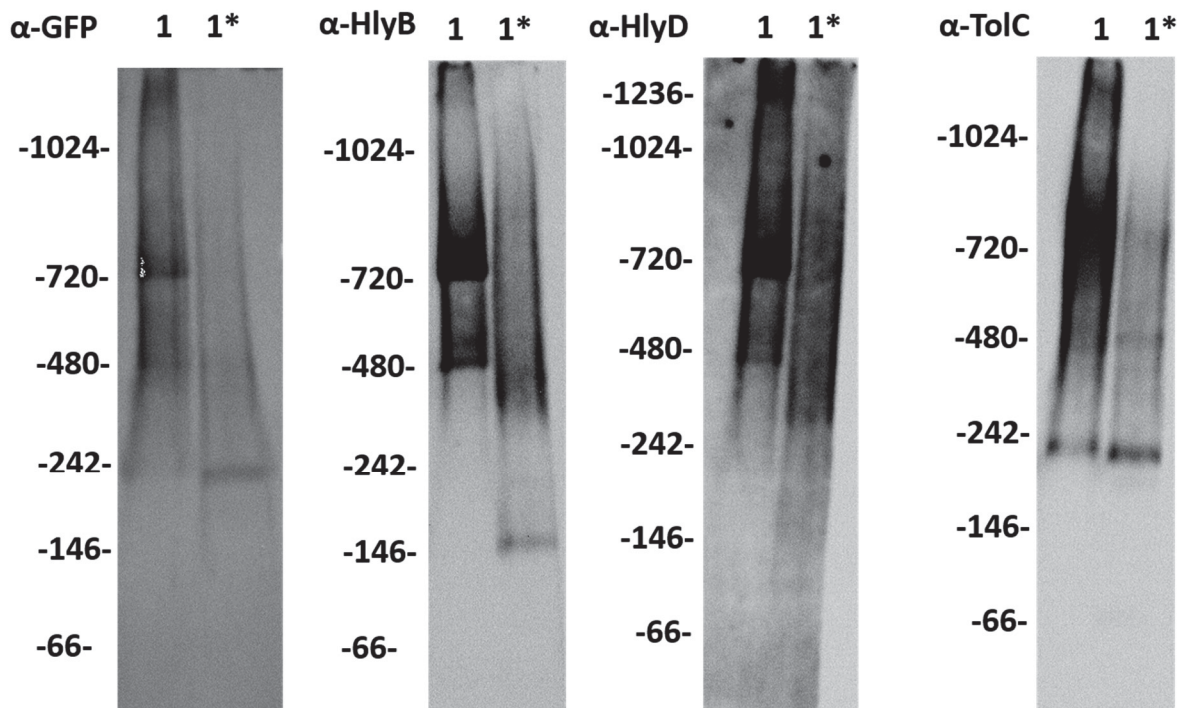
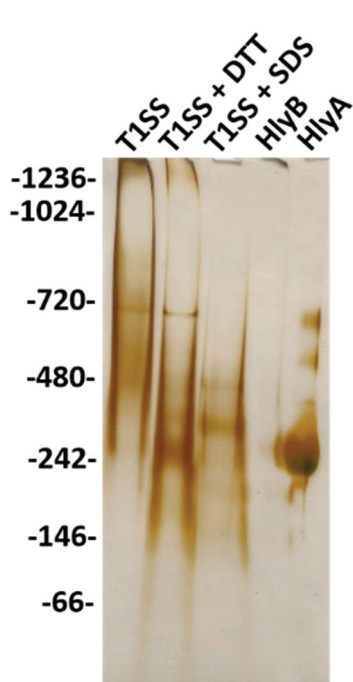


Figure 7. Immunoblot analysis of the reinjected SEC fraction from TISS purification. All parts of the HlyA TISS were detected by immunofluorescence in the collected SEC fractions. The sample derived from DSP crosslinked, solubilized membranes from *E.coli* BL21(DE3). The sample was applied to a NativePAGE with a Bis-Tris 4-16 % gradient gel. The protein was transferred by tank-blot to the PVDF membrane. The blotted membranes then were examined by using specific antibodies against eGFP, HlyB, HlyD and TolC. The * indicates an addition of 50mM DTT and 1 % (w/v) SDS during sample preparation to reduce the DSP disulfide bonds and separate the components of the TISS.

To evaluate the running behavior of the single components of the TISS the pooled sample was compared with purified reference from HlyB in detergent (LMNG) and HlyA. Also the supposed complex was added with DTT respectively DTT and SDS. The samples were applied to a NativePAGE and was subsequently silver stained. The pooled sample showed on band at 720 kDa with a background smearing of protein. When disulfide bounds were dissolved the background vanished and the 720 kDa band was still visible. Also a ladder of different bands appeared between 480 kDa and 146 kDa. Also the addition of SDS changed the pattern again and the 720 kDa band disappeared. Furthermore a band between 480 and 242 got more intense while a band around 242 was dissolved. The reference protein HlyB showed no normal running behavior (Figure 8).



While in other cases the HlyB would form a band at 146 kDa (supposed dimer, data not shown but observable in Figure 7), the HlyB here stopped migrating at the height of HlyA around 242 kDa. The interaction of the reference samples disrupted the normal migration.

While the Westernblot showed the different immunofluorescence signals the same bands were not detectable when silver stained. The further improvement of the purification guided to the use of a different strain to reduce possible impurities like AcrAB. Therefore, the strain C43 Δ acrAB was used for further purification. In addition, the purification without crosslink was investigated to reduce the smearing background resulting from various possible crosslinking products.

Figure 8 Silverstain of the reinjected SEC fraction from the T1SS purification on a NativePAGE. The pooled fractions from the reinjected T1SS was applied to a NativePAGE, Bis-Tris 4-16 % gradient gel. The gel run was stopped after the running front reached the bottom of gradient gel. The protein was fixed with methanol and acetic acid and silver stained. Additional supplements to the sample are indicated by + DTT (50 mM) and + SDS (1 % and 50 mM DTT). HlyB and HlyA was applied as purified reference.

Affinity purification and size exclusion chromatography of T1SS in C43 Δ acrAB

The established expression protocol for the T1SS was used in the C43 Δ acrAB strain. The membranes were collected and solubilized like stated before. To reduce the smearing background, the purification was carried out without crosslink reagent. As described above the affinity purification and SEC were performed. The resulting SEC chromatogram and NativePAGE is shown in Figure 9. The corresponding Western blot in Figure 10.

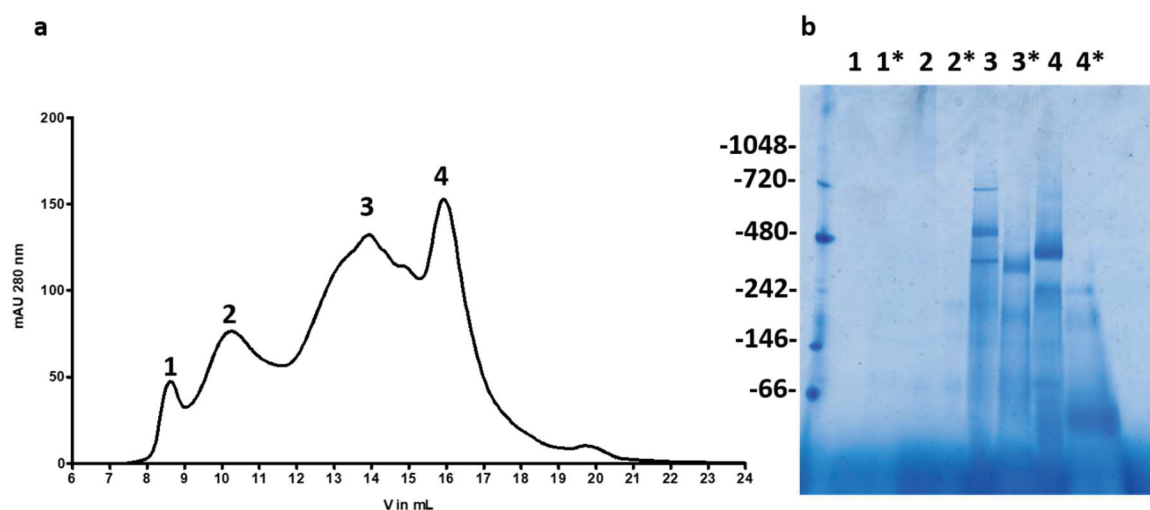


Figure 9. SEC of affinity purified T1SS from C43 Δ acrAB and corresponding NativePAGE. (a) The eluted fractions from the CBP-resin containing the T1SS were concentrated using an Amicon Ultra centrifugal filter unit and 500 μ L was loaded on a Superose6 increase 10/300 column. The

numbers indicates the selected peaks 1 to 4, which were used for further investigation. (b) collected fractions from the TISS purification were applied to a NativePAGE, Bis-Tris 4-16 % gradient gel. The gel run was stopped after the running front reached the bottom of gradient gel. The protein was fixed with methanol and acetic acid and stained with colloidal Coomassie. The * indicates an addition of 50 mM DTT and 1 % (w/v) SDS during sample preparation to reduce the DSP disulfide bonds and separate the components of the TISS.

The SEC chromatogram of the CBP-tag purified TISS showed a novel pattern. The main signal shifted from the initial peak at 10 mL to the peaks at 14 and 16 mL. This could be through the new strain or the abdication of crosslinker. The blue native PAGE showed no significant bands in the first and second peak. In contrast, the previously positive tested band close to 720 kDa was detectible in peak three. To check for identity immunofluorescence was used as shown in Figure 10.

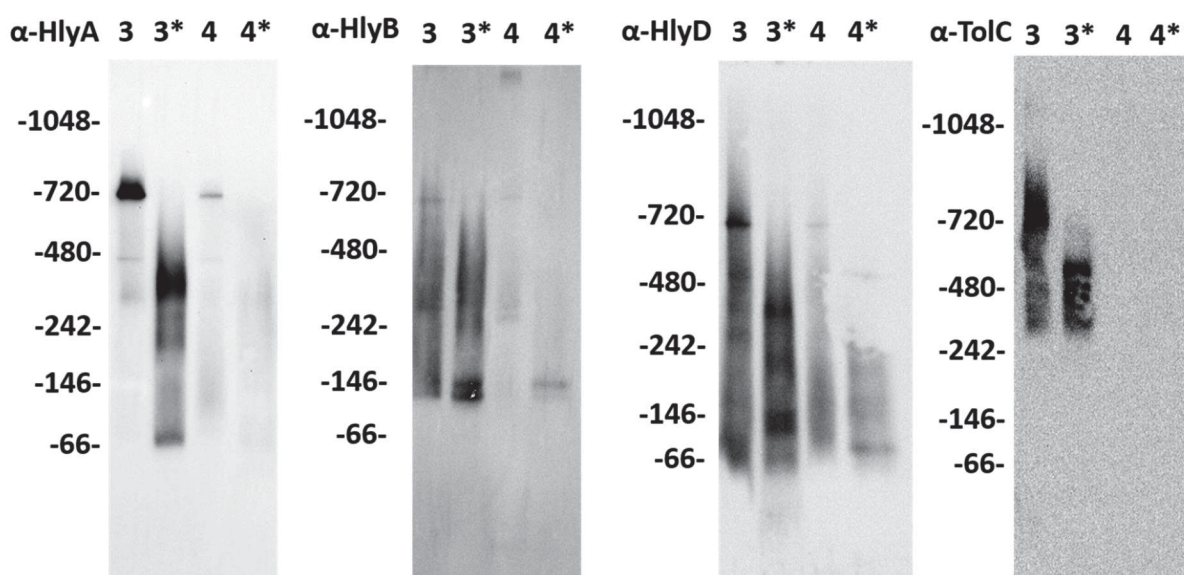


Figure 10. NativePAGE Immunofluorescence analysis of TISS SEC fractions from C43 Δ acrAB. The sample was applied to a NativePAGE with a Bis-Tris 4-16 % gradient gel. The protein was transferred by tank-blot to the PVDF membrane. The sample 3 indicates the third peak respectively 4, the fourth peak from the SEC shown in **Figure 8**. The blotted membranes then were examined by using specific antibodies against HlyA, HlyB, HlyD and TolC. The * indicates an addition of 50 mM DTT and 1 % (w/v) SDS during sample preparation to reduce the DSP disulfide bonds and separate the components of the TISS.

The immunofluorescence showed all components in the 720 kDa band for peak three. When DTT and SDS was added the pattern was altered. HlyA showed then bands below 480 to 66 kDa but also at around 242 kDa, as described before. For HlyB the band around 146 kDa is observable when DTT and SDS was added. HlyD showed a staircase pattern beginning at below 480 kDa to near the 66 kDa marker band. TolC in contrast showed signals between 242 and 480 kDa band up to a little above the 480 kDa band resulting in a smearing signal.

The three most prominent bands in Figure 9 (b) from peak three at around 720 kDa, 480 kDa and between 480 kDa to 242 kDa were analyzed. Due to the improved background signal the bands were cut from the NativePAGE and analyzed via mass spectrometry (MS) to validate the result of the immunofluorescence and ensure the identity of different bands. While between 480 kDa to 242 kDa the different components of the TISS were identified by MS, the band at 480

kDa showed TolC and impurities. The band at 720 kDa harbored a major impurity. GroEL was detected there. A HSP60 homolog protein expressed as stress regulator to cope with miss folding, overexpression or molecular crowding [207]. Puppala et al. showed for GroEL while overexpression protein in E.coli that a 720 kDa complex of GroEL was present and appeared as a single band on NativePAGE [208] similar to the observed band during purification. Additionally the analyzed T1SS samples showed OmpF as a major impurity.

To avoid the identified impurities the strain used for purification was changed to C43 Δ acrAB, Δ ompF. To prevent copurification of GroEL an additional washing step at the affinity purification was established. A washing step containing ATP to enforce the substrate release of GroEL by traversing the ATP cycle as described by Chaudhuri et al. [207].

Affinity purification and size exclusion chromatography of T1SS in C43 Δ acrAB Δ ompF without crosslinking

While the expression, stalling and membrane preparation was not altered the additional washing step during the CBP affinity purification was established. The eluted protein was then applied to SEC. The resulting chromatogram and the corresponding Western blot is shown in Figure 11 respectively the blue NativePAGE in Figure 12.

The changes in the purification resulted in a shift in the chromatogram to higher volumes. Also the vanishing of the GroEL impurities at 720 kDa on NativePAGE. The immunofluorescence showed signal for every component of the T1SS but the overall MW suggested that the complex is not intact. The major signals were located between the 242 and 480 kDa bands. eGFP-HlyA plus a trimer of TolC would lead to a MW of approximately 294 kDa. A dimer of HlyB together with a hexamer of HlyD 485 kDa. A HlyB dimer with a HlyD trimer 322 kDa. So different permutations of the T1SS components could lead to the emerging signals. When SDS and DTT were added to the shoulder peak indicated as “1”, the signal for HlyA and TolC was minimally altered. While the signal for HlyB and HlyD was disrupted and resulted in a signal at 146 kDa for HlyB and one band around 146 kDa with a broad band at 66 kDa for HlyD. This could be an indication for disruption of the IMC and a more stable complex of stalled eGFP-HlyA caged in TolC.

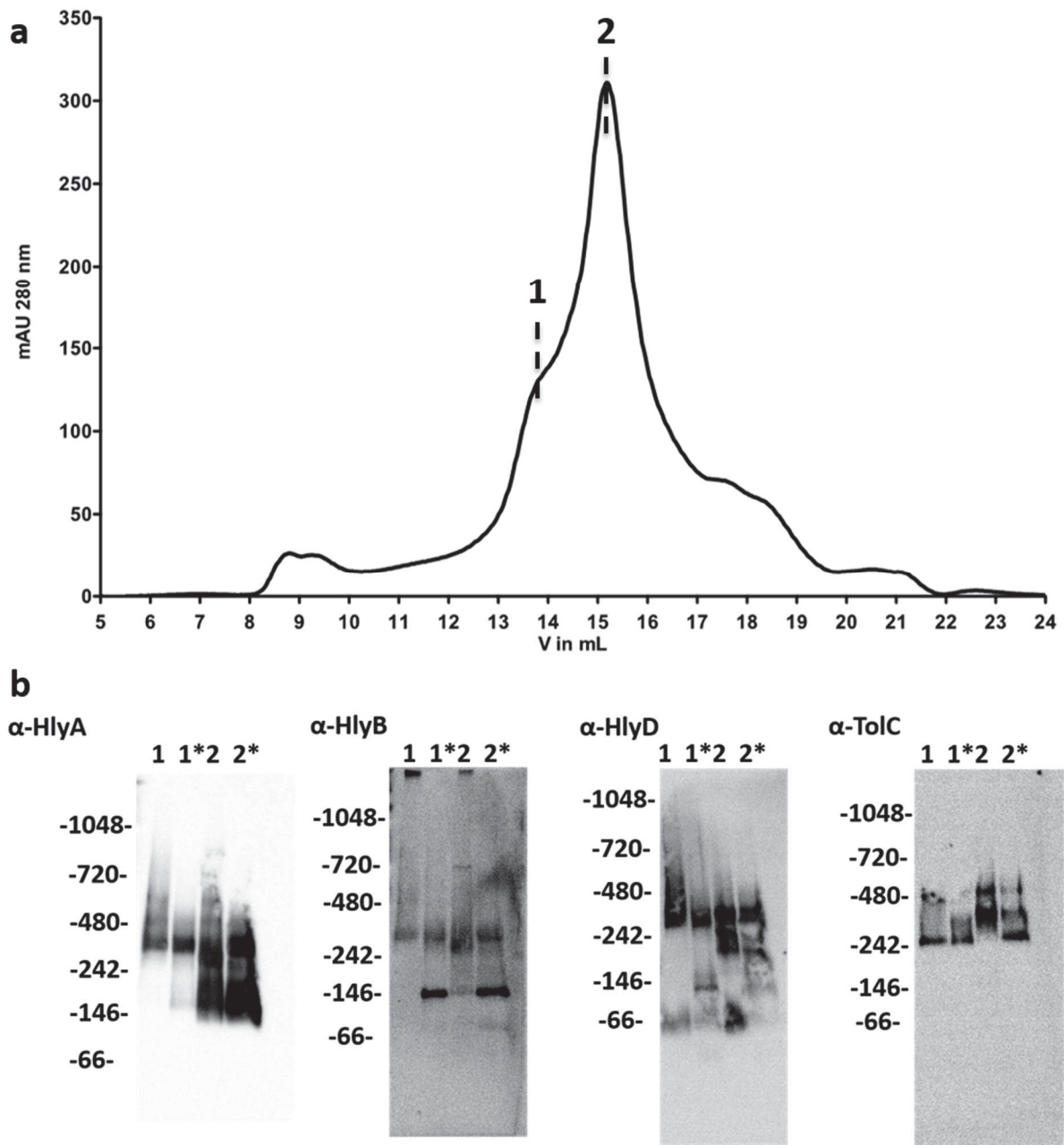


Figure 11. SEC after CBP affinity purification, of stalled, not crosslinked TISS, expressed in C43 Δ acrAB Δ ompF. (a) The eluted fractions from the CBP-resin containing the TISS were concentrated using an Amicon Ultra centrifugal filter unit and 500 μ L was loaded on a Superose6 increase 10/300 column. 1 indicates the front shoulder of the major peak (around 13.5 mL) 2 indicates the top of the major peak (near 15 mL). (b) All parts of the HlyA TISS were detected by immunofluorescence in the collected SEC fractions. The sample was applied to a NativePAGE with a Bis-Tris 4-16 % gradient gel. The protein was transferred by tank-blot to the PVDF membrane. The blotted membranes then were examined by using specific antibodies against HlyA, HlyB, HlyD and TolC. The * indicates an addition of 50mM DTT and 1 % (w/v) SDS during sample preparation to reduce separate the components of the TISS.

The blue NativePAGE showed a similar pattern to the Western blot. A band between 242 to 480 kDa at around 13 mL elution volume followed by smaller bands in the higher elution volume.

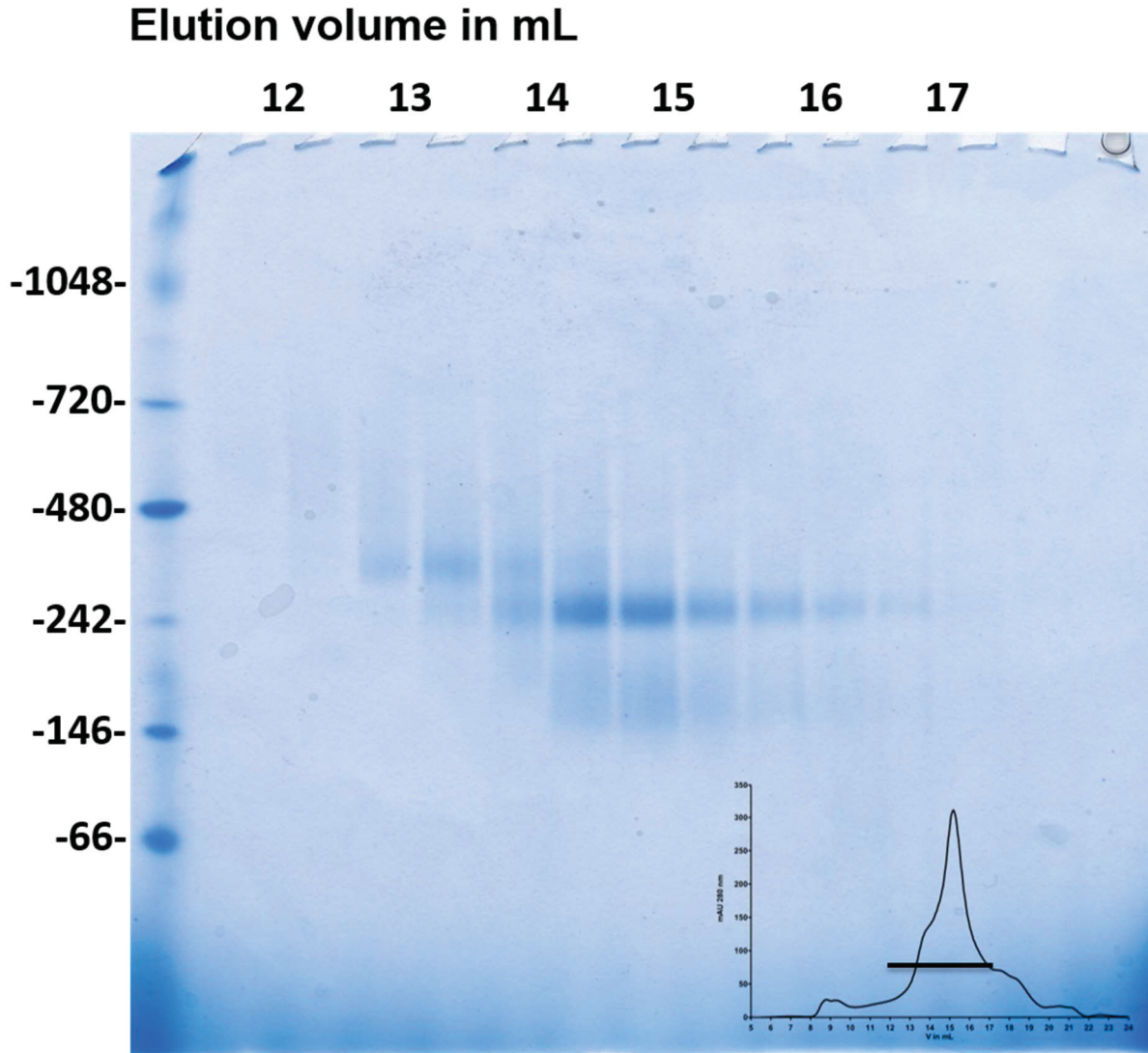


Figure 12. Blue NativePAGE of SEC after CBP affinity purification, of stalled, not crosslinked TISS, expressed in C43 Δ acrAB Δ ompF. The eluted fractions from the CBP-resin containing the TISS were concentrated using an Amicon Ultra centrifugal filter unit and 500 μ L was loaded on a Superose6 increase 10/300 column. The numbers on top indicating the elution volume of the applied sample. On the right bottom corner a schematic of the SEC chromatogram is shown with a black bar indicating the selected range applied to the gel. Collected fractions from the TISS purification were applied to a NativePAGE, Bis-Tris 4-16 % gradient gel. The gel run was stopped after the running front reached the bottom of gradient gel. The protein was fixed with methanol and acetic acid and stained with colloidal Coomassie.

The eradication of the impurities revealed that the higher molecular weight bands were mimicking the complex by unspecific binding and showed that in the C43 Δ acrAB Δ ompF strain the complex is not stable without crosslinking when purified as described before. Therefore, the purification with DSP crosslink was tried to isolate the TISS in the C43 Δ acrAB Δ ompF strain.

Affinity purification and size exclusion chromatography of T1SS in C43 Δ acrAB Δ ompF using DSP as crosslinker

The purification of the T1SS in the C43 Δ acrAB Δ ompF strain without crosslinker resulted in a disintegration of the complex. Therefore the next step was to stabilize the complex. In the experiments before, the usage of crosslinker versus no crosslinker showed no significant difference but there were impurities present which masked the actual results why the usage of crosslinker had to be evaluated again.

The membranes were crosslinked before solubilization. The solubilized membranes then were used for affinity purification followed by SEC. The SEC fractions were analyzed by silver stained NativePAGE and immunofluorescence (Figure 13).

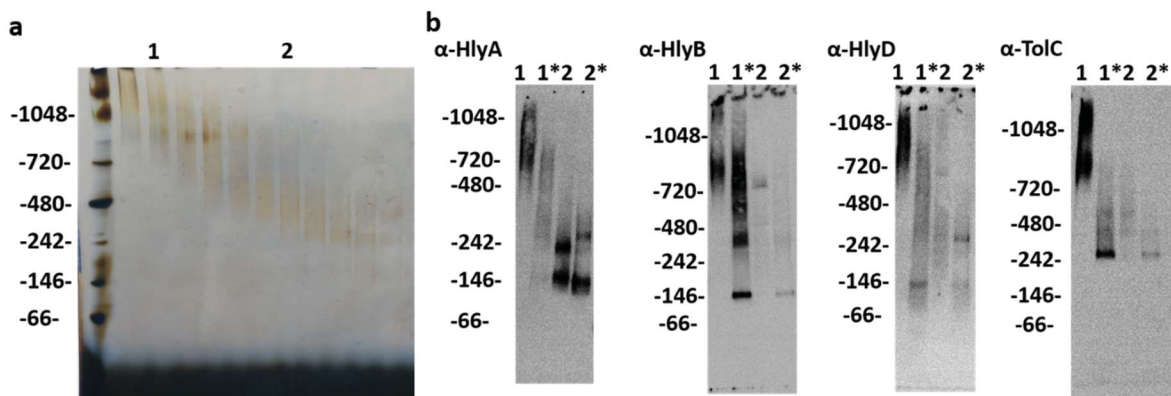


Figure 13. Analysis of SEC after CBP affinity purification, of stalled and crosslinked T1SS, expressed in C43 Δ acrAB Δ ompF. (a) The eluted fractions from the CBP-resin containing the T1SS were concentrated using an Amicon Ultra centrifugal filter unit and 500 μ L was loaded on a Superose6 increase 10/300 column. 1 indicates the front shoulder of the major peak (nearly 11 mL). 2 indicates the back shoulder of the major peak (around 13 mL). Silver stained NativePAGE of the SEC from 11 to 15 mL, shifting in every lane 0.5 mL. (b) All proteins of the HlyA T1SS were detected by immunofluorescence in the collected SEC fractions. The sample was applied to a NativePAGE with a Bis-Tris 4-16 % gradient gel. The protein was transferred by tank-blot to the PVDF membrane. The blotted membranes then were examined by using specific antibodies against HlyA, HlyB, HlyD and TolC. The * indicates an addition of 50mM DTT and 1 % (w/v) SDS during sample preparation to reduce the disulfide bonds from DSP and separate the components of the T1SS.

By reintroducing the crosslinking, the first major peak shifted to earlier elution volume during SEC Figure 13 (a) to about 11 mL to 13 mL. When applied to NativePAGE for immunofluorescence signals can be detected for every component at a height range between 720 to 1048 kDa. The signals exhibits a high smearing but can be dissolved when DTT and SDS is added. The signal for HlyA is like HlyD very faint in the presence of DTT and SDS. HlyB shows a ladder pattern when the crosslink is dissolved. While TolC shows a clear signal at approximately 242 kDa with some background and signals in the higher MW range. The silver stained NativePAGE underlined this findings and showed a staircase like pattern from higher to lower MW signals with no clear bands visible.

While stabilizing the interaction between the components of the T1SS no clear band pattern was observable and it was not clear if the integrity of the complex was ensured. The signals could also be a result of the proximity during crosslinking.

Recent studies showed an importance of peptidoglycan for interactions between IMC and outer membrane protein for AcrAB [186]. Therefore, it was investigated if the purification in the presents of peptidoglycan can stabilize the T1SS complex with no need for crosslinking. Further, instead of the C43 Δ acrAB Δ ompF strain the C43 Δ acrAB strain was used. Experiments with the IMC showed a tendency for higher stability (data not shown) when OmpF was present.

Affinity purification and size exclusion chromatography of T1SS in C43 Δ acrAB Δ ompF using DSP as crosslinker

The standard expression followed the altered membrane preparation. To ensure that the peptidoglycan layer around TolC was preserved, the cells were incubated with lysozyme while thawing and during the cell cracking. An additional incubation step was added to ensure sufficient time for the activity of the lysozyme. A second method was tried in parallel according to Hu *et al.* [81]. Here the whole cell was lysated using lauryldimethylamine oxide (LDAO), a non-denaturing detergent. Also in this method the peptidoglycan was digested by lysozyme. Therefore, the purification was compared with the established Fos-Choline-16 method. For further comparison the methods are abbreviated by Fos and accordingly LDAO.

Both collected membranes were solubilized and applied to CBP-resin. The eluted protein was then applied to SEC and the eluted protein was tested on the T1SS components. The chromatogram of both SEC is shown in Figure 14.

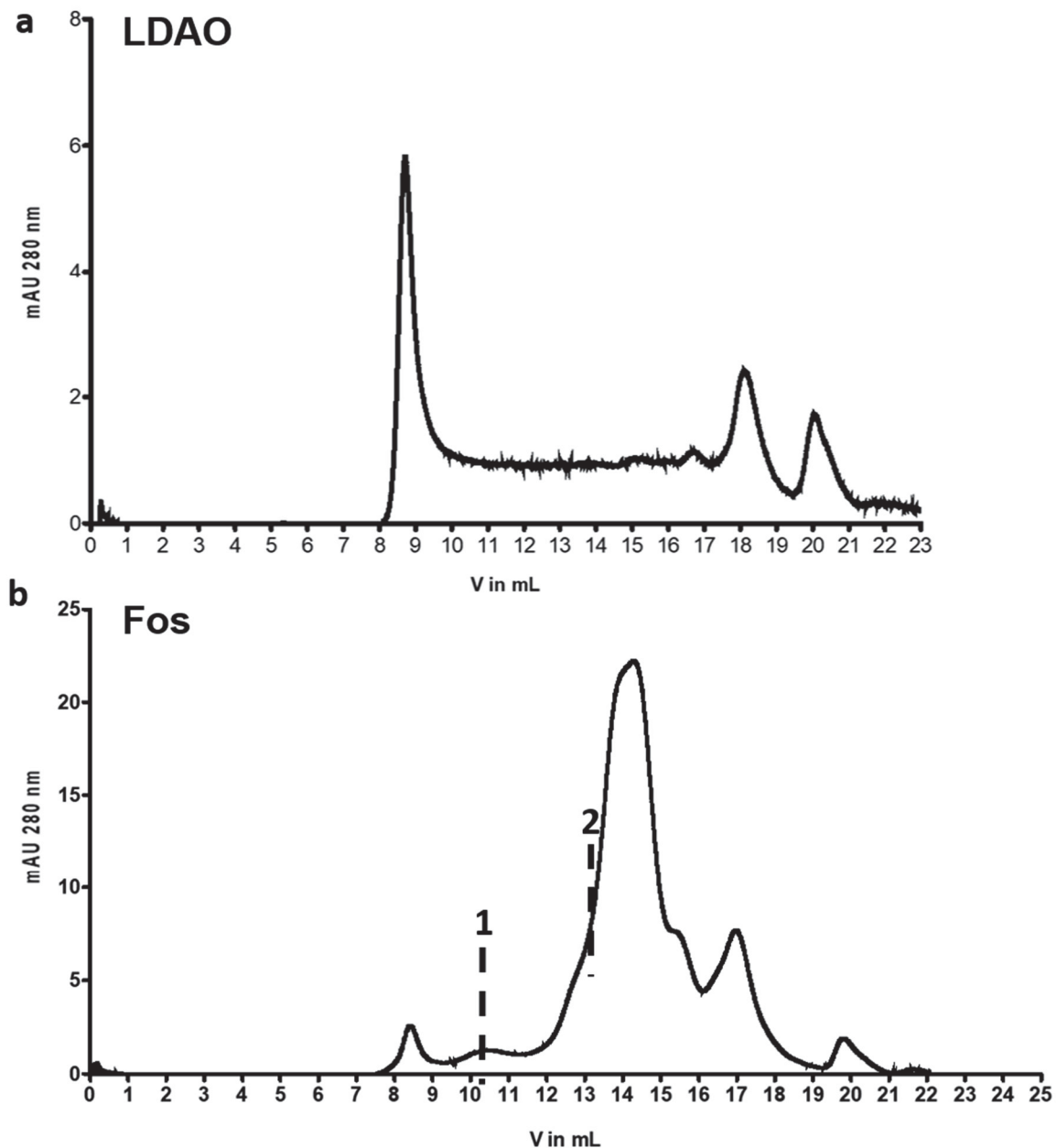
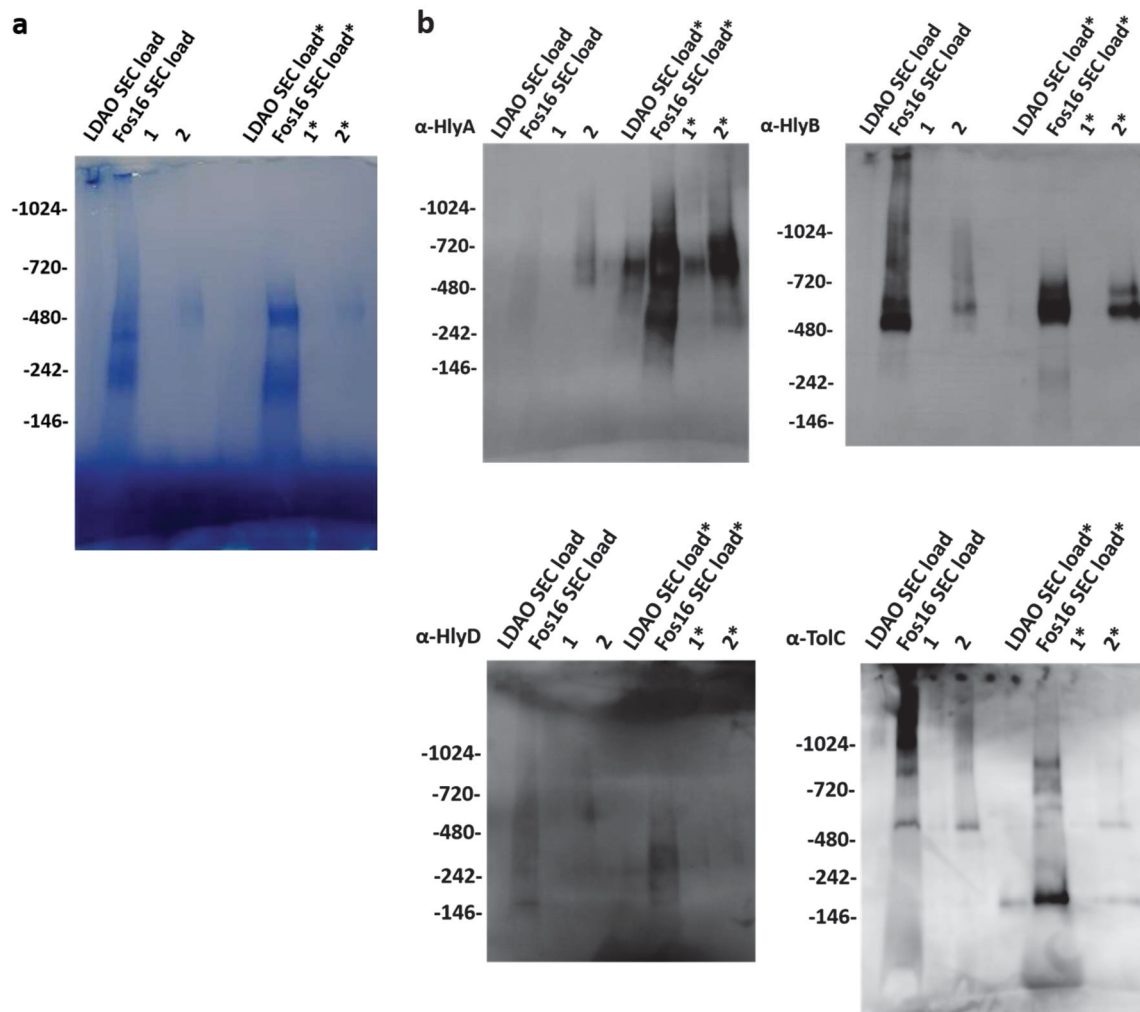


Figure 14. Comparison of “LDAO” versus “Fos” purification showing the SEC after CBP affinity purification, of stalled, not crosslinked TISS with peptidoglycan digest, expressed in C43 Δ acrAB (a) LDAO purification. The eluted fractions from the CBP-resin containing the TISS were concentrated using an Amicon Ultra centrifugal filter unit and 500 μ L was loaded on a Superose6 increase 10/300 column. (b) Fos purification. The eluted fractions from the CBP-resin containing the TISS were concentrated using an Amicon Ultra centrifugal filter unit and 500 μ L was loaded on a Superose6 increase 10/300 column. (b) 1 indicates the first peak (near 10.5 mL) 2 indicates the front shoulder of the major peak in the chromatogram (around 13 mL)

The SEC chromatogram of LDAO showed only a small peak for aggregate followed from a minimal signal with no clear peak profile. The purification from whole cell solubilization with LDAO showed no sufficient yield for purification, therefore the SEC loaded sample was further investigated. The Fos purification showed a small peak for about 10 ml and a major peak beginning from 12 to 15 ml. The fractions around 10 ml were collected, the same was done for the fractions from 12.5 to 13.5 ml to collect the front shoulder of the peak.

The fractions were concentrated and applied to NativePAGE for further investigation via Coomassie stain and immunofluorescence displayed in Figure 15.



*Figure 15. Comparison of “LDAO” versus “Fos” blue NativePAGE and immunofluorescence of SEC load and peaks from Fos purification of stalled, not crosslinked TISS with peptidoglycan digest, expressed in C43 Δ acrAB. (a) Load indicates the samples protein applied to the SEC for purification. The numbers correspond to the samples taken from the chromatogram shown in **Figure 13**. The * indicates an addition of 50 mM DTT and 1 % (w/v) SDS during sample preparation to reduce the disulfide bonds from DSP and separate the components of the TISS. Collected fractions from the TISS purification were applied to a NativePAGE, Bis-Tris 4-16 % gradient gel. The gel run was stopped after the running front reached the bottom of gradient gel. The protein was fixed with methanol and acetic acid and stained with colloidal Coomassie. (b) All proteins of the HlyA TISS were detected by immunofluorescence in the collected SEC fractions. The sample was applied to a NativePAGE with a Bis-Tris 4-16 % gradient gel. The protein was transferred by Trans-Blot® Turbo™ to the PVDF membrane. The blotted membranes then were examined by using specific antibodies against HlyA, HlyB, HlyD and TolC. The * indicates an addition of 50 mM DTT and 1 % (w/v) SDS during sample preparation to reduce the disulfide bonds from DSP and separate the components of the TISS.*

The low yield of protein for LDAO purification was also displayed on the blue NativePAGE and the Western blot with no visible bands. The purification with Fos-choline 16 instead showed protein in the sample and the different components of the TISS were detectable. The

application of the SEC load resulted in a smearing band on blue NativePAGE and for TolC respectively HlyB detected by immunofluorescence. For HlyD and HlyA only faint bands were visible. When SDS and DTT is applied, more signals are emerging. Even the LDAO sample shows some faint signal for HlyA. In contrast to the faint bands of HlyA in “load” without denaturation with SDS and DTT intense signals are detectable. Overall, smeary background was reduced and the specific signals became clearer visible. Only HlyD showed faint signals in all cases but was observable in the SEC load and the sample indicated as “2”, when SDS and DTT was added. The major bands for HlyB and HlyA migrated with the addition of denaturing reagents to a MW of approximately 480 kDa. For TolC some signals around 480 kDa were visible but the major signal when SDS was added was observable between 242 and 146 kDa.

From the emerged signals no intact complex was observable when the suggested stoichiometry of the T1SS is correct, regardless of HlyD trimer or hexamer.

Discussion

For obtaining detailed information about the structural properties the isolation of the functional translocation system was crucial. It was demonstrated that the HlyA T1SS can be stalled *in vivo* [173]. The stalling prevented the disassembly by arresting the secretion system in a transient active state. We showed for the first time that we were able to isolate membranes containing all components of the stalled T1SS, which is essential to enable further steps for purification of the complex. Until now only separated parts of the HlyA T1SS are structurally characterized, like the NBD by Zaitseva et al. respectively CLD Lecher et al. [157, 164] and a periplasmic soluble fragment of HlyD by Kim et al. [181]. The whole T1SS in action is not understood and characterized so far. The method of stalling the T1SS now gave us the opportunity to characterize the whole complex. The first step to enable the characterization was obtaining the membrane containing the intact complex. By using Western blot analysis we demonstrated that all T1SS forming proteins, eGFP-HlyA, HlyB, HlyD and TolC were present in the purified membrane.

To access the complex for further investigation a solubilization assay was used to identify potential detergents suited for purification. The zwitterionic Fos-Cholines® -14, 15 and 16 and Cyclofos™-5 as well as the non-ionic pyranosides n-Dodecyl- β -D-maltopyranoside and n-Dodecyl- β -D-thiomaltopyranoside and digitonin seemed to be good candidates to reach this ambition. Nevertheless, a positive fluorescence signal of eGFP-HlyA, HlyB, HlyD and TolC during this solubilization screen gave only a first hint of a successful solubilization. The integrity of the protein complex was not confirmed. To verify this, density gradient centrifugation was the method of choice. Only if eGFP-HlyA, HlyB, HlyD and TolC are co-localized within the same layer the complex is still assembled. The gradient showed signals by immunofluorescence for all components in the sucrose gradient around 20 to 25 % w/w. The spread of signal for some components led to the assumption that the overall stability of the complex could be influenced during the purification. Therefore, the usage of DSP as a crosslinker was established. The crosslinker was introduced to increase the stability of the stalled complex during the cell disruption and solubilization.

For the first time we were able to purify all components of the T1SS via CBP-tag. The identity of the components was confirmed by immune fluorescence on NativePAGE and SDS PAGE. High background on the NativePAGE indicated an inhomogeneous sample containing a lot of different crosslinking products. Even though the release of the crosslink by the addition of DTT did not alter the signal pattern. On SDS PAGE the complex was disrupted when DTT was added and the single components were present. While the presence of all components was necessary to open the opportunity to purify the T1SS, the correct assembly was not assured. The high MW would have been a hint for a hexameric stoichiometry for HlyD (779 kDa for the stalled complex).

The further purification improved the sample smearing on the NativePAGE and led to better visible bands in the MW area close to the 720 kDa band. The sample was still inhomogeneous and not suited for methods like multi angle light scattering (MALS) to determine an absolute MW. It was concluded that on one hand the crosslinking also resulted in broadening of the sample by crosslinking impurities and on the other hand the possibility to crosslink proteins which are not involved in the translocation but have an affinity to the complex like unsecreted HlyA [57]. Even when there is no unspecific crosslink between the T1SS and other proteins, eGFP-HlyA has 106 lysine in its primary sequence. Therefore many lysine residues can crosslink via DSP. Additionally, to reduce the amount of impurities it was decided to use a delta *acrAB* strain. The AcrAB complex also uses TolC as a component, therefore the solubilization of TolC could lead to copurification by interaction between the components [53, 186].

The change to C43 Δ *acrAB* strain resulted in a reduction of the background visible on NativePAGE. The absence of crosslinker also led to clearer band patterns. The immunofluorescence led to positive signals for all components of the T1SS. The identity check of the different bands on NativePAGE via MS resulted in a contrary result. The main band around 720 kDa was a complex of GroEL described also for other purifications by Puppala et al. [208]. GroEL is able to bind unfolded proteins and is upregulated when a lot of protein is unfolded in the cytosol [28]. Through the overexpression of all components it is possible that GroEL binds to the unfolded parts of HlyA and is then copurified by the nature of the interactions between unfolded HlyA and HlyB [57], also visible on the gel shown in Figure 8 (silver stain of Native PAGE). Also it is possible that GroEL associates to some impurities which are copurified. After applying the samples to PVDF membrane for Western blot the binding pockets of the chaperones could be accessible what resulted then in an unspecific interaction with the primary antibody. The complex disintegrated into segments between 242 and 480 kDa when SDS and DTT was added. Resulting in a hypothesis that the T1SS falling apart into two segments. Assumed the complex is composed of the dimer HlyB, hexamer HlyD, trimer TolC and stalled with the eGFP-HlyA the size MW would be around 779 kDa. From the appearing band pattern, the size of the fragments is around 320 to 380 kDa. Permutation of the possible protein assemblies allows different combinations. The hexamer of HlyD would be located around 325 kDa while the trimer would be around 163 kDa. Also, a dimer of HlyB and a trimer of HlyD would be around 320 kDa. HlyA with HlyB dimer 300 kDa and TolC with a single HlyA to approximately 290 kDa. While the hexamer of HlyD together with TolC would reach a size of around 480 kDa and TolC with a trimeric HlyD 315 kDa. This possible combinations together with the known interactions between HlyA and HlyB investigated by Lecher et al. [57] and the MFP analog from HlyD (AcrB) and TolC by Shi et

al. [186] allowing no clear conclusion what parts formed the band for this pattern. Higher resolution would be needed to further specify the results. To stabilize the complex the crosslink was reintroduced. Furthermore, an additional washing step during the affinity purification was introduced, to get rid of GroEL. The properties of GroEL allowed the depletion through the usage of ATP during the washing step of the CBP-resin based on the ATP hydrolysis cycle described by Chaudhuri et al. [207]. Additionally a new strain was established to reduce impurities produced by OmpF. Therefore our two new expression strains C41 $\Delta ompF \Delta acrAB$ and C43 $\Delta ompF \Delta acrAB$ created in the institute with excellent properties for protein production were used (Kanonenberg et al.) [209].

The expression of the C43 $\Delta ompF \Delta acrAB$ strain when no crosslink was introduced, produced a more homogeneous sample with less background. The 720 kDa impurity from GroEL vanished through the optimized purification. Nevertheless, the diffracted pattern via immunofluorescence, seen in the former experiment for the T1SS components, was still visible. While the purity of the sample was increased the stability of the complex was not given. The assumption of disintegration of the complex appeared possible. Therefore, we compared the results with the purification in C43 $\Delta ompF \Delta acrAB$ while the complex was crosslinked. The SEC profile showed again an elution volume near 12 mL with a major peak. Earlier elution indicated an increase in size for the eluted sample. The 720 kDa GroEL impurity was not visible while signal for the T1SS components were detectable via immunofluorescence between 720 kDa and 1024 kDa on the NativePAGE, dissolvable by SDS and DTT into the single components of the complex. Only hints of eGFP-HlyA were visible after dissolving of the crosslink. While the presence of all components of the T1SS in a higher MW band was achieved, the bands also became much broader. The sample inhomogeneity was too high for applying to MALS. The behavior of the complex became a quandary between more homogeneous sample and possible intact complex. As a result, newly appeared methods for the purification of other TSS were used in hope to isolate the intact complex.

A type III secretion system from *Salmonella enterica serovar Typhimurium* was isolated by lysating the whole cell by using the non denaturing detergent LDAO in presence of peptidoglycan (Hu et al.) [81]. Furthermore the Luisi Lab found a distinct interaction between AcrAB the peptidoglycan and the C-terminal part of TolC in the periplasm [186]. The new insights lead to the assumption that the presents of the peptidoglycan could also be crucial for the integrity of the T1SS. Therefore, the whole cell solubilization approach was tried for and the established purification method with peptidoglycan digest to conserve the peptidoglycan around the TolC (proposed by Meroueh et al.) [10] while disrupting the sacculus in the periplasm. The use of LDAO unfortunately did not result in a sufficient yield and while protein was detected in the sample, barely detectable on native PAGE and only HlyA and TolC were clearly detectable via immunofluorescence when SDS and DTT was added. The established purification method altered with peptidoglycan digestion resulted in a low yield after SEC resulting in faint signals even when SDS and DTT were added. In contrast to the load sample, which showed all components are present before applied to SEC. The behavior of bad staining (Coomassie and immunofluorescence) of HlyD and HlyA when native buffer used was observed during daily routine. A possible explanation can be the interaction between HlyD and HlyA [65, 185]. This effect could be reinforced by the strong intrinsic hydrophobic interactions of the GG-repeats when unfolded previously described by O'Brien et al [210]. The resulting

band pattern was similar to other purifications when no crosslink was present. Leading to the conclusion that the complex has to be stabilized favorable through crosslink to enable the purification of the whole complex. Unfortunately, by crosslinking also band broadening is introduced. Therefore, optional crosslinking or purification methods should be evaluated to acquire homogeneous samples of the T1SS.

In summary, it was shown that we were able to express cells where the T1SS is present and obtain membranes with the T1SS components. Through a detergent screen, feasible candidates for solubilization were found and introduced. An affinity purification method was established producing samples with all T1SS components present. Immunofluorescence analysis of purifications with crosslinker present and absent are indicating that the solubilized complex is not stable during the purification when no crosslink is present. The use of primary amine crosslinker leads to a major increase in species with different MW making it impossible to determine the actual size or multimeric state of the complex. Therefore, the crosslink path should be further investigated in the future to obtain a feasible method to obtain the T1SS in conditions that allow structural analysis of the complex.

4 Discussion

This thesis focused on several aspects of the HlyA T1SS, new findings and their consequences. The first chapter describes the *in vivo* quantification of the secretion rate in *E. coli* BL21 in dependence of the extracellular added calcium ion concentration. The second chapter deals with the quantification of active T1SS and TolC in the UPEC strain UTI89 and in BL21. Thirdly, possible strategies and approaches to enable purification of the entire T1SS for further studies are presented.

The HlyA secretion rate and its independence on extracellular calcium ions

The ability to quantify the secretion rate of the HlyA T1SS relied on former experiments and observations. To calculate the secretion rate per transporter and per second the actual number of T1SS had to be determined. Thus, the experimental setup developed for the investigation of the C-directional transport (shown by Lenders et al.) [173] of HlyA was used. The translocation pore was arrested through the use of a fast folding eGFP fused to the N-terminus of HlyAc, a truncated HlyA variant of full length HlyA consisting of only the last 218 aa [173]. After 1 h of co-expression of HlyB, HlyD and eGFP-HlyAc all functional T1SS were arrested (see chapter 3.1). Furthermore, immunofluorescence was used to measure the absolute amount of active T1SS. The determined amount of HlyA T1SS was comparable with the results of the HlyB quantification via quantitative Western blot analysis (see chapter 3.1). This confirms the suggested dimer of HlyB proposed from the NBD structure [157, 158], mass spectrometry [205] and MALS [211] leading to a total number of about 5000 (4532 ± 966) active T1SS per cell.

The determination of HlyB via Western blot allowed the quantification of the amount of transporter present in the cell. For the quantification of the secretion rate this method alone was not sufficient. The amount of HlyB alone does not ensure that the amount of detected transporter in the cell is equal to the amount of active T1SS. Therefore, a method was developed to quantify the amount of active T1SS. This also allowed conclusions about how many HlyB transporters were involved to form active T1SS compared to the overall amount in the cell.

Based on the structure of the AcrAB-TolC complex determined by cryo-EM (Du et al. and Shi et al.), it is known that the membrane spanning part has a length of about 320 Å [53]. Furthermore, it is known that the HlyA T1SS is only able to secret unfolded protein through the translocation pathway [52]. For the T1SS pathway a similar length (like the AcrAB-TolC complex) of about 320 Å was assumed. To evaluate the possible use of HlyA respectively HlyAc to bridge the pathway different assumptions were made to decide which substrate would be sufficient for the experiment. Assuming that the substrate is completely unfolded a length of the polypeptide chain can be calculated. Using a length of 3.5 Å per aa (actual 4.07 Å but altered by torsion angles) [212], results in a length of 3584 Å for unfolded HlyA and 763 Å for unfolded HlyAc. In the cytosol, HlyB forms a translocation pore and the estimated length to span also the NBD is about 45 Å, derived from the crystal structure of the HlyB-NBD [157]. Therefore, it was assumed that 365 Å have to be bridged to span the distance between cytosol and the outer extracellular space. For HlyA the possible extracellular part on the surface would be approximately 3200 Å in length (919 aa) and begin to fold on the surface by binding calcium ions to the RTX motifs. Furthermore, in the case of HlyAC only 398 Å in length reach the cell surface (113 aa). The surface reaching fragment will begin to fold and only a small globular

binding target will be accessible in comparison to HlyA. Since no monoclonal antibody was available several antibodies would be able to bind to HlyA. Therefore the shorter construct HlyAc was used to ensure a single binding event. When the size of a single binding groove is about 20 to 40 Å³ (pdb 1MEL) [213] only one antibody can bind per T1SS to HlyAc (see chapter 3.1). Thus, a number of approximately 5000 (4532 ± 966) active T1SS per cell, which is equal to the amount of HlyB in the cell is equal to the amount of active T1SS. The quantification method for active T1SS via antibody staining also allowed the determination of active T1SS in *E. coli* UTI89 (approximately 800), while the calculation through the amount of HlyB was not feasible in UTI89 because of the high proteolytic digestion of the transporter (see chapter 3.4).

With the amount of active T1SS and the determination of secreted protein by supernatant analysis, we were able to determine the secretion rate for HlyA and HlyAc to 16.0 ± 1.3 and 16.6 ± 1.4 amino acids per second and transporter. The secretion rate was not influenced by the concentration of calcium ions in the extracellular space. Additionally, when HlyA is compared to HlyAc no significant change was observed.

T1SS substrates share the repeat in toxins (RTX) motif (GGXGXDXUX, where X can be any amino acid and U is a large, hydrophobic amino acid), which is also called glycine-rich repeat (GG-repeat). In previous studies, the affinity of calcium ions to GG repeats in HlyA was determined to approximately 100 μM by Thomas et al. [150]. The GG repeats are essential for the correct folding of the protein and through their location in the sequence, accumulated in the C-terminal [167, 197], it was suggested that the induced folding promotes a driving force for RTX-proteins (like HlyA and CyaA from *Bordetella pertussis*) that pulls the protein in a ratchet like motion out of the translocator [167, 169]. With the above described experimental setup it was possible to address this theory by determining the secretion rate at different calcium ion concentrations. The calcium ion concentration showed no influence on the secretion rate even below the K_D (100 μM) or in complete absence of calcium ions (adjusted with EGTA). The secretion rate was not altered and in the same range with approximately 16 amino acids per second and transporter. The experiments showed that calcium ions are a major factor for the stability of the HlyA in the supernatant, but no difference in the actual secretion rate was observed. Furthermore, no difference between HlyA and HlyAc was detected, which concluded that the proposed ratchet like pulling mechanism does not exist for HlyA. Therefore, while essential for protein stability the binding of calcium ions to the GG repeats does not represent the driving force of secretion.

Furthermore, it was possible to investigate the influence of the GG repeat proportion per aa on the secretion rate in HlyA. HlyAc contains 3 GG repeats with a length of 218 aa and HlyA 6 GG repeats in 1024 aa. While HlyA contains 4.7 times more aa compared to HlyAc, it only has twice as many GG repeats. Therefore, it was demonstrated that the number of GG repeats per aa has no influence on the actual secretion rate for the HlyA T1SS.

The HlyA T1SS quantification in BL21 and UTI89 and its influence on TolC expression level.

An initial quantification of the T1SS in *E. coli* BL21 determined approximately 4500 active HlyA T1SS and about the same amount of HlyB dimeric complexes. It was concluded from these findings that almost every HlyB participates in the T1SS. What was baffling was the inability to further increase the amount of T1SS. This raised the obvious question whether the level of expression is co-regulated (see chapter 3.4). From this finding an investigation was started to determine contributing factors resulting in an restricted T1SS expression. A closer look was taken to an essential protein involved in the T1SS formation, TolC [214]. It was decided to quantify the amount of TolC in the laboratory strain BL21 and the influence of the overexpression of the other T1SS components on the amount of TolC. For the determination, we used again quantitative Western blot analysis with purified TolC to calculate the amount of TolC in BL21 cells. The amount of TolC was equal to the determined number of active T1SS with approximately 5000 TolC trimers. This indicates that every TolC trimer is occupied by HlyB and HlyD when overexpressed and arrested by eGFP-HlyA. Guided by this result, the experiment was repeated in the *E. coli* strain UTI89, parental host of the HlyA T1SS. In these experiments, only the substrates, eGFP-HlyA and eGFP-HlyAc, respectively, were overexpressed, while the amount of HlyB, HlyD and TolC remained at endogenous levels. The quantification of TolC also resulted in about 5000 TolC trimers per cell in the UPEC strain. Combining all measurements, 4472 ± 1231 TolC trimers per cell were quantified as summarized in Figure 2 in chapter 3.4.

The expression and assembly of the T1SS had no significant influence on the overall amount of TolC in *E. coli* BL21 or UTI89. Nonetheless, the amount of active HlyA T1SS in UTI89 was determined to approximately 800 systems (796 ± 62). This concludes that while overexpressed in BL21 the whole TolC pool is depleted by the T1SS. However, cells show no altered behavior as no influence on cell growth or viability was detected. Other systems using TolC such as the tripartite efflux pumps AcrAB and MacAB rely on TolC and are crucial for drug resistance in *E. coli* [54, 215, 216]. This raises the obvious question why is there no phenotype? A possible explanation is that *E. coli* can compensate the loss of TolC by upregulation homologs, which substitute the outer membrane protein similar to strains in which *acrAB* is deleted (described by Sulavik et al, Nichols et al. and Alon et al.) [216-218]. Originally, TolC homologs in *E. coli* were discovered by the homology to the OMP of *Pseudomonas aeruginosa*, YjcP (MdtP) (26% identity and 47% similarity over 466 residues), and YohG (MdtQ) (27% identity and 45% similarity over 345 residues) [216]. Sulavik et al. [216] showed that in the absence of TolC the amount of these homologs are significantly increased especially in presence of antibacterial agents and affect intrinsic resistance and later found to have an effect on antibiotic resistance mechanism against fluorquinolones (Ciprofloxacin) [219]. Alon et al. 2019 [218] showed how *E. coli* can compensate the loss of ArcAB by up regulation of redundant multidrug transporters. The TolC independent major facilitator superfamily (MFS) transporters identified were MdfA a multidrug resistance transporter, which is able to bind cationic and zwitterionic lipophilic compounds and transports these from the cytosol into the periplasm by utilizing the PMF for active transport (showed by Heng et al.) [220]. MdtM is like MdfA located in the cytosolic membrane facing to the periplasm and is a polyspecific, promiscuous protein and transports a

diverse range of antibiotics, antimicrobial peptides or lipophilic cations. Ensuring transport from the cytosol, MdtM is supposed to deliver the antimicrobial substances to other efflux systems to subsequently transport these out of the periplasm (Law et al.) [221]. Additionally to the MFS the small multidrug resistance (SMR) protein EmrE, 111 aa in size, possesses 4 TMDs and forms dimer, is able to transport cationic drugs from the cytoplasm using a substrate / H⁺ antiport mechanism (Rotem et al.) [222]. While AcrAB has a major role in providing resistance to cells, the above mentioned TolC independent efflux and transport systems can compensate the predicted occupation of TolC through the T1SS at least to some degree.

While our experiment showed no influence on TolC expression, recent studies described several factors, which influence the regulation of TolC. Antibiotics [223], pH [224], flavonoids, indole, metal ions [225], EDTA or ethanol [226]. The *mar-sox* regulon responsible for the TolC expression was identified in the late 90s [227], while it was unclear how the actual regulation was maintained. Important for the ability to deal with reactive oxygen species (ROS), it was shown that the addition of H₂O₂ to an *E. coli* culture was sufficient to induce the *soxRS* regulon [228]. But it took ten years to identify the actual regulation (Zhang et al. 2008) [223]. A *marbox* activates the transcription of *tolCp3* and *tolCp4* through the transcriptional regulators MarA SoxS and Rob [223]. Further studies by Rosner et al. [229] suggested that some metabolites like *p*-hydroxybenzoate (pHBA), salicylate [230], indole [231] and other components [232, 233] can function as trigger for *marA soxS* and *rob* [229]. The transcriptional upregulation of TolC results in higher excretion of the trigger metabolites which than leads to basal expression of TolC. When mutants of TolC, which are deficient for secretion, are present the amount of TolC rises but the *marA soxS* and *rob* level stays elevated [229]. However, by having a closer look on the regulation of TolC and inducing upregulation via suitable metabolites or ROS producer like H₂O₂ the overall amount of TolC could be increased.

The 5000 TolC trimers on endogenous level seems reasonable when considering the amount of systems using the T1SS. In the laboratory strain *Escherichia coli* K-12 substr. MG1655 eight different RND-efflux systems rely on TolC (MdtEF-TolC, AcrDA-TolC, AcrEF-TolC, EmrAB-TolC, EmrKY-TolC MdtABC-TolC, AcrAB-TolC and MacAB-TolC)[234]. This does not include the HlyA and ColV T1SS [235] found in pathogenic strains like UTI89. Therefore, 10 systems rely on TolC to be operational when all mentioned RND-efflux systems and the two T1SS are present. The quantification of AcrAB-TolC determined approximately 500 systems [53, 215] while the HlyA T1SS on endogenous level is around 800. This would implicate that 3700 TolC trimers would be still available in the pool for other systems. The other efflux systems have a broad range of substrates: amino acids (described by Franke et al. and Yamada et al.) [232, 233], detergents (SDS, cholates by Nishino et al.) [236], while other efflux systems show some degree of redundancy to AcrAB like EmrKY or MacAB (detergents, antibiotics described by Sulavik et al. and Crow et al.) [237, 238]. This leads to the hypothesis that the different systems support each other to provide the cell with the required efflux capabilities while being able to secret toxins into the extracellular space.

Kanonenberg et al. 2019 [209] showed that the genomic deletion of *acrAB* and *ompF* did not altered the overall vitality and growth behavior of the *E. coli* strain [209]. This observation is similar to the experiments in which the T1SS was overexpressed in *E. coli* BL21. There was also no change in vitality and growth observed (chapter 3.4). Proteome analysis of the Δ *acrAB*

ΔompF strain revealed no obvious explanation to the observed behavior. An interesting hypothesis could be the regulatory influence of efflux systems in situations when the T1SS is arrested in an overexpressed system. When all TolC are occupied by the T1SS, the cell has to compensate in a way which is not investigated and understood yet. This obviously leads to interesting experiments that could also provide a better understanding of the T1SS.

T1SS surface localization

While the overexpression of the T1SS components had no influence on the amount of TolC, the question arises whether overexpression influences the surface pattern and accumulation of the T1SS. The experimental setup of the stalled T1SS allowed to use immunofluorescence labels for structured illumination microscopy (SIM) to address this question. In 2017 Jeong et al. [239] showed that the T4SS of *Legionella pneumophila* is strictly located to both poles of the cell with $92\% \pm 2\%$. While not clear, whether the secretion complex has to be located on the poles or the substrates must be transported from the poles [239] it has been shown that substrates are specifically located to the membrane adjacent to both poles [240-242]. Another prime example is the *Shigella* T3SS. Here, the secretion machinery was observed diffusely over the surface while the ipaC translocon component was only present at one pole during cell invasion ($70\% \pm 12\%$) by Jaumouillé et al. [243]. Therefore, some secretion systems show distinct polarization especially when active transport is conducted. But how is the situation for the T1SS? The Hensel laboratory Barlag et al. 2016 showed via single super-resolution imaging of self-labeled proteins that the SPI4-T1SS shows no specific localization on the cell surface while the SiiE adhesin secreting T1SS clustered in a unspecific manner [244]. SiiE is a giant adhesin (595 kDa) important for biofilm formation and cell adhesion [245]. While SiiE is not a toxin, HlyA is. Therefore, this difference was addressed by investigating the surface distribution and particularly the influence of overexpression in comparison to the endogenous situation in the wild type strain UTI89. The experiment was based on the stalled T1SS experiment (3.1) and the protocol was modified for usage in the *E. coli* UTI89 strain respectively for the laboratory strain to obtain better resolution for the data collection. For high throughput of the data an automated evaluation routine based on (Fiji) ImageJ [246] was developed. It was demonstrated that the HlyA T1SS showed no distinct localization on the cell surface regardless of endogenous expression (800 active T1SS) or overexpression (4500 active T1SS). Only a small fraction of bacteria accumulated the HlyA T1SS in both tips of the cell, $\sim 10\% \pm 7\%$. $\sim 29\% \pm 8\%$ roughly a quarter of the cells showed accumulation in one of the tips while the majority of all analyzed cells did not show any specific accumulation of the stalled HlyA T1SS, $\sim 61\% \pm 9\%$. While no specific polarization was observed, the signals clustered across the surface in non-repeating patterns. The acquired signal distribution from the cell surface showed similarities to the SiiF pattern from *Salmonella* [244]. A comparison of the signals is shown in Figure 1.

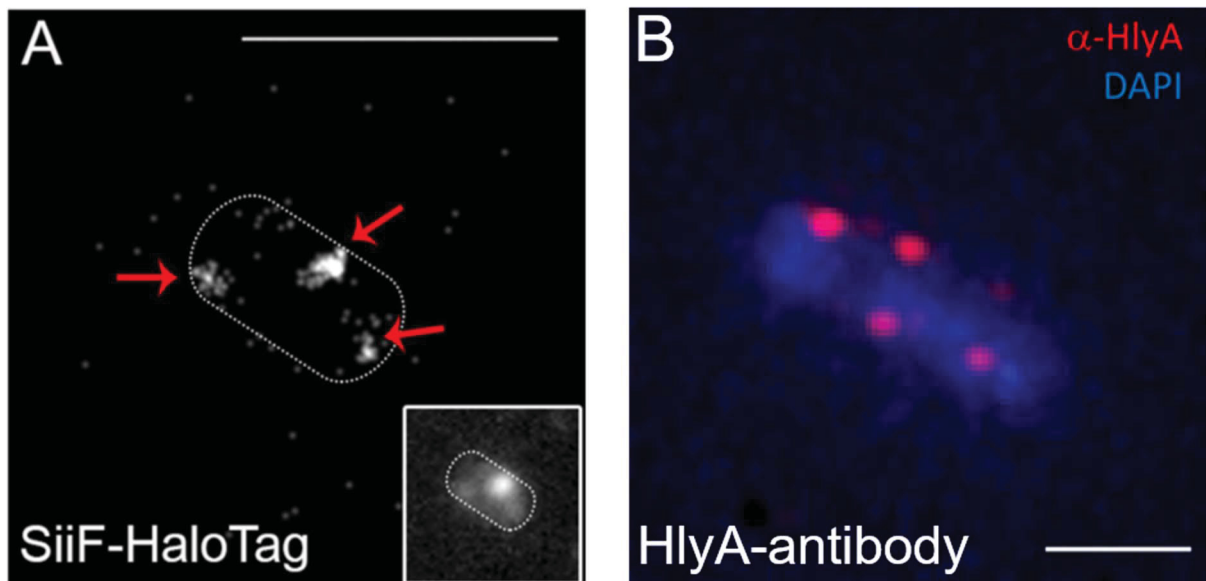


Figure 1. Comparison of surface distribution of different TISS. Showing labeled TISS in *Salmonella enterica* and *E. coli* BL21. (A) Single molecule localization microscopy of SiiF with a Halo-tag in living cells of *Salmonella*. Labeled with TMR-Star. Cells were imaged by super-resolution microscopy (SRM). 500 consecutive frames were acquired with 5 mW laser power at the focal plane. Cumulative maximum intensity projections with bilinear interpolation of all 500 frames are shown. Scale bar 5 μ m. Taken from [244] (B) HlyA TISS stalling was induced in BL21(DE3). DNA was stained by DAPI and cell surface exposed HlyA was stained by immunofluorescence labelling. Cells were imaged by SIM. Maximum intensity projections (MIPs) of raw data before processing show the DAPI channel in blue (DAPI), and the HlyA channel in red (α -HlyA). Scale bar: 1 μ m.

It can be concluded that no specific pattern is adopted by the HlyA TISS and the pattern is not influenced by overexpression of the TISS components. Moreover, despite of the different functions of the substrate, the SiiE secretion machinery has the same partial clustering as the HlyA secretion system. The experiment of Rassam et al 2015 demonstrated that proteins inserted by the Bam complex are forming rigid OMP islands [247]. The concept of OMP islands leads to the hypothesis that the actual localization could be determined by another factor(s). The most rigid part of the secretion machinery is the outer membrane protein TolC. This would also be in line with experiment in *Salmonella typhimurium* in which the diffusion rate of the TolC homolog SiiC was measured by Barlag et al. [244]. Here, the experiment demonstrated that the diffusible part of the secretion machinery was SiiF, while SiiC were mostly stationary [244]. Furthermore, it is in line with the similar behavior for the Tol-Pal system investigated by Rassam et al. [248]. The IM complex consisting of TolQ, TolA and TolR can lateral diffuse in the membrane, while the OMPs such as OmpF and the vitamin B₁₂ specific porin BtuB are located in sequestered OMP island [247]. In the presence of the bacteriocin colicin E9 (ColE9) the Tol-Pal system binds the ColE9 and the inner membrane complex lateral mobility is reduced while a clustering occurs.

For SecYEG a helical distribution was observed by Shiomi et al. [249]. By fusing GFP to a non-secretion competent mutant of MBP (maltose binding protein) and CFP-MreB the distribution of the Sec translocon during translocation was investigated [249]. Here, the translocation complex is rigid and located in the inner membrane. It was suggested that the rigid

helical distribution of the Sec translocation machinery may have an advantage through a more equal translocation over the entire cell than a random distribution. The first is achieved by using MreB as “support structure”.

An additional insight in the TolC distribution was observed by Bergmiller et al, 2017 [250]. Here, the uneven distribution of TolC in the outer membrane was observed and investigated through the accumulation of AcrB fused to eGFP. The fluorescence measurement showed an uneven distribution of AcrB during cell division. 42 % of eGFP-AcrB remained in the newly formed cell compared to 58 % in the maternal cell. It was concluded that this distribution has a long-term effect on the accumulation of AcrAB-TolC to one pole of the cell. A possible explanation to the uneven distribution was provided by Wang *et al* who investigated the distribution of protein clusters in bacterial cells during growth [251]. Here, a model was proposed to explain the observed lateral movement of protein clusters in the outer membrane to the poles on both ends of the cell. The formed clusters are unevenly formed and nucleate spontaneously while moving to both poles during growth. The insertion in the membrane occurs in the middle of the cell, where also the constriction takes place during cell division. The explanation is that through the clustering it is ensured that every new cell have at least some OMP clusters and can sufficiently thrive during growth. Gunasinghe et al, 2017, reviewed the location of secretion system on the cell surface of Gram-negative bacteria [252]. The authors proposed that the uneven distribution via OMP islands is a form of adaptation to variations in the amount of OMP in the daughter cells to increase the adaptation ability to possible environmental challenges. The asymmetry quantified by Bergmiller et al. [250] showed an asymmetry of approximately 10 % in the 2h time window from parental to the daughter cells. In the same time window the experiment with the cells (chapter 3.4) showed signals in one of the tips with approximately $29\% \pm 8\%$ of the cases. Therefore, some of the one sided polarized cell showed the observed polarization through a parental ancestry. This tendency can shift the results to some degree to one sided tip polarization. Nevertheless, for the HlyA T1SS no clear tip accumulation was observed with signals in both tips of the cell ($\sim 10\% \pm 7\%$) while the majority of all analyzed cells did not show any specific accumulation of the stalled HlyA T1SS ($\sim 61\% \pm 9\%$)

TolC will display the same behavior as other OMP islands (investigated by Rassam et al.) [247], since TolC is threaded through the peptidoglycan layer [10] and therefore constrained in diffusion in the outer membrane. The peptidoglycan is in steady reconstruction for inserting new proteins in the sacculus, which could lead to a cluster like insertion mechanism in the membrane (described by Typas et al.) [191]. These hypothesis is in good agreement with the ‘patch like growing’ described for the peptidoglycan sacculus [191]. When the supposed TolC localization is correct, the unfolding consequence would be beneficial for the knowledge about other system that use TolC. Because a rigid localization of TolC then implies the localization of the many systems that use TolC as an adaptor protein, the various RND-pumps and TolC using systems: MdtEF-TolC, AcrDA-TolC, AcrEF-TolC. EmrAB-TolC, EmrKY-TolC MdtABC-TolC, AcrAB-TolC and MacAB-TolC [234] respectively the T1SS of HlyA and ColV [235].

Strategies for the HlyA T1SS isolation

In this thesis, the first steps for the purification of an entire T1SS were established. While developing these methods, different major obstacles appeared. They cumulated in the quandary between an unstable complex, that disintegrates during purification or inhomogeneous samples which provide no basis for further experiments. The results were described in chapter 3.5. Therefore, this segment discusses new strategies to open up new options for purification.

While it was shown that it is possible to obtain membranes containing all components of the T1SS, a major constriction for the further purification was the maintenance of the integrity of the secretion system. The use of formaldehyde respectively para-formaldehyde resulted in large protein aggregates through crosslinks that did not migrate in a gradient native gel to estimate a molecule weight (MW). The use of DSP (dithiobis(succinimidyl propionate)) resulted in samples containing all T1SS components but at the same time, the homogeneity of the sample was severely decreased. For this reason methods like MALS were not applicable to obtain an absolute MW. The knowledge of the absolute MW of the complex could provide new insights into the multimeric state of the T1SS. In addition, homogenous samples would be highly favorable for structural methods such as cryo electron microscopy (EM) and X-ray crystallography.

In other cases the issue of stability was addressed by creating fusion constructs. For example AcrA was fused to AcrZ to stabilize the interaction between AcrZ and AcrAB (Du et al.) [53]. Recombinant proteins for AcrBZ were purified and crystallized. Structures obtained by X-ray crystallography were used for docking into electron density maps determined by single particle cryo-EM to obtain near atomic structural information of AcrABZ-TolC. In another case AcrB was fused to one AcrA while 5 transmembrane helices (TMH) were fused as a membrane inserted linker between the AcrB and first AcrA. Additionally a second AcrA was fused by a linker to the first AcrA (Jeong et al.) [188]. This fusion construct allowed purification of AcrAB resulting in a structure at 8.2 Å resolution obtained via cryo-EM. A third experiment resulted in the structure of MacAB-TolC by Fritzpatrick et al. determined again by single particle cryo-EM by fusing MacA via a single TMH to MacB. Additionally introduced cysteine residues and subsequent crosslinking stabilized the complex [54]. In all cases the components were purified by affinity chromatography and used for crystallization trials [53] or cryo-EM [188] [53]. Can this approach also be applied to the HlyA T1SS? While the construct of two HlyB with several TMH as linker could be challenging but somehow manageable the fusion of several HlyD could be even more complicated. HlyD has an N-terminal cytosolic and C-terminal periplasmic domain connected by a single TMH [181, 185]. Unpublished data showed that if the C-terminal part of HlyD was fused to an affinity tag the secretion ability of the T1SS with non-tagged HlyB was abolished. Therefore, it is not clear if the complex still assembles or whether secretion is disturbed. When fusing an affinity tag to the N-terminal side the secretion is possible but severely reduced (unpublished data, approximately > 95 %). Considering the impact of altering the terminus of HlyD, fusion of several HlyD could lead to an inability to assemble the IMC.

While the purification and reconstitution of HlyB was recently published from Kanonenberg et al. [211] the purification of the IMC is still problematic. As described, the activity of the single components is sensible to fusion at the termini of the transporter. Therefore, similar experiments used to purify the *Salmonella* SPI-1 T3SS by pulling on a single component of the needle complex, which is 4 MDa in size, did not result in stable a HlyB / HlyD complex. The laboratory of Prof. Luisi demonstrated that the interaction between the IMC of AcrAB and TolC is essential for the stability of the RND-efflux pump [186]. This could be an additional factor for the inability to obtain a stable IMC HlyB/HlyD complex. One possibility would be that the affinity tag of HlyB prevents a stable interaction with HlyD or TolC. For some secretion systems such as the EscN EscO T3SS complex from *E. coli* it is possible to isolate the components separately and assemble the components from scratch for further experiments (shown by Mejewski et al) [253]. For the T3SS the ATPase EscN was separately purified to the central stalk EscO. After affinity purification the separate proteins were mixed and incubated before they were applied to cryo-EM, which demonstrated formation of a homohexameric stalk similarly to F₁/V₁-ATPases [253]. Due to the properties of HlyD, this approach unfortunately is not feasible. Unpublished experiments showed that the expression of HlyD in the absence of HlyB is cytotoxic even in C41 and C43 strains and additionally leads to aggregation, which cannot be overcome. This also is a possible explanation why only a crystal structure of a truncated periplasmic fragment of HlyD is available [181]. Nevertheless, the restraints for the HlyB and HlyD purification might be resolved by stabilizing the IMC via TolC.

In chapter (3.5) it was shown, that through the introduction of amine specific crosslink the produced samples showed immunospecific signals for all components of the T1SS but the homogeneity was very low. It can be assumed that the many primary amines of the lysine from HlyA lead to a multitude of crosslink products. This might create a problem in reproducibility. Nevertheless, a new approach was developed. Kim et al. (2016) showed that the periplasmic part of HlyD probably forms a hexamer [181] while the lipoyl motif interacts with TolC [181], which was also predicted by Pimenta et al. [185]. In combination with the structures of AcrAB, which confirmed a tip to tip interaction between TolC and the AcrAB machinery [53, 186, 188], a different approach could be envisioned. In the periplasmic part, suggested to interact with the tip of TolC, a serine residue (S242) is present in the adjacent domain. This serine could be changed to cysteine to enable the use of a hetero bifunctional crosslinker. The second crosslink target is an exposed lysine (K130) of TolC. Through its trimeric nature 3 crosslinks between HlyD and TolC would be established to stabilize the assembled T1SS. A scheme of the proposed approach is shown in Figure 2.

The stalled, crosslinked complex could then be purified by density gradient centrifugation and affinity purification. Furthermore, the density gradient might be further stabilized by the GraFix method developed by Kastner et al. [254] which was invented for complex preparation intended for single particle cryo-EM analysis.

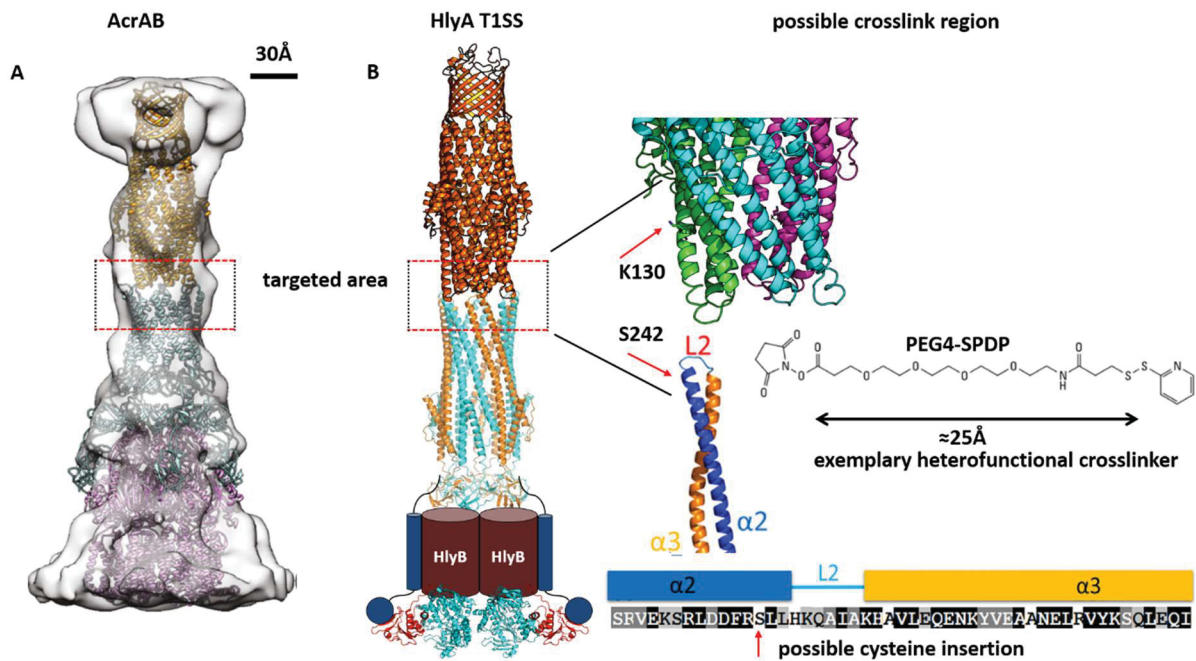


Figure 2. Novel crosslink approach to stabilize the HlyA T1SS for purification. (A) Image of the AcrAB-TolC RND complex, taken from [186]. The red dotted box indicates the region where TolC and AcrA are interacting via tip to tip interaction. (B) Scheme of the HlyA T1SS, generated from TolC (2XMN), HlyB NBD (2PMK) and CLD (3ZUA), HlyD modified from [181]. The red dotted line indicates the proposed interaction region between TolC and HlyD, which is magnified on the right side. The domain structure and sequence of the periplasmic part is shown on the bottom right side helices $\alpha 2$, $\alpha 3$ and the interaction loop L2. Lysine 130 of one TolC monomer and serine 242 of the HlyD monomer are indicated by the red arrows. A possible crosslinker is shown on the middle right side PEG4-SPDP (2-Pyridyldithiol-tetraoxatetradecane-N-hydroxysuccinimide)

Also a second experiment can be suggested. The transporter SiiF of the SiiE-T1SS diffuses freely in the inner membrane if no secretion occurs (investigated by Barlag et al.) [244]. In addition, it is known that TolC is recruited when the substrate HlyA is present in the cytosol [52]. Therefore, crosslinking could be used to investigate interactions between TolC and HlyD. HlyD colocalizes with HlyB in the inner membrane forming the IMC (shown by Pimenta et al. and Blakrishnan et al.) [62, 65]. If HlyD acts similar to SiiF, the IMC could also diffuse in the cytosolic membrane. When successful, this approach would allow purification of the T1SS in the absence of substrate and therefore in a resting state. This approach would be ideal for cryo electron tomography, which allowed obtaining the structure of different secretion systems. To highlight a few examples: the *in vivo* structure of a Type IV secretion system in *Helicobacter pylori* cag (Chang et al.) [255], the *in vivo* structure of AcrAB (Shi et al.) [186] or during infection the T3SS of *Salmonella enterica* serovar Typhimurium, where acquired by cryo electron tomography (Majewski et al.) [253].

A third approach for a novel purification strategy is based on an observation described in chapter 3.5. Here HlyB interacted with HlyA according to the migration behavior on native PAGE. Former studies showed that the IMC consisting of HlyB and HlyD interacts with the substrate HlyA inducing recruitment of TolC [65]. It is proposed that the interaction of the HlyB CLD is responsible for the chaperone-like function with HlyA [163, 165]. This interaction could be utilized for a pulldown of the IMC. The observed interaction on native PAGE of the

transporter HlyB with the substrate HlyA is shown in Figure 3 and was described in chapter 3.5. There on the height of approximately 242 kDa an intense signal for HlyA is visible. The HlyB signal migrated to the left side of the HlyA signal in a semicircular style.

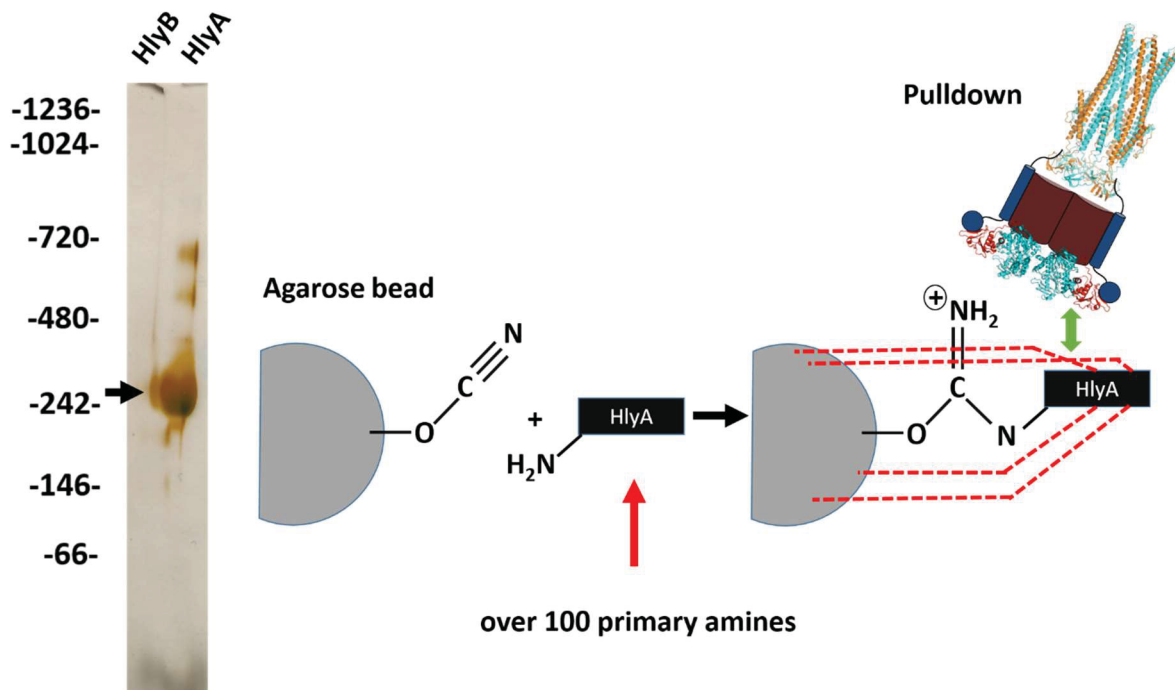


Figure 3 Schematic approach for pulldown of the HlyA T1SS IMC. On the left side a silver stained native PAGE with HlyB and HlyA is shown where the HlyB stopped migration together with HlyA indicated with an arrow. Right from the PAGE a schematic of the CNBr-Agarose beads is shown and the binding of HlyA to the nitrile group creating an agarose bead coated with HlyA (indicated by red dotted line). A model of the HlyA T1SS IMC (HlyB NBD (2PMK) and CLD (3ZUA), HlyD modified from [181]) interacts with the immobilized HlyA and then can be used for a pulldown.

For the supposed experiment, the interaction observed between HlyA and the IMC is assumed of sufficient strength to allow pulldown. The molecular properties of HlyA could be used to coat the surface of CNBr-agarose beads with unfolded respectively folded HlyA. HlyA possesses 106 lysine residues distributed across the entire primary sequence. Therefore, HlyA is an excellent candidate to be linked to CNBr-agarose beads. This would be comparable to the experiments of Frick-Cheng et al. 2016 in which a monoclonal antibody bound to CNBr-agarose beads was used to purify the core complex of the Type IV secretion system from *Helicobacter pylori cag* [256]. Established for linking antibodies or antibody fragments to the beads [257] this approach could also be utilized to create a platform for protein-protein interaction between the T1SS components. While it is known that the IMC interacts with unfolded HlyA [52, 163, 185] the stoichiometry of the interacting partner is unknown. This novel experiment could provide a method to access the IMC or even the whole T1SS without introducing any affinity tags.

To conclude, there are two suggested approaches to isolate the T1SS from the bacterial cell. The first is to stabilize the complex by introducing specific crosslinks to prevent disassembly or disintegration during purification. The second is to try a new capture method by using the interaction between HlyA and the IMC utilizing agarose-CNBr beads to bind HlyA on its

surface. However, when the IMC alone is immobilized, the T1SS is not assembled. The isolation of the IMC would be a major step forward but consequently lead to an approach where the T1SS could be assembled *in vitro*. The major challenge would be to form the complex and stabilize it afterwards. For further experiments, a two membrane system is a necessity. Therefore, the OMP TolC has to be reconstituted in a membrane system like a giant unilamellar vesicle (GUV) to create a compartment where the extracellular space can be simulated. Second the IMC has to be reconstituted to enable proper investigation. The IMC in detergent could be an initial step, but the detergent would prevent the usage of GUVs for TolC. Kanonenberg et al. [209, 211] established an important fundament for future purifications. Using a novel strain for improved purification of membrane proteins [209] and reconstitution of HlyB in Saposin-A [211], a possible direction to reconstitute the HlyA T1SS *in vitro* would pave a novel and interesting but furthermore very challenging path for future experiments.

5 Bibliography

1. Alberts, B., et al., *Molecular Biology of the Cell*. 2008: Garland Science.
2. Gennis, R.B., *Biomembranes - Molecular Structure and Function*. Springer, New York, NY, 1989. **1**: p. 533.
3. Sohlenkamp, C. and O. Geiger, *Bacterial membrane lipids: diversity in structures and pathways*. FEMS Microbiol. Rev., 2016. **40**(1): p. 133-159.
4. Gidden, J., et al., *Lipid compositions in Escherichia coli and Bacillus subtilis during growth as determined by MALDI-TOF and TOF/TOF mass spectrometry*. Int J Mass Spectrom. 2009. **283**(1-3): p. 178-184.
5. Rappolt, M., et al., *Mechanism of the Lamellar/Inverse Hexagonal Phase Transition Examined by High Resolution X-Ray Diffraction*. Biophys. J., 2003. **84**(5): p. 3111-3122.
6. OADC/DNEM, *Image Library | CDC Online Newsroom | CDC*. 2019.
7. Koster, M., W. Bitter, and J. Tommassen, *Protein secretion mechanisms in Gram-negative bacteria*. Int. J. Med. Microbol. 2000. **290**(4-5): p. 325-331.
8. Costa, T.R., et al., *Secretion systems in Gram-negative bacteria: structural and mechanistic insights*. Nat Rev Microbiol, 2015. **13**(6): p. 343-59.
9. *Microbial Cell Walls and Membranes | H. R. Perkins | Springer*. 1980.
10. Meroueh, S.O., et al., *Three-dimensional structure of the bacterial cell wall peptidoglycan*, in *Proc Natl Acad Sci U S A*. 2006. p. 4404-9.
11. Rawicz, W., et al., *Effect of Chain Length and Unsaturation on Elasticity of Lipid Bilayers*. Biophys. J., 2000. **79**(1): p. 328-339.
12. Gan, L., S. Chen, and G.J. Jensen, *Molecular organization of Gram-negative peptidoglycan*. Proc Natl Acad Sci U S A, 2008. **105**(48): p. 18953-18957.
13. De Geyter, J., et al., *Protein folding in the cell envelope of Escherichia coli*. Nat. Microbiol. 2016. **1**(8): p. 16107.
14. Singer, S.J. and G.L. Nicolson, *The Fluid Mosaic Model of the Structure of Cell Membranes*. Science, 1972. **175**(4023): p. 720-731.
15. Van Meer, G., D.R. Voelker, and G.W. Feigenson, *Membrane lipids: where they are and how they behave*. Nat. Rev. Mol. Cell Biol., 2008. **9**(2): p. 112-124.
16. Gouaux, E., *Principles of Selective Ion Transport in Channels and Pumps*. Science, 2005. **310**(5753): p. 1461-1465.
17. Lanyi, J.K., *Bacteriorhodopsin*. Annu. Rev. Physiol. 2004. **66**(1): p. 665-688.
18. Skou, J.C., *The influence of some cations on an adenosine triphosphatase from peripheral nerves*. BBA, 1957. **23**: p. 394-401.
19. Nikaido, H. and M. Saier, *Transport proteins in bacteria: common themes in their design*. Science 1992. **258**(5084): p. 936-942.

20. Padan, E., *Bacterial Membrane Transport: Secondary Transport Proteins*, in *eLS*. 2019. p. 1-13.
21. Gerlach, R.G. and M. Hensel, *Protein secretion systems and adhesins: the molecular armory of Gram-negative pathogens*. *Int J Med Microbiol*, 2007. **297**(6): p. 401-15.
22. Nijeholt, J.A.L.a. and A.J.M. Driessen, *The bacterial Sec-translocase: structure and mechanism*. *Philos. Trans. R. Soc. Lond., B, Biol. Sci.* 2012.
23. Ullers, R.S., et al., *Sequence-specific interactions of nascent Escherichia coli polypeptides with trigger factor and signal recognition particle*. *J Biol Chem*, 2006. **281**(20): p. 13999-4005.
24. Beck, K., et al., *Discrimination between SRP- and SecA/SecB-dependent substrates involves selective recognition of nascent chains by SRP and trigger factor*. *Embo J*, 2000. **19**(1): p. 134-43.
25. von Heijne, G., *The signal peptide*. *J Membr Biol*, 1990. **115**(3): p. 195-201.
26. Gilmore, R., G. Blobel, and P. Walter, *Protein translocation across the endoplasmic reticulum. I. Detection in the microsomal membrane of a receptor for the signal recognition particle*. *J Cell Biol*, 1982. **95**(2 Pt 1): p. 463-9.
27. Walter, P. and G. Blobel, *Translocation of proteins across the endoplasmic reticulum III. Signal recognition protein (SRP) causes signal sequence-dependent and site-specific arrest of chain elongation that is released by microsomal membranes*. *J Cell Biol*, 1981. **91**(2 Pt 1): p. 557-61.
28. Lecker, S., et al., *Three pure chaperone proteins of Escherichia coli--SecB, trigger factor and GroEL--form soluble complexes with precursor proteins in vitro*. *Embo J*, 1989. **8**(9): p. 2703-9.
29. Randall, L.L., et al., *Binding of SecB to ribosome-bound polypeptides has the same characteristics as binding to full-length, denatured proteins*. *Proc Natl Acad Sci U S A*, 1997. **94**(3): p. 802-7.
30. Mori, H. and K. Ito, *The Sec protein-translocation pathway*. *Trends Microbiol.*, 2001. **9**(10): p. 494-500.
31. Dilks, K., et al., *Prokaryotic utilization of the twin-arginine translocation pathway: a genomic survey*. *J Bacteriol*, 2003. **185**(4): p. 1478-83.
32. Ize, B., et al., *Novel phenotypes of Escherichia coli tat mutants revealed by global gene expression and phenotypic analysis*. *J Biol Chem*, 2004. **279**(46): p. 47543-54.
33. Létoffé, S., et al., *Bacteria capture iron from heme by keeping tetrapyrrol skeleton intact*. *PNAS* 2009. 106 (28): p. 11719-11724
34. Mickael, C.S., et al., *Salmonella enterica Serovar Enteritidis tatB and tatC Mutants Are Impaired in Caco-2 Cell Invasion In Vitro and Show Reduced Systemic Spread in Chickens*. *ASM Infect. Immun.* 2010.
35. Jongbloed, J.D., et al., *TatC is a specificity determinant for protein secretion via the twin-arginine translocation pathway*. *J Biol Chem*, 2000. **275**(52): p. 41350-7.

36. Stanley, N.R., et al., *Escherichia coli* strains blocked in Tat-dependent protein export exhibit pleiotropic defects in the cell envelope. *J Bacteriol*, 2001. **183**(1): p. 139-44.
37. Sauve, V., et al., *The SoxYZ complex carries sulfur cycle intermediates on a peptide swinging arm*. *J Biol Chem*, 2007. **282**(32): p. 23194-204.
38. Tottey, S., et al., *Protein-folding location can regulate manganese-binding versus copper- or zinc-binding*. *Nature*, 2008. **455**(7216): p. 1138-42.
39. Palmer, T. and B.C. Berks, *The twin-arginine translocation (Tat) protein export pathway*. *Nat. Rev. Microbiol.*, 2012. **10**(7): p. 483-496.
40. Pohlschröder, M., et al., *Translocation of proteins across archaeal cytoplasmic membranes*. *FEMS Microbiol. Rev.*, 2019. **28**(1): p. 3-24.
41. *A common export pathway for proteins binding complex redox cofactors? - Berks - 1996 - Mol. Microbiol. - Wiley Online Library*. 2019.
42. Sargent, F., et al., *Sec-independent protein translocation in Escherichia coli. A distinct and pivotal role for the TatB protein*. *J Biol Chem*, 1999. **274**(51): p. 36073-82.
43. Muller, M. and R.B. Klosgen, *The Tat pathway in bacteria and chloroplasts (review)*. *Mol Membr Biol*, 2005. **22**(1-2): p. 113-21.
44. Smith, T.J., et al., *An N-Terminal Retention Module Anchors the Giant Adhesin LapA of Pseudomonas fluorescens at the Cell Surface: a Novel Subfamily of Type I Secretion Systems*. *J. Bacteriol.*, 2018. **200**(8): p. e00734-17.
45. Nikaido, H., *Structure and mechanism of RND-type multidrug efflux pumps*. *Adv. Enzymol. Relat. Areas Mol. Biol.*, 2011. **77**: p. 1.
46. Daury, L., et al., *Tripartite assembly of RND multidrug efflux pumps*. *Nat. Commun.*, 2016. **7**: p. 10731.
47. Piddock, L.J.V., *Multidrug-resistance efflux pumps ? not just for resistance*. *Nat. Rev. Microbiol.*, 2019. **4**(8): p. 629-636.
48. Šmajš, D., et al., *Bacteriocin synthesis in uropathogenic and commensal Escherichia coli: colicin E1 is a potential virulence factor*. *BMC Microbiol.*, 2010. **10**(1): p. 288.
49. Izadi-Pruneyre, N., et al., *NMR studies of the C-terminal secretion signal of the haem-binding protein, HasA*. *Eur. J. Biochem. FEBS* 1999. **261**(2): p. 562-568.
50. Kanonenberg, K., C.K. Schwarz, and L. Schmitt, *Type I secretion systems - a story of appendices*. *Res Microbiol*, 2013. **164**(6): p. 596-604.
51. Guo, S., et al., *Structure of a 1.5-MDa adhesin that binds its Antarctic bacterium to diatoms and ice*. *Sci. Adv.*, 2017. **3**(8): p. e1701440.
52. Thanabalu, T., et al., *Substrate-induced assembly of a contiguous channel for protein export from E.coli: reversible bridging of an inner-membrane translocase to an outer membrane exit pore*. *Embo J*, 1998. **17**(22): p. 6487-96.
53. Du, D., et al., *Structure of the AcrAB-TolC multidrug efflux pump*. *Nature*, 2014. **509**(7501): p. 512-5.

54. Fitzpatrick, A.W.P., et al., *Structure of the MacAB-TolC ABC-type tripartite multidrug efflux pump*. Nat Microbiol, 2017. **2**: p. 17070.
55. Neuberger, A., D. Du, and B.F. Luisi, *Structure and mechanism of bacterial tripartite efflux pumps*. Res. Microbiol., 2018. **169**: p. 401.
56. Eicher, T., et al., *Coupling of remote alternating-access transport mechanisms for protons and substrates in the multidrug efflux pump AcrB*. Elife, 2014. **3**.
57. Lecher, J., et al., *An RTX transporter tethers its unfolded substrate during secretion via a unique N-terminal domain*. Structure, 2012. **20**(10): p. 1778-87.
58. Kieuvongngam, V., et al., *Structural basis of substrate recognition by a polypeptide processing and secretion transporter*. eLife, 2020. **9**: p. e51492.
59. Wu, K.-H., Y.-H. Hsieh, and P.C. Tai, *Mutational Analysis of Cvab, an ABC Transporter Involved in the Secretion of Active Colicin V*. PLoS 2012. **7**(4): p. e35382.
60. Ostolaza, H., A. Soloaga, and F.M. Goni, *The binding of divalent cations to Escherichia coli alpha-haemolysin*. Eur J Biochem, 1995. **228**(1): p. 39-44.
61. Chenal, A., et al., *RTX calcium binding motifs are intrinsically disordered in the absence of calcium: implication for protein secretion*. J Biol Chem, 2009. **284**(3): p. 1781-9.
62. Pimenta, A.L., et al., *Antibody analysis of the localisation, expression and stability of HlyD, the MFP component of the E. coli haemolysin translocator*. Mol Gen Genet, 1999. **261**(1): p. 122-32.
63. Wang, R.C., et al., *Analysis of the membrane organization of an Escherichia coli protein translocator, HlyB, a member of a large family of prokaryote and eukaryote surface transport proteins*. J Mol Biol, 1991. **217**(3): p. 441-54.
64. Mackman, N., et al., *Genetical and functional organisation of the Escherichia coli haemolysin determinant 2001*. Mol Gen Genet, 1985. **201**(2): p. 282-8.
65. Balakrishnan, L., C. Hughes, and V. Koronakis, *Substrate-triggered recruitment of the TolC channel-tunnel during type I export of hemolysin by Escherichia coli*. J Mol Biol, 2001. **313**(3): p. 501-10.
66. Nivaskumar, M. and O. Francetic, *Type II secretion system: a magic beanstalk or a protein escalator*. BBA-MOL CELL RES., 2014. **1843**(8): p. 1568-77.
67. Korotkov, K.V., M. Sandkvist, and W.G.J. Hol, *The type II secretion system: biogenesis, molecular architecture and mechanism*. Nat. Rev. Microbiol., 2012. **10**(5): p. 336-351.
68. Nivaskumar, M., et al., *Distinct docking and stabilization steps of the Pseudopilus conformational transition path suggest rotational assembly of type IV pilus-like fibers*. Structure, 2014. **22**(5): p. 685-96.
69. Korotkov, K.V. and W.G.J. Hol, *Structure of the GspK–GspI–GspJ complex from the enterotoxigenic*. Nat. Struct. Mol. Biol., 2008. **15**(5): p. 462-468.

70. Korotkov, K.V., J.R. Delarosa, and W.G.J. Hol, *A dodecameric ring-like structure of the N0 domain of the type II secretin from enterotoxigenic Escherichia coli*. J Struct Biol, 2013. **183**(3): p. 354-362.
71. Reichow, S.L., et al., *Structure of the cholera toxin secretion channel in its closed state*. Nat. Struct. Mol. Biol., 2010. **17**(10): p. 1226-1232.
72. Gray, M.D., et al., *In vivo cross-linking of EpsG to EpsL suggests a role for EpsL as an ATPase-pseudopilin coupling protein in the Type II secretion system of Vibrio cholerae*. Mol Microbiol, 2011. **79**(3): p. 786-98.
73. Cornelis, G.R., *The type III secretion injectisome*. Nat. Rev. Microbiol., 2019. **4**(11): p. 811-825.
74. Buttner, D., *Protein export according to schedule: architecture, assembly, and regulation of type III secretion systems from plant- and animal-pathogenic bacteria*. Microbiol Mol Biol Rev, 2012. **76**(2): p. 262-310.
75. Galan, J.E. and H. Wolf-Watz, *Protein delivery into eukaryotic cells by type III secretion machines*. Nature, 2006. **444**(7119): p. 567-73.
76. Kubori, T., *Supramolecular Structure of the Salmonella typhimurium Type III Protein Secretion System*. Science, 1998. **280**(5363): p. 602-605.
77. Marlovits, T.C., et al., *Structural insights into the assembly of the type III secretion needle complex*. Science, 2004. **306**(5698): p. 1040-2.
78. Marlovits, T.C., et al., *Assembly of the inner rod determines needle length in the type III secretion injectisome*. Nature, 2006. **441**(7093): p. 637-40.
79. Schraidt, O. and T.C. Marlovits, *Three-dimensional model of Salmonella's needle complex at subnanometer resolution*. Science, 2011. **331**(6021): p. 1192-5.
80. Schraidt, O., et al., *Topology and organization of the Salmonella typhimurium type III secretion needle complex components*. PLoS Pathog, 2010. **6**(4): p. e1000824.
81. Hu, J., et al., *T3S injectisome needle complex structures in four distinct states reveal the basis of membrane coupling and assembly*. Nat. Microbiol., 2019.
82. Loquet, A., et al., *Atomic model of the type III secretion system needle*. Nature, 2012. **486**(7402): p. 276-9.
83. Radics, J., L. Königsmaier, and T.C. Marlovits, *Structure of a pathogenic type 3 secretion system in action*. Nat. Struct. Mol. Biol., 2013. **21**(1): p. 82-87.
84. Galan, J.E., et al., *Bacterial type III secretion systems: specialized nanomachines for protein delivery into target cells*. Annu Rev Microbiol, 2014. **68**: p. 415-38.
85. Bradley, D.E., *Morphological and serological relationships of conjugative pili*. Plasmid, 1980. **4**(2): p. 155-69.
86. Durrenberger, M.B., W. Villiger, and T. Bachi, *Conjugational junctions: morphology of specific contacts in conjugating Escherichia coli bacteria*. J Struct Biol, 1991. **107**(2): p. 146-56.

87. Grohmann, E., G. Muth, and M. Espinosa, *Conjugative Plasmid Transfer in Gram-Positive Bacteria*. *Microbiol Mol Biol Rev* 2003. **67**(2): p. 277-301.
88. Alvarez-Martinez, C.E. and P.J. Christie, *Biological diversity of prokaryotic type IV secretion systems*. *Microbiol Mol Biol Rev*, 2009. **73**(4): p. 775-808.
89. Trokter, M., et al., *Recent advances in the structural and molecular biology of type IV secretion systems*. *Curr Opin Struct Biol*, 2014. **27**: p. 16-23.
90. Chandran, V., et al., *Structure of the outer membrane complex of a type IV secretion system*. *Nature*, 2009. **462**(7276): p. 1011-5.
91. Low, H.H., et al., *Structure of a type IV secretion system*. *Nature*, 2014. **508**(7497): p. 550-553.
92. Rivera-Calzada, A., et al., *Structure of a bacterial type IV secretion core complex at subnanometre resolution*. *Embo J*, 2013. **32**(8): p. 1195-204.
93. Cascales, E. and P.J. Christie, *Agrobacterium VirB10, an ATP energy sensor required for type IV secretion*. *Proc Natl Acad Sci U S A*, 2004. **101**(49): p. 17228-33.
94. Ripoll-Rozada, J., et al., *Functional interactions of VirB11 traffic ATPases with VirB4 and VirD4 molecular motors in type IV secretion systems*. *J Bacteriol*, 2013. **195**(18): p. 4195-201.
95. Hu, B., et al., *In Situ Molecular Architecture of the Helicobacter pylori Cag Type IV Secretion System*. *mBio*, 2019. **10**(3).
96. Aly, K.A. and C. Baron, *The VirB5 protein localizes to the T-pilus tips in Agrobacterium tumefaciens*. *Microbiology*, 2007. **153**(Pt 11): p. 3766-75.
97. Pukatzki, S., et al., *Identification of a conserved bacterial protein secretion system in Vibrio cholerae using the Dictyostelium host model system*. *Proc Natl Acad Sci U S A*, 2006. **103**(5): p. 1528-33.
98. Leiman, P.G., et al., *Type VI secretion apparatus and phage tail-associated protein complexes share a common evolutionary origin*. *Proc Natl Acad Sci U S A*, 2009. **106**(11): p. 4154-9.
99. Zoued, A., et al., *TssK is a trimeric cytoplasmic protein interacting with components of both phage-like and membrane anchoring complexes of the type VI secretion system*. *J Biol Chem*, 2013. **288**(38): p. 27031-41.
100. Zoued, A., et al., *Architecture and assembly of the Type VI secretion system*. *BBA-MOL CELL RES.*, 2014. **1843**(8): p. 1664-73.
101. Boyer, F., et al., *Dissecting the bacterial type VI secretion system by a genome wide in silico analysis: what can be learned from available microbial genomic resources?* *BMC Genom.*, 2009. **10**: p. 104.
102. Ho, B.T., T.G. Dong, and J.J. Mekalanos, *A view to a kill: the bacterial type VI secretion system*. *Cell Host Microbe*, 2014. **15**(1): p. 9-21.
103. Chen, W.-J., et al., *Involvement of type VI secretion system in secretion of iron chelator pyoverdine in Pseudomonas taiwanensis*. *Sci. Reports*, 2016. **6**: p. 32950.

104. Si, M., et al., *Manganese scavenging and oxidative stress response mediated by type VI secretion system in Burkholderia thailandensis*. Proc Natl Acad Sci U S A, 2017. **114**(11): p. E2233-E2242.
105. Wang, T., et al., *Type VI Secretion System Transports Zn²⁺ to Combat Multiple Stresses and Host Immunity*. PLoS Pathogens 2015. **11**(7): p. e1005020.
106. Lin, J., et al., *A Pseudomonas T6SS effector recruits PQS-containing outer membrane vesicles for iron acquisition*. Nat. Commun., 2017. **8**(1): p. 14888.
107. Silverman, J.M., et al., *Structure and Regulation of the Type VI Secretion System*. Annu. Rev. Microbiol., 2012. **66**(1): p. 453-472.
108. Ma, L.S., J.S. Lin, and E.M. Lai, *An IcmF family protein, ImpLM, is an integral inner membrane protein interacting with ImpKL, and its walker a motif is required for type VI secretion system-mediated Hcp secretion in Agrobacterium tumefaciens*. J Bacteriol, 2009. **191**(13): p. 4316-29.
109. Basler, M., et al., *Type VI secretion requires a dynamic contractile phage tail-like structure*. Nature, 2012. **483**(7388): p. 182-6.
110. Vettiger, A. and M. Basler, *Type VI Secretion System Substrates Are Transferred and Reused among Sister Cells*. Cell, 2016. **167**(1): p. 99-110.e12.
111. Voulhoux, R., et al., *Role of a highly conserved bacterial protein in outer membrane protein assembly*. Science, 2003. **299**(5604): p. 262-5.
112. Leo, J.C., I. Grin, and D. Linke, *Type V secretion: mechanism(s) of autotransport through the bacterial outer membrane*. Philos Trans R Soc Lond B Biol Sci, 2012. **367**(1592): p. 1088-101.
113. Wu, T., et al., *Identification of a multicomponent complex required for outer membrane biogenesis in Escherichia coli*. Cell, 2005. **121**(2): p. 235-45.
114. Hagan, C.L., S. Kim, and D. Kahne, *Reconstitution of outer membrane protein assembly from purified components*. Science, 2010. **328**(5980): p. 890-2.
115. Ieva, R., et al., *Sequential and spatially restricted interactions of assembly factors with an autotransporter beta domain*. Proc Natl Acad Sci U S A, 2011. **108**(31): p. E383-91.
116. Mu, X.Q. and E. Bullitt, *Structure and assembly of P-pili: a protruding hinge region used for assembly of a bacterial adhesion filament*. Proc Natl Acad Sci U S A, 2006. **103**(26): p. 9861-6.
117. Phan, G., et al., *Crystal structure of the FimD usher bound to its cognate FimC-FimH substrate*. Nature, 2011. **474**(7349): p. 49-53.
118. Hahn, E., et al., *Exploring the 3D molecular architecture of Escherichia coli type I pili*. J Mol Biol, 2002. **323**(5): p. 845-57.
119. Robinson, L.S., et al., *Secretion of curli fibre subunits is mediated by the outer membrane-localized CsgG protein*. Mol Microbiol, 2006. **59**(3): p. 870-81.
120. Goyal, P., et al., *Structural and mechanistic insights into the bacterial amyloid secretion channel CsgG*. Nature, 2014. **516**(7530): p. 250-3.

121. Nenninger, A.A., L.S. Robinson, and S.J. Hultgren, *Localized and efficient curli nucleation requires the chaperone-like amyloid assembly protein CsgF*. Proc Natl Acad Sci U S A, 2009. **106**(3): p. 900-5.
122. Wang, X., et al., *In vitro polymerization of a functional Escherichia coli amyloid protein*. J Biol Chem, 2007. **282**(6): p. 3713-9.
123. Leyton, D.L., A.E. Rossiter, and I.R. Henderson, *From self sufficiency to dependence: mechanisms and factors important for autotransporter biogenesis*. Nat. Rev. Microbiol., 2012. **10**(3): p. 213-225.
124. Junker, M., R.N. Besingi, and P.L. Clark, *Vectorial transport and folding of an autotransporter virulence protein during outer membrane secretion*. Mol Microbiol, 2009. **71**(5): p. 1323-32.
125. Ieva, R. and H.D. Bernstein, *Interaction of an autotransporter passenger domain with BamA during its translocation across the bacterial outer membrane*. Proc Natl Acad Sci U S A, 2009. **106**(45): p. 19120-5.
126. Ieva, R., K.M. Skillman, and H.D. Bernstein, *Incorporation of a polypeptide segment into the beta-domain pore during the assembly of a bacterial autotransporter*. Mol Microbiol, 2008. **67**(1): p. 188-201.
127. Oomen, C.J., et al., *Structure of the translocator domain of a bacterial autotransporter*. Embo J, 2004. **23**(6): p. 1257-66.
128. van den Berg, B., *Crystal structure of a full-length autotransporter*. J Mol Biol, 2010. **396**(3): p. 627-33.
129. Meng, G., et al., *Structure of the outer membrane translocator domain of the Haemophilus influenzae Hia trimeric autotransporter*. Embo J, 2006. **25**(11): p. 2297-304.
130. Lillington, J., S. Geibel, and G. Waksman, *Reprint of "Biogenesis and adhesion of type I and P pili"*. BBA-MOL CELL RES., 2015. **1850**(3): p. 554-64.
131. Wright, K.J., P.C. Seed, and S.J. Hultgren, *Development of intracellular bacterial communities of uropathogenic Escherichia coli depends on type I pili*. Cell Microbiol, 2007. **9**(9): p. 2230-41.
132. Hultgren, S.J., S. Normark, and S.N. Abraham, *Chaperone-assisted assembly and molecular architecture of adhesive pili*. Annu Rev Microbiol, 1991. **45**: p. 383-415.
133. Vetsch, M., et al., *Pilus chaperones represent a new type of protein-folding catalyst*. Nature, 2004. **431**(7006): p. 329-33.
134. Remaut, H., et al., *Donor-strand exchange in chaperone-assisted pilus assembly proceeds through a concerted beta strand displacement mechanism*. Mol Cell, 2006. **22**(6): p. 831-42.
135. Verger, D., et al., *Molecular mechanism of P pilus termination in uropathogenic Escherichia coli*. EMBO Rep, 2006. **7**(12): p. 1228-32.

136. Olsen, A., A. Jonsson, and S. Normark, *Fibronectin binding mediated by a novel class of surface organelles on Escherichia coli*. *Nature*, 1989. **338**(6217): p. 652-5.
137. Dueholm, M.S., et al., *Curli Functional Amyloid Systems Are Phylogenetically Widespread and Display Large Diversity in Operon and Protein Structure*. *PLoS ONE*, 2012. **7**(12): p. e51274.
138. Barnhart, M.M. and M.R. Chapman, *Curli Biogenesis and Function*. *Annu. Rev. Microbiol.*, 2006. **60**(1): p. 131-147.
139. Kikuchi, T., et al., *Curli Fibers Are Required for Development of Biofilm Architecture in Escherichia coli K-12 and Enhance Bacterial Adherence to Human Uroepithelial Cells*. *Microbiol. Immunol.*, 2005. **49**(9): p. 875-884.
140. Hufnagel, D.A., W.H. Depas, and M.R. Chapman, *The Biology of the Escherichia coli Extracellular Matrix*. *Microbiology Spectrum*, 2015. **3**(3).
141. Hung, C., et al., *Escherichia coli Biofilms Have an Organized and Complex Extracellular Matrix Structure*. *mBio*, 2013. **4**(5): p. e00645-13-e00645.
142. Margery, et al., *The Bacterial Curli System Possesses a Potent and Selective Inhibitor of Amyloid Formation*. *Mol. Cell* 2015. **57**(3): p. 445-455.
143. Van Gerven, N., et al., *Bacterial Amyloid Formation: Structural Insights into Curli Biogenesis*. *Trends Microbiol.*, 2015. **23**(11): p. 693-706.
144. Chapman, M.R., *Role of Escherichia coli Curli Operons in Directing Amyloid Fiber Formation*. *Science*, 2002. **295**(5556): p. 851-855.
145. Bian, Z. and S. Normark, *Nucleator function of CsgB for the assembly of adhesive surface organelles in Escherichia coli*. *Embo J* 1997. **16**(19): p. 5827-5836.
146. Takagi, F., N. Koga, and S. Takada, *How protein thermodynamics and folding mechanisms are altered by the chaperonin cage: molecular simulations*. *Proc Natl Acad Sci U S A*, 2003. **100**(20): p. 11367-72.
147. Brinker, A., et al., *Dual function of protein confinement in chaperonin-assisted protein folding*. *Cell*, 2001. **107**(2): p. 223-33.
148. Springer, W. and W. Goebel, *Synthesis and secretion of hemolysin by Escherichia coli*. *J. Bacteriol.*, 1980. **144**(1): p. 53-59.
149. Holland, I.B., et al., *Type I Protein Secretion-Deceptively Simple yet with a Wide Range of Mechanistic Variability across the Family*. *EcoSal Plus*, 2016. **7**(1).
150. Thomas, S., I.B. Holland, and L. Schmitt, *The Type I secretion pathway - the hemolysin system and beyond*. *BBA-MOL CELL RES.*, 2014. **1843**(8): p. 1629-41.
151. Lenders, M.H., et al., *Molecular insights into type I secretion systems*. *Biol Chem*, 2013. **394**(11): p. 1371-84.
152. Higgins, C.F., *ABC Transporters: From Microorganisms to Man*. *Annu. Rev. Cell Biol.*, 1992. **8**(1): p. 67-113.

153. Xiong, J., et al., *Tracing the structural evolution of eukaryotic ATP binding cassette transporter superfamily*. Sci. Rep., 2015. **5**(1): p. 16724.
154. Walker, J.E., et al., *Distantly related sequences in the alpha- and beta-subunits of ATP synthase, myosin, kinases and other ATP-requiring enzymes and a common nucleotide binding fold*. Embo J, 1982. **1**(8): p. 945-951.
155. Oswald, C., I.B. Holland, and L. Schmitt, *The motor domains of ABC-transporters*. Naunyn-Schmiedeberg's Arch Pharmacol 2006. **372**(6): p. 385-399.
156. Ames, G.F., Mimura, C. S., Holbrook, S. R. and Shyamala, *Traffic ATPases: A Superfamily of Transport Proteins Operating from Escherichia coli to Humans*, in Adv. Enzymol. Relat. Areas. Mol. Biol.. 1992 p. 1-47.
157. Zaitseva, J., et al., *H662 is the linchpin of ATP hydrolysis in the nucleotide-binding domain of the ABC transporter HlyB*. Embo J, 2005. **24**(11): p. 1901-10.
158. Zaitseva, J., et al., *A structural analysis of asymmetry required for catalytic activity of an ABC-ATPase domain dimer*. Embo J, 2006. **25**(14): p. 3432-43.
159. Smith, P.C., et al., *ATP Binding to the Motor Domain from an ABC Transporter Drives Formation of a Nucleotide Sandwich Dimer*. Mol. Cell, 2002. **10**(1): p. 139-149.
160. Benabdelhak, H., et al., *A Specific Interaction Between the NBD of the ABC-transporter HlyB and a C-Terminal Fragment of its Transport Substrate Haemolysin A*. J. Mol. Biol., 2003. **327**(5): p. 1169-1179.
161. Morgan, J.L.W., J.F. Acheson, and J. Zimmer, *Structure of a Type-I Secretion System ABC Transporter*. Structure, 2017. **25**(3): p. 522-529.
162. Zolnerciks, J.K., et al., *Structure of ABC transporters*. Essays Biochem., 2011. **50**: p. 43-61.
163. Zhang, F., J.A. Sheps, and V. Ling, *Complementation of transport-deficient mutants of Escherichia coli alpha-hemolysin by second-site mutations in the transporter hemolysin B*. JBC, 1993. **268**(26): p. 19889-19895.
164. Lecher, J., et al., *¹H, ¹⁵N and ¹³C resonance assignment of the N-terminal C39 peptidase-like domain of the ABC transporter Haemolysin B (HlyB)*. Biomol NMR Assign 2011. **5**(2): p. 199-201.
165. Holland, I.B., L. Schmitt, and J. Young, *Type I protein secretion in bacteria, the ABC-transporter dependent pathway (Review)*. Mol. Membr. Biol, 2009. **22**(1-2): p. 29-39.
166. Noegel, A., et al., *Plasmid cistrons controlling synthesis and excretion of the exotoxin alpha-haemolysin of Escherichia coli*. Mol Gen Genet, 1979. **175**(3): p. 343-50.
167. Linhartova, I., et al., *RTX proteins: a highly diverse family secreted by a common mechanism*. FEMS Microbiol Rev, 2010. **34**(6): p. 1076-112.
168. Welch, R.A., *Pore-forming cytolysins of gram-negative bacteria*. Mol Microbiol, 1991. **5**(3): p. 521-8.

169. Bumba, L., et al., *Calcium-Driven Folding of RTX Domain β -Rolls Ratchets Translocation of RTX Proteins through Type I Secretion Ducts*. Mol. Cell 2016. **62**(1): p. 47-62.
170. Delepelaire, P., *Type I secretion in gram-negative bacteria*. BBA-MOL CELL RES., 2004. **1694**(1-3): p. 149-61.
171. Gangola, P. and B.P. Rosen, *Maintenance of intracellular calcium in Escherichia coli*. JBC, 1987. **262**(26): p. 12570-12574.
172. Jones, H.E., et al., *Slow changes in cytosolic free Ca²⁺ in Escherichia coli highlight two putative influx mechanisms in response to changes in extracellular calcium*. Cell Calcium 1999. **25**(3): p. 265-274.
173. Lenders, M.H.H., et al., *Directionality of substrate translocation of the hemolysin A Type I secretion system*. Sci. Rep., 2015. **5**: p. 12470.
174. Holland, I.B., B. Kenny, and M. Blight, *Haemolysin secretion from E coli*. Biochimie 1990. **72**(2-3): p. 131-141.
175. Stanley, P., et al., *Fatty acylation of two internal lysine residues required for the toxic activity of Escherichia coli hemolysin*. AAAS, Science 1994. **266**(5193): p. 1992-1996.
176. Hardie, K.R., et al., *In vitro activation of Escherichia coli prohaemolysin to the mature membrane-targeted toxin requires HlyC and a low molecular-weight cytosolic polypeptide*. Mol. Microbiol. 1991. **5**(7): p. 1669-1679.
177. Bakás, L., et al., *Reversible adsorption and nonreversible insertion of Escherichia coli alpha-hemolysin into lipid bilayers*. Biophys. J., 1996. **71**(4): p. 1869-1876.
178. Hyland, C., et al., *Membrane Interaction of Escherichia coli Hemolysin: Flotation and Insertion-Dependent Labeling by Phospholipid Vesicles*. J. Bacteriol., 2001. **183**(18): p. 5364-5370.
179. Bhakdi, S., et al., *Escherichia coli hemolysin may damage target cell membranes by generating transmembrane pores*. Infect. Immun., 1986. **52**(1): p. 63-69.
180. Yum, S., et al., *Crystal structure of the periplasmic component of a tripartite macrolide-specific efflux pump*. J Mol Biol, 2009. **387**(5): p. 1286-97.
181. Kim, J.S., et al., *Crystal Structure of a Soluble Fragment of the Membrane Fusion Protein HlyD in a Type I Secretion System of Gram-Negative Bacteria*. Structure, 2016. **24**(3): p. 477-85.
182. Zgurskaya, H.I., et al., *Structural and functional diversity of bacterial membrane fusion proteins*. BBA-Proteins Proteom., 2009. **1794**(5): p. 794-807.
183. Lee, M., et al., *Membrane fusion proteins of type I secretion system and tripartite efflux pumps share a binding motif for TolC in gram-negative bacteria*. PLoS One, 2012. **7**(7): p. e40460.
184. Xu, Y., et al., *Functional Implications of an Intermeshing Cogwheel-like Interaction between TolC and MacA in the Action of Macrolide-specific Efflux Pump MacAB-TolC*. JBC 2011. **286**(15): p. 13541-13549.

185. Pimenta, A.L., et al., *Mutations in HlyD, part of the type I translocator for hemolysin secretion, affect the folding of the secreted toxin*. J Bacteriol, 2005. **187**(21): p. 7471-80.
186. Shi, X., et al., *In situ structure and assembly of the multidrug efflux pump AcrAB-TolC*. Nat. Commun., 2019. **10**(1): p. 2635.
187. Xu, Y., et al., *The tip region of the MacA α -hairpin is important for the binding to TolC to the Escherichia coli MacAB-TolC pump*. Biochem Biophys Res Commun, 2010. **394**(4): p. 962-965.
188. Jeong, H., et al., *Pseudoatomic Structure of the Tripartite Multidrug Efflux Pump AcrAB-TolC Reveals the Intermeshing Cogwheel-like Interaction between AcrA and TolC*. Structure, 2016. **24**(2): p. 272-6.
189. Koronakis, V., et al., *Crystal structure of the bacterial membrane protein TolC central to multidrug efflux and protein export*. Nature, 2000. **405**(6789): p. 914-919.
190. Hagan, C.L., T.J. Silhavy, and D. Kahne, *beta-Barrel membrane protein assembly by the Bam complex*. Annu Rev Biochem, 2011. **80**: p. 189-210.
191. Typas, A., et al., *From the regulation of peptidoglycan synthesis to bacterial growth and morphology*. Nat. Rev. Microbiol., 2011. **10**: p. 123.
192. Koronakis, V., J. Eswaran, and C. Hughes, *Structure and function of TolC: the bacterial exit duct for proteins and drugs*. Annu Rev Biochem, 2004. **73**: p. 467-89.
193. Vaccaro, L., K.A. Scott, and M.S. Sansom, *Gating at both ends and breathing in the middle: conformational dynamics of TolC*. Biophys J, 2008. **95**(12): p. 5681-91.
194. Létoffé, S., P. Delepelaire, and C. Wandersman, *Protein secretion in gram-negative bacteria: assembly of the three components of ABC protein-mediated exporters is ordered and promoted by substrate binding*. Embo J., 1996. **15**(21): p. 5804-5811.
195. Eswaran, J., C. Hughes, and V. Koronakis, *Locking TolC Entrance Helices to Prevent Protein Translocation by the Bacterial Type I Export Apparatus*. JMB 2003. **327**(2): p. 309-315.
196. Bakkes, P.J., et al., *The rate of folding dictates substrate secretion by the Escherichia coli hemolysin type I secretion system*. J Biol Chem, 2010. **285**(52): p. 40573-80.
197. Thomas, S., et al., *Equilibrium folding of pro-HlyA from Escherichia coli reveals a stable calcium ion dependent folding intermediate*. BBA-Proteins Proteom., 2014. **1844**(9): p. 1500-1510.
198. Litwin, M., et al., *UROLOGIC DISEASES IN AMERICA PROJECT: ANALYTICAL METHODS AND PRINCIPAL FINDINGS*. J Urol.2005. **173**(3): p. 933-937.
199. Casadevall, A., et al., *ASM Journals Eliminate Impact Factor Information from Journal Websites*. mBio, 2016. **7**(4): p. e01150-16.
200. Arnoux, P., et al., *The crystal structure of HasA, a hemophore secreted by Serratia marcescens*. Nat. Struct. Biol., 1999. **6**(6): p. 516-520.

201. Hinsa, S.M., et al., *Transition from reversible to irreversible attachment during biofilm formation by Pseudomonas fluorescens WCS365 requires an ABC transporter and a large secreted protein*. Mol. Microbiol. 2003. **49**(4): p. 905-918.
202. Debarbieux, L., *Folded HasA inhibits its own secretion through its ABC exporter*. Embo J., 2001. **20**(17): p. 4657-4663.
203. Koronakis, V., E. Koronakis, and C. Hughes, *Isolation and analysis of the C-terminal signal directing export of Escherichia coli hemolysin protein across both bacterial membranes*. Embo J., 1989. **8**(2): p. 595-605.
204. Jarchau, T., et al., *Selection for transport competence of C-terminal polypeptides derived from Escherichia coli hemolysin: the shortest peptide capable of autonomous HlyB/HlyD-dependent secretion comprises the C-terminal 62 amino acids of HlyA*. Mol. Gen. Genet., 1994. **245**(1): p. 53-60.
205. Reimann, S., et al., *Interdomain regulation of the ATPase activity of the ABC transporter haemolysin B from Escherichia coli*. Biochem J 2016. **473**(16): p. 2471-2483.
206. Lenders, M.H., et al., *In vivo quantification of the secretion rates of the hemolysin A Type I secretion system*. Sci Rep, 2016. **6**: p. 33275.
207. Chaudhuri, T.K., V.K. Verma, and A. Maheshwari, *GroEL assisted folding of large polypeptide substrates in Escherichia coli: Present scenario and assignments for the future*. Prog. Biophys. Mol. Biol.2009. **99**(1): p. 42-50.
208. Puppala, A.K., et al., *Structural basis for early-onset neurological disorders caused by mutations in human selenocysteine synthase*. Sci Rep, 2016. **6**: p. 32563.
209. Kanonenberg, K., et al., *Shaping the lipid composition of bacterial membranes for membrane protein production*. Microb. Cell Factories, 2019. **18**(1).
210. O'Brien, D.P., et al., *Calcium-dependent disorder-to-order transitions are central to the secretion and folding of the CyaA toxin of Bordetella pertussis , the causative agent of whooping cough*. Toxicon, 2018. **149**: p. 37-44.
211. Kanonenberg, K., S.H.J. Smits, and L. Schmitt, *Functional Reconstitution of HlyB, a Type I Secretion ABC Transporter, in Saposin-A Nanoparticles*. Sci Rep, 2019. **9**(1).
212. Bhagavan, N.V., *CHAPTER 4 - Three-Dimensional Structure of Proteins*, in *Medical Biochemistry (Fourth Edition)*, N.V. Bhagavan, Editor. 2002, Academic Press: San Diego. p. 51-65.
213. Desmyter, A., et al., *Crystal structure of a camel single-domain VH antibody fragment in complex with lysozyme*. Nat Struct Biol, 1996. **3**(9): p. 803-11.
214. Wandersman, C. and P. Delepelaire, *TolC, an Escherichia coli outer membrane protein required for hemolysin secretion*. Proc Natl Acad Sci U S A, 1990. **87**(12): p. 4776-80.
215. Tikhonova, E.B. and H.I. Zgurskaya, *AcrA, AcrB, and TolC of Escherichia coli Form a Stable Intermembrane Multidrug Efflux Complex*. J Biol Chem, 2004. **279**(31): p. 32116-24.

216. Sulavik, M.C., et al., *Antibiotic Susceptibility Profiles of Escherichia coli Strains Lacking Multidrug Efflux Pump Genes*. *Antimicrob. Agents Chemother.*, 2001. **45**(4): p. 1126-1136.
217. Nichols, R.J., et al., *Phenotypic Landscape of a Bacterial Cell*. *Cell*, 2011. **144**(1): p. 143-156.
218. Alon Cudkowicz, N. and S. Schuldiner, *Deletion of the major Escherichia coli multidrug transporter AcrB reveals transporter plasticity and redundancy in bacterial cells*. *PLOS ONE*, 2019. **14**(6): p. e0218828.
219. Goswami, M., et al., *Involvement of Antibiotic Efflux Machinery in Glutathione-Mediated Decreased Ciprofloxacin Activity in Escherichia coli*. *Antimicrob. Agents Chemother.* 2016. **60**(7): p. 4369-4374.
220. Heng, J., et al., *Substrate-bound structure of the E. coli multidrug resistance transporter MdfA*. *Cell Res.* 2015. **25**(9): p. 1060-1073.
221. Law, C.J. and K.O. Alegre, *Clamping down on drugs: the Escherichia coli multidrug efflux protein MdtM*. *Res Microbiol.*, 2018. **169**(7): p. 461-467.
222. Rotem, D. and S. Schuldiner, *EmrE, a Multidrug Transporter from Escherichia coli, Transports Monovalent and Divalent Substrates with the Same Stoichiometry*. *JBC* 2004. **279**(47): p. 48787-48793.
223. Zhang, A., J.L. Rosner, and R.G. Martin, *Transcriptional activation by MarA, SoxS and Rob of two tolC promoters using one binding site: a complex promoter configuration for tolC in Escherichia coli*. *Mol. Microbiol.*, 2008. **69**(6): p. 1450-1455.
224. Masuda, N. and G.M. Church, *Regulatory network of acid resistance genes in Escherichia coli*. *Mol. Microbiol.*, 2003. **48**(3): p. 699-712.
225. Leblanc, S.K.D., C.W. Oates, and T.L. Raivio, *Characterization of the Induction and Cellular Role of the BaeSR Two-Component Envelope Stress Response of Escherichia coli*. *J. Bacteriol.*, 2011. **193**(13): p. 3367-3375.
226. Bury-Moné, S., et al., *Global Analysis of Extracytoplasmic Stress Signaling in Escherichia coli*. *PLOS Genet.*, 2009. **5**(9): p. e1000651.
227. Aono, R., N. Tsukagoshi, and M. Yamamoto, *Involvement of Outer Membrane Protein TolC, a Possible Member of the mar-sox Regulon, in Maintenance and Improvement of Organic Solvent Tolerance of Escherichia coli K-12*. *J. Bacteriol.*, 1998. **180**(4): p. 938.
228. Liochev, S.I., et al., *Induction of the soxRS Regulon of Escherichia coli by Superoxide*. *JBC* 1999. **274**(14): p. 9479-9481.
229. Rosner, J.L. and R.G. Martin, *An Excretory Function for the Escherichia coli Outer Membrane Pore TolC: Upregulation of marA and soxS Transcription and Rob Activity Due to Metabolites Accumulated in tolC Mutants*. *J. Bacteriol.* 2009. **191**(16): p. 5283-5292.
230. Van Dyk, T.K., et al., *Characterization of the Escherichia coli AaeAB Efflux Pump: a Metabolic Relief Valve?* *J. Bacteriol.*, 2004. **186**(21): p. 7196-7204.

231. Kawamura-Sato, K., et al., *Role of multiple efflux pumps in Escherichia coli in indole expulsion*. FEMS Microbiol. Lett., 1999. **179**(2): p. 345-352.
232. Franke, I., et al., *YfiK from Escherichia coli Promotes Export of O-Acetylserine and Cysteine*. J. Bacteriol. 2003. **185**(4): p. 1161-1166.
233. Yamada, S., et al., *Effect of Drug Transporter Genes on Cysteine Export and Overproduction in Escherichia coli*. Appl. Environ. Microbiol 2006. **72**(7): p. 4735-4742.
234. Keseler, I.M., et al., *The EcoCyc database: reflecting new knowledge about Escherichia coli K-12*. Nucleic Acids Res., 2017. **45**(D1): p. D543-D550.
235. Zhang, L.H., et al., *Genetic analysis of the colicin V secretion pathway*. Genetics, 1995. **141**(1): p. 25-32.
236. Nishino, K. and A. Yamaguchi, *Analysis of a Complete Library of Putative Drug Transporter Genes in Escherichia coli*. J. Bacteriol. 2001. **183**(20): p. 5803-5812.
237. Sulavik, M.C., et al., *Antibiotic susceptibility profiles of Escherichia coli strains lacking multidrug efflux pump genes*. Antimicrob. Agents Chemother., 2001. **45**(4): p. 1126.
238. Crow, A., et al., *Structure and mechanotransmission mechanism of the MacB ABC transporter superfamily*. Proc Natl Acad Sci U S A, 2017. **114**(47): p. 12572.
239. Jeong, K.C., et al., *Polar delivery of Legionella type IV secretion system substrates is essential for virulence*. Proc Natl Acad Sci U S A, 2017. **114**(30): p. 8077-8082.
240. Conover, G.M., et al., *The Legionella pneumophila LidA protein: a translocated substrate of the Dot/Icm system associated with maintenance of bacterial integrity*. Mol. Microbiol. 2003. **48**(2): p. 305-321.
241. Bardill, J.P., J.L. Miller, and J.P. Vogel, *IcmS-dependent translocation of SdeA into macrophages by the Legionella pneumophila type IV secretion system*. Mol. Microbiol. 2005. **56**(1): p. 90-103.
242. Vincent, C.D., et al., *Identification of the DotL coupling protein subcomplex of the Legionella Dot/Icm type IV secretion system*. Mol. Microbiol. 2012. **85**(2): p. 378-391.
243. Jaumouillé, V., et al., *Cytoplasmic targeting of IpaC to the bacterial pole directs polar type III secretion in Shigella*, in *Embo J*. 2008. p. 447-57.
244. Barlag, B., et al., *Single molecule super-resolution imaging of proteins in living Salmonella enterica using self-labelling enzymes*. Sci. Rep., 2016. **6**: p. 31601.
245. Barlag, B. and M. Hensel, *The Giant Adhesin SiiE of Salmonella enterica*. Molecules, 2015. **20**(1): p. 1134-1150.
246. Schindelin, J., et al., *Fiji: an open-source platform for biological-image analysis*. Nat. Methods, 2012. **9**: p. 676.
247. Rassam, P., et al., *Supramolecular assemblies underpin turnover of outer membrane proteins in bacteria*. Nature 2015. **523**(7560): p. 333-336.

248. Rassam, P., et al., *Intermembrane crosstalk drives inner-membrane protein organization in Escherichia coli*. Nat. Commun., 2018. **9**(1).
249. Shiomi, D., et al., *Helical distribution of the bacterial chemoreceptor via colocalization with the Sec protein translocation machinery*. Mol. Microbiol. 2006. **60**(4): p. 894-906.
250. Bergmiller, T., et al., *Biased partitioning of the multidrug efflux pump AcrAB-TolC underlies long-lived phenotypic heterogeneity*. Science, 2017. **356**(6335): p. 311-315.
251. Wang, H., N.S. Wingreen, and R. Mukhopadhyay, *Self-Organized Periodicity of Protein Clusters in Growing Bacteria*. Phys. Rev. Lett. 2008. **101**(21).
252. Gunasinghe, S.D., et al., *Super-Resolution Imaging of Protein Secretion Systems and the Cell Surface of Gram-Negative Bacteria*. Front. Cell. Infect. Microbiol., 2017. **7**(220).
253. Majewski, D.D., et al., *Cryo-EM structure of the homohexameric T3SS ATPase-central stalk complex reveals rotary ATPase-like asymmetry*. Nat. Commun., 2019. **10**(1).
254. Kastner, B., et al., *GraFix: sample preparation for single-particle electron cryomicroscopy*. Nat Methods, 2008. **5**(1): p. 53-5.
255. Chang, Y.-W., et al., *In Vivo Structures of the Helicobacter pylori cag Type IV Secretion System*. Cell Rep., 2018. **23**(3): p. 673-681.
256. Frick-Cheng, A.E., et al., *Molecular and Structural Analysis of the Helicobacter pylori cag Type IV Secretion System Core Complex*. ASM mBio 2016. **7**(1): p. e02001-15.
257. Besselink, T., et al., *Comparison of activated chromatography resins for protein immobilization*. J. Sep. Sci., 2013. **36**(7): p. 1185-1191.

6 List of Abbreviations

Å	Ångstrom
ABC	ATP-binding cassette
ACP	acyl carrier protein
ADP	Adenosine diphosphate
ATP	Adenosine triphosphate
CLD	C39-peptidase like domain
CNBr	Cyanogen bromide
CMC	critical micellar concentration
Cryo-EM	cryo electron microscopy
Cryo-ET	cryo electron tomography
<i>csg</i>	curli-specific genes
CU	chaperone-usher
CyaA	adenylate cyclase toxin-haemolysin
DNA	deoxyribonucleic acid
<i>E. coli</i>	<i>Escherichia coli</i>
EDTA	ethylenediaminetetraacetic acid
eGFP	enhanced Green Fluorescence protein
EGTA	ethylene glycol-bis(β -aminoethyl ether)-tetraacetic acid
EM	electron microscopy
ET	electron tomography

GSP	general secretion pathway
HlyA	haemolysin A
HlyAc	N-terminally truncated variant of HlyA
HlyB	haemolysin B
HlyC	haemolysin C
HlyD	haemolysin D
IM	inner membrane
IMAC	immobilized metal-ion-affinity chromatography
KD	dissociation constant
kDa	kilo Dalton
LPS	lipopolysaccharide
MD	molecular dynamic
MFP	membrane fusion protein
MFS	major facilitator superfamily
μg	microgram
mg	milligram
min	minutes
μL	microlitre
mL	millilitre
μM	micromolar
mM	millimolar
NBD	nucleotide-binding domain
nm	nanometer
NMR	nuclear magnetic resonance
OEP	outer membrane efflux proteins
OM	outer membrane
OMP	outer membrane protein
PAGE	polyacrylamide gel electrophoresis
PCAT	C39-peptidase containing ABC transporter

pdb	Protein Data Bank
pI	isoelectric point
PMF	proton motive force
PP	periplasm
pro-HlyA	non-toxic pre-protein
RND	resistance-nodulation-division
RTX	repeats in toxin
RTX repeats	glycine-rich repeats of the RTX domain
SDS	sodium dodecyl sulphate
SEC	size exclusion chromatography
Sec	general secretory
SMR	small multidrug resistance
SPR	surface plasmon resonance
SRP	signal recognition particle
T1SS	Type I secretion system
T2SS	Type II secretion system
T3SS	Type III secretion system
T4SS	Type IV secretion system
T5SS	Type V secretion system
T6SS	Type VI secretion system

T7SS	Type VII secretion system
T8SS	Type VIII secretion system
Tat	twin arginine translocation
TBS	Tris-buffered saline
TBS-T	TBS with Tween 20
TEV	tobacco etch virus
TMD	transmembrane domain
TMH	transmembrane helix
UPEC	uropathogenic Escherichia coli

7 List of Figures

Introduction

Figure 1 Phospholipids and the bilayer. a) Major contributors of the Escherichia coli membrane PE, PG and CL. Fatty acid chains are indicated by the dark yellow with the chain length's normally varying between 14 and 19 carbon atoms in E.coli [4]. b) Detergents and fatty acids are forming a micelle while phospholipid favorably arrange as a bilayers except pure PE, which will form hexagonal cubic phases [5]. 8

Figure 2 Medical illustration of carbapenem-resistant Enterobacteriaceae. A figurative illustration of a Gram-negative carbapenem-resistant bacteria from the CDC-Website for public domain. 2019.09.11[6] 9

Figure 3 Scheme of the TF path for Sec translocation (post translational secretion). The nascent chain is recognized through the signal peptide and SecB can bind the unfolded protein to prevent aggregation. The precursor protein SecB-complex is recognized by SecA and mediates the binding to the SecYEG translocation complex. The initiation step requires ATP but not its hydrolysis. Continued translocation requires cycles of ATP hydrolysis. The translocation is occurring in a step-wise fashion with a steps of 20–30 amino acid residues and is the released in the periplasm. Figure based on [30] 11

Figure 4 Scheme of the different Tat mediated translocations which have been identified. The first possibility is the acquisition of their cofactor prior to transport across the cytoplasmic membrane. Only certain cofactors are associated with Tat-mediated transport. These can be broadly divided into metal–sulphur clusters and cofactors containing a nucleotide moiety. Metal ions compete for binding sites in proteins. The second case of Tat mediated secretion is the possibility to obtain metal ions under controlled conditions in the cytoplasm. [38]. The third known use of the Tat pathway allows hetero-oligomeric complexes to form in the cytoplasm and then be transported by a signal peptide in just one of the constituent subunits. Figure based on [39] 12

Figure 5 Scheme of the different double-membrane spanning secretion systems. (A) From left to right. Resistance–nodulation–division (RND) pumps are able to secrete a broad range of different substrates in particular small hydrophobic substances. Type I secretion systems (TISSs) secretes an unfolded substrate across both membranes in a single step (except for some bacteriocins and adhesins which own a cleavable N-terminal secretionsignal [44]). The correct folding is induced by Ca^{2+} binding in the extracellular space. The secretion systems T3SS (B) T4SS and T6SS are directly targeting a host cell across a third membrane. These sophisticated machineries are used to directly inject proteins, DNA or effector molecules into the targeted cell to manipulate or infect it. Figure based on [8] 13

Figure 6. Outer membrane secretion systems. On the left the type V secretion system. T5SS autotransporter (type Va) carboxy-terminal domain (CTD) (the EstA translocator) is inserted into the outer membrane (OM) as a β -barrel, whereas the amino-terminal domain (NTD) of the protein (the EstA passenger) is exposed to the extracellular space after translocation through the β -barrel. The Bam complex (BamA–BamB–BamC–BamD–BamE) is involved in the insertion of the EstA translocator domain into the OM and is also possibly involved in secretion of the EstA passenger domain [111-115]. Shown in the middle is the chaperone–usher pathway. A type I pilus is shown, with the subunits FimH, FimG and FimF forming the tip (known as the fibrillum), and ~1,000 FimA subunits forming a thick rod. The usher (which is composed of FimD) contains a pore, plug, NTD, CTD1 and CTD2. The penultimate FimA subunit traverses the pore, whereas the final FimA subunit is on the periplasmic side of the pore and is still bound to the FimC chaperone [116-118]. The right side displays the curli biogenesis system. The secretion channel in the OM is composed of the protein CsgG and is capped on the periplasmic side by the protein CsgE. The minor curli subunit CsgB anchors the major curli subunit CsgA to

the OM and nucleates its polymerization. The secretion process is mediated by the two accessory proteins CsgF and CsgC[119-122]. The Figure is based on [8]. 17

Figure 7. Structure of Sav1866 from *Staphylococcus aureus* with bound ADP (pdb entry 2HYD). One of the two monomers is colored dark gray. The other monomer's TMD is colored blue, cyan, yellow and green, while the corresponding NBD is colored red. Coupling helix 1 (magenta helix) is thought to make contact with the cis NBDs during formation of the nucleotide sandwich. Coupling helix 2 (orange helix) is always domain swapped to interact with the trans NBD. (B) Close-up view of the gray NBD and the sandwiched ADP molecule. Motifs which are directly involved in ATP binding and hydrolysis are colored as follows: Walker A, red; Q-loop, green; H-loop, purple; Walker B, cyan; A-loop, blue; C-loop, yellow; D-loop, black. Figure is taken and modified from [151] 19

Figure 8. X-ray structure of a folded GG-repeat in CyaA. The N-terminal consecutive nonapeptide tandem repeats (GGxGxDxxx) are arranged in a regular right-handed helix of parallel β strands (β -roll). The first six residues of the RTX motif (GGxGxD) constitute a turn with bound calcium ion (yellow ball), while the last three non conserved residues (xxx) form a short β strand. Calcium ions are numbered for clarity, and the residues 1,636–1,642 of the TDDALTV segment involved in initiation of Ca^{2+} -induced folding of the RTX domain are colored in magenta. Taken and modified from [169] 21

Figure 9. Domain organization of HlyA, HlyAc and fusion proteins used in the experiments. Yellow indicates the N-terminal region containing the membrane insertion domain of the toxin. The blue box the C-terminal secretion signal consisting of 50-60 aa. Black boxes represent conserved RTX-domain also called GG-repeats with the conserved consensus sequence GGXGXGUX. The marked aa represent the position for fatty acid acylation via HlyC. Green indicates the N-terminal eGFP in fusion proteins used in for stalling the TISS. 22

Figure 10. Hexameric model of HlyD. (A) Six HlyD protomers (cyan and orange) are assembled in a side-by-side arrangement. This funnel-like hexamer is also observed for MacA and AcrA [53, 180]. (B) Interaction between two adjacent protomers. The intermolecular interaction between $\alpha 2$ and $\alpha 3$ observed while electrostatic interaction of Arg186 and Asp309 also occurs. Figure from [181]. 23

Figure 11. TolC integrated into the peptidoglycan. Stereoviews from the side of (A) and above (B) the crystal structure of TolC outer-membrane channel embedded into a pore of the cell wall. TolC is shown in ribbon and surface representations as a solvent-accessible Connolly surface (purple). The protruding TolC β -barrel domain (shown in ribbon) is fully embedded into the outer-membrane bilayer of the Gram-negative bacterium. Figure was taken from [10] 24

Figure 12. Assembly, secretion and stalling of the TISS. The inner membrane complex of HlyB purple (CLD based on pdb file: 3ZUA in red, NBD based on pdb file: 2PMK cyan) and HlyD in blue (periplasmic part based on pdb file: 5C21) is colocalized. In the presence of the substrate HlyA, HlyB and HlyD recruit TolC, the OMP of the TISS. The unfolded substrate is threaded into the translocation pore with the C-terminus first, while ATP binding is mediated by the interaction of the secretion signal with HlyB. The unfolded substrate is displaced into the translocator and moves through TolC until the extracellular space is reached. Here, the GG-repeats bind to extracellular Ca^{2+} (indicated by dark green spheres) which induces folding of the substrate while transport is continued. When HlyA completely passed the translocator, it is presumed that this triggers the release of the OMP and ADP and phosphate is released into the cytosol while the initial state of the IMC is restored. When eGFP (in light green based on the pdb file: 5DY6) or any fast folding protein is fused to the N-terminal site of HlyA the initial secretion occurs until the fast folding N-terminal part reaches the translocation pore. It is too narrow to enter and the secretion system is arrested in this state by preventing the disassembly of the TISS. In the extracellular space the surface reaching part is folded by binding Ca^{2+} , which prevents backsliding into the translocation pore. 25

Chapter V – Isolation of the hemolysin A Type I secretion system in action

Figure 1. Western blot of prepared *E. coli* membranes containing stalled HlyA TISS. All parts of the HlyA TISS were detected by immunofluorescence in the collected membranes from *E. coli* BL21 DE3. The used antibody is labeled above while specific bands (eGFP-HlyA, HlyB, HlyD and TolC) are indicated by arrows. 121

Figure 2. Solubilization screen from membranes containing the stalled HlyA TISS. Solubilization screen of *E. coli* membranes containing the via eGFP-HlyA stalled HlyA TISS. For the screen 92 different detergents were tested. Non-ionic detergents are marked by green boxes, zwitterionic by blue boxes and anionic are marked by red boxes. SDS and the solubilization buffer without detergent are used as control in line H7 and H8. The list of all used detergents is shown in Table 1. The solubilized membranes were spotted on a nitrocellulose membrane via dot blot method. The blotted membranes then were examined by using specific antibodies against (a) HlyA, (b) HlyB, (c) HlyD and (d) TolC. 122

Figure 3. Western blot from sucrose gradient with the solubilized TISS membrane. All parts of the HlyA TISS were detected by immunofluorescence in the collected gradient fractions. The used sample derived from, Fos16 solubilized membranes from *E. coli* BL21(DE3) The sample was applied to SDS-PAGE with a continuous 10 % polyacrylamide gel. The Protein was transferred by tank-blot to the PVDF membrane. The blotted membranes then were examined by using specific antibodies against eGFP, HlyB, HlyD and TolC 123

Figure 4. SEC profile of DSP cross-linked CBP-eGFP-HlyA stalled TISS. The eluted fractions from the CBP-resin containing the TISS were concentrated using an Amicon Ultra centrifugal filter unit and 500 μ L was loaded on a Superose6 increase 10/300 column. 1 indicates the first major peak (near 10 to 11 mL) for further investigation. 2 indicates the second major peak (around 12-13 mL) for further investigation. Peak 1 and 2 was applied to NativePAGE and SDS-PAGE for immunoblot analysis (Figure 4). 124

Figure 5. Immunoblot analysis of the SEC fractions from TISS purification. All parts of the HlyA TISS were detected by immunofluorescence in the collected SEC fractions. The sample derived from DSP crosslinked, solubilized membranes from *E. coli* BL21(DE3). (a) the sample was applied to a Native PAGE with a Bis-Tris 4-16 % gradient gel. The protein was transferred by tank-blot to the PVDF membrane. (b) the sample was applied to SDS-PAGE with a continuous 10 % polyacrylamide gel. The Protein was transferred by tank-blot to the PVDF membrane. The blotted membranes then were examined by using specific antibodies against eGFP, HlyB, HlyD and TolC. The * indicates an addition of 50mM DTT during sample preparation to reduce the DSP disulfide bonds. 125

Figure 6. SEC profile of DSP cross-linked CBP-eGFP-HlyA stalled TISS and reinject of selected fractions on same column. (a) The eluted fractions from the CBP-resin containing the TISS were concentrated using an Amicon Ultra centrifugal filter unit and 500 μ L was loaded on a Superose6 increase 10/300 column. The dotted line indicates the selected peak (about 10 to 14 mL) for reinject. (b) The selected 4 mL fraction were concentrated using an Amicon Ultra centrifugal filter unit to 500 μ L and was reinjected on the Superose6 increase. The dotted lines indicates the selected peak (about 11-15 mL) for further investigation. The pooled peak (indicated as 1) was applied to NativePAGE and for immunoblot analysis and silver stain (Figure 7 & 8). 127

Figure 7. Immunoblot analysis of the reinjected SEC fraction from TISS purification. All parts of the HlyA TISS were detected by immunofluorescence in the collected SEC fractions. The sample derived from DSP crosslinked, solubilized membranes from *E. coli* BL21(DE3). The sample was applied to a NativePAGE with a Bis-Tris 4-16 % gradient gel. The protein was transferred by tank-blot to the PVDF membrane. The blotted membranes then were examined by using specific antibodies against eGFP, HlyB, HlyD and TolC. The * indicates an addition of

50mM DTT and 1 % (w/v) SDS during sample preparation to reduce the DSP disulfide bonds and separate the components of the TISS. 128

Figure 8 Silverstain of the reinjected SEC fraction from the TISS purification on a NativePAGE. The pooled fractions from the reinjected TISS was applied to a NativePAGE, Bis-Tris 4-16 % gradient gel. The gel run was stopped after the running front reached the bottom of gradient gel. The protein was fixed with methanol and acetic acid and silver stained. Additional supplements to the sample are indicated by + DTT (50 mM) and + SDS (1 % and 50 mM DTT). HlyB and HlyA was applied as purified reference. 129

Figure 9. SEC of affinity purified TISS from C43 Δ acrAB and corresponding NativePAGE. (a) The eluted fractions from the CBP-resin containing the TISS were concentrated using an Amicon Ultra centrifugal filter unit and 500 μ L was loaded on a Superose6 increase 10/300 column. The numbers indicates the selected peaks 1 to 4, which were used for further investigation. (b) collected fractions from the TISS purification were applied to a NativePAGE, Bis-Tris 4-16 % gradient gel. The gel run was stopped after the running front reached the bottom of gradient gel. The protein was fixed with methanol and acetic acid and stained with colloidal Coomassie. The * indicates an addition of 50 mM DTT and 1 % (w/v) SDS during sample preparation to reduce the DSP disulfide bonds and separate the components of the TISS. 129

Figure 10. NativePAGE Immunofluorescence analysis of TISS SEC fractions from C43 Δ acrAB. The sample was applied to a NativePAGE with a Bis-Tris 4-16 % gradient gel. The protein was transferred by tank-blot to the PVDF membrane. The sample 3 indicates the third peak respectively 4, the fourth peak from the SEC shown in Figure 8. The blotted membranes then were examined by using specific antibodies against HlyA, HlyB, HlyD and TolC. The * indicates an addition of 50 mM DTT and 1 % (w/v) SDS during sample preparation to reduce the DSP disulfide bonds and separate the components of the TISS. 130

Figure 11. SEC after CBP affinity purification, of stalled, not crosslinked TISS, expressed in C43 Δ acrAB Δ ompF. (a) The eluted fractions from the CBP-resin containing the TISS were concentrated using an Amicon Ultra centrifugal filter unit and 500 μ L was loaded on a Superose6 increase 10/300 column. 1 indicates the front shoulder of the major peak (around 13.5 mL) 2 indicates the top of the major peak (near 15 mL). (b) All parts of the HlyA TISS were detected by immunofluorescence in the collected SEC fractions. The sample was applied to a NativePAGE with a Bis-Tris 4-16 % gradient gel. The protein was transferred by tank-blot to the PVDF membrane. The blotted membranes then were examined by using specific antibodies against HlyA, HlyB, HlyD and TolC. The * indicates an addition of 50mM DTT and 1 % (w/v) SDS during sample preparation to reduce separate the components of the TISS. 132

Figure 12. Blue NativePAGE of SEC after CBP affinity purification, of stalled, not crosslinked TISS, expressed in C43 Δ acrAB Δ ompF. The eluted fractions from the CBP-resin containing the TISS were concentrated using an Amicon Ultra centrifugal filter unit and 500 μ L was loaded on a Superose6 increase 10/300 column. The numbers on top indicating the elution volume of the applied sample. On the right bottom corner a schematic of the SEC chromatogram is shown with a black bar indicating the selected range applied to the gel. Collected fractions from the TISS purification were applied to a NativePAGE, Bis-Tris 4-16 % gradient gel. The gel run was stopped after the running front reached the bottom of gradient gel. The protein was fixed with methanol and acetic acid and stained with colloidal Coomassie. 133

Figure 13. Analysis of SEC after CBP affinity purification, of stalled and crosslinked TISS, expressed in C43 Δ acrAB Δ ompF. (a) The eluted fractions from the CBP-resin containing the TISS were concentrated using an Amicon Ultra centrifugal filter unit and 500 μ L was loaded on a Superose6 increase 10/300 column. 1 indicates the front shoulder of the major peak (nearly 11 mL). 2 indicates the back shoulder of the major peak (around 13 mL). Silver stained NativePAGE of the SEC from 11 to 15 mL, shifting in every lane 0.5 mL. (b) All proteins of the HlyA TISS were detected by immunofluorescence in the collected SEC fractions. The sample was applied to

a NativePAGE with a Bis-Tris 4-16 % gradient gel. The protein was transferred by tank-blot to the PVDF membrane. The blotted membranes then were examined by using specific antibodies against HlyA, HlyB, HlyD and TolC. The * indicates an addition of 50mM DTT and 1 % (w/v) SDS during sample preparation to reduce the disulfide bonds from DSP and separate the components of the TISS. 134

Figure 14. Comparison of “LDAO” versus “Fos” purification showing the SEC after CBP affinity purification, of stalled, not crosslinked TISS with peptidoglycan digest, expressed in C43 *ΔacrAB* (a) LDAO purification. The eluted fractions from the CBP-resin containing the TISS were concentrated using an Amicon Ultra centrifugal filter unit and 500 μ L was loaded on a Superose6 increase 10/300 column. (b) Fos purification. The eluted fractions from the CBP-resin containing the TISS were concentrated using an Amicon Ultra centrifugal filter unit and 500 μ L was loaded on a Superose6 increase 10/300 column. (b) 1 indicates the first peak (near 10.5 mL) 2 indicates the front shoulder of the major peak in the chromatogram (around 13 mL) 136

Figure 15. Comparison of “LDAO” versus “Fos” blue NativePAGE and immunofluorescence of SEC load and peaks from Fos purification of stalled, not crosslinked TISS with peptidoglycan digest, expressed in C43 *ΔacrAB*. (a) Load indicates the samples protein applied to the SEC for purification. The numbers correspond to the samples taken from the chromatogram shown in Figure 13. The * indicates an addition of 50 mM DTT and 1 % (w/v) SDS during sample preparation to reduce the disulfide bonds from DSP and separate the components of the TISS. Collected fractions from the TISS purification were applied to a NativePAGE, Bis-Tris 4-16 % gradient gel. The gel run was stopped after the running front reached the bottom of gradient gel. The protein was fixed with methanol and acetic acid and stained with colloidal Coomassie. (b) All proteins of the HlyA TISS were detected by immunofluorescence in the collected SEC fractions. The sample was applied to a NativePAGE with a Bis-Tris 4-16 % gradient gel. The protein was transferred by Trans-Blot® Turbo™ to the PVDF membrane. The blotted membranes then were examined by using specific antibodies against HlyA, HlyB, HlyD and TolC. The * indicates an addition of 50 mM DTT and 1 % (w/v) SDS during sample preparation to reduce the disulfide bonds from DSP and separate the components of the TISS. 137

Discussion

Figure 1. Comparison of surface distribution of different TISS. Showing labeled TISS in *Salmonella enterica* and *E. coli* BL21. (A) Single molecule localization microscopy of SiiF with a Halo-tag in living cells of *Salmonella*. Labeled with TMR-Star. Cells were imaged by super-resolution microscopy (SRM). 500 consecutive frames were acquired with 5 mW laser power at the focal plane. Cumulative maximum intensity projections with bilinear interpolation of all 500 frames are shown. Scale bar 5 μ m. Taken from [244] (B) HlyA TISS stalling was induced in BL21(DE3). DNA was stained by DAPI and cell surface exposed HlyA was stained by immunofluorescence labelling. Cells were imaged by SIM. Maximum intensity projections (MIPs) of raw data before processing show the DAPI channel in blue (DAPI), and the HlyA channel in red (α -HlyA). Scale bar: 1 μ m.

Figure 1. Novel crosslink approach to stabilize the HlyA TISS for purification. (A) Image of the AcrAB-TolC RND complex, taken from [186]. The red dotted box indicates the region where TolC and AcrA are interacting via tip to tip interaction. (B) Scheme of the HlyA TISS, generated from TolC (2XMN), HlyB NBD (2PMK) and CLD (3ZUA), HlyD modified from [181]. The red dotted line indicates the proposed interaction region between TolC and HlyD, which is magnified on the right side. The domain structure and sequence of the periplasmic part is shown on the bottom right side helices α 2, α 3 and the interaction loop L2. Lysine130 of one TolC monomer and serine242 of the HlyD monomer are indicated by the red arrows. A possible crosslinker is shown on the middle right side PEG4-SPDP (2-Pyridyldithiol-tetraoxatetradecane-N-hydroxysuccinimide) 151

Figure 2 Schematic approach for pulldown of the HlyA TISS IMC. On the left side a silver stained native PAGE with HlyB and HlyA is shown where the HlyB stopped migration together with HlyA indicated with an arrow. Right from the PAGE a schematic of the CNBr-Agarose beads is shown and the binding of HlyA to the nitrile group creating an agarose bead coated with HlyA (indicated by red dotted line). A model of the HlyA TISS IMC (HlyB NBD (2PMK) and CLD (3ZUA), HlyD modified from [181]) interacts with the immobilized HlyA and then can be used for a pulldown. 152

8 Danksagung

An erster Stelle möchte ich meinem Doktorvater Prof. Dr. Lutz Schmitt danken. Vielen Dank, du hast es mir ermöglicht zu promovieren. Unsere zahlreichen Gespräche waren mir eine Inspiration und lieferten stets neue Ideen und Ansätze für meine Experimente. Dank dir habe ich einiges über Hochschulpolitik lernen dürfen, dies eröffnete mir völlig neue Perspektiven und wird mir sicher in Zukunft helfen meine Ziele zu verfolgen. Vielen Dank dafür, dass du mich immer wieder eingefangen hast, wenn meine Ideen meine Arbeitskapazitäten mal wieder überstiegen. Am meisten danke ich dir dafür, dass du mir, einem jungen Familienvater mit zwei kleiner Kinder, ermöglicht hast seinen Dokortitel zu erlangen. Ich konnte immer auf dich zählen, auch wenn kurzfristig etwas mit den Kindern war. Du sagtest einmal für dich wäre dies selbstverständlich, aber die Realität ist für viele eine andere. Ich hoffe, dass in der Zukunft sich mehr Verantwortliche so wie du verhalten.

Großen Dank möchte ich auch an Dr. Sander Smits richten. Deine einzigartige Art war anfangs schwierig für mich zu verstehen, hat mir aber sehr geholfen mich persönlich weiter zu entwickeln. Durch die interessanten Gespräche mit dir habe ich oft neue Perspektiven entwickeln können, was mir sehr dabei geholfen hat meine Ziele zu verfolgen. Du hattest immer ein offenes Ohr für mich und meist sehr pragmatische Lösungsvorschläge, was mir sehr entgegen kam. Deine „*can do*“ Mentalität finde ich sehr erfrischend und inspirierend. Insbesondere danke ich dir für die Hilfe bei der Korrektur dieser Arbeit.

An dieser Stelle möchte ich mich bei Prof. Dr. Michael Feldbrügge für die freundliche Übernahme des Korreferates bedanken und die vielen Tipps während unsere Follow-Up Meetings für mein Projekt.

Wenn ich zurückschaue auf meinen Weg an der Universität und wer diesen geprägt hat, möchte ich unbedingt PD. Dr. Ulrich Schulte danken. Als Begleiter durch das Studium hast du maßgeblich mein Interesse an der Biochemie mitgestaltet. Sympathisch und herzlich hast du mich auch durch die Promotionszeit begleitet und mir immer Gehör geschenkt wenn etwas anlag oder ich fragen hatte.

Im SFB1208 gibt es eine Person der ich sehr danken möchte, Dr. Cordula Kruse. Danke für die Hilfe mit all den bürokratischen Hindernissen und Vorgaben die mit einer Promotion einhergehen und für deine Unterstützung, wenn mal etwas nicht so klappte. Des Weiteren will ich mich auch bei dir entschuldigen, dass du mich manchmal genau an diese bürokratischen Aufgaben erinnern musstest. Du hast mir mit deiner freundlichen und offenen Art sehr geholfen.

Meinen größten Dank widme ich meiner Familie. Natalia, Finn und Leif. Nata du hast mir immer den Rücken freigehalten und immer zugehört, wenn ich mir Gedanken über vieles an

der Arbeit gemacht habe und mich stets unterstützt. Ohne dich wäre meine Promotion so nicht möglich gewesen. Da verstehe ich wenn man sagt, dass hinter jedem starken Mann eine starke Frau steht. Finn und Leif, ihr gebt mir so viel Freude auch wenn ich manchmal gerne etwas mehr Schlaf hätte. Wenn ich mit euch zusammen bin, weiß ich warum sich der Aufwand lohnt. Ich liebe euch alle drei.

Nicht minder möchte ich meinen Eltern Sigrid und Lothar, Schwiegereltern Valery und Elena sowie meinen Schwestern Kristina und Mareike, meinem Schwager Christian, meinen kleinen Nichten Maja, Jette und Lilli und meiner Oma Lilo danken. Ihr habt mich während meines Studiums immer wieder unterstützt, mir zugehört und Ratschläge gegeben. Ohne die Hilfe von euch wäre mein Studium so nicht möglich gewesen und ich bin sehr dankbar dafür. Es ist schön wenn die Familie zusammensteht und sich gegenseitig hilft. Ich wünsch mir, dass wir dies auch in Zukunft tun.

Meinen Kollaborationspartnern vom Institut für Krankenhaushygiene möchte ich meinen Dank aussprechen. Prof. Dr. Klaus Pfeffer, vielen Dank für die Möglichkeit die S2 Arbeiten mit unserem uropathogenen Stamm durchzuführen. Vielen Dank an Prof. Dr. med. Colin R. MacKenzie der initial den Stamm für mich kultivierte. Weiter möchte ich Larissa Legewie und Jens Lichte danken. Ihr habt mir die Einrichtungen in eurem Institut gezeigt und geholfen, sodass ich meine Experimente erfolgreich durchführen konnte. Danke, dass ihr euch die Zeit dafür genommen habt. Ich hoffe meine Unterstützung bei euren Proteinreinigungen hat euch auch etwas geholfen.

Ein herzliches Dankeschön geht an Dr. Stefanie Weidtkamp-Peters vom Center for Advanced Imaging (CAi) für die tolle Betreuung bei den Mikroskopen und eine wunderbare Einführung in die Fluoreszenzmikroskopie und die Hilfe bei der Konzipierung einiger Experimente.

Meinem Mitstreiter Dr. Sebastian Hänsch möchte ich auch meinen Dank aussprechen. Es hat mir große Freude gemacht zusammen mit dir die Experimente für unsere Publikation zu planen und zu realisieren. Ich konnte viel von dir lernen und genoss unseren regen Austausch über unsere Daten, die möglichen Folgeexperimente und Möglichkeiten. Die Entdeckung unserer gemeinsamen Interessen, wie beispielsweise Pen and Paper Rollenspiele, machten mir die Zeit mit dir noch wesentlich angenehmer, auch wenn die Probenvorbereitung von über 12 Stunden nicht immer hätten sein müssen, aber geteiltes Leid ist bekanntlich halbes Leid.

Für den alltäglichen Kampf gegen die Bürokratie im Labor danke ich Tatjana Platz und der langjährigen Vorgängerin Mathilde Blum, vielen Dank an euch beide. Ihr habt mir viel Papierarbeit abgenommen, an der ich ohne euch vielleicht noch immer sitzen würde.

Als nächstes möchte ich dem Doppelpack Sven Reimann und Michael Lenders danken. Michael du hast mir viel beigebracht und mich ins Labor eingearbeitet. Du warst der Kaiser und ich dein Generalfeldmarschall, deine ausführende Gewalt. Zusammen haben wir viel geschafft und hatten selbst bei ermüdenden Aufgaben noch Spaß. Dein Input war immer sehr reflektiert und deine unaufgeregte Art in Fragen der Wissenschaft stand im Kontrast zu deinem Hungerhirn (und den dann folgenden Schreien über den Flur). Ohne Zucker funktioniert der Michael einfach nicht! Selbst als du dein Referendariat begannst, warst du immer bei Fragen verfügbar. Vielen Dank dafür.

Sven, mein Benchnachbar. Michael und ich hatten dich in der Zange und dein Unverständnis über uns wurde oft mit einem Kopfschütteln honoriert, gefolgt von einem ausgiebigen Lachen. Du hattest immer ein offenes Ohr, wenn ein Experiment mal nicht so lief wie es sollte und hast mir viele hilfreiche Tipps gegeben. Und wenn es zu frustrierend wurde, konnten wir uns immer noch am Wochenende auf einen gepflegten Whisky zusammensetzen. Entschuldige, dass du meine Tiraden über die Tagespolitik so oft ertragen musstest, auch wenn wir oft tolle Diskussionen daraus entwickelten. Die Arbeit mit dir war mir immer eine Freude und dafür danke ich dir.

Zu meinen Laborpartnern zählt auch Marcel, der dunkle Lord. Zusammen waren wir im Lab29 oder wie wir gerne sagten: „Unser Inklusionslabor im Institut“. Wir standen uns an der Bench gegenüber, besprachen ausgiebig unsere Daten, blickten hoch und wussten beide „Läuft“, um dann ein „Ohhh Isabelle“ dran zu hängen. Wir teilten unsere Freude, unser Leid und konnten mal endlich gute Musik im Labor etablieren. Du hattest oft hilfreiche Tipps für mich und es war mir immer eine Freude, wenn wir unsere Ideen im wissenschaftlichen Austausch besprechen und vor allem verbessern konnten. Die ÄKTA hast du immer in Schuss gehalten und ich konnte einiges über Wartung der Säulen und der Geräte von dir lernen. Du hast mir sehr geholfen bei der Sache zu bleiben und ich wünsche dir viel Erfolg im Süden. War eine super Zeit mit dir. Darauf ein Espresso oder doch Whisky?

Liebe Isabelle, du warst meine erste zu betreuende Studentin und musstest deswegen wohl auch am längsten unter mir leiden. Denn du warst das Hauptopfer, wenn ich mal wieder meine Flachwitze oder „Dadjokes“ rausgehauen habe. Ein Augenrollen gefolgt von „echt jetzt Tobi?“ war dabei schon fast eine Ehrung. Marcel und ich hatten einen Heidenspaß daran dich mit Katzenkunst und netten Memes zu versorgen. Du bist nun unsere Institutskünstlerin und Beauftragte für Mobbing, daher haben wir prinzipiell alles richtig gemacht. Aber auch abseits dessen, war es mir eine riesen Freude mit dir zusammen zu arbeiten. Ich kann mich glücklich schätzen eine so fleißige, selbständige und kluge Studentin bekommen zu haben, die dann auch bei uns blieb (war wohl doch nicht so schlimm) und „Rücken an Rücken“ mit mir arbeitete als neues Mitglied im Lab29. Immer an die Schutzbrille denken und tut mir leid mit dem S2-Bereich. Danke, dass du es mit mir ausgehalten hast.

Olivia „Oli“, du bist, wie wir oft schon Kund getan haben, die Person die ich am längsten an der Uni kenne. Seit dem ersten Tag verstehen wir uns gut und unser Weg scheint miteinander verbandelt zu sein. Wir trafen immer wieder zusammen und haben dabei immer gut

zusammengearbeitet. Da wir uns gut verstehen, etablierten wir eine Arbeitsehe, geschmiert von literweise Kaffee und Zigarettenpausen, die uns beiden halfen die anstehenden Arbeiten im Institut möglichst unkompliziert zu bewältigen und unsere Projekte und Ergebnisse immer wieder zu besprechen und zu evaluieren. Wir wissen wo unsere Stärken liegen und haben uns zusammen gut ergänzt um mehr Zeit für Kaffee, ich meine unsere Experimente, zu haben. Dann abends nach dem SFB noch mal treffen auf eine Runde Shadowrun oder doch lieber ein anderes Rollenspiel? Wir hatten viel Spaß damit und ich fand es immer wieder schön dein entflammtes Interesse an WOW und Rollenspielen zu sehen. Ich hoffe du kannst dir den Spaß bewahren und findest einen wohl gesonnenen GM für regelmäßige Spielabende. Vielen Dank für die tolle Zeit, die vielen Kaffeegespräche, deine Hilfe, wenn mal wieder etwas „schnell“ gemacht werden sollte. Danke, dass du unkompliziert deine Mithilfe angeboten hast und an der richtigen Stelle eingesprungen bist. Eine bessere Arbeitsehefrau und Kollegin kann ich mir nicht vorstellen.

Und wenn wir schon beim Thema Kaffee sind. Die zweite Person die meinen sowieso schon immensen Kaffeekonsum weiter erhöht hat: Julia. Julia wir haben uns oft beim Kaffee über unsere Projekte, aber auch viele andere Dinge unterhalten. Ich finde es immer schön, wenn jemand zu seiner Meinung steht auch wenn diese konträr zu meiner ist. Ich schätze Menschen mit Rückgrat und das hast du auf jeden Fall! Ein „kurasche Weech“, dass auch mal Klartext reden kann und die bestimmt eine tolle Mutter wird. Hier auch nochmal alles Gute euch dreien. Vielen Dank für die schöne Zeit.

Nicht vergessen möchte ich Tim, meinen Büronachbarn. Vereint im Hass auf den Mac der nicht tut was er soll und Graphen die springen als wären sie auf einem Turnier. Es ist immer schön, wenn man seine Resultate auch aus anderen Blickwinkeln betrachten kann. Daher schauten wir uns gegenseitig auf unsere Ergebnisse und hinterfragten sie, um sicher zu sein, dass die Schlussfolgerungen in die richtige Richtung gehen. Vielen Dank fürs Zuhören, auch wenn ich manchmal einfach Dampf ablassen musste. Wenn ich dich suchte, war es eigentlich relativ einfach dich an deinem einzigartigen Lachen quer durch das Institut zu hören. Danke, dass du mir immer geholfen hast, wenn ich Unterstützung brauchte.

Wenn es mal darum ging anzupacken und einfach was zu bewegen, im wahrsten Sinne des Wortes, waren wir die Leute die man gerufen hat. Und das entspricht auch deinem Naturell, Jens. Du packst die Sachen an und machst sie einfach. Ein konservativer Fels in der Linken Hochburg Uni, auch das gehört zur Vielfalt. Bei Kaffee über aktuelle Experimente, Politik und Whisky zu fachsimpeln war stets interessant und die Etablierung des Düsseldorfers Whiskykreises mit dir war mir eine Freude. Als Meister des SAXS wünsche ich dir viel Erfolg und hoffentlich darf ich mich noch einige Male an deiner Backkunst erfreuen (machst einfach den besten Kuchen). Als Techniker des Instituts hast du mir auch sehr mit der HPLC geholfen, wenn sie mal wieder nicht so wollte wie sie sollte. Vielen Dank für die Hilfe und tollen Gespräche.

Manuel und Martin euch nenne ich jetzt im Doppelpack, weil ihr von einem ähnlichen Schlag Mensch seid. Ihr beide seid nicht die Lautesten und gebt nicht zu allem euren Senf ab, aber wenn spricht es für euer überlegtes Handeln und Denken. Martin, vielen Dank für die persönlichen Gespräche und dein Input zu meiner Arbeit. Deine, im Vergleich zu mir, ruhigere Art war für mich ein guter Gegensatz um neue Denkweisen aufgezeigt zu bekommen. Manuel bei dir war es ähnlich, oft hast du zugehört und dein Gesicht hat meist schon gezeigt wie du zu der Sache stehst, bevor du ein Wort gesagt hast. In Diskussionen haben wir manchmal andere Ansichten gehabt, aber stets konstruktiv und freundschaftlich miteinander geredet. Wir haben aber auch fundamentale Fragen über unsere Arbeit und Experimente besprochen, was mir sehr geholfen hat neue Experimente zu entwickeln und zu überlegen wie es weitergeht. Vielen Dank für eure offenen Ohren und die tolle Hilfe, Martin und Manuel.

Florestan der zweite Masterstudent, der nach meiner Betreuung im Institut geblieben ist und Manuel (A). Euch gibt es wahrscheinlich nur im Doppelpack. Ihr habt eine tolle Gruppendynamik und ich wünsche euch, dass ihr diese erhalten und weiter in eure Arbeit einbringen könnt. Manuel, du kamst zu Oli als Masterstudent und warst mir als Memelord direkt sympathisch. Du hast dich von den ATPasen nicht entmutigen lassen und bist dann glücklicherweise auch bei uns im Institut geblieben, was mich sehr freut. Die Montagabende mit den aktuellen und ehemaligen Institutsleuten ist eine wahre Freude und der „Trashtalk“ bringt direkt noch mal eine neue Qualität dazu. Marcel hat dich mit der ÄKTA beerbt und ich glaube du bist der Richtige für diese Aufgabe, da ich dich als verantwortungsbewusst und sorgsam wahrgenommen habe und du deshalb auch die erste Wahl für mich warst, um die Kaffeekasse mit zu übernehmen. Ja, Florestan, du sollst ihm dabei helfen! Du warst mein letzter Masterstudent und hast mich mit deiner gewissenhaften Arbeitsweise und dem Anspruch alles super zu machen, von dir überzeugt. Ich hatte große Freude daran zusammen mit dir am Typ I Sekretionssystem zu arbeiten und ehrlich gesagt, würde ich dies auch gerne weiter tun, da ich glaube, dass wir dort noch eine ganze Reihe reißen könnten. Deine Arbeiten bei der Rekonstitution von TolC haben auf jeden Fall schon mal einen guten Grundstein gelegt und ich bin überzeugt, dass du den IMC auch noch packst. Der Input von dir zu den Experimenten war mir stets sehr willkommen und dein ruhige, bedachte, aber dennoch humorvolle Art hat mir die letzten Monate im Labor noch einmal versüßt. Manuel, Florestan vielen Dank, dass ich mit euch zusammenarbeiten durfte.

Hans und Tri. Ihr wart immer mal wieder im Institut, erst als Bachelorstudenten, dann Hans als SHK und dann beide wieder im Master. Es ergibt Sinn, dass es hieß: „Ihr seid wie Herpes, man wird euch einfach nicht los.“ Im Gegensatz zum Virus war eure Anwesenheit aber stets eine Freude. Gerade dir Hans danke ich für die Unterstützung bei alltäglichen Arbeiten während deiner SHK Zeit, du hast viel Last von meinen Schultern genommen.

Also to you Zoreh, many thanks for the many fruitful discussions and steady communication about our projects. I really appreciated your input on our experiments and fresh view on many

“old” discussion positions in our project. You showed me that it is always beneficial to acquire “fresh blood” for the group, to not be stuck in old patterns.

Diana vielen Dank, dass du immer ein offenes Ohr hattest, wenn es um Klonierungen oder Papierkram ging. Wenn es nicht weiter ging wusste ich immer, dass du weisst wie es trotzdem klappt. Das war einfach unbezahlbar. Wenn die Nacht dann mal wieder zu kurz war, weil die Kinder krank waren oder Probleme beim Schlafen hatten (wer braucht schon Schlaf), war der mentale Aufbau immer sehr willkommen. Deine direkte Art war stets erfrischend und angenehm. In diesem Zusammenhang möchte ich auch meinen Dank an Iris richten. Genau wie Diana, warst du stets integer, direkt und immer hilfsbereit, wenn ich Fragen zur Klonierung hatte. Ich durfte dich auch immer fragen, wo ich eigentlich alles finde. Deine freundliche Art ist mir sehr willkommen und die vielen Tipps zu Klonierung, Plasmiddesign und Erfahrungen mit PCR haben mir gerade am Anfang meiner Promotion sehr geholfen.

Es gibt Personen die „den Laden“ am Laufen halten und immer wenn man mal nicht weiß wo etwas ist bzw. wie es weitergeht, kommt der Satz: „Frag mal Martina.“ Vielen Dank Martina, dass du dich der vielen Aufgaben im Institut angenommen hast und ich immer zu dir kommen konnte. Wenn etwas kaputt gegangen war oder bestellt werden musste, warst du immer die erste Anlaufstelle. Nein, nicht erstmal zum Chef. Lieber erstmal Martina fragen, vielleicht weiß sie ob man es noch retten kann. Du kennst die Abläufe und hast dafür gesorgt, dass die Lager gefüllt waren, damit „Wir“ einfach arbeiten können. Vielen Dank! Nicht minder möchte ich Silke danken. Wenn ich neue Zellen brauchte oder Vorräte bestellt werden mussten, konnte ich immer zu dir kommen. Die Arbeit mit dir war mir eine Freude.

Stefanie vielen Dank für deine Hilfe mit den ATPasen und, dass du es mit Tim ausgehalten hast. Deine norddeutsch wirkende Art passt wunderbar ins Labor und ist sehr erfrischend. Vivien vielen Dank für deine Hilfe mit dem IMC, das Thema verfolgt dich ja nun auch seit der Bachelorzeit. Trotzdem bist du nicht geflohen, dafür Respekt! Viel Erfolg mit dem neuen Thema und danke nochmals, dass du bei Fragen immer ansprechbar warst. Zusätzlich möchte ich dir Alex für den experimentellen Input und die interessanten Gespräche über dein Projekt danken. Ich wünsche dir viel Erfolg beim Aufbau des Projekts.

Ein großer Dank an die vielen ehemaligen Kollegen Katja, Rebecca, Kalpana, Katharina, und Sakshi. Ihr habt mir gerade am Anfange der Promotion viel mit eurem Know-How geholfen meine Experimente ans Laufen zu bekommen. Eure freundlichen Worte, wenn es mal wieder nicht geklappt hat, waren mir stets willkommen und eure Tipps für meine Experimente habe ich gerne angenommen, vielen Dank.

Many thanks to the whole group of Synthetic Membrane Systems. Alexej, thank you so much for your advices for experiments and with the reconstitution of the IMC. You were the ideal

sparring partner for new ideas and hypothesizes. The boss with the boots on the ground was a new experience for me and I learned a lot from you and your leading style. Thank you for giving me this insight. Maryna a strong woman with strong opinions, it was wonderful to work and discuss with you. I really enjoyed your scientific input, thank you for sharing with me. Athanasios, many thanks to you for the nice discussions and the input to my experiments. Your scientific background is really interesting and helped me obtain views from a different angle which helped me a lot. Michael thanks for being such a great guy. You provided me with MSP when I needed some, discussed my experiments with me and I learned a lot about your homeland Egypt. Alexej, Maryna, Athanasios and Michael thank you for giving me the opportunity to get to know you all. I am wishing the best for your future experiments you deserve the best results. I always had a nice time in your lab when doing the Western blots and I did a lot of them. Thanks!

An dieser Stelle möchte ich mich auch bei Kerstin bedanken. Du hast mich in die Fermentation eingeführt und zusammen haben wir am IMC gearbeitet und so viele Proben für das MALS vorbereitet, dass ich mich zwischenzeitlich schon selbst total verstreut gefühlt habe. Danke für die viele Unterstützung und das Wissen warum das B in HlyB für Bitch steht.

Ich bedanke mich bei der DFG für den SFB 1208 und die finanzielle Unterstützung. Die vielen interessanten Vorträge, Veranstaltungen, Symposien und Konferenzen die durch die Finanzierung ermöglicht wurden.

Zuletzt möchte ich meinen Freunden danken, die mich außerhalb der Arbeit immer unterstützt und aufgebaut haben. Boray, Sabrina, Christoph, Robert(s), Christian(s), Simon, Laura, Jenny, Erika, Flo und Claudia euch allen vielen Dank. Euer Rückhalt hat mich auch durch schwere Phasen gebracht.

Ich danke allen Leuten, die hier zwar nicht namentlich erwähnt wurden, aber trotzdem zum Gelingen dieser Arbeit beigetragen haben.

9 Curriculum vitae

Personal data

Name	Tobias Beer
Date of birth	05th February 1986, Paderborn
Mobile	+49 (0) 176 / 38959886
e-Mail	Tobias.Beer@uni-duesseldorf.de
Family status	married, 2 children

Doctorate

Since 01.2016	at the Heinrich-Heine-University Dusseldorf
04.2020	Doctor rerum naturalium (Dr.rer.nat.)
PhD thesis	Isolation and cellular characterization of the hemolysin A type I secretion system in <i>Escherichia coli</i>
First examiner	Univ. Prof. Dr. Lutz Schmitt, Institute for Biochemistry, Heinrich-Heine-University Düsseldorf
Second examiner	Prof. Dr. Michael Feldbrügge, Institute for Mikrobiology, Heinrich-Heine-University Düsseldorf

Studies

Master of Science „Biochemistry“	
10/2013 – 10/2015	at the Heinrich-Heine-Universität Düsseldorf, Overall grade: 2.1
17.10.2018	Master of Science (M.Sc.)
Master thesis	„Isolation eines Typ I Sekretionssystems“ (grade 1.3)
First examiner	Univ. Prof. Dr. Lutz Schmitt, Institute for Biochemistry, Heinrich-Heine-University Düsseldorf
Second examiner	PD Dr. Ulrich Schulte, Institute for Biochemistry, Heinrich-Heine-University Düsseldorf
Bachelor of Science „Biochemistry“	
10/2010 – 10/2013	at the Heinrich-Heine-Universität Düsseldorf, Overall grade: 2.4
03.09.2013	Bachelor of Science (Ba.Sc.)

Bachelor thesis	„Optimierung der HLA-Klasse I Sequenz-basierenden Typisierung“ (grade 2.0)
First examiner	PD Dr. Rüdiger Sorg, Institute for Transplantation Diagnostic and Cell Therapeutics, University Hospital of Düsseldorf I UKD
Second examiner	PD Dr. Ulrich Schulte, Institute for Biochemistry, Heinrich-Heine-University Düsseldorf

Apprenticeship

08/2007 – 06/2010	Apprenticeship as staatlich geprüfter Chemielaborant Currenta GmbH und Co. OHG / Bayer Healthcare Wuppertal
-------------------	--

Military Service

10/2006 – 06/2007	Draft, Augustdorf (PzGdr) => Medical Service and doctoral assistant
-------------------	---

School education

09/1996 – 06/2006	Gesamtschule Paderborn Elsen (Allgemeine Hochschulreife) 2.7
-------------------	--

Publications

2019	Type I Secretion Systems—One Mechanism for All? Spitz, O., Erenburg, I. N., Beer, T., Kanonenberg, K., Holland, I. B., Schmitt, L., Microbiology Spectrum 2019. 7(2)
2018	Type I secretion system—it takes three and a substrate Kanonenberg, Kerstin Spitz, Olivia Erenburg, Isabelle N Beer, Tobias Schmitt, Lutz FEMS Microbiol. Lett., 2018. 365(11)
2016	In vivo quantification of the secretion rates of the hemolysin A Type I secretion system Lenders, M. H. Beer, T. Smits, S. H. Schmitt, L. Nature Sci. Rep. 2016. 6: p. 33275

Participation at scientific conferences

2019 „Dynamics of Membrane Systems“: 2nd International Conference in Düsseldorf, Germany, poster presentation (The hemolysin A secretion machinery of *E.coli* and it's *in vitro* reconstitution.)

2017 „Dynamics of Membrane Systems“: 1st International Conference in Düsseldorf, Germany, poster presentation (The hemolysin A secretion machinery of *E.coli*.)

Gordon Research Seminar and Conference: Mechanisms of Membrane Transport, New London, NH, United States of America, poster presentation (*In vivo* quantification of the secretion rates of the hemolysin A Type I secretion system from *E.coli*)

10 Erklärung

Ich versichere an Eides Statt, dass die Dissertation von mir selbständig und ohne unzulässige fremde Hilfe unter Beachtung der „Grundsätze zur Sicherung guter wissenschaftlicher Praxis an der Heinrich-Heine-Universität Düsseldorf“ erstellt worden ist. Die Dissertation wurde in der vorgelegten oder in ähnlicher Form noch bei keiner anderen Fakultät eingereicht. Ich habe bisher keine erfolglosen und erfolgreichen Promotionsversuche unternommen.

(Ort, Datum)

(Tobias Beer)